Viking '75 Spacecraft Design and Test Summary

Volume I - Lander Design

Neil A. Holmberg, Robert P. Faust,
and H. Milton Holt

NOVEMBER 1980

CASE FILE COPY

NASA

Viking '75 Spacecraft Design and Test Summary

Volume I - Lander Design

Neil A. Holmberg, Robert P. Faust,
and H. Milton Holt
Langley Research Center
Hampton, Virginia

PREFACE

This publication, in three volumes, discusses the design of the Viking lander and orbiter as well as the engineering test program developed to achieve confidence that the design was adequate to survive the expected mission environments and to accomplish the mission objective. Volume I includes a summary of the Viking Mission and the design of the Viking lander. Volume II consists of the design of the Viking orbiter and Volume III comprises the engineering test program for the lander and the orbiter.

The material contained in this report was assembled from documentation produced by the Martin Marietta Corporation (now Martin Marietta Aerospace) and the Jet Propulsion Laboratory during the Viking spacecraft design and test program. Viking Project personnel contributing to the preparation of this publication and their area of contribution are as follows:

Lander science design and test . . . . Joseph C. Moorman

Lander guidance and control design and test . . . . . Anthony Fontana

Lander propulsion design and test . . . . Anthony Fontana

Lander thermal design and test . . . . T. W. Edmund Hankinson

Viking orbiter detailed design information:
   Command and sequencing . . . . Carl R. Pearson
   Computer command subsystem . . . . Carl R. Pearson
   Flight data subsystem . . . . Carl R. Pearson
   Data storage subsystem . . . . Carl R. Pearson
   Visual imaging subsystem . . . . Carl R. Pearson
   Infrared thermal mapper subsystem . . . . Carl R. Pearson
   Mars atmospheric water detector subsystem . . . . . Carl R. Pearson
   Temperature control . . . . William A. Carmines
   Structure subsystem . . . . William A. Carmines
   Pyrotechnic subsystem . . . . William A. Carmines
   Cabling subsystem . . . . William A. Carmines
   Propulsion subsystem . . . . William A. Carmines
   Mechanical devices subsystem . . . . William A. Carmines

Test data and information . . . . William A. Carmines

CONTENTS

INTRODUCTION

The Viking Project was initiated in 1968 and was climaxed with the launching of two Viking spacecraft in 1975. The first landing on Mars was July 20, 1976, and the second landing was September 3, 1976. Each spacecraft contained an orbiter and a lander. The objective of the Viking Mission was to increase significantly man's knowledge of the planet Mars through orbital observations by the orbiter as well as by direct measurements made by the lander during Martian atmospheric entry, descent, and landing. Particular emphasis was placed on obtaining biological, chemical, and environmental data relevant to the existence of life on the planet at the present time, at some time in the past, or the possibility of life existing at a future date. Orbiter observations consisted of radio-science, imaging, thermal, and water-vapor measurements used to assist landing-site selection and the study of the dynamic and physical characteristics of Mars and its atmosphere. Lander direct measurements consisted of radio science; atmospheric structure and composition; landing-site imaging; atmospheric pressure, temperature, and wind velocity; identification of the elemental composition of the surface material; physical properties of the surface material; the search for evidence of living organisms and organic materials; and determination of seismological characteristics of the planet. The Viking scientific return was further expanded by the capability of simultaneous Martian observations from orbit and the surface.

This document, divided into three volumes, summarizes the design of the Viking lander and orbiter as well as the engineering test program developed to achieve confidence that the design was adequate to survive the expected mission environments and accomplish the mission objective. The engineering test program covered those aspects of testing prior to delivery of the Viking landers and orbiters to the John F. Kennedy Space Center. Most of the material contained in this document was taken from documentation prepared by Martin Marietta Corporation (now Martin Marietta Aerospace) and the Jet Propulsion Laboratory during the Viking spacecraft design and test program. This volume contains a summary of the Viking Mission and a detailed description of the Viking lander design. All abbreviations and symbols used in this volume are defined in an appendix.

Use of trade names in this report does not constitute an official endorsement of such products or manufacturers, either expressed or implied, by the National Aeronautics and Space Administration.

VIKING MISSION SUMMARY

MISSION CONSTRAINTS

The Viking spacecraft like all other NASA planetary spacecraft met the internationally established planetary quarantine requirement. The internationally accepted criterion for planetary quarantine is that there be only 1 chance

in 1000 (0.001 probability) of contamination by terrestrial organisms during the 50-year period beginning January 1, 1969. Because other spacecraft may be exploring Mars during the 50-year period, the Viking sterilization requirements were more stringent: less than 1 chance in 10 000 (0.0001 probability).

In order to avoid Earth organic contamination from invalidating Martian sample analysis, the lander surface sample and organic analysis instruments were cleaned and maintained such that surface samples would contain less than 1 ppm of terrestrial organic material.

MISSION PHASES

The five phases of the Viking mission, which are described in this section, were launch; cruise; orbital; separation, entry, and landing; and landed.

Launch phase: Two Viking spacecraft were launched on a Titan-IIIE/Centaur launch vehicle which first placed the spacecraft in a 165-km (90 n. mi.) orbit and then injected the spacecraft on a heliocentric trajectory which intercepted Mars almost a year later. (See fig. 1.)
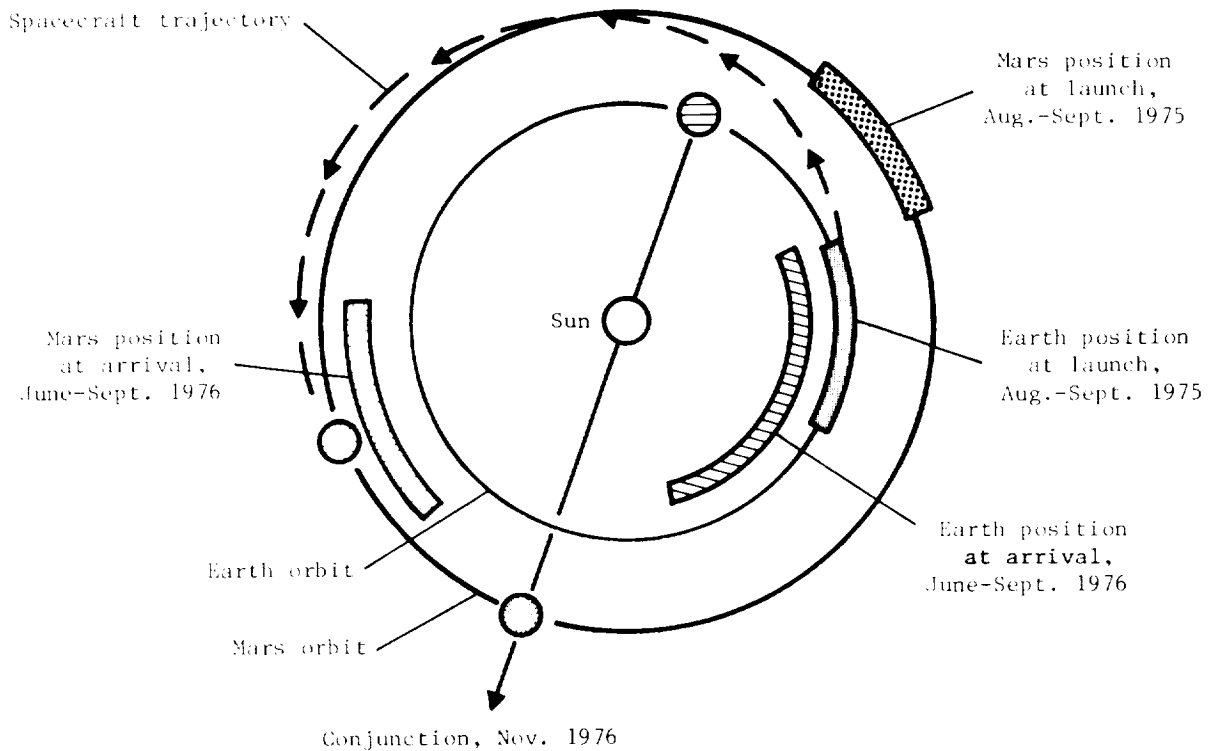

Figure 1.- Relative positions of Earth and Mars.

Cruise phase: During the cruise to Mars, the orbiter provided all space-craft power, communications, velocity control, and navigation. The lander

activity consisted of functional tests to assess postlaunch environmental effects and to perform tape-recorder conditioning and battery conditioning.

Orbital phase: After the orbiter placed the spacecraft into Martian orbit, observations were made to identify potential landing sites for the lander. Lander functional performance was verified and the orbit determined such that lander separation time could be calculated. After lander separation, the orbiter continued Martian scientific observations and also supported lander data (4000 or 16 000 bps), stored the data on a digital tape recorder, and retransmitted the data to Earth. (See fig. 2.)

Orbiter-to-Earth two-way radio link
Orbiter science data
Lander relay data
Engineering telemetry
Doppler and range signals
Commands

Earth

Orbiter

Lander-to-orbiter one-way relay radio link
Lander science data
Engineering telemetry

Lander-to-Earth two-way radio link
Lander science data
Engineering telemetry
Doppler and range signals
Commands
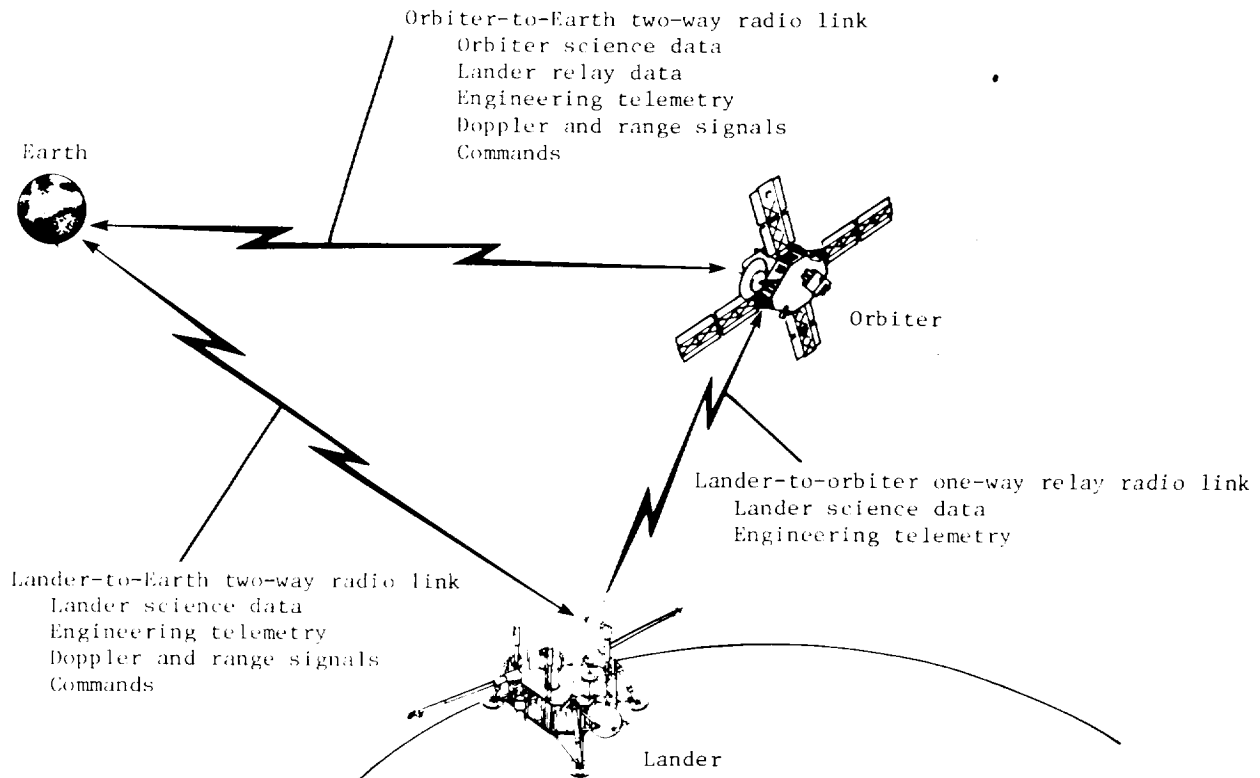
Lander

Figure 2.- Radio links between Earth and orbiter and lander.

Separation, entry, and landing phase: At the selected orbital point, the lander separated from the orbiter, and the lander deorbit engines were fired. (See fig. 3.) The lander coasted a minimum of 2.25 hr until atmospheric forces on the aeroshell initiated deceleration. (See fig. 4.) At an altitude of approximately 6 km (19 500 ft), a parachute was deployed, the aeroshell cap separated from the lander, and the landing legs were deployed; at an altitude of approximately 1.4 km (4600 ft), the terminal descent engines ignited, the parachute was released, and the total velocity was reduced to the landing velocity of 2.4 m/sec (8 ft/sec).

3
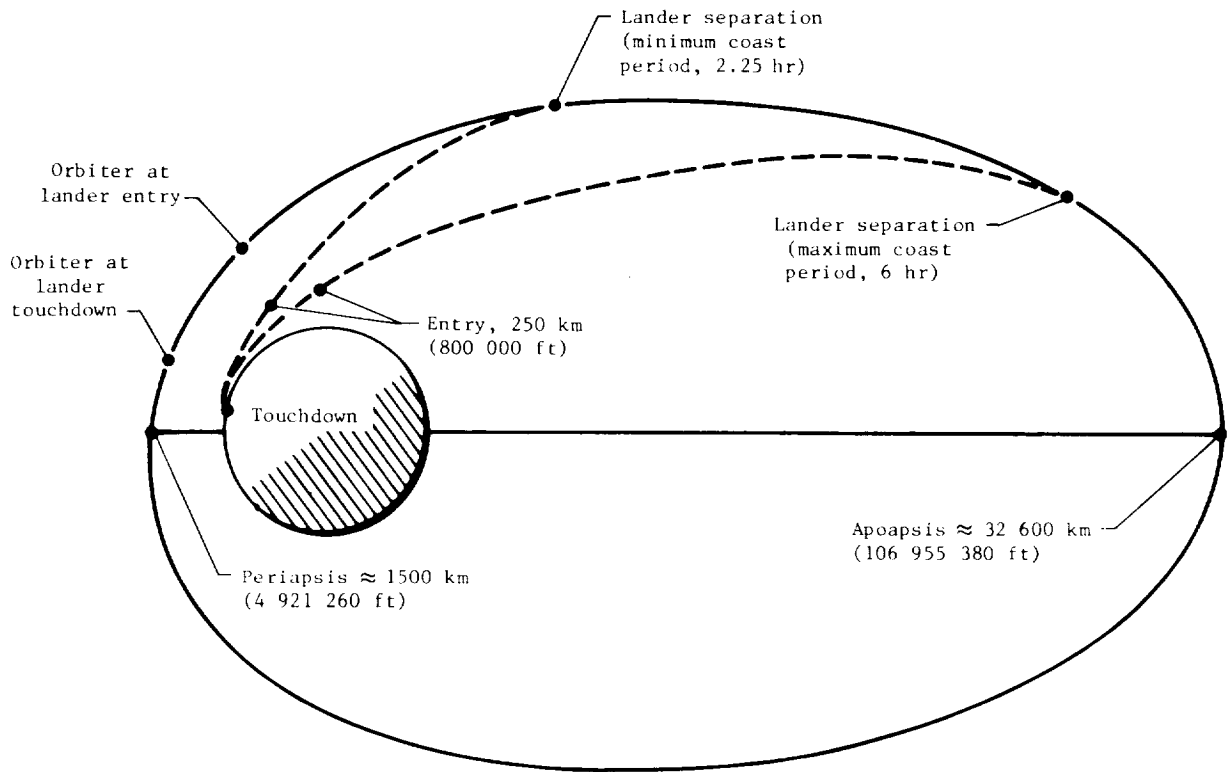
Figure 3.- Orbital phase.
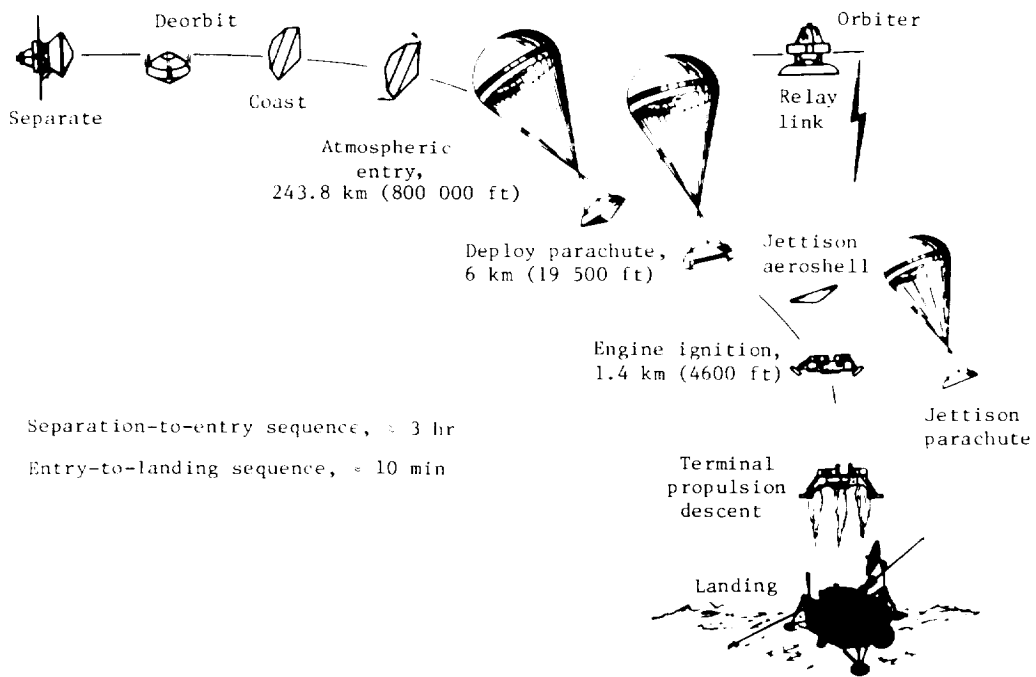
Figure 4.- Lander deorbit, coast, entry, and landing sequence.

Landed phase: The landers operated from a preprogrammed mission which was modified as planned after landing by commanding through the direct link. Data were returned by a UHF relay link via the orbiter as well as by a direct link to Earth. (See fig. 2.)

MISSION ENVIRONMENTS

Typical mission-phase environments are summarized in table 1. The natural and spacecraft induced environments formed a basis for mechanical and thermal designs as well as the test environments used for design qualification and workmanship testing. Transportation and other Earth environments such as humidity were not a basis for spacecraft design as the philosophy was to design shipping containers and system test equipment to control ambient environmental conditions.

TABLE 1.- TYPICAL MISSION-PHASE ENVIRONMENTS

(a) Lander prelaunch terminal sterilization environment

Maximum temperature, ^{O}C (^{O}F) 131 (326)
Humidity at 0° C, percent . . . . <2.5
Gas composition . . . . N_2 + <2.5% O_2
Duration . . . . As required to insure <0.001 probability of contaminating Mars with terrestrial biological organisms

(b) Spacecraft launch induced environment

Maximum sustained acceleration, Earth g units 4
Random vibration:
  rms overall, Earth g units 3.2
  20 to 450 Hz, dB/octave 3
  450 to 1000 Hz, g^2/Hz 0.008
  1000 to 2000 Hz, dB/octave 6
  Duration, sec 60
Maximum acoustics, dB 137
Pressure decay rate, mm Hg/sec (in. Hg/sec) . . . . <36 (<1.42)

(c) Lander entry, terminal descent, and landing induced environments

Entry:
  Sustained acceleration, Earth g units . . . . -13.6
  Peak transient vibration, Earth g units 7.2
  Peak aerodynamic noise, dB 126
Terminal descent and landing:
  Sustained acceleration, Earth g units . . . . -1.0
  rms overall transient vibration, Earth g units 4.1
  Peak aerodynamic noise, dB 122
  Landing velocity:
    Vertical, m/sec (ft/sec) . . . . 2.4 ± 1 (8 ± 3)
    Horizontal, m/sec (ft/sec) . . . . 0 ± 1 (0 ± 3)

(d) Mars surface (landed) environment

Surface atmospheric pressure, mbars (1 bar = 10^5 Pa) . . . . 4 to 7.5
Surface temperature, K . . . . 155 to 275
Maximum wind velocity, m/sec 90
Acceleration of gravity, m/sec^2 . . . . 3.7

DESIGN AND TEST MANAGEMENT APPROACH

As shown in figure 5, the Viking Program, which is part of the NASA Planetary Exploration Program, was managed by NASA Headquarters at the Program Level and by the Langley Research Center at the Project Level. The Viking Project was divided into six basic "systems": lander, orbiter, launch and flight operations, launch vehicle, tracking and data, and the mission control and computing center. Each of the six system managers reported to the Project Manager who integrated the systems into one project. The Project Manager was assisted by the Martin Marietta Corporation (now Martin Marietta Aerospace) in its role as integration contractor and the Re-entry and Environmental Systems Division, General Electric Company, which provided support in the areas of mission analysis and design, reliability and quality assurance, data and configuration management, and project administration functions.

System Definitions

The Viking lander system was defined as VLC, VLC AGE, software, simulators, and special facilities required for VLC fabrication, sterilization, and testing. The VLC consisted of structures and mechanisms, thermal, propulsion, pyrotechnic, communications, telemetry, power, guidance and control, entry-science, and landed-science subsystems.

The Viking orbiter system was defined as the Viking orbiter, the spacecraft adapter, VLC adapter, VO AGE, software, and all special facilities required for fabrication and testing. The Viking orbiter consisted of structure, power, propulsion, stabilization and control, communication, and science subsystems.

The launch and flight operations system was defined as the equipment, software, personnel, and procedures required to plan, design, and conduct spacecraft preflight readiness evaluation, prelaunch and launch operations, and the flight control necessary for the accomplishment of mission objectives.

The launch vehicle system was defined as the Titan IIIE/Centaur, nose fairing, launch vehicle mission-peculiar equipment, LVS AGE, LVS facilities, and the personnel required to accomplish the LVS functions.

The tracking and data system was defined as a selected collection of Earth-based equipment, software, personnel, and procedures required to transmit commands, to acquire, relay, and process science and engineering data, and to generate, transmit, and process radiometric data.

The mission control and computing center system was defined as a selected collection of Earth-based facilities, equipment, software, personnel, and procedures required to prepare and transmit commands, to acquire, process and display metric, science, and engineering data and to furnish the data in an organized format to project personnel for analysis.
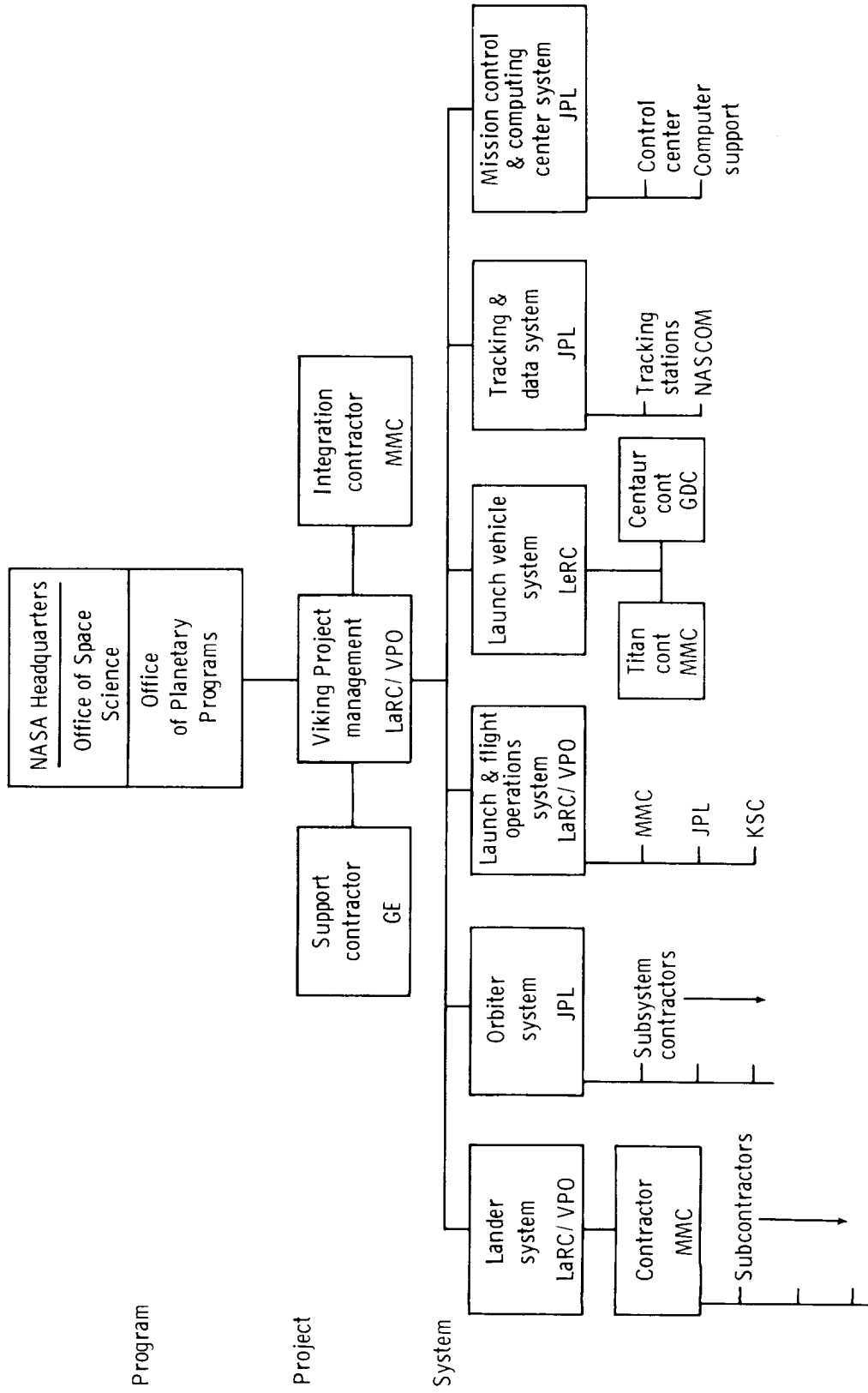
6

Figure 5.- Viking Project organization.

7

System Interface Management

The Viking Project management recognized the need for strict integration and control of system interfaces and instituted system IRD's and appropriate change control procedures to insure project-wide visibility and coordination of any system changes which affected interfaces.

A Management Council consisting of the Project Manager as chairman, the System Managers, and key project staff members was established to provide a mechanism for management personnel to meet regularly to discuss Viking problems and to mutually plan and review the conduct of the Viking Project.

Steering groups consisting of senior Viking personnel were established to provide guidance and direction in the disciplines of science, engineering, mission analysis and design; launch and flight operations; and mission planning. (See fig. 6.) Steering groups were responsible for identifying major problems in their discipline and assigning the development of solutions to the working groups reporting to them, for reviewing actions and recommendations of their working groups, and for resolving issues the groups were unable to resolve. Working groups were composed of personnel of three or more Viking system organizations which were directly affected by a subsystem or activity which crossed system interfaces.

Design and Test Reviews

Design and test reviews for both the lander and the orbiter were held to verify compatibility with system, subsystem, and component design requirements. Preliminary design reviews evaluated design concepts prior to the building of development hardware. Critical design reviews evaluated development test results and proposed modifications prior to the building of flight hardware.

Problem Management

When critical problems within a system were recognized, the Project Manager assigned the problem to the Viking Project top ten problem list, approved the selection of the person responsible for the solution of the problem, and approved the resulting plan and schedule for resolution of the problem. The problem status was reported weekly in the Project Manager's Staff Meeting until he concurred that the problem had been resolved.

Schedules

Performance evaluation and review technique (PERT) was used to identify and resolve schedule conflicts at the system levels as well as within a system. Gantt project planning charts were used to provide top management visibility. A typical master schedule employing a Gantt chart is shown as figure 7.
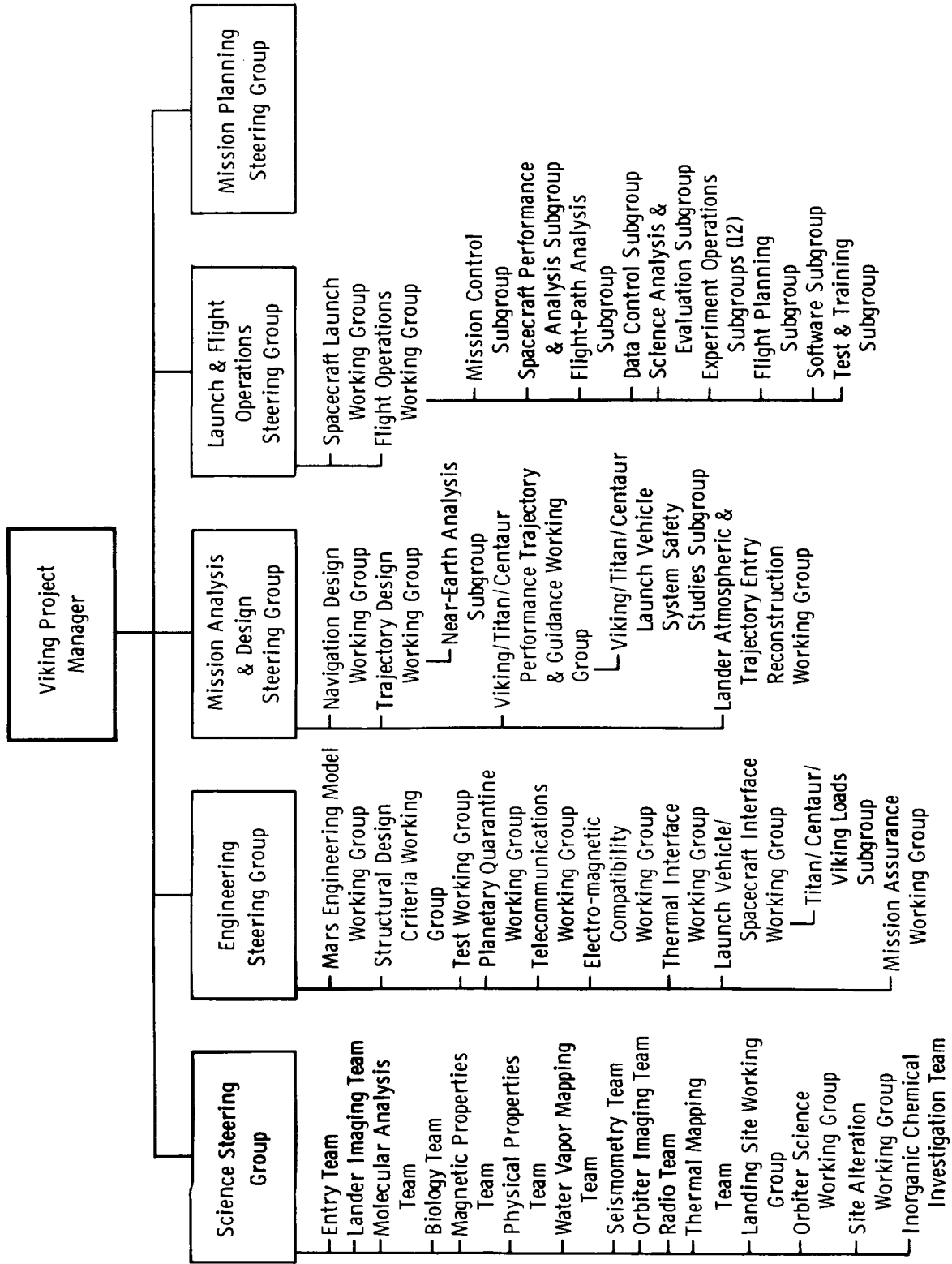
Viking Project Manager

- **Science Steering Group**
  - Entry Team
  - Lander Imaging Team
  - Molecular Analysis Team
  - Biology Team
  - Magnetic Properties Team
  - Physical Properties Team
  - Water Vapor Mapping Team
  - Seismometry Team
  - Orbiter Imaging Team
  - Radio Team
  - Thermal Mapping Team
  - Landing Site Working Group
  - Orbiter Science Working Group
  - Site Alteration Working Group
  - Inorganic Chemical Investigation Team

- **Engineering Steering Group**
  - Mars Engineering Model Working Group
  - Structural Design Criteria Working Group
  - Test Working Group
  - Planetary Quarantine Working Group
  - Telecommunications Working Group
  - Electro-magnetic Compatibility Working Group
  - Thermal Interface Working Group
  - Launch Vehicle/Spacecraft Interface Working Group
    - Titan/Centaur/Viking Loads Subgroup
  - Mission Assurance Working Group

- **Mission Analysis & Design Steering Group**
  - Navigation Design Working Group
  - Trajectory Design Working Group
    - Near-Earth Analysis Subgroup
  - Viking/Titan/Centaur Performance Trajectory & Guidance Working Group
    - Viking/Titan/Centaur Launch Vehicle System Safety Studies Subgroup
  - Lander Atmospheric & Trajectory Entry Reconstruction Working Group

- **Launch & Flight Operations Steering Group**
  - Spacecraft Launch Working Group
  - Flight Operations Working Group
    - Mission Control Subgroup
    - Spacecraft Performance & Analysis Subgroup
    - Flight-Path Analysis Subgroup
    - Data Control Subgroup
    - Science Analysis & Evaluation Subgroup
    - Experiment Operations Subgroups (12)
    - Flight Planning Subgroup
    - Software Subgroup
    - Test & Training Subgroup

- **Mission Planning Steering Group**
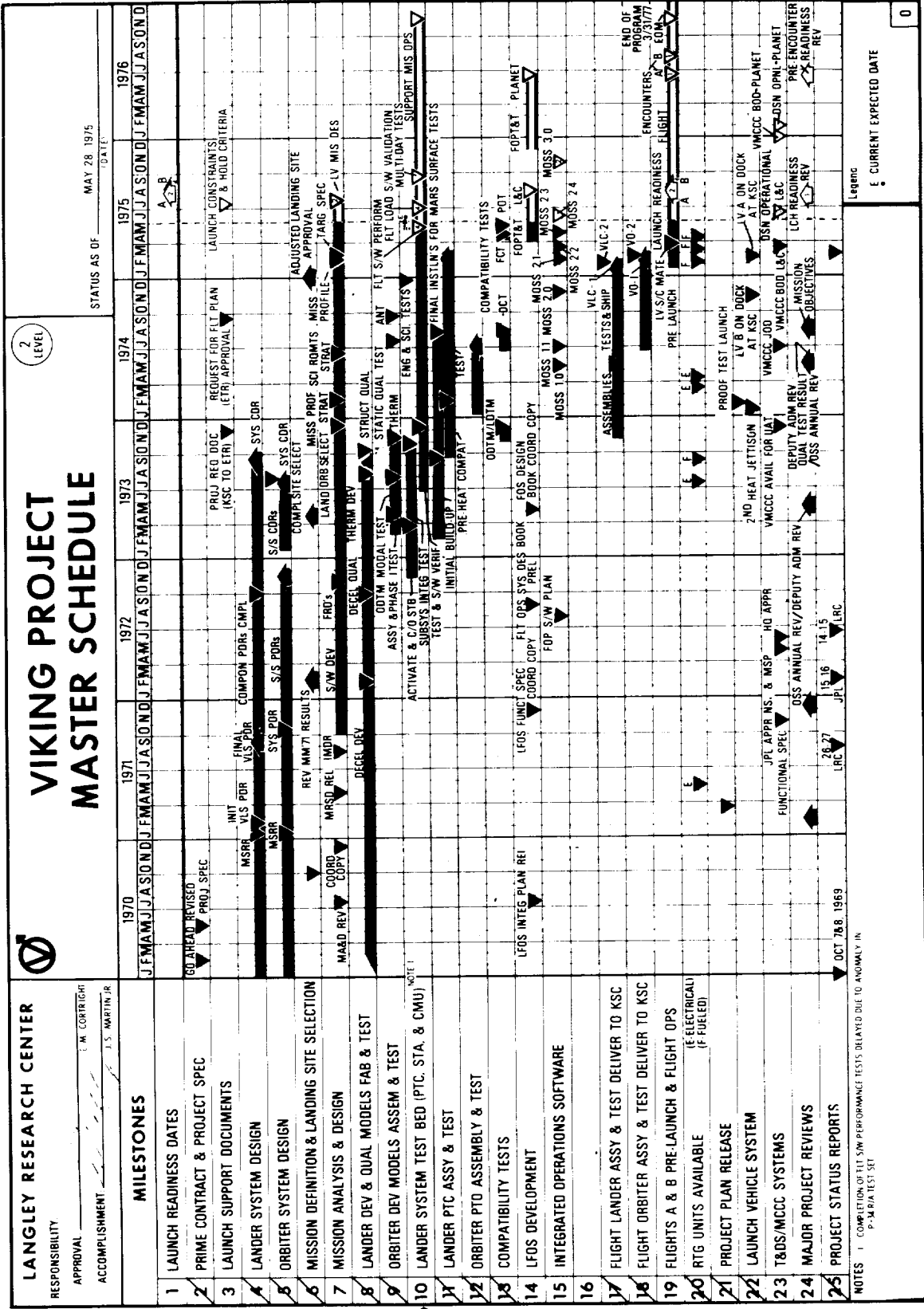
Figure 6.- Working groups.

9

Figure 7.- Master schedule.

VIKING LANDER DESIGN

FUNCTIONS AND REQUIREMENTS

The VLC, shown in the exploded view of figure 8, was designed to separate from the VO once the spacecraft was in orbit around Mars and to descend to a soft landing on the surface of the planet. The VLC was also designed to be heat sterilized to meet the criterion, which had been recommended by COSPAR, that the probability of contaminating the planet with terrestial organisms during the period of biological exploration would be less than 0.001. During the descent of the VL to the surface of the planet, the automated spacecraft was controlled by an on-board computer with attitude and acceleration data supplied by an inertial reference unit, altitude data supplied by a radar altimeter, and velocity data from a four-beam Doppler radar. Also during this phase of the mission, entry-science instruments took measurements of composition, pressure, temperature, and density variations of the Martian atmosphere. Once on the surface, the VL was controlled by the same computer utilized during descent and landing while two cameras photographed the Martian landscape and other instruments collected data about surface characteristics, atmospheric characteristics, meteorologic activity, and physical structure of the planet. Biological and organic analysis of surface samples tested for existence of life as microorganisms in the surface material. Data from the VL during descent were relayed to Earth by the VO and also recorded on the VO for later playback. Most of these data were also recorded on board the lander for playback after landing. After landing, data were relayed to the VO where the data were recorded for subsequent playback to Earth. A direct communication link to Earth from the VL was also provided for commanding and as a backup to the relay link for data return to Earth. A functional block diagram of the VLC is given in figure 9. Each subsystem and its major functional requirements are given in the following sections. More detail on each subsystem design is given in later sections of this report.
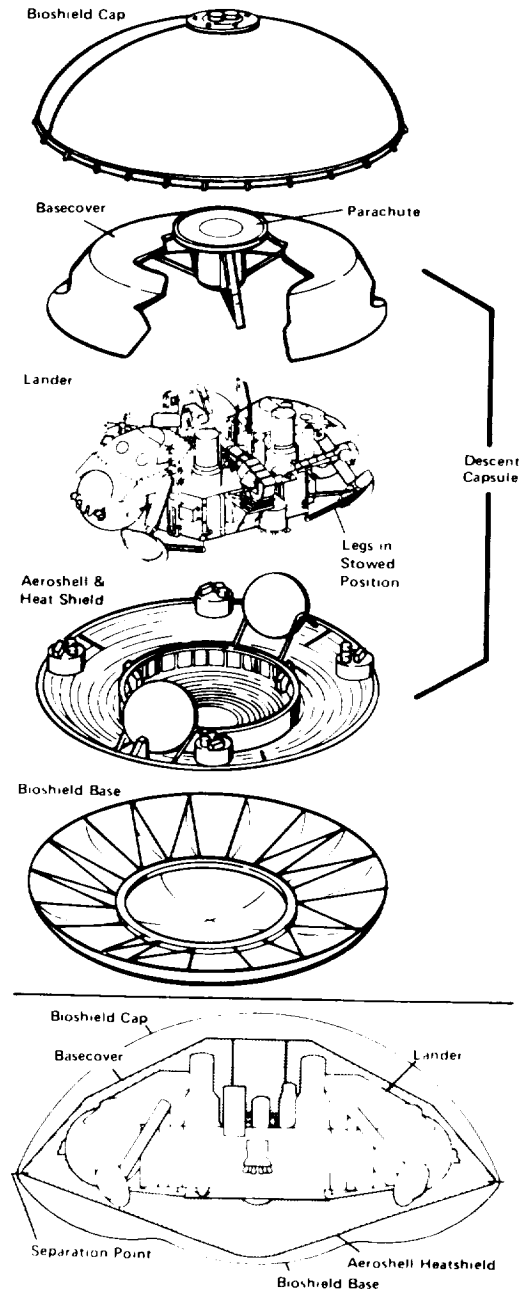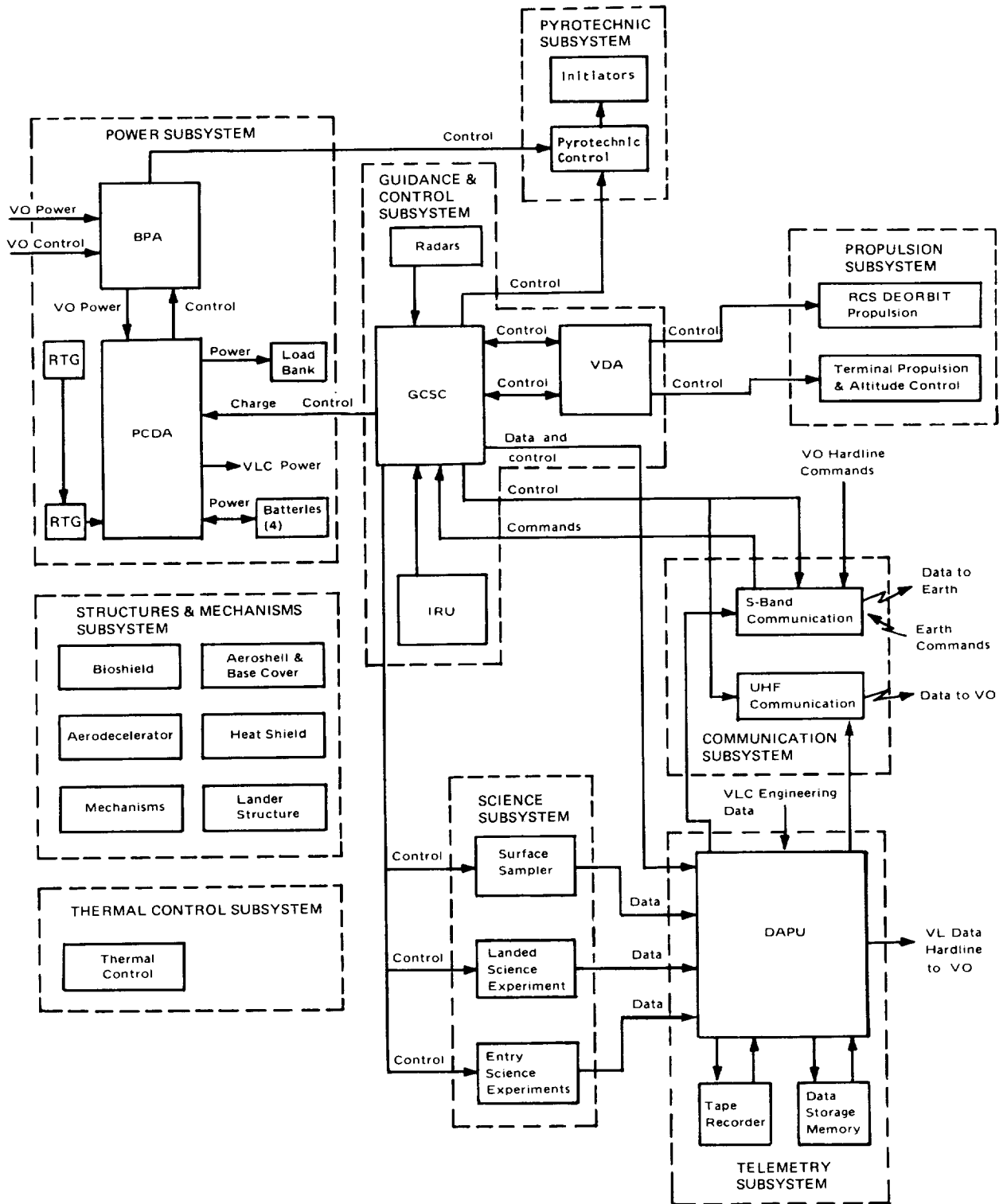
Figure 8.- Viking lander capsule.

11

Figure 9.- Functional block diagram of VLC.

Structures and Mechanisms Subsystem

The structures and mechanisms subsystem consisted of the bioshield, aerodecelerator made up of an aeroshell and parachute, the lander body structure, landing legs, deployment mechanism for the high-gain antenna, and venting assembly. The bioshield prevented recontamination of the sterilized VLC with Earth organisms by completely encapsulating it during and after sterilization. The aerodecelerator provided aerodynamic deceleration and lifting entry into the Martian atmosphere with the aeroshell and provided deceleration and stabilization with a disc-gap-band parachute. The three landing legs provided a stable landing on the surface with energy absorption to minimize landing shock. The deployment mechanism for the high-gain antenna provided structural support for the high-gain antenna in the stowed position during flight and landing. After landing, the mechanism was deployed and it supported the HGA in the deployed position. The venting assembly maintained the pressure differential between the inside and outside of the VLC at a safe level during launch and entry into the Mars atmosphere.

Thermal Control Subsystem

The thermal control subsystem provided an acceptable temperature environment for all components and structures with the use of both passive and active techniques. Passive thermal control was accomplished through selective component location and selection of materials that had the desired surface optical properties. Optimization of equipment location and material selection was used to achieve the required thermal balance. Wind covers were used to prevent excessive cooling by isolating the RTG's from Mars surface winds and to prevent overheating in the cruise vacuum environment by allowing adequate heat loss through radiation. Thermal insulations were used to control heat flow between equipment and the environment. Active thermal control techniques included electrical heaters and variable thermal resistance devices (thermal switches). Cycling of the RCS thrusters during orbit coast provided a source of heat for temperature-sensitive valves.

Communications Subsystem

The communications subsystem shown in the simplified block diagram of figure 10 included the UHF RCE and the S-band DCS. The RCE was used to transmit data to the orbiter for subsequent transmission to Earth. The DCS was a quasi-redundant subsystem used for direct transmission of data to Earth by using the transponders, TWTA's, circulator switch, diplexer, and HGA. The DCS was fully redundant when used for receiving commands transmitted from Earth by using the transponders, command detectors/decoders, diplexer, LGA, and HGA. In addition, the communications subsystem with its ranging capability was used to support radio science experiments.
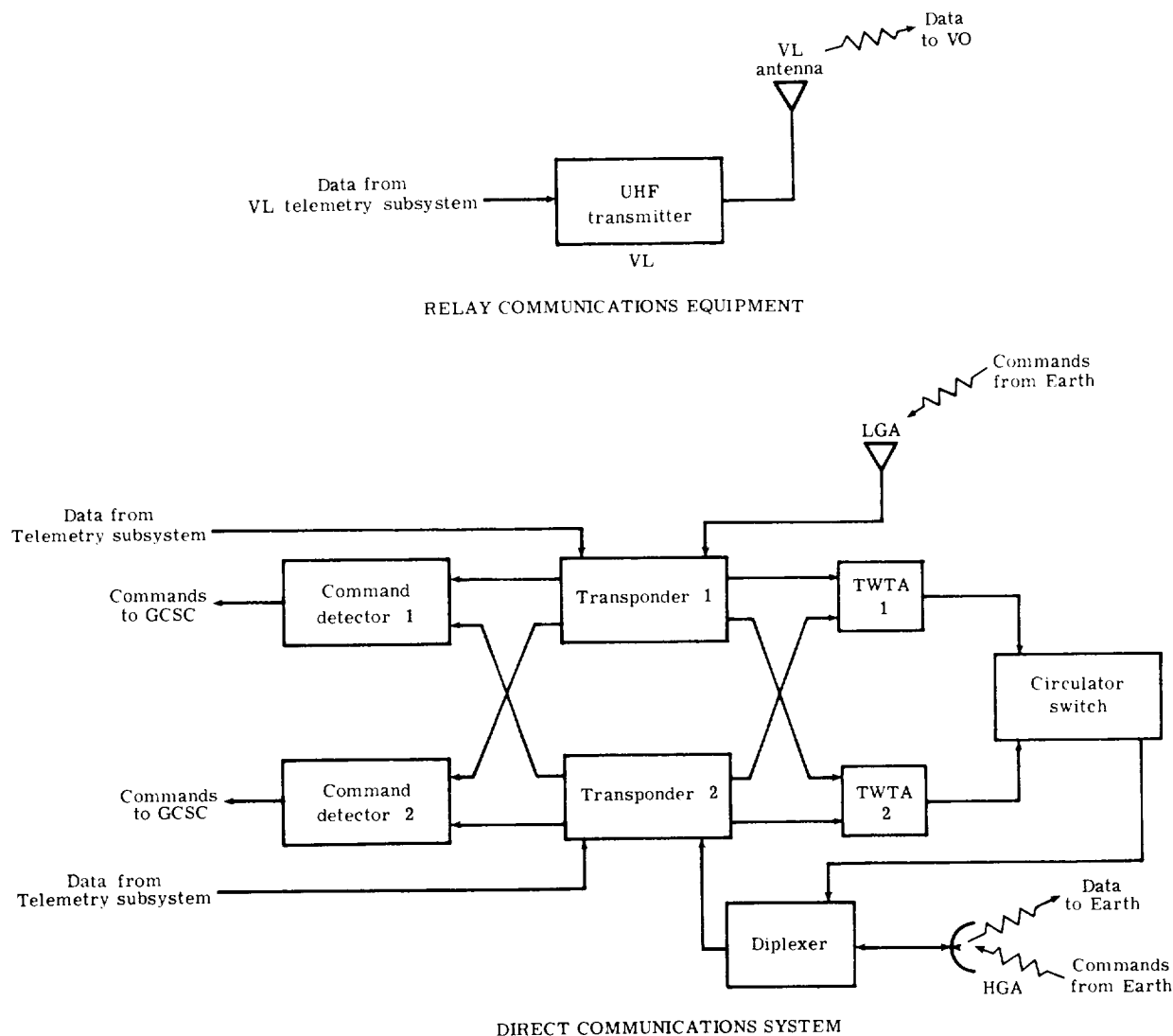
Figure 10.- Block diagram of communications subsystem.

Guidance and Control Subsystem

The guidance and control subsystem, shown in the block diagram of figure 11, embodied the GCSC, IRU, RA, TDLR, VDA, and flight software. The GCSC was a block-redundant random-access, stored-program, general-purpose digital computer. It interfaced with other lander subsystems and utilized the flight software to perform guidance, steering, and control of the lander from separation to landing; command processing and sequencing for all mission phases; and computation of lander orientation and S-band antenna pointing after landing. The IRU was a strap-down sensor system with gyros and accelerometers on each of the three principal axes that provided inputs to a software-controlled navigator. A redundant fourth gyro was skewed equally with respect to the principal axes, and a fourth redundant accelerometer was in the critical X-axis. The two
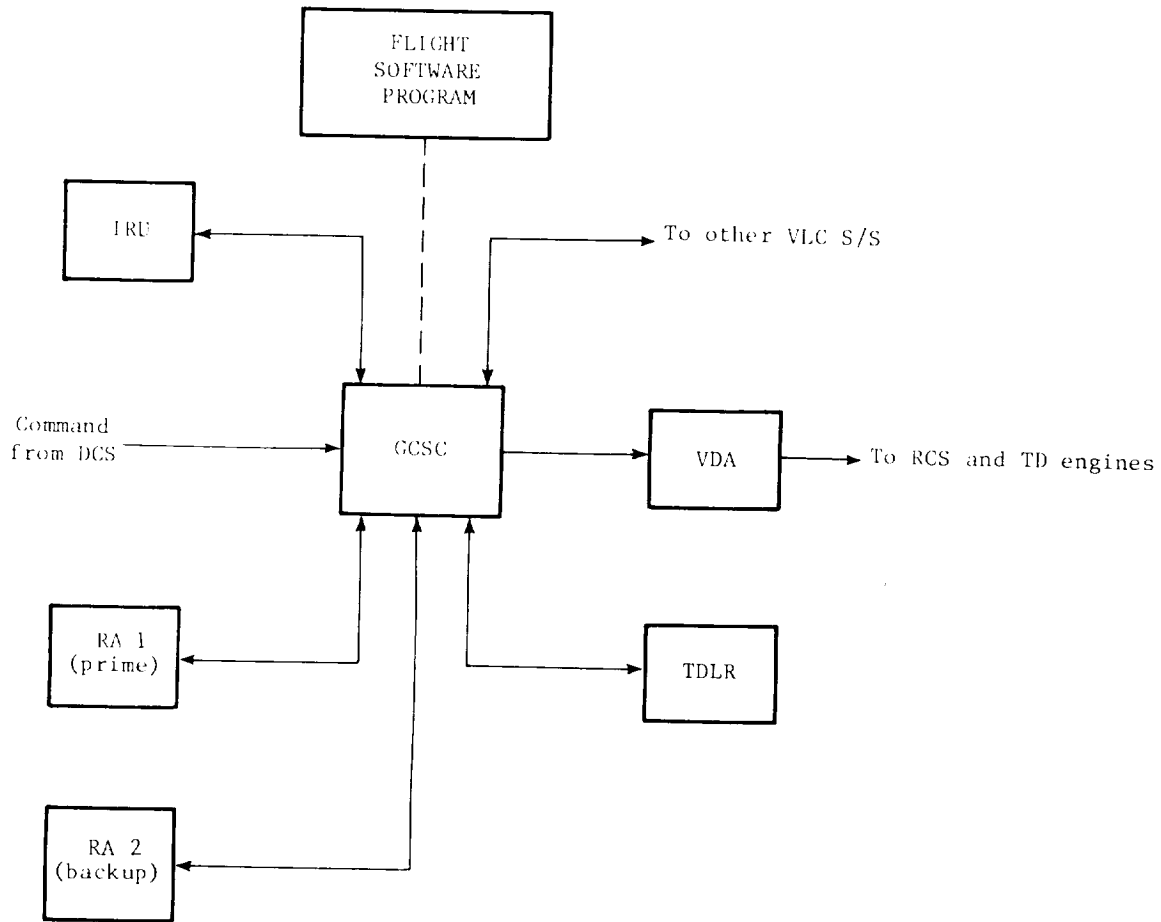
14

Figure 11.- Block diagram of guidance and control subsystem. IRU, VDA, TDLR, and GCSC have internal redundancy.

redundant radar altimeters provided altitude data to the software-controlled inertial navigator from entry to near touchdown. The TDLR was composed of four independent Doppler radars integrated into one unit. The four measured beam velocities relative to the surface of the planet were converted to the lander principal axes by software and used to update the inertial navigator during terminal descent. The VDA decoded and implemented GCSC commands for the reaction control engines, the terminal descent engines, and the terminal roll thrusters. The flight software contained the necessary routines to perform the guidance, control, command, and sequencing functions.

Power Subsystem

The power subsystem, shown in the bock diagram of figure 12, was composed of the BPA, the PCDA, batteries, RTG, and load banks. The BPA conditioned and distributed VO input power to the lander for cruise operations. The PCDA provided switching for various electrical loads, conditioned RTG power for dis-
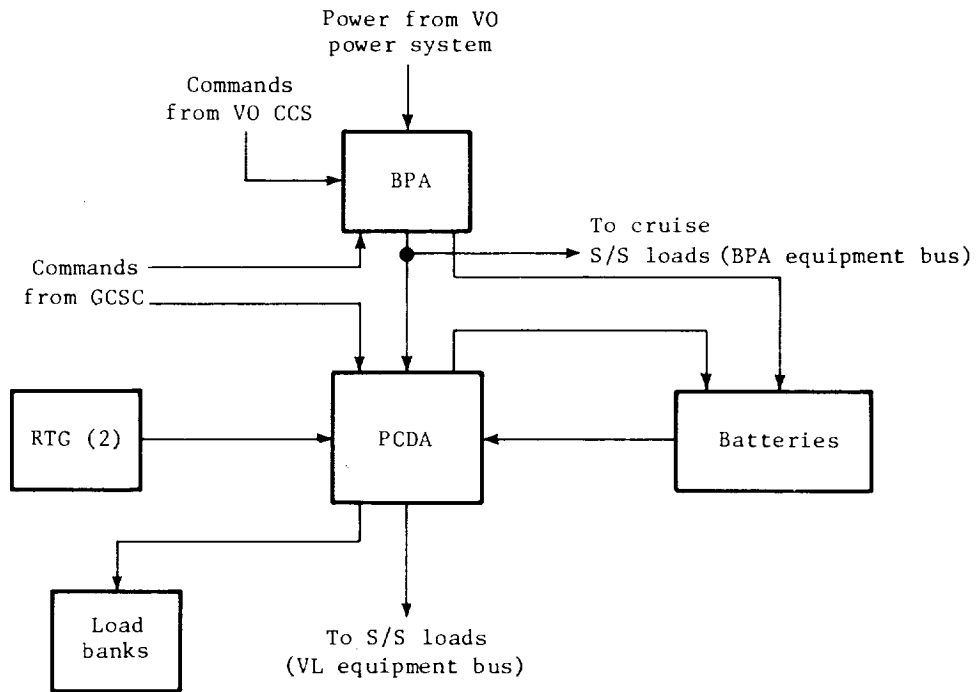
Figure 12.- Block diagram of power subsystem.

tribution to lander loads or battery charging, provided sensors for detecting several unsafe operating conditions on the lander, and provided the control for making the lander safe if any of these unsafe conditions exist. Two RTG's were provided as the source of power for the lander. Four nickel-cadmium batteries were used for energy storage to meet electrical demands when the peak RTG output was exceeded. Load banks were provided for discharging the batteries and as a load for shunt regulators used by the PCDA for regulating the VL bus voltage.

Propulsion Subsystem

The monopropellant propulsion subsystem consisted of the RCS and the TDS. The RCS shown in the flow diagram of figure 13 consisted of four three-engine clusters and two fuel tanks to provide impulse energy for deorbit and attitude control through entry. The TDS represented by the flow diagram of figure 14 contained three throttleable engines, four roll engines, and two fuel tanks for controlling velocity and attitude during terminal descent.

Pyrotechnics Subsystem

The pyrotechnics subsystem, shown in the block diagram of figure 15, was made up of redundant LPCA's, pyrotechnic devices, and pyromechanical devices. The LPCA controlled all pyrotechnic functions on the lander by responding to
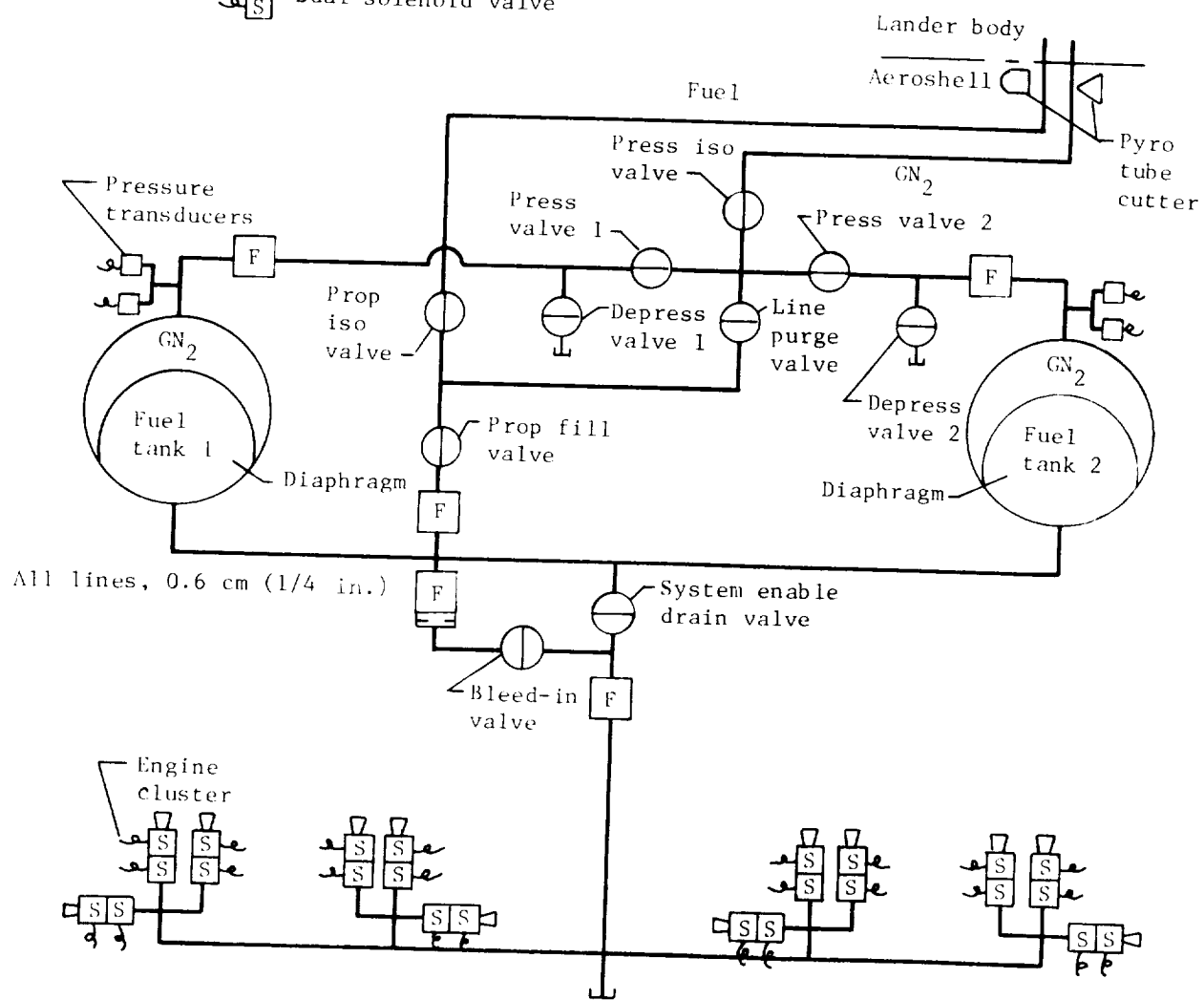
16

Figure 13.— Flow diagram of RCS.
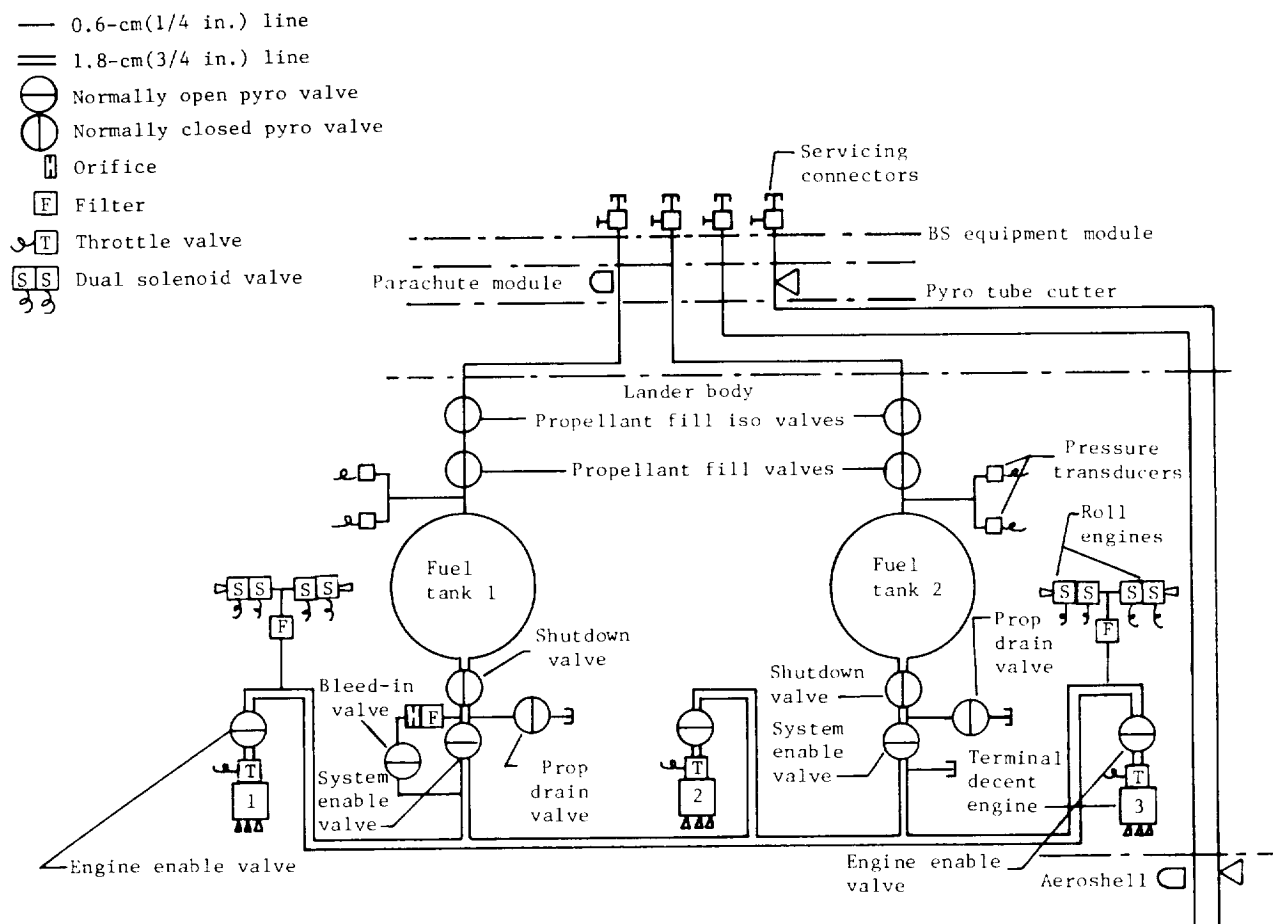
Figure 14.- Flow diagram of terminal propulsion system.
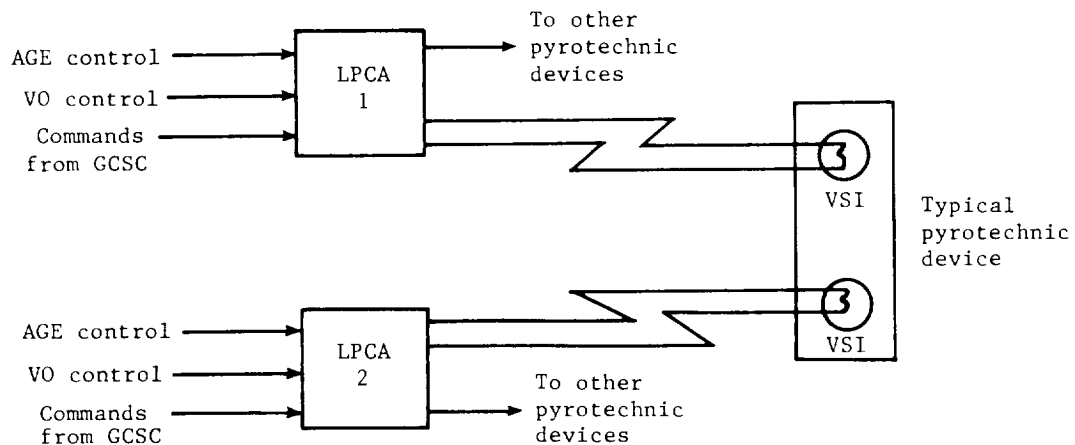
Figure 15.- Block diagram of pyrotechnics subsystem.

commands from the AGE, the VO, or the GCSC. The Viking standard initiator was used with all devices to perform the necessary pyrotechnic functions on the lander.

Telemetry and Data Handling Subsystem

The telemetry and data handling subsystem, shown in the block diagram of figure 16, was composed of the DAPU, the DSM, and the TR. The DAPU acquired, processed, modulated, and controlled storage of all VLC data during the mission. The DSM utilized a plated-wire memory for storing approximately 200 000 bits of data and the tape recorder can store 10^7 bits of data on each of four tracks of metal tape.
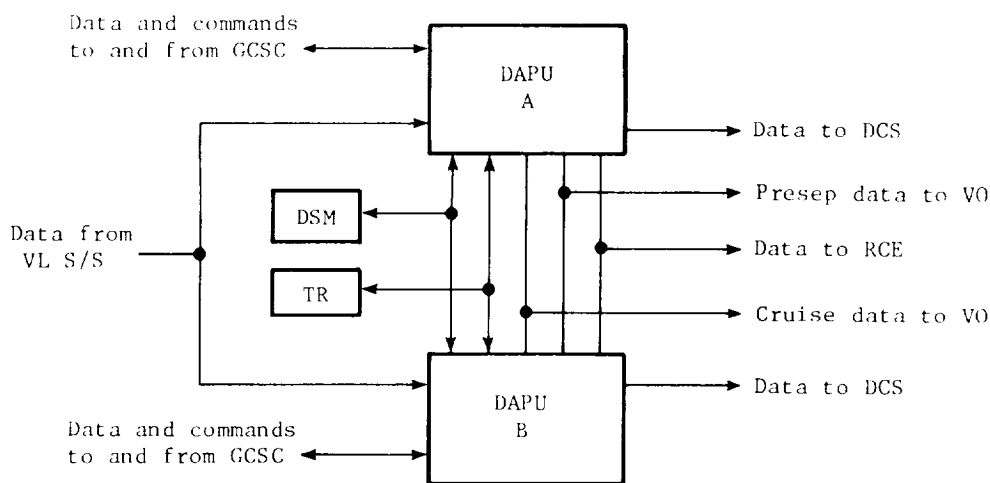
Figure 16.- Block diagram of telemetry and data handling subsystem.

Science Subsystem

The science subsystem included the instruments used for the entry- and landed-science investigations.

Entry Science

The overall objective of the entry-science investigations was to define the present physical and chemical state of the Martian atmosphere and its inter- action with the solar wind. In the upper atmosphere, the composition and abun- dance of neutral species were determined by the UAMS. The ion concentration and ion and electron energy distributions were determined by the RPA. In the lower atmosphere, pressure, temperature, density, and mean molecular weight were determined by pressure and temperature measurements together with data from the VL guidance system.

Landed Science

The primary emphasis of the Viking Mission was on gathering information on biological, chemical, and environmental characteristics most relevant to the search for extraterrestrial life - either past, present, or potential for the future. In addition, investigations of the interior, surface, and meteorology of Mars were carried out. The landed-science instruments and their major scientific objectives are discussed here but a more detailed discussion of the design is given in later sections of this report.

Biology: The biology instrument contains GEX, LR, and PR experiments. These three experiments analyze Martian surface samples for life that may exist as microorganisms on Mars.

Gas chromatograph and mass spectrometer: The GCMS contained an LPA, a GCA, an MSA, an IEA, a HSA, and an AFA. The GCMS was used to analyze the Martian atmosphere and to analyze surface material for organic constituents that may corroborate the biological results.

Lander camera system: The lander camera system utilized two facsimile-type cameras to take pictures of the scene around the lander. The cameras provided color, black and white, infrared, and stereoscopic photographs. Imaging data were used primarily to characterize the site and determine its geologic setting. Images also enhanced data from some experiments and were necessary for the success of other experiments.

Meteorology: The meteorology instrument contained three hot-film anemometers for measuring wind speed and direction, four thermocouples mounted to a heated post for removing wind-direction ambiguities and a three-thermocouple array for measuring temperature. This instrument in conjunction with the ambient pressure sensor used during entry characterized the meteorological conditions in the vicinity of the lander.

Seismometer: The seismometer contained three moving mass-coil assemblies in three mutually perpendicular axes. The instrument was coupled to the surface through the lander body and legs to measure seismic activity of the planet.

Surface sampler assembly: The surface sampler assembly includes the SSAA, GCMS, biology PDA's, and the SSCA. The surface sampler acquired surface samples for distribution to the GCMS and biology and X-ray fluorescence instruments and supported the physical and magnetic properties investigations.

X-ray fluorescence spectrometer: The XRFS contained two radioisotope sources that irradiate surface material introduced into the instrument. Four thin window proportional counters detected fluorescent X-rays emitted by the irradiated samples and the data were used to determine chemical characteristics of the surface material.

Magnetic properties: The magnetic properties experiment utilized magnets located on the surface sampler boom and the lander body. These magnets attracted magnetic materials that may have been suspended in the atmosphere or may have been in the surface material that came in contact with the magnets.

20

SUBSYSTEM DESIGN

The design of each VLC subsystem is described in detail in this section. The purpose of each component of a subsystem, the function of the component within the VLC, operating modes of each component, and a general description of each are given.

Structures and Mechanisms Subsystem

The detailed design of the bioshield, aerodecelerator, the lander body structure, landing legs, high-gain antenna deployment mechanism, and the venting assembly is discussed.

Bioshield

The bioshield prevented recontamination of the sterilized VLC with Earth organisms by completely encapsulating it during and after sterilization. The bioshield, shown in figure 17, was composed of three major subassemblies: the equipment module, the bioshield cap, and the bioshield base.
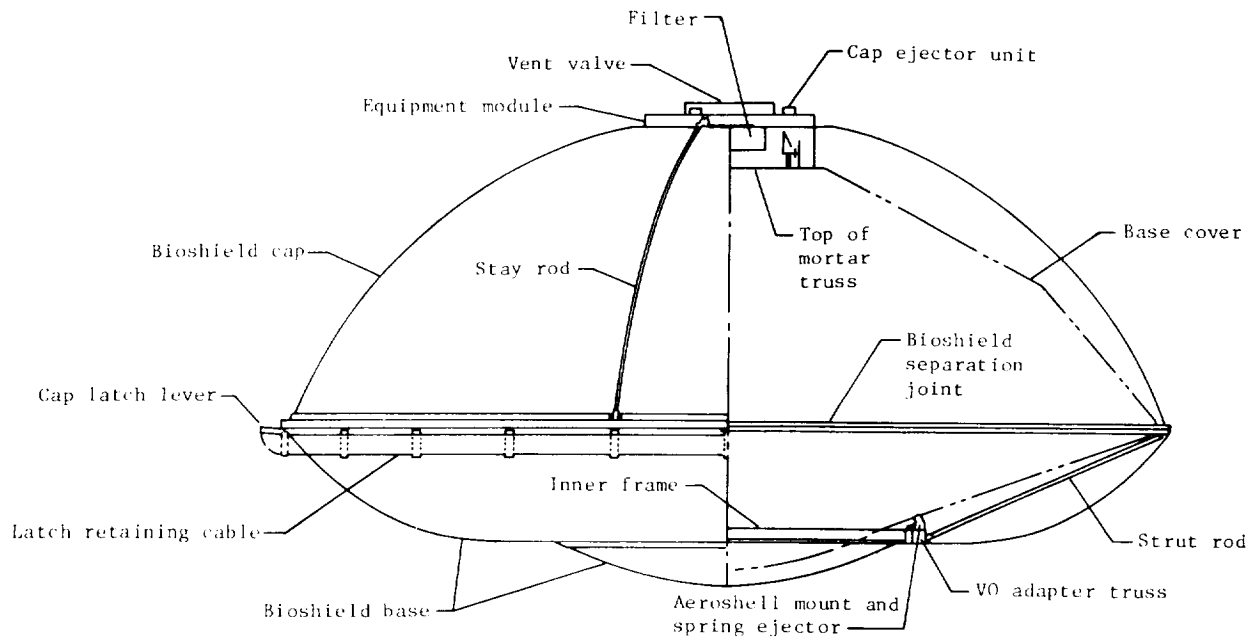
Figure 17.- Bioshield assembly.

Equipment module: The equipment module, shown in figure 18, supported the bioshield cap at the forward end of the VLC and provided a bulkhead through which passed various electrical and instrumentation harnesses and pressurization and propellant lines. The equipment module also contained the bioshield vent
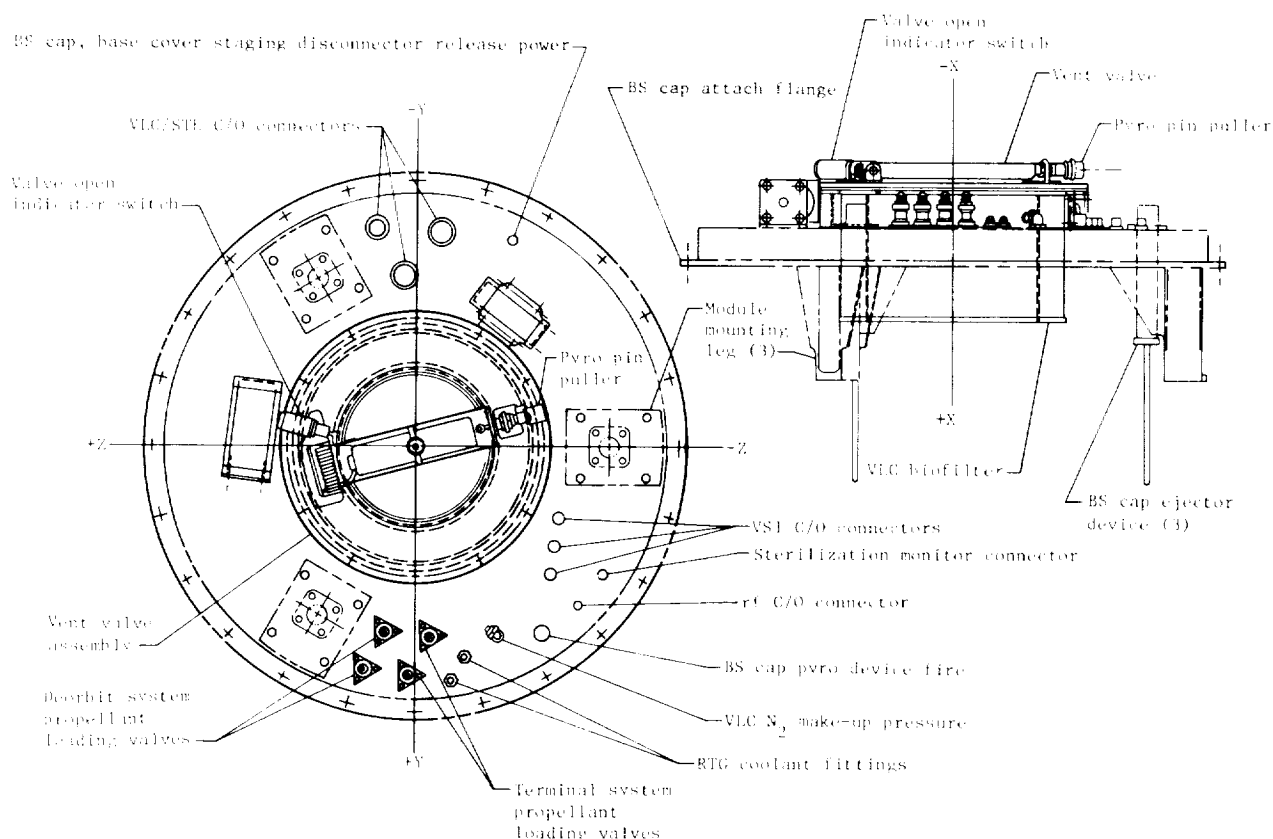
Figure 18.- Equipment module assembly.

valve and biofilter. The vent valve was opened at launch from Earth to permit the pressurized bioshield to vent to zero to prevent bursting of the assembly. The bioshield maintained internal pressure throughout sterilization and subsequent ground operations. When the VLC was launched, the bioshield vent valve was opened to permit the bioshield to vent to atmospheric pressure. The bioshield maintained a pressure of 1244 Pa (5.0 in. H_2O) above ambient pressure until approximately 0.5 sec before launch. A biofilter prevented any contamination of the bioshield interior during periods when the positive differential pressure was not maintained. The equipment module contained three ejector devices that provided the forces for separation of the bioshield cap and equipment module assembly when the cruise portion of the mission was attained.

Bioshield cap: The bioshield cap, covering the upper portion of the VLC and interfacing with the equipment module and the bioshield base, was a fabric assembly supported by stays of aluminum tubes when unpressurized. Its function was that of a pressure vessel that was pressurized at terminal sterilization and remained pressurized until launch. The bioshield cap interfaced with the bioshield base to form the rest of the pressure vessel. The cap contained the

cable and latch assemblies that provided a means for sealing the base and cap. The latches were held in the closed position by steel cable assemblies that were tightened by means of turnbuckles. At separation, a pyrotechnic-actuated cable cutter cut the cable at three locations to permit the latches to rotate and free the cap from the base. The equipment module was attached to the base cover and mortar support truss by three bolts threaded into three pyrotechnic-actuated separation nuts. Upon actuation, the nuts released the equipment module and the three spring-loaded ejector devices propelled the equipment module and bioshield cap assemblies away from the VLC.

Bioshield base: The bioshield base, covering the lower portion of the VLC and interfacing with the aeroshell, the bioshield cap, and the VO adapter truss, was a fabric assembly supported by stays of aluminum tubes similar to the bioshield cap. Its function was that of a pressure vessel, the same as the bioshield cap. The bioshield base contained a structural ring that provided a load-carrying path between the VO adapter truss and the VLC. The ring also had provisions for electrical and instrumentation harnesses, gas-supply connections, and orbiter-to-lander umbilical power. The thermal insulation blanket attached to the bioshield base was installed after mating with the VO adapter truss.

Aerodecelerator

The aerodecelerator system provided lifting entry into the Mars atmosphere; deployed the parachute (by pyrotechnically energized mortar) upon command from the VLC systems (e.g., RA mark based on terrain); used the parachute to reduce the VLC relative velocity (no wind) to the range of 31 to 94 m/sec (100 to 300 ft/sec) and reduced the relative flight-path angle to 20° or less from the local vertical before the VLC descended below a predetermined altitude; utilized differential drag between the parachute-VLC combination and the aeroshell to separate the aeroshell from the VLC by at least 15 m (50 ft) in 3 sec; and used the parachute drag force after aeroshell release to carry the parachute mortar, support truss, and the base cover away from the VLC after terminal descent engine ignition. After entry into the Mars atmosphere, the aerodecelerator system decelerated and stabilized the VLC until terminal propulsion ignition. After use, the aerodecelerator system separated from the VLC body structures. The aerodecelerator system, shown in figure 19, consisted of an aeroshell, a base cover, a disc-gap-band parachute, a parachute mortar with associated pyrotechnics, and a mortar support truss.

Aeroshell: The aeroshell conical shape provided the aerodynamic configuration of a lifting body to permit entry into the Mars atmosphere. Entry heat was dissipated by an ablative coating on the aeroshell exterior surface. The aeroshell interfaced with the VL at the three main support fittings and with the base cover at the periphery of both assemblies. Multiple leaf-spring seals around the periphery of the aeroshell sealed the gap between the assemblies from potential ablative products during entry. The aeroshell provided mounting provisions for the UAMS, the RPA, the stagnation-temperature sensor, and the stagnation-pressure sensor. Four pressure ports were mounted on the Y- and
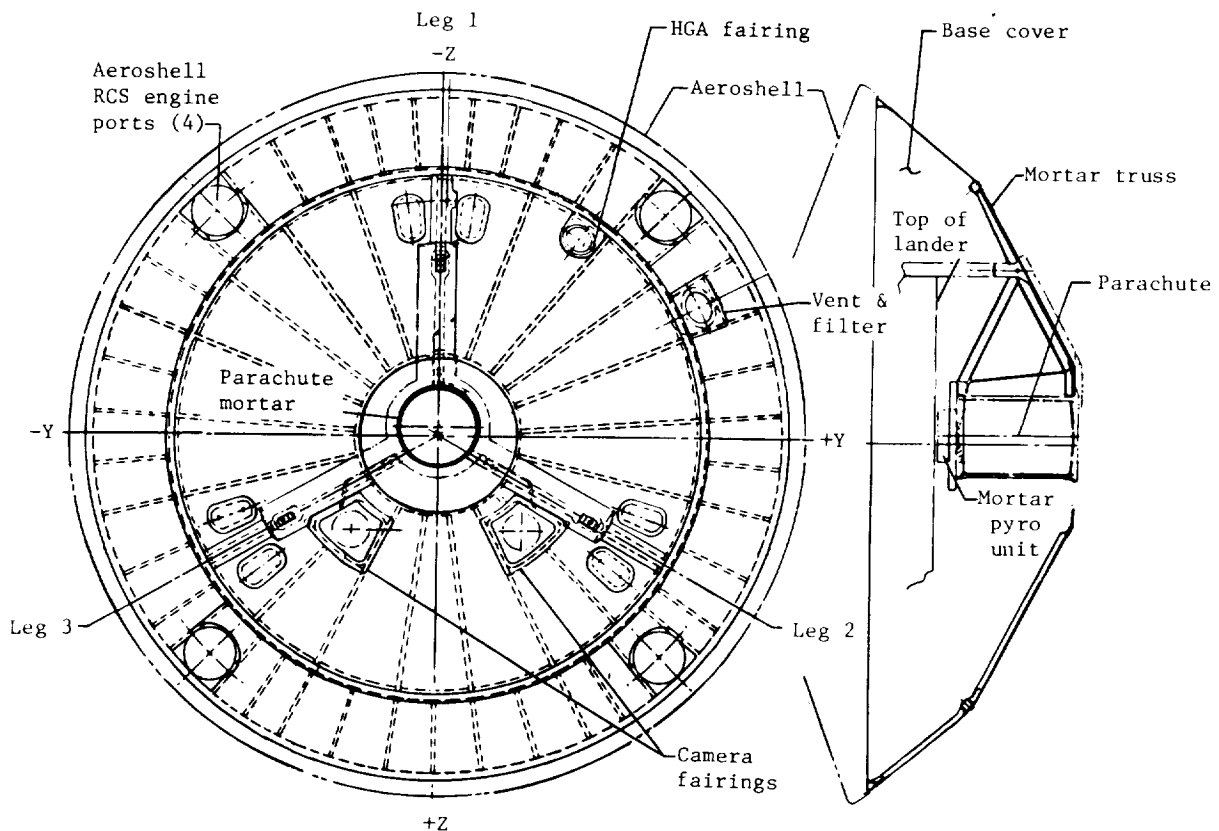
Figure 19.- Aerodecelerator system.

Z-axes of the aeroshell. The transducers for these ports were on the payload adapter frame. The aeroshell also provided a mounting structure for the RA antenna. Mounted on the aeroshell structure and projecting through the base cover in the assembled entry configuration were four deorbit engine assemblies. The two propellant tanks for these engines were also mounted in the aeroshell.

Base cover: The base cover provided protection from entry heat for the upper portion of the VL body. It interfaced with the VL body through the mortar support structure. The base cover was attached to the mortar truss for structural support. The mortar truss was attached to the main support fittings of the VL body.

Parachute and mortar: At approximately 6096 to 7620 m (20 000 to 25 000 ft) above the Mars terrain, the mortar was initiated to deploy the parachute and bridle. The parachute and bridle interfaced with the VL at the mortar truss. Loads were transferred directly to the VL through the main support fittings.

Mortar support truss: The separation nuts that attached the aeroshell to the VL were fired 7 sec after parachute deployment; this left the VL and base cover suspended from the parachute. The landing legs were then deployed by firing three pin pullers. At an altitude of approximately 1400 m (4600 ft), the

24

terminal engines were started and 2 sec later the separation nuts retaining the parachute, base cover, and mortar truss to the VL were fired. The VL then completed the landing phase of the mission controlled by the terminal propulsion system.

Lander Body Structure

The VL body structure shown in figure 20 provided structural integrity for all mission phases and mounting provisions for all equipment required to soft-land on the Mars surface. All power, communication, terminal propulsion, and science components for the Mars Mission (postlanded phase) were contained in and on the VL body. The VL was constructed primarily of machined aluminum and titanum and was configured and sized to provide minimum weight and optimum instrument placement. Cabling, propellant tanks, plumbing, and insulation were
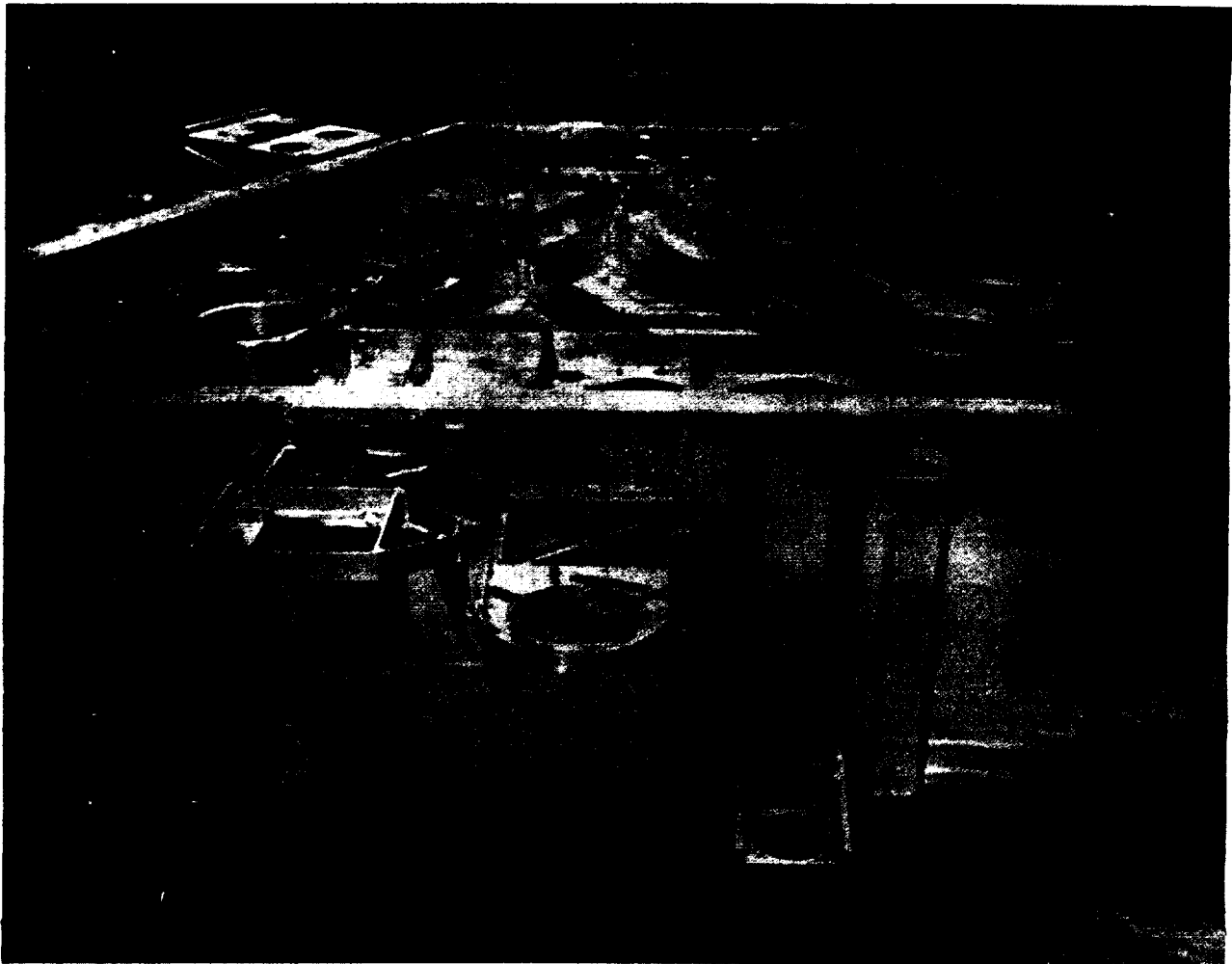
Figure 20.- Lander body.

protected by sand- and dust-resisting materials. The VL and most externally mounted components were painted with a thermal paint containing silicone that provided resistance to sand and dust abrasion. The RTG's were mounted directly on the VL primary structure and heat generated by the RTG's was conducted through a thermal switch directly under the RTG's to the interior of the VL when the lander temperature decreased to less than 3.3° C (38° F). Fins on the RTG's dissipated any remaining thermal energy. Figure 21 shows the location of the components on the equipment plate. The equipment plate was constructed of aluminum and was supported by nine titanium fittings that were attached to the VL body sides and the equipment plate. Titanium provided thermal transfer protection so that little conduction took place between the VL exterior and the equipment plate which was the support for the majority of the VL components. The bottom cover of the VL had a filtered vent for pressure
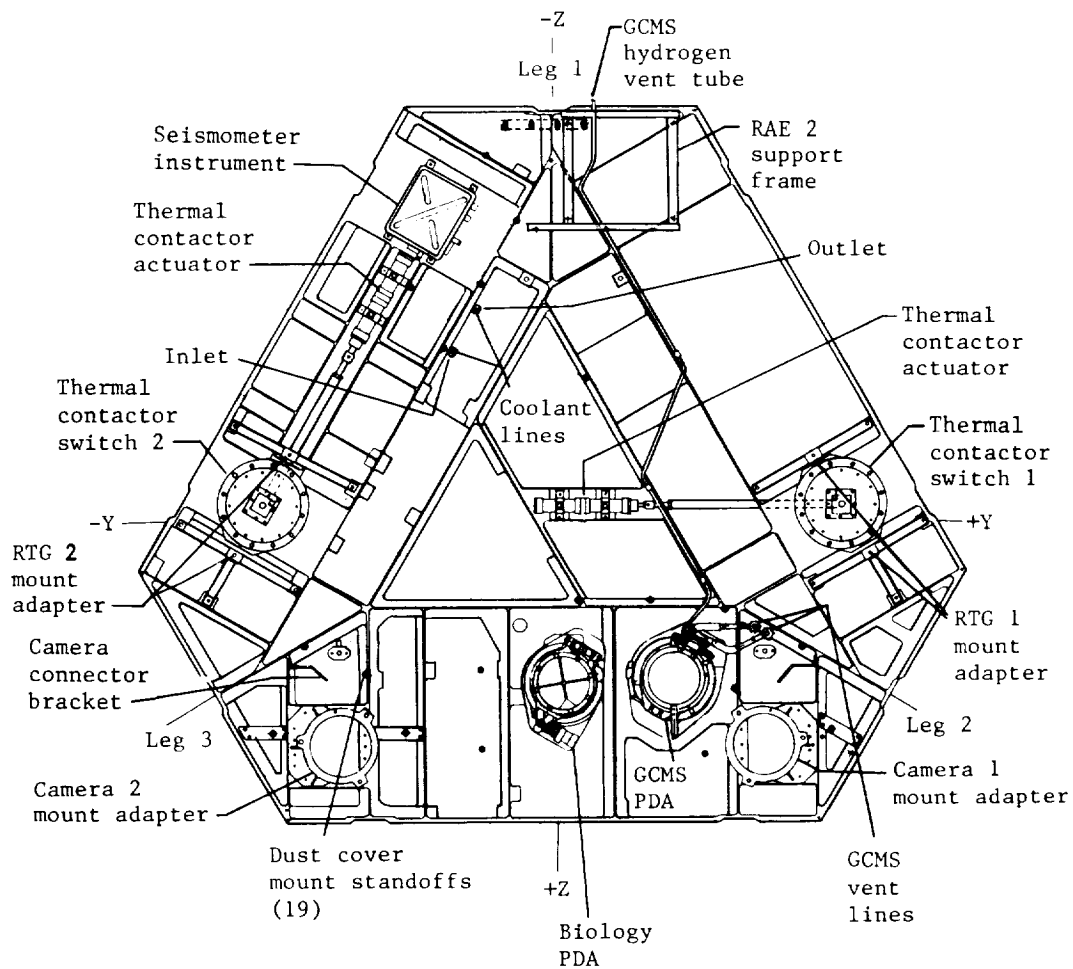
(a) Top view.

Figure 21.- Component arrangement of lander equipment plate.
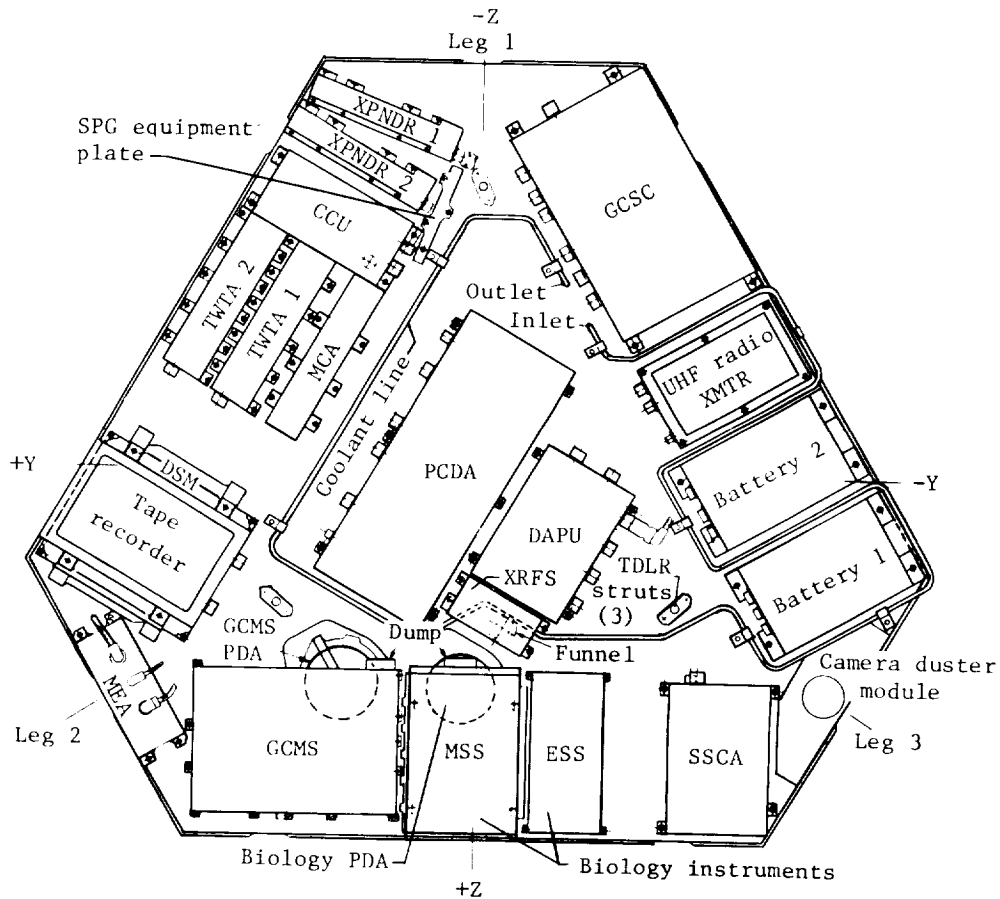
(b) Bottom view.

Figure 21.- Concluded.

stabilization. Electrical bonding was accomplished by metal contact in most instances. The equipment not installed on the equipment plate was as follows:

S-band low-gain antenna on top of the main support fitting at leg 3

UHF antenna on the side between legs 1 and 3

Surface sample acquisition assembly and collector head on side between legs 2 and 3

Meteorology boom and sensors on VL side at leg 2

Three terminal descent engines on each of the three VL sides

Two VL pyrotechnic control assemblies, one on the side at leg 1 and the other on the side between legs 1 and 3

One valve drive amplifier on the side between legs 1 and 2

Two radar altimeter electronic assemblies, one on the side between legs 1 and 3 and the other on top of VL at leg 1

One inertial reference unit on the side at leg 1

Two terminal propulsion tanks, one on the side between legs 1 and 2 and the other on the side between legs 1 and 3

One high-gain antenna on the side between legs 1 and 2

VL radar altimeter antenna on the bottom of VL between legs 1 and 2

Terminal descent and landing radar antenna on bottom of VL

Landing Legs

The VL had three legs that were designed for the following purposes: to actuate the TESS at first leg contact, to provide a stable (upright) landing on the Mars surface, to provide for energy absorption that minimized the landing shock loads on the VL, and to support the VL during its operational life on Mars in a manner that satisfied the transmissibility requirements imposed by the seismometer and the stiffness requirements imposed by the lander cameras and the high-gain antenna assembly. The landing legs shown in figure 22 included a main strut assembly and an A-frame assembly which included the foot pad for each leg. The upper end of the main strut interfaced with a fitting on the VL and was attached with a shear pin. The inboard ends of the A-frame were attached through load limiters to the VL body. The load limiters were designed to bend plastically when the limiting load was applied; thus, the VL body and its equipment were protected. Both ends of the main strut and the inboard ends of the A-frame were connected with ball joints to provide universal motion. The foot pad was rigidly attached to the A-frame. Bonded crushable aluminum honeycomb was used in the strut for load attenuation at landing. The legs were restrained in the stowed position by pyrotechnic pin pullers and were independent of the aeroshell and base cover. After aeroshell separation, a signal from the GCSC activated the pin pullers to release the legs. A spring extended the strut and latches locked the legs in the extended position. The landing leg assemblies also provided mounting and actuation for the TESS, main strut stroke gages which could be viewed by the camera, and an installation site for the parachute phase temperature transducer on foot pad 2.
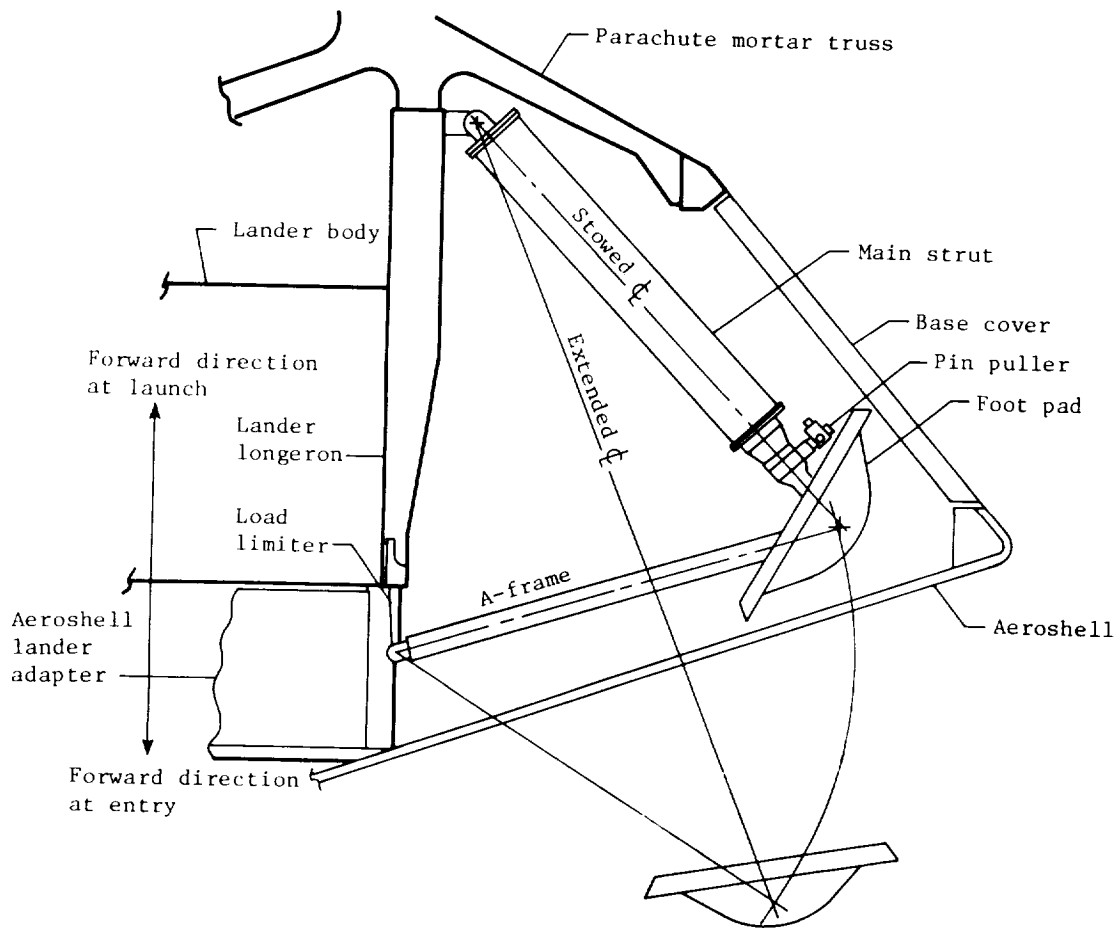
Figure 22.- Viking lander leg.

High-Gain Antenna Deployment Mechanism

The HGADM (fig. 23) provided structural support for the HGA in the stowed position during flight and landing. After landing it released, deployed, locked in place, and supported the HGA in the deployed position. The fixed portion of the HGADM mast interfaced with the VL body and was aligned with the VL axes through tooled alignment pins. The pins were installed in the VL and protruded through the HGADM mast base. The rotating portion of the mast interfaced with

the antenna. Rotational forces about the hinge line applied to the assembly rotated the antenna to its deployed position after the pyroactuated pin puller in the down-lock bracket was released. The down-lock bracket supported and restrained the HGA during flight and landing. Upon GCSC command, the pin puller was actuated and the down lock rotated away from the HGADM and deployment took place. A governor in the HGADA regulated the deployment motion to limit acceleration and shock on the antenna assembly. When deployed, the HGADM was locked in a manner that prevented any motion of the HGADM and supported the antenna within specified angular tolerances and the required rigidity. The antenna location and deployment mechanism were designed to provide the maximum clearance to the Mars surface upon landing.

FOLDED CONFIGURATION   ERECTED CONFIGURATION
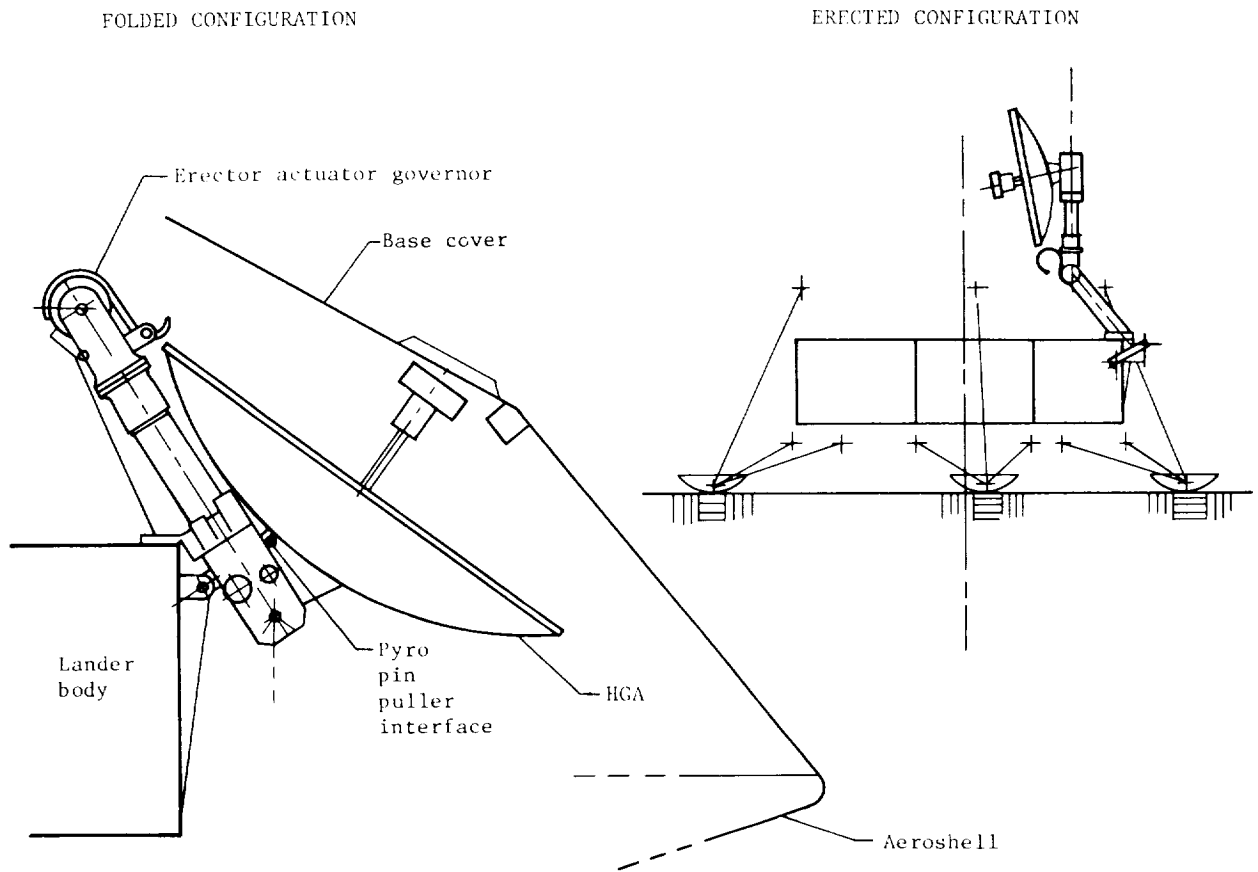
Figure 23.- High-gain antenna deployment mechanism.

Venting Assembly

The varying pressure within the shroud payload compartment surrounding the VLC caused differential pressures across the walls of enclosed spaces within the spacecraft. These spaces were adequately vented during launch and Mars entry to prevent excessive structural loads and consequent deflection, distortion, or damage. The VLC consisted of three main chambers which were nested within each

other. The inner chamber, the VL, had a vent in the center of the bottom cover
which allowed gas to flow into the second chamber formed by the aeroshell and
base cover. (See fig. 24(a).) A vent in the side of the base cover permitted
gas flow into the cavity enclosed by the bioshield cap and base but outside of
the aeroshell and base cover. (See fig. 24(b).) The gas escaped from the bio-
shield through the bioshield vent valve assembly at the top of the bioshield
cap, when it was opened. (See fig. 24(c).) The bioshield vent valve was a
spring loaded normally open valve. During the prelaunch mission phase it was
held closed by a pyro-actuated pin puller. At 1.2 sec before launch, an LCE
discrete signal fired the pin puller and opened the valve.

The structural design limit pressures for the three main chambers of the
VLC were as follows:

	Burst	Crush
Bioshield	4137 Pa (0.6 psid)	------------------
Aeroshell and base cover . .	689 Pa (0.1 psid)	144 Pa (3.0 lb/ft^2)
Leader	345 Pa (0.05 psid)	144 Pa (3.0 lb/ft^2)

Internal thermal balance considerations imposed a requirement on the venting
system. Insulation was ineffective unless the gas pressure was low enough to
eliminate conduction effects. The specific requirement was to lower pressure
to 0.013 Pa (10^{-3} torr) within 1 1/2 hr after lift-off. Additional require-
ments were imposed upon the vents themselves. The bioshield vent assembly
included a biofilter which prevented the entry of biota as small as 0.3 μm.
The base-cover vent was designed to diffuse the hot wake gases which flowed in
during entry. The VL vent included a 70-μm mesh screen to keep out dust par-
ticles during operations on the Mars surface. In addition, to permit contin-
uous insulation across the VL bottom cover, a layer of insulation comprised
part of the vent and the outflow passed directly through it.

During the mission, four time periods that were of interest from the vent-
ing standpoint were the initial depressurization, launch ascent, parking orbit
through TMI, and Mars entry.

Initial depressurization: Initial depressurization was the rapid blowdown
of the entire VLC which occurred at 1.2 sec before launch. The bioshield vent
valve was opened to release the 3.45 ± 0.7 kPa (0.5 ± 0.1 psi) positive differen-
tial pressure which was maintained until launch for planetary quarantine purposes.

Launch ascent: Launch ascent included the first 100 sec or so following
lift-off. Most of the atmosphere of the Earth was traversed during this period
and peak pressures were encountered.

Parking orbit through TMI: The period for parking orbit through TMI
extended from the shroud separation at about 270 sec after lift-off through
5400 sec (1 1/2 hr). Outgassing within the VLC became the prime consideration
during this period because it delayed attainment of the required low internal
pressure. At about 270 sec after lift-off, the Centaur shroud parted like a

Filter area, cm^2 (in^2)

1064 (165) (blanket, 70-μm conical screen filter)

504 (78.2) (150-μm screen diffuser)

23 774 (3530) (pleated, 0.3 μm)

Orifice diameter, cm (in.)

20.32 (8.0) (annular gap, 1.27 cm (0.5 in.))

17.78 (7.0) (8 mesh screen)

20.32 (8.0) Cyclindrical biofilter (0.3 μm)

Conical filter

Thermal blanket

Annular gap

TDLR

Support screen

(a) VL vent.

Cyclindrical diffuser

Screen

Aeroshell base cover

(b) Base-cover vent.
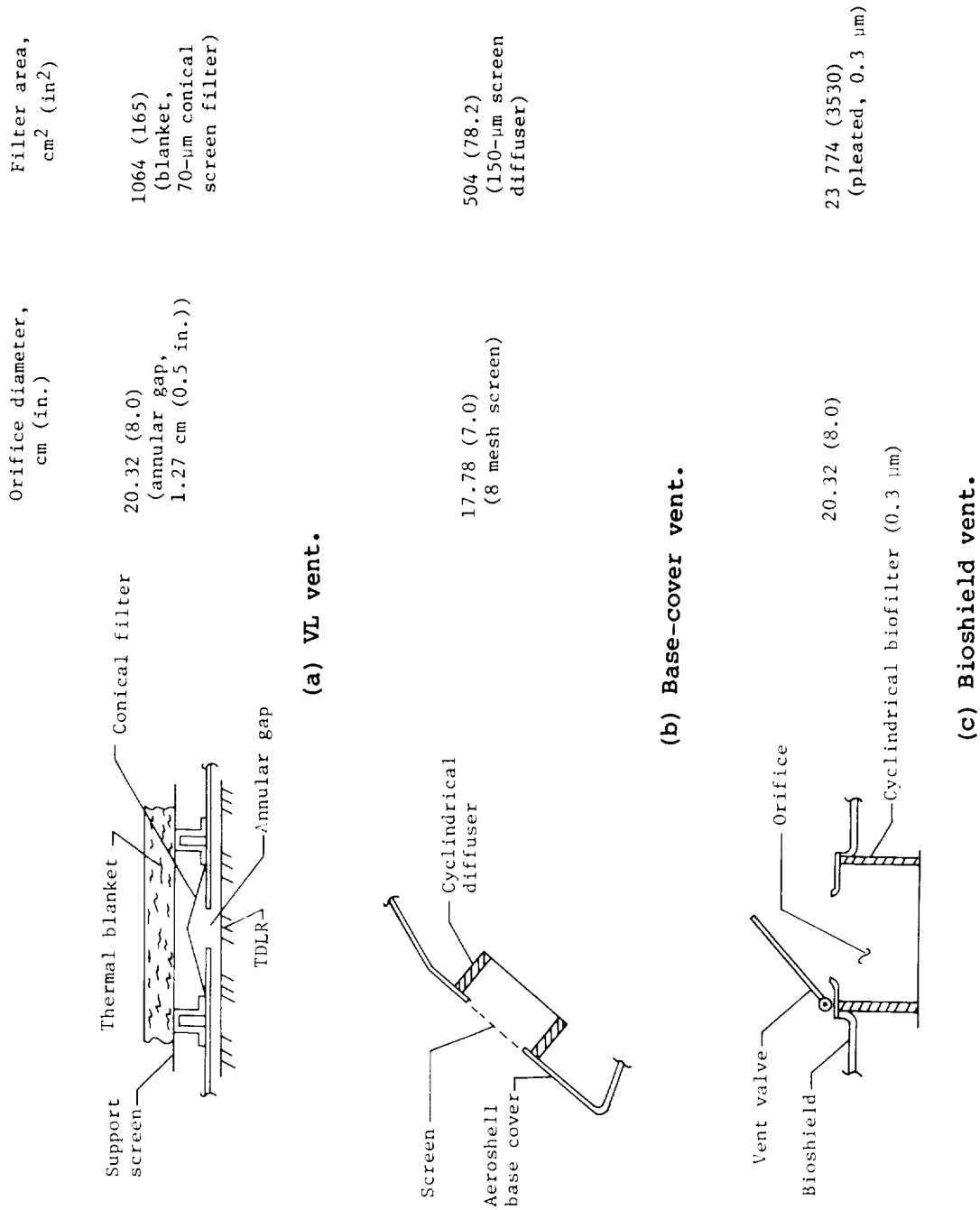
Orifice

Vent valve

Bioshield

(c) Bioshield vent.

Figure 24.- Vent assembly configurations.

clam shell and was jettisoned. The bioshield vent orifice became the forward stagnation point of the V S/C and a spike increase in external pressure was experienced. Jettisoning the bioshield cap at 4560 sec after lift-off caused a step decrease in the external pressure on the base cover.

Mars entry: As the VLC descended through the Mars atmosphere, the venting system allowed sufficient in-flow of gas to prevent excessive differential pressures. Because of the vent's location on the base cover, the entering gas was hot wake gas and the external pressure was the base pressure. Fine mesh screening in the base-cover vent diffused the gas and prevented an entering jet from creating a local hot spot.

Thermal Control Subsystem

The VLC thermal control subsystem was designed to provide an acceptable temperature environment for all VLC components and structures. The subsystem was designed to function during the prelaunch, launch, cruise, and descent phases of the mission, entry into the Mars atmosphere, and for a minimum of 90 days into the postlanded phase. Thermal control was achieved for all mission phases by utilizing a combination of passive and active thermal control systems. The passive techniques - use of geometry, thermal coatings, equipment location, and insulation - were preferred for simplicity and reliability; however, active techniques - thermal switches, heaters, and water cooling - were used in conjunction with the passive techniques where necessary.

Passive Thermal Control

Passive thermal control was accomplished through geometrical considerations and selection of materials which have desired surface optical properties. In addition, equipment location optimization and selected materials are utilized throughout the VLC to achieve the required thermal balance between components, structure, and the external environment. Notable examples are as follows:

Geometrical considerations: RTG wind covers were used to isolate the RTG's from the wind on the Mars surface; thus, overcooling was prevented. Maximum heat loss was provided for by radiation to prevent the RTG from overheating in a vacuum environment during cruise or in a hot calm environment on Mars.

Thermal control coatings: Coatings with the desired infrared emittance and solar absorptance optical properties were used to provide the required thermal radiation characteristics on all surfaces of the VLC.

Equipment location: Most equipment that had to survive and operate on the Mars surface was located in a single thermally controlled compartment.

Thermal insulation: Thermal isolation by insulation was achieved in various areas of the VLC to control heat flow between the equipment and the environment during cruise, postseparation, and postlanded mission phases. Two types of thermal insulation used were: multilayer radiation shield insulation for use in vacuum and bulk fibrous insulation for use in vacuum and Mars atmosphere.

Active Thermal Control

Active thermal control techniques included water cooling system (prelaunch phase only), electrical heaters, and thermal switches. Notable examples are as follows:

Water cooling system: The water cooling system was used to remove thermal energy from the RTG's and the VLC during all prelaunch activities. It could not be used after launch. This fluid, water with a sporicide added, was purged from the airborne portion of the system by sterile nitrogen gas just prior to launch, and the ground portion of the system was severed from the VLC.

Heaters: The VLC used both continuous operation and thermostatically controlled electrical heaters, many of which had redundant systems. Cycling of the RCS engines during deorbit provided a source of heat for sensitive engine valves.

Thermal switches: Thermal switches were used to maintain internal equipment above specified minimum temperature limits by controlling the heat transfer from each RTG and the equipment mounting plate. The control was effected by changing the resistance of the thermal switch contact areas between the hot RTG mounting plate and the cool equipment mounting plate. The switch responded to equipment mounting plate temperatures by a change in gas vapor pressure in the bellows; thus, the switch was activated. A schematic drawing of the thermal switch is shown in figure 25.
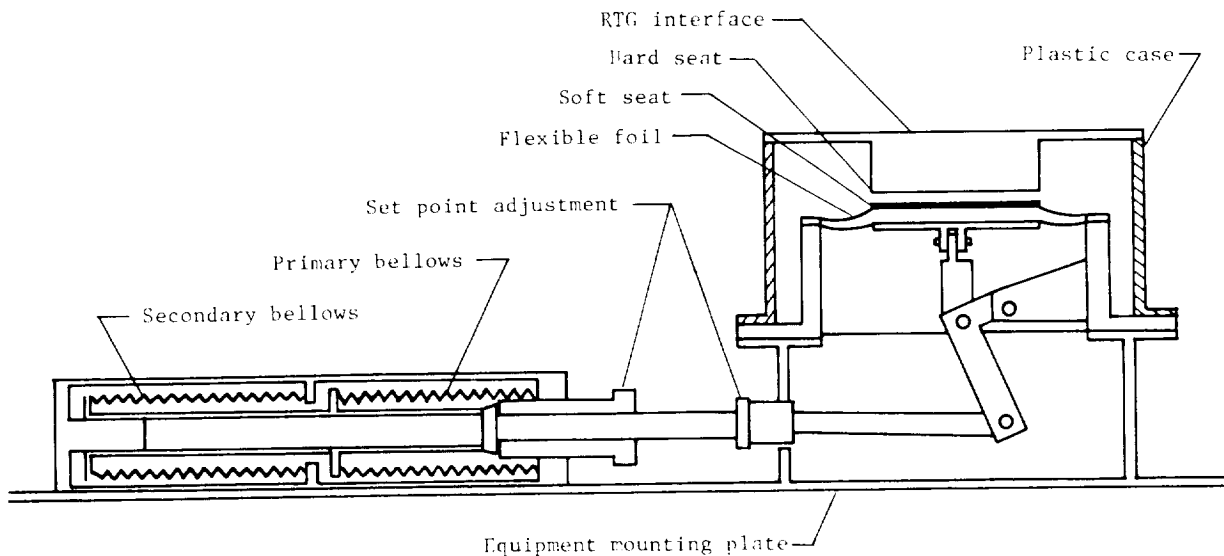
Figure 25.- Schematic drawing of thermal switch.

Operating Modes

Operating modes for the thermal control subsystem for each mission phase were as follows:

Prelaunch: Thermal control during the prelaunch phase was provided by external air conditioning and a water cooling system in the VLC. During sterilization, the water system was used to assist the hot nitrogen gas in heating the VLC. The systems operated continuously until launch except for limited periods when one or both systems were permitted to be inoperable.

Launch to cruise: Thermal control during ascent was achieved through payload fairing protection of the VLC from the aerodynamic heating pulse. The fairing ejection was optimized to minimize heat transfer to the VLC from the external environment. Furthermore, the transient of less than 2 hr between ascent and Sun acquisition was of relatively short duration compared with the thermal time constant of the VLC.

Cruise: Thermal control during cruise was primarily passive with the exception of thermostatically controlled heaters on the propulsion system and IRU cover. During this period, the VLC was in a vacuum environment, was radiating to a deep-space temperature of -3.7 K (-453° F), and was exposed to a solar flux varying from 1371 to 485 W/m^2 (435 to 154 Btu/ft^2-hr). The VLC was designed to be virtually independent of the solar intensity so that the large variation from Earth to Mars was of no consequence. This independence from solar intensity was accomplished by insulating the Sun side of the VLC with highly effective multilayer radiation shield insulation. Also, the VLC was partially shaded by the VO. To provide for proper rejection to deep space of the RTG thermal energy, the base cover infrared emissivity was optimized. Internal VLC equipment was isolated from the hot RTG and from the cold base cover and aeroshell environments by both multilayer and fibrous insulation. During midcourse maneuvers, the large thermal time constant of the VLC and the low solar absorptivity of the base cover provided sufficient thermal protection.

Postseparation to landing: The thermal control system for the mission phase from postseparation to landing used most of the features of the cruise thermal control system and, in addition, used the aeroshell ablator to minimize the entry heating effects. During the deorbit coast the optimization of base cover and aeroshell optical properties provided the proper thermal balance between solar irradiation, engine plume heating, and radiation to deep space. The aeroshell ablator protected against the aerodynamic heat pulse during entry. During the parachute and terminal descent phase, convective heat transfer became significant but was of short duration, and the VLC equipment compartment was thermally protected by insulation and a large thermal time constant.

Landed - Mars surface: The VL experienced a wide variety of thermal environments on Mars. These environments are shown in figure 26. The VL

Sky temperature, 99 to 144 K (−281° to −**200° F**)

Atmospheric radiation

Atmospheric temperature, 153 to 308 K (−184° to 95° F)

Wind velocity, 0 to 39.6 m/sec (0 to 130 ft/sec)

Ground IR

Ground temperature 153 to 308 K (−184° to 95° F)

Radiation to space

Direct solar (24.66-hr diurnal cycle) noon flux, 485 to 634 W/m² (**154** to 201 Btu/ft²-hr) at 45° to 90° Sun elevation angle
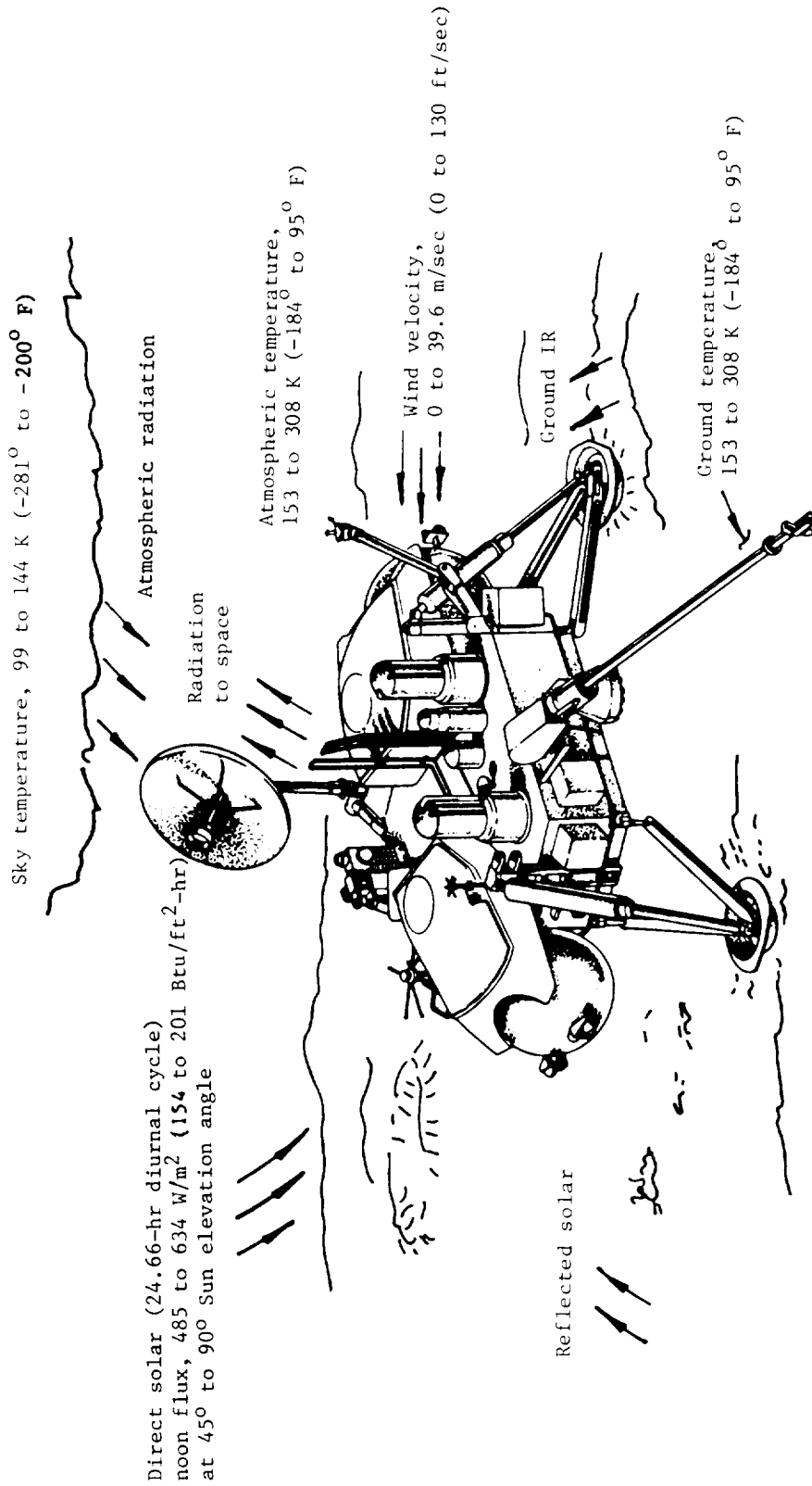
Reflected solar

Figure 26.− Mars surface thermal environments.

36

exterior surfaces were covered with erosion-resistant thermal coatings having intermediate solar absorptance and high infrared emissivity. The internal equipment compartment was enclosed in fibrous insulation to provide isolation from the Mars environments. Insulation penetrations required for structural supports, electrical cables, and science experiments were designed for minimum conductance. All VL external surfaces and penetrations were designed to prevent penetration of Mars winds into the internal equipment compartment. Heat from both RTG's was provided to the internal equipment through thermal switches as required by cold environments and/or equipment inactivity. RTG wind shields were installed to insure that heat would be available in cold windy environments. The required energy distribution within the internal equipment compartment was achieved by selection of surface optical properties, equipment arrangement, mounting techniques, and equipment mounting plate design.

Communications Subsystem

The relay communications equipment operated at a UHF frequency of approximately 381 MHz and consisted of a transmitter and an antenna assembly. The RCE transmitted data to the VO for subsequent transmission to Earth. The DCS operated at S-band frequencies with DSN channel 13a, approximately 2294 MHz, used for downlink transmitting and channel 13b, approximately 2112 MHz, used for uplink receiving. The DCS contained the SBRA, an S-band LGA, and an HGA. The DCS was used for direct communications between the VL and Earth.

Relay Communications Equipment

The RCE was part of the V S/C RCL shown in figure 27 and was used for separation, deorbit, entry, and postlanded data transmission. The RCL included the VO RRS as a complementary subsystem to the RCE. The VL was required to have the capability of transmitting at least 1×10^7 bits of data daily via the relay link from landing to EOM when the VO was in an overhead periapsis passage. The data quality required was fewer than 3 bit errors per 1000 bits. During entry and landing, degradation of this performance was expected for short-time durations as a result of attitude maneuvers, parachute oscillations, etc. The RCE performed the following functions:

Frequency shift key modulation of the carrier signal accomplished with a composite telemetry signal which had been split phase coded by the DAPU; a data bit "1" consisted of a (10) symbol pair and a data bit "0" consisted of a (01) symbol pair

Transmitted the modulated rf signal to the VO RRS via a right-hand circularly polarized antenna

Transmitted data to the RRS during the VLC separation, deorbit, entry, terminal descent, landing, and postlanded phases of the mission at power levels and data rates in accordance with commands from the GCSC

VIKING LANDER CAPSULE RELAY
COMMUNICATIONS EQUIPMENT

VIKING ORBITER RELAY EQUIPMENT CONFIGURATION
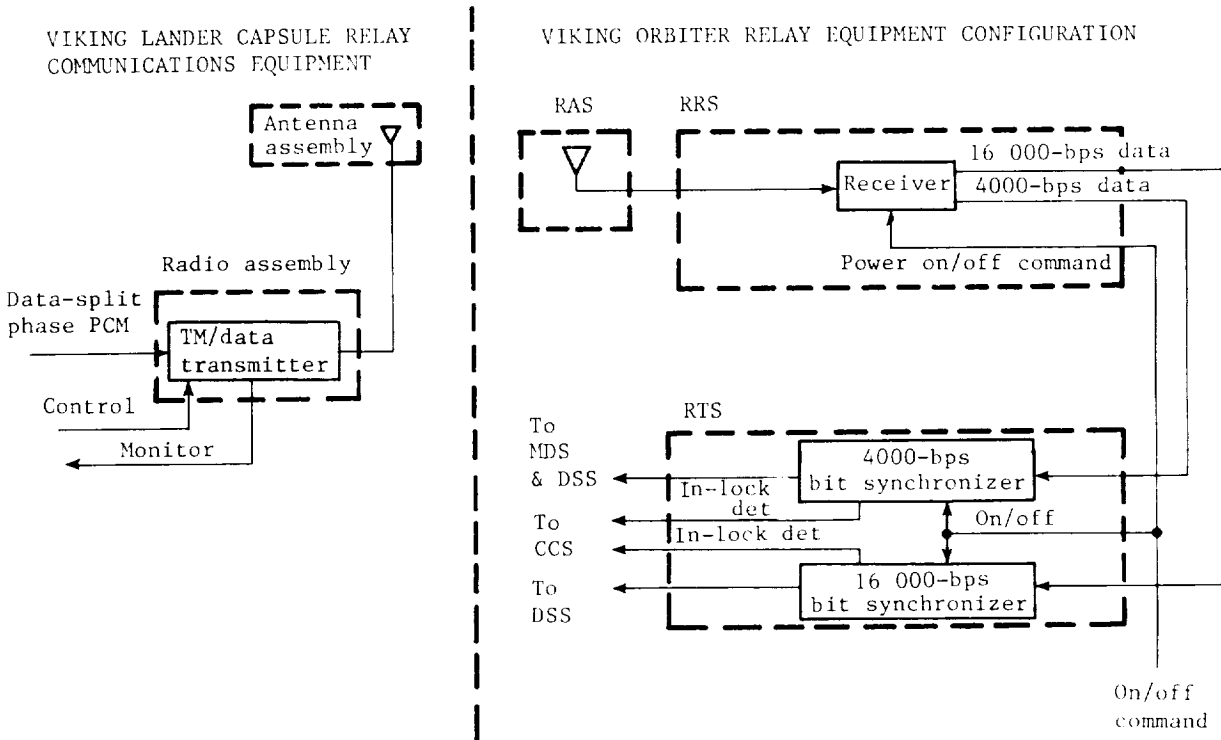
Figure 27.- Block diagram of relay communications link.

UHF transmitter.- The purpose of the UHF transmitter was to generate the
rf signal frequencies and levels necessary to provide the specified data qual-
ity when operating in conjunction with the UHF antenna, to modulate the rf
signal with the split phase composite telemetry signal at 4 000 or 16 000 bps,
and to operate at three commandable power levels, depending on the mission pro-
gramming. The UHF transmitter operated at three discrete power modes called
mode I, mode II, and mode IV, which were nominally the 30-W, 10-W, and
1-W modes, respectively. These modes were command selectable by pulse discrete
commands from the GCSC or, in the event no commands were received by the trans-
mitter subsequent to power application, it would automatically sequence to the
30-W mode. These three modes were obtained by two techniques within the trans-
mitter: bypass switching of rf stages and control of driver amplifier collector
voltages. The significant electrical parameters of the transmitter are as
follows:

Frequency for -
  Mark, MHz 381.063303
  Space, MHz 380.863303

Frequency stability . . . . $\pm38.4 \times 10^{-6}$

Frequency deviation, kHz 200

38

Power output for -
  Mode I, dBm 44.8
  Mode II, dBm 40.0
  Mode IV, dBm 30.0

Waveform characteristics for -
  Asymmetry, nsec . . . . ±625
  Jitter, nsec 700
  Droop, percent 2.5
  Overshoot, percent 5.0
  Rise and fall times, μsec 1.5

     UHF antenna.- The UHF antenna, shown in figure 28, radiated the rf signal
to the VO during preseparation, checkout, separation, deorbit, landing, and
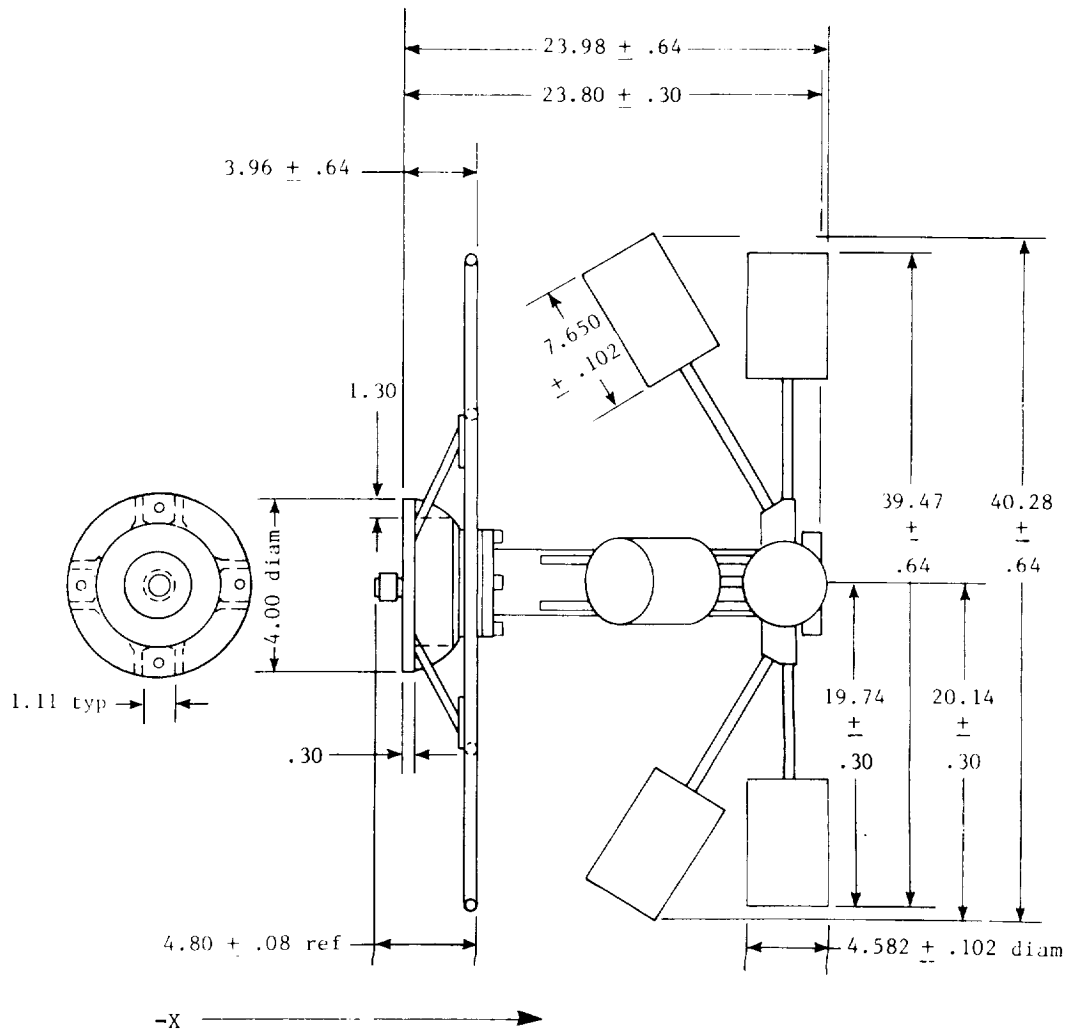
Figure 28.- UHF antenna. All dimensions are in cm.

postlanded operations. The UHF antenna provided an approximately hemispherical radiation pattern about the negative X-axis of the VL during these mission phases. The UHF antenna was a right-hand circularly polarized eight-element crossed dipole above a tuned ground plane. The free-space gain as specified through any planar cut containing the axis of the antenna is plotted in figure 29. This type of radiation pattern could not be obtained with the usual
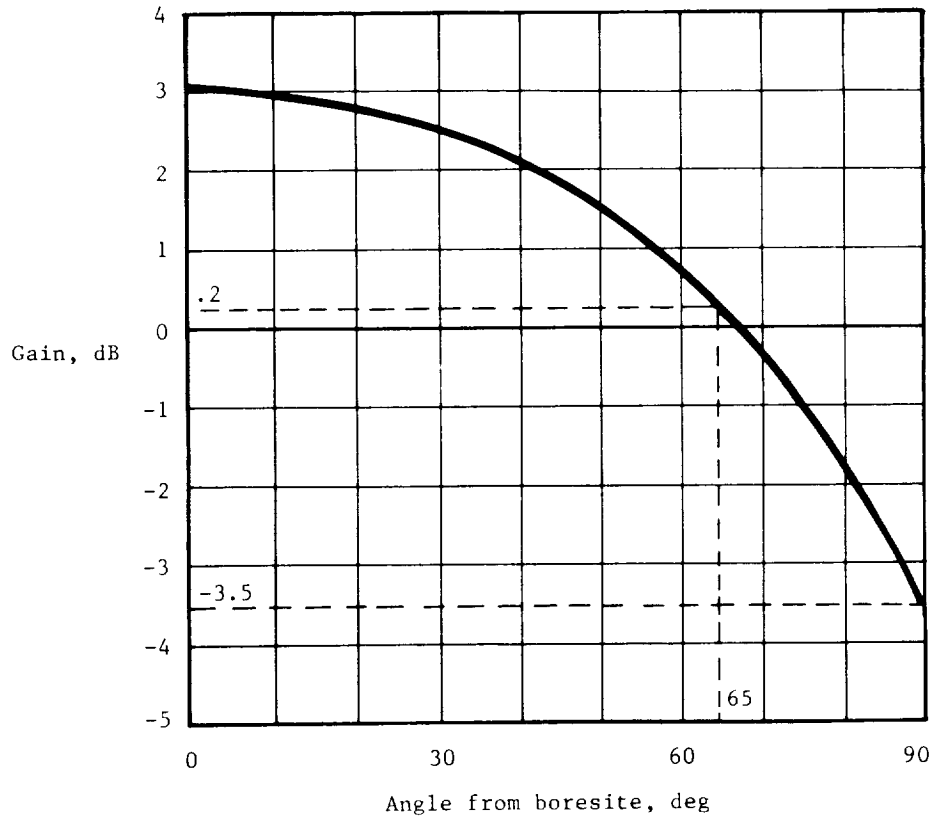
Figure 29.- Typical radiation pattern of UHF antenna.

planar arrangement of turnstile antennas of crossed dipoles over a ground screen or crossed slots in a conducting ground plane since they supplied only a radial mode of radiation. An additional mode of radiation was required which basically consisted of a doughnut shape with its null along the axis of symmetry of the antenna. These two modes were obtained with the UHF antenna design by incorporating additional dipole elements depressed by a selected angle below the normal dipole elements. The desired radiation characteristics in the upper hemisphere were achieved by proper choice of the lengths and inclination angles of the radiating elements and their heights above the ground plane. The geometry and dimensions of the grid-wire ground-plane configuration, with a maximum size less than 1/2 wavelength, were chosen so that suppression of the backward radiation

40

was greater than would be obtained with a much larger continuous sheet. The
ends of the dipole elements were loaded with 6.4-mm-diameter (1.25 in.) corona
balls, which were covered with a low-density polyurethane foam encased in a
thin-wall fiberglass tubing to increase the power-handling capability to approx-
imately 100 W which was well above the 60 W that was specified. The electrical
parameter variation of the UHF antenna was basically controlled by the local
rf environment in which the antenna functioned. Characteristics of the antenna
were measured on a 3/8-scale model of the VL in the four pertinent flight
configurations.

Direct Communications System

The DCS shown in the functional block diagram of figure 30 provided a
direct communication link between Mars and Earth after the VL had landed. Prior
to separation of the VLC from the VO, a portion of the DCS provided the capabil-
ity to detect and decode a command signal received from Earth through the VO
radio frequency subsystem. The DCS contained the SBRA, the S-band LGA, and the
HGA. The functions of the DCS were as follows:

To receive and demodulate the S-band signals transmitted by DSN

To coherently translate the frequency of the received signal in the ratio
240/221 when operating in the two-way mode

To detect and decode the command signals transmitted by the DSN and to sup-
ply decoded command data to the GCSC and emergency commands to the PCDA

To transmit to the DSN a modulated S-band signal that was phase coherent
with the received signal in the two-way mode or derived from an internal
frequency source in the one-way mode

To provide a turnaround channel for the DSN ranging signal

To modulate the transmitted signal with composite telemetry or telemetry
and ranging waveforms

To receive HGA articulation pulses from the GCSC and to step the HGA in
azimuth and elevation

To provide data for engineering telemetry

To monitor status of the SBRA and to supply status data to the GCSC

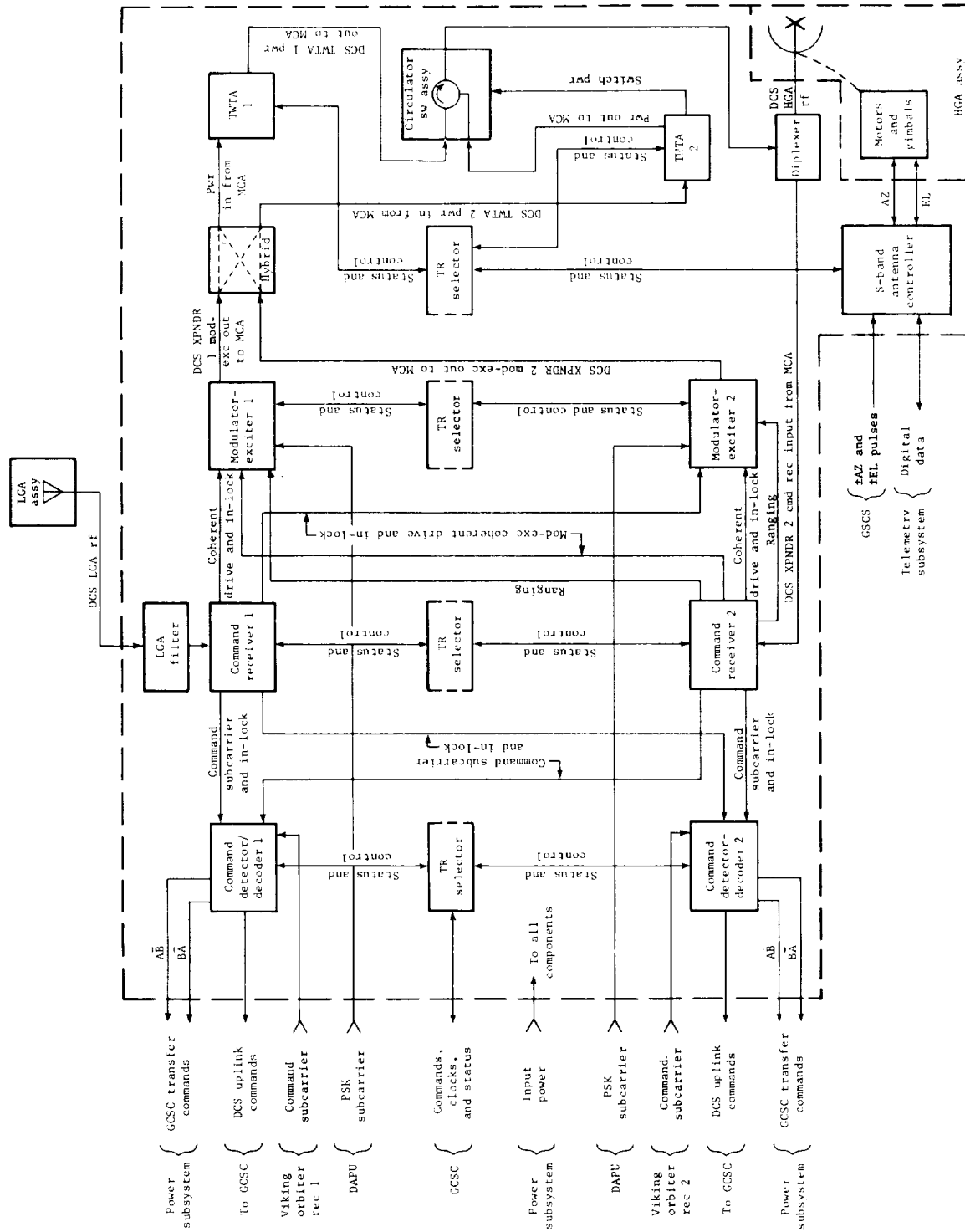To receive commands from the GCSC and to perform appropriate switching
within the SBRA

Figure 30.- Functional block diagram of DCS.

42

S-band radio assembly.- The SBRA contained a CCU, an MCA and block-redundant TWTA's, and transponders.

Command control unit: The CCU was made up of block-redundant command detectors and decoders, a TRS, and an HGAC. The functions of the CCU were as follows:

To detect and decode the composite command signal received from the transponder receiver (or VO receiver), to determine if the command was a normal GCSC command or PCDA emergency command, and to supply the command to the correct user

To accept NRZ-PCM command signals consisting of 5 command bits and a parity check bit from the GCSC, to verify correct parity, to decode the serial command bits, and to generate a continuous level output for SBRA component switching and control

To provide status information on SBRA component operation to the GCSC

To receive HGA stepping commands from the GCSC and to convert these commands into the proper sequence, duration, and level to assure positive indexing of the stepper motors

To generate resolver excitation, to provide signal processing to convert the HGA position readout signals into a digital form, and to supply these data to the telemetry subsystem

Transmit-receive selector: The TRS provided the status monitoring, generation of control signals, and command interface functions within the CCU. A functional block diagram of the TRS is shown in figure 31. GCSC commands to the TRS were used for cross strapping of receivers and modulator-exciters, cross strapping of receivers and detectors, selecting the internal oscillator, initiating ranging with receiver 2, and interrogating the DCS status register. Implementation of the cross-strapping commands by the DCS was a function of the command receiver in-lock status.

Command detectors: The command detectors shown in the block diagram of figure 32 accepted a composite command signal from the VLC command receivers during postlanded operations or from the VO radio frequency subsystem prior to separation of the VLC. This composite input signal was a 384-Hz sinewave subcarrier that was modulated by PSK with NRZ-PCM command data. The command data symbol rate was 4 symbols/sec with a transition density of at least 4 transitions in every block of 32 symbols. At the beginning of each command transmission, an idle sequence of alternating 1 and 0 was transmitted to allow the detector to acquire subcarrier lock and bit timing. This idle sequence had a minimum of 256 symbols. The detector recovered and demodulated the subcarrier, rejected signals intended for the VO, extracted bit timing information from the transmitted commands, and outputted to the command decoders an NRZ-PCM command data bit stream with a 180° polarity ambiguity and outputted an indication of combined subcarrier and bit-sync status. With an input signal-noise ratio of

43

From
S-band components

Enable ──▷── Status control ◀── Readout complete

Status input interface circuits

Interrupt status and shift control

Interrupt

Comparator (parallel) ──▷── Interrupt to GCSC

10-bit status store ── Formatter ──▷── Status data to GCSC

Incorrect parity

TRS timing 288 kHz ──▷── Countdown timing   Clock

Parity

Shift pulses ──▷── 6-bit decode register

Command data ──▷──

Parity

Decode

Power convert & regulator ──▷── TRS OC to TM

Decode control

OC detector

Clock

Command memory

Output interface (9 circuits)

To S-band subsystem components
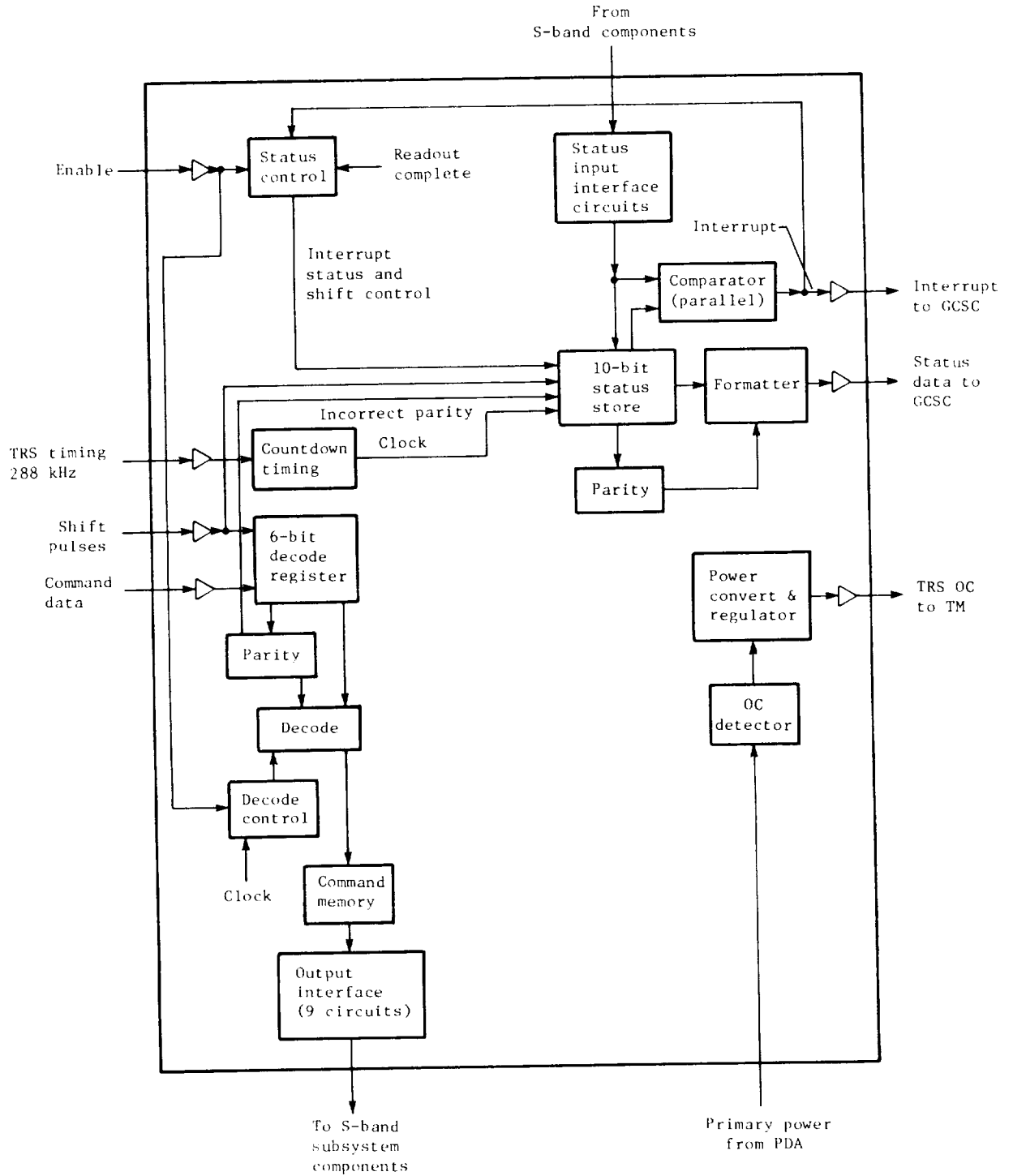
Primary power from PDA
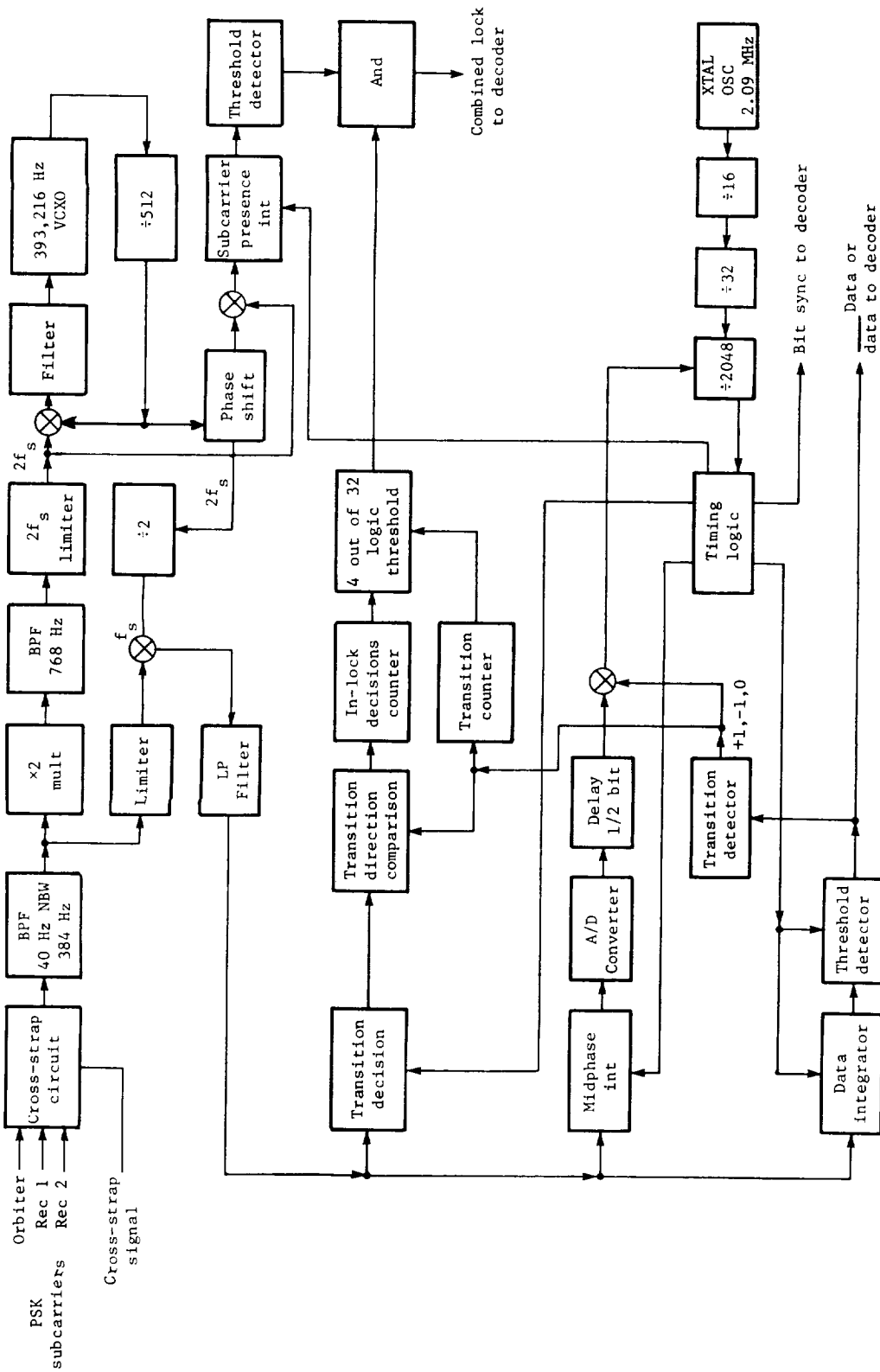
Figure 31.- Functional block diagram of TRS.

44

Figure 32.- Block diagram of command detector.

11.5 ± 0.5 dB, the symbol error rate of the output data stream was $\leq 10^{-5}$. The major functions of the detector were:

(1) Subcarrier recovery: Subcarrier recovery was accomplished by doubling the input signal frequency, filtering and limiting this signal, and phase-locking the detector VCXO to this signal.

(2) Coherent demodulation: The recovered subcarrier was used to synchronously demodulate the composite input signal. The output of the demodulator was supplied to the transition decision circuit, the midphase integrator, and the inphase integrator.

(3) Bit lock: The transition decision circuit sampled the output of the data demodulator before and after a bit transition and compared this sample with the data integrator output. These comparisons were processed through a two-level decision circuit which declared valid bit lock when 4 out of 11 valid bit-lock decisions were detected. Since this detection process required the presence of data transitions before the bit-lock decision could be valid, circuitry was also included to detect transitions and inhibit the bit-lock decision process if data transitions were not present.

(4) Bit-timing recovery: Bit-timing recovery was accomplished by integrating across a bit transition and by using the output of the integrator to either advance or retard the timing such that the value of the integrator output is forced to 0. When the transition detector indicated four in-lock indications, the bit-timing recovery circuit integration time was reduced from 100 percent to 50 percent of a bit period to reduce the effect of noise at the output of the integrator.

(5) Data detection: Data detection was accomplished by the data integrator and threshold detector. The demodulated composite input signal was integrated for a data period and the output supplied to the threshold detector where the decision of 1 or 0 was made based on whether the integrator output was positive or negative.

(6) Detector lock: Detector lock decisions were based on the logical ANDing of the transition decision and the subcarrier presence integrator. The error rate of the transition detector remained low with small timing errors; however, if a signal dropout occurred the bit-lock indicator would indicate "in-lock" at an unacceptable rate. It was for this reason that the subcarrier presence indicator was ANDed with the bit lock since its output was sensitive to signal power.

(7) Inphase integrator telemetry: The inphase integrator TM circuit was used to facilitate testing at system level and to provide an estimate of the command channel performance during mission operations. This TM measurement sensed the output of the inphase integrator for transmitted 1's and was capable of holding the sample value within 2 percent for a 16-bit delay.

Command decoders: The command decoders accepted the NRZ-PCM command data stream from the command detectors. The decoders processed the 4-symbol/sec data stream to remove the 180° ambiguity, recognized either a "normal" or "emergency"

46

symbol preamble, decoded 32-symbol Hamming coded command words, corrected single bit errors per word, detected double errors per word, and transmitted the corrected 24-bit command words to the GCSC. In addition, indication of decoder lock was also supplied to the GCSC. If the "emergency" preamble were decoded, two output pulses of 250 nsec were supplied to the power control and distribution assembly for switching GCSC's. The command decoder shown in the block diagram of figure 33 performed the following major functions:

(1) Idle-preamble state counter: The idle-preamble state counter controlled the command decoder during the idle and preamble recognition phase of a complete cycle. Upon recognition of 24 correct and contiguous bits of idle sequence, the bit counter overflowed and the idle-preamble state counter enabled a search for the preamble (Barker code) or either of the two emergency preamble codes. Correct decoding of either emergency code allowed the generation of the associated emergency command and caused the idle-preamble state counter to revert to the idle search mode and inhibited generation of any additional emergency commands until the decoder was reset.

(2) Load shift state counter: Correct decoding of the Barker preamble allowed the load shift state counter to assume control of the command decoder, obviated any further emergency commands until reset, and provided for the generation of the decoder in-lock signal to the GCSC.

(3) Syndrone and storage registers: The load shift state counter enabled the syndrone register for error detection and allowed the decoded to accept command words from the storage registers.

(4) Bit counter: During this portion of the cycle, bit counter overflow indicated that 32 command symbols had been received. At this time, if the stored command word did not contain two or more errors, the load shift state counter enabled the shift clock and a 24-bit command word was transmitted to the GCSC.

(5) Word counter: After the word had been shifted out, the word counter was incremented and the count was compared with the total number of words to be processed. If the total had not been transmitted, the load-shift subcycle was repeated. When the total number of words had been transmitted to the GCSC, the decoder reverted to the idle-preamble subcycle. If any stored command word contained two errors, the in-lock signal to the GCSC was dropped and the decoder reverted to the idle-preamble subcycle.

High-gain antenna controller: The HGAC accepted an HGA command from the GCSC, converted this signal to the proper drive for the stepping motors in the HGA. The HGAC also provided excitation to the resolvers in the HGA, processed the resolver outputs, and upon command from the TM subsystem, converted these signals to a digital representation of the HGA position. A functional block diagram of the HGAC is shown in figure 34. The input specifications to the HGAC are shown in the following table:
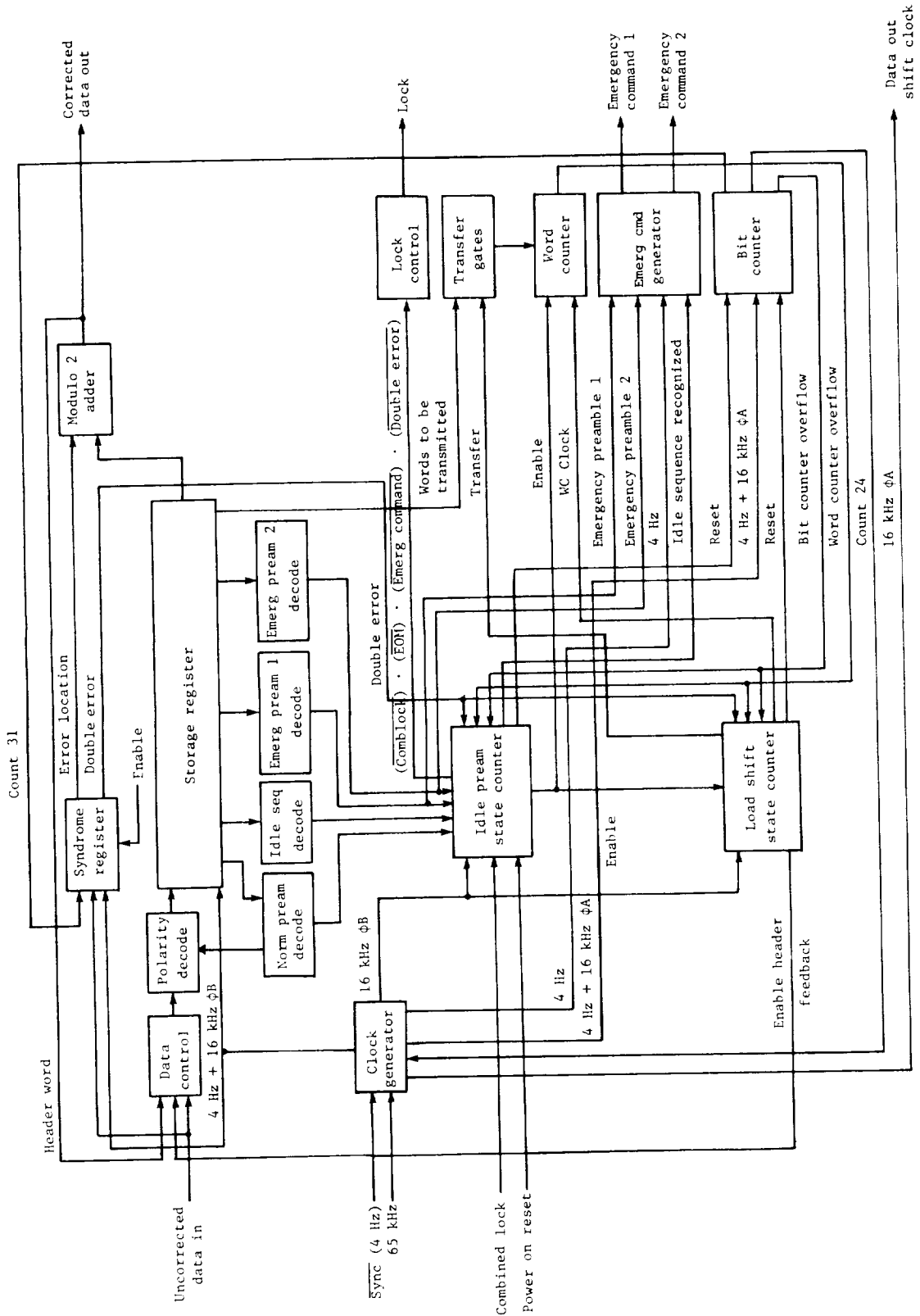
47

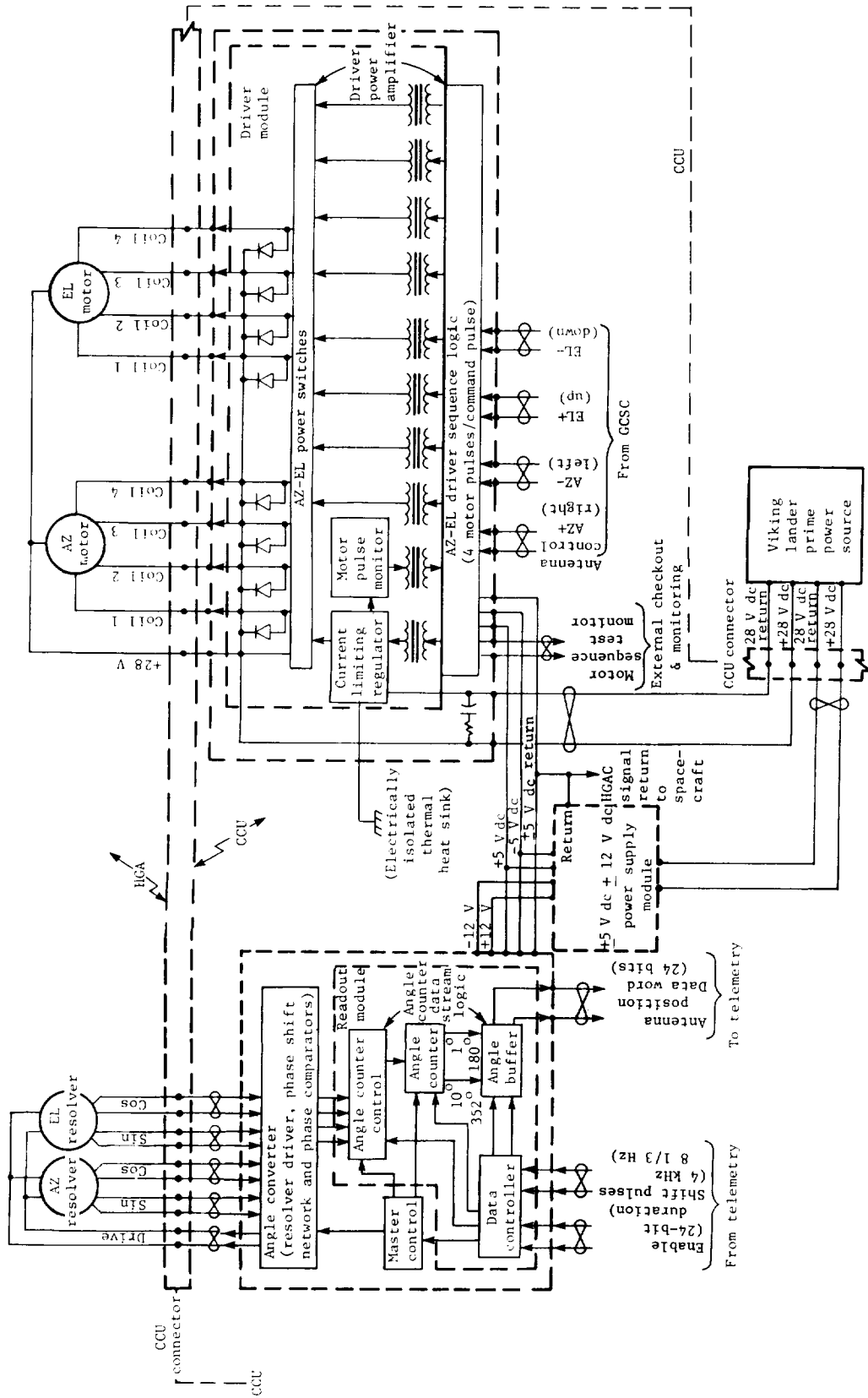Figure 33.- Block diagram of command decoder.

48

Figure 34.- Block diagram of antenna controller.

```
Elevation or azimuth step command from
  GCSC, nsec pulse . . . . . . . . . . . . . . . . . . . . . . . . . . . . . . . . . .  500 ± 100
Stepping rate, pulses/sec . . . . . . . . . . . . . . . . . . . . . . . . . . . . . . . . . . . . 1.64
TM shift pulses, sec⁻¹ . . . . . . . . . . . . . . . . . . . . . . . . . . . .  8 1/3 or 4000
TM enable duration, sec or msec . . . . . . . . . . . . . . . . . . . . . . . .  2.88 or 6
Resolver sine and cosine from HGA, $V_{p-p}$ . . . . . . . . . . . . . . . .  0 to 5.6
```

The output specification corresponding to these inputs were as follows:

```
Motor drive pulses (four per step command):
  Voltage, V . . . . . . . . . . . . . . . . . . . . . . . . . . . . . . . . . . . . . . . . . 19 to 33
  Current, A . . . . . . . . . . . . . . . . . . . . . . . . . . . . . . . . . . . . . . . 0.35 to 0.5
  Duration, msec . . . . . . . . . . . . . . . . . . . . . . . . . . . . . . . . . . . . . 55 ± 6
  Dwell, msec . . . . . . . . . . . . . . . . . . . . . . . . . . . . . . . . . . . . . . . 55 ± 6

HGA position data (three 8-bit words):
  Data rate, bps . . . . . . . . . . . . . . . . . . . . . . . . . . . . . . . 8 1/3 or 4000
  Word length, bits . . . . . . . . . . . . . . . . . . . . . . . . . . . . . . . . . . . 24

Resolver excitation:
  Voltage, $V_{p-p}$ . . . . . . . . . . . . . . . . . . . . . . . . . . . . . . . . . . 10 ± 20%
  Frequency (sinewave), kHz . . . . . . . . . . . . . . . . . . . . . . . . . . . . . . 4
```

The HGAC consisted of two major modules, readout module and driver module, that operated in the following manner. The readout module provided the 4-kHz sinewave excitation to both the azimuth and elevation resolvers and received the sine and cosine outputs from both resolvers. The sine and cosine outputs were processed through circuitry that converted the amplitude output of the resolver to phase information and the resolver position was determined by measuring the time interval between the zero crossings of these two signals. The readout of the HGA position was initiated upon receipt of the enable signal and shift pulses from the TM subsystem. The driver module accepted the appropriate HGAC step (±EL or ±AZ) command from the GCSC, determined whether the command was ±EL (AZ), converted the command signal to four current-limited stepping signals, and sequenced the power switches in the proper order to cause the HGA stepping motors to index 1 full revolution (360°). The stepping motors in the HGA were four phase dc brushless motors. As such the driver module converted each GCSC stepping command into four motor driver pulses to index the stepping motor through four 90° steps. The power switches controlled the selection of motor coils and the current-limiting regulator controlled the magnitude and duration of the pulse. The rise and fall times of the current pulses were also controlled by the regulator to insure proper acceleration and deceleration characteristics of the HGA.

Command system: During a command period the following sequence was followed:

(1) An uplink frequency sweep was used to acquire and lock the command receiver.

(2) After command-receiver lock, the command message was executed. The command message consisted of all sequences of subcarrier modulation including

idle sequences, preambles, coded data, and end flags. A command message was the total uplink transmission for each commanding period and was made up of blocks of data words and their attendant overhead. A block was called a command message segment. A command message segment consisted of a preamble, message segment header, from 1 to 31 command data words, and a check-sum word. The VLC was designed to receive, validate, and execute uplink command data on the basis of a command message segment. A typical command message and command message segment are shown in figure 35. An idle sequence of alternate 1 and 0 was transmitted just prior to the beginning of a commanding period and any other time when it was desired to maintain the uplink command capability. The idle sequence was not transmitted during command receiver acquisition. A minimum of 256 idle sequence symbols were transmitted prior to the start of the first command message segment to achieve command detector bit-sync status. An additional 60 idle sequence symbols were transmitted prior to but contiguous with each preamble at the beginning of all command message segments. These 60 idle sequence symbols maintained polarity and time phasing throughout and always ended with a transmitted 1. Idling sequence periods, other than the above defined periods of 60 symbols, maintained time phasing with the 60 symbols.

Preamble: An 11-symbol preamble was utilized by the VLC to determine the proper polarity and word boundaries of the incoming data. The preamble was transmitted immediately following the final 1 of each preceding 60-symbol idle sequence at the beginning of each message segment. The preamble word was a particular symbol pattern recognized only by the command decoders.

Figure 35.- Typical command message.
N ≤ 30.

Command data coding: All command data transmitted subsequent to the preamble and contained in a message segment was coded to provide for the detection and correction of all single errors within a word and the detection of all double errors. The uncoded data word was 24 bits in length. The coding technique utilized a Hamming code in which 6 additional parity check bits were added to the 24 data bits increasing the coded word length to 30 symbols. In addition, two more symbols were added to increase transition density to make each transmitted word a total of 32 symbols in length. The last coded data word in each message segment was a 24-bit check-sum word which was compared
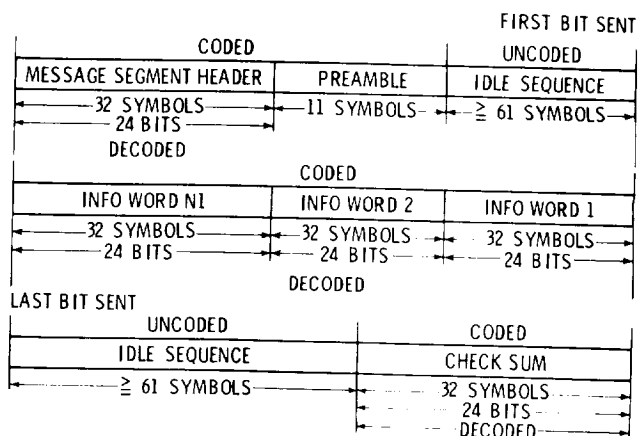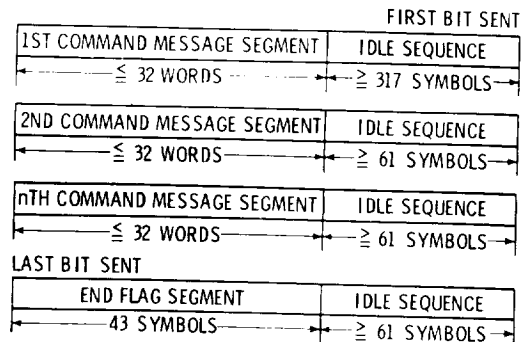
with the sum of all previously coded words in the message segment to verify overall segment parity and to identify undetected errors. The relative positions of the data, parity, and transition symbols are shown below:

```
                              UNCODED DATA WORD
                            [24    DATA BITS    1]
  LBS                                                                    FBS
                              CODED DATA WORD
  [ 32   31   30   29   28   27   26   25│ 24    DATA BITS    1 ]
     T    C    C    C    C    C    C    T │
```

T = Transition bit;   C = Parity check bit
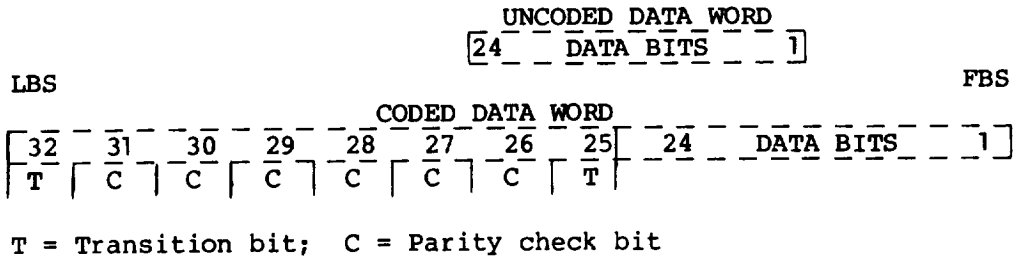
An end flag was sent at the end of a command message to signal termination of the uplink. The end flag was a unique message segment header transmitted immediately following an idle sequence and a preamble word. The end flag is coded and its bit pattern, as shown in figure 36, was different from all other legitimate headers to insure a minimum Hamming distance of 4.

MESSAGE SEGMENT HEADER WORD

BIT POSITION 1 IS SENT FIRST

```
1  2  3  4  5  6  7  8  9 10 11 12 13 14 15 16 17 18 19 20 21 22 23 24
X  X  X  X  X  X  X  X  Y  Y  Y  Y  Y  Y  Y  Y  Y  Y  0  W  W  W  W  W
|-------- LANDER --------|-------- COMPUTER --------|---- WORD ----|
         ADDRESS                 INSTRUCTIONS            COUNT

                                                        TWO'S
                                                     COMPLEMENT
```

| 0 | 1 | 1 | 0 | 1 | 0 | 0 | 0 |
LANDER A ADDRESS

| 0 | 0 | 0 | 1 | 0 | 1 | 1 | 0 |
LANDER B ADDRESS

| 1 | 0 | 0 | 0 | 0 | 0 | 0 | 1 |
LANDER C ADDRESS

The addresses are representative and do not indicate actual addresses.

1 WORD	1	1	1	1	1
2 WORDS	0	1	1	1	1
3 WORDS	1	0	1	1	1
4 WORDS	0	0	1	1	1
5 WORDS	1	1	0	1	1
30 WORDS	0	1	0	0	0
31 WORDS	1	0	0	0	0

END FLAG

BIT POSITION 1 SENT FIRST

```
1  2  3  4  5  6  7  8  9 10 11 12 13 14 15 16 17 18 19 20 21 22 23 24
X  X  X  X  X  X  X  X  X  0  0  0  0  0  0  0  0  0  0  1  0  0  0  0  0
```

Figure 36.- Message segment header and end flag.

52

(3) Upon receipt of the detector lock, the decoder idle sequence search was enabled.
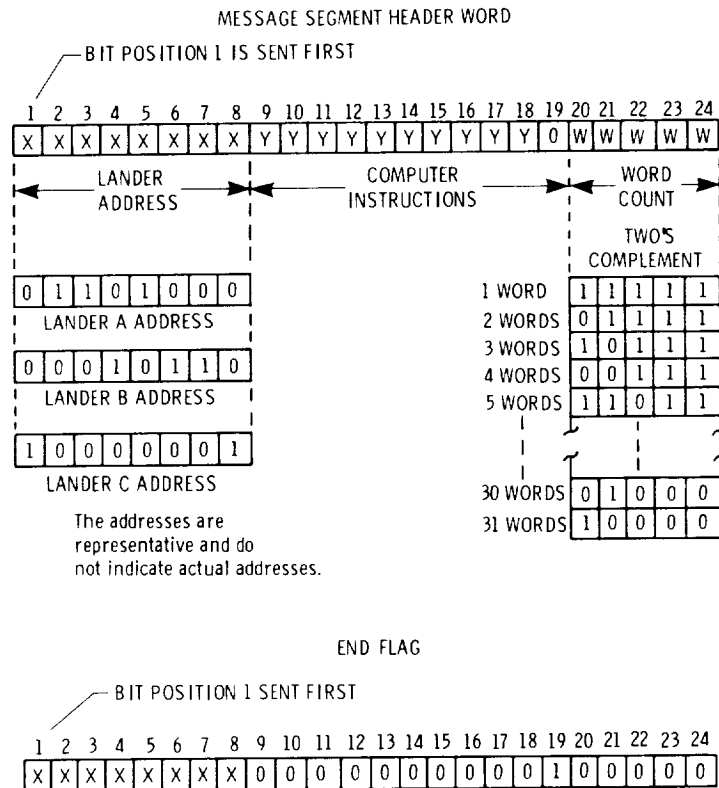
(4) When recognition of a normal preamble or its complement inhibited any further emergency decodes, the decoder enabled search for the succeeding 32 bits, which was the message segment header, with the input data being inverted if the complement of the preamble was recognized. Upon receipt of the 32 bits, the 24 bits of command data with errors corrected were sent to the GCSC. The corrected data were also recirculated within the decoder where the word count was decoded and established the number of words to follow the message segment header. The bit locations for the message segment header as well as the end flag are shown in figure 36.

(5) The command decoder continued to process the command symbols following the preamble, to supply the corrected data to the GCSC, and to count the words processed. When the word counter overflowed, the command decoder reverted to the idle search mode.

(6) If additional message segments were to be transmitted, the command uplink continued starting with at least 60 bits of idle sequence. If additional message segments were not to be transmitted or the time period between segments was long and the desire was to maintain command detector lock, idle sequence was continued until the next message segment was sent or the command uplink was terminated.

(7) If the command decoder detected an emergency command, a momentary discrete was sent to the PCDA, further searches for the emergency command were inhibited, and the command decoder reverted to the idle search mode in preparation for normal commands.

(8) If another emergency command was to be sent, the inhibit was cleared by power cycling of the command decoder or forcing the command detector to drop-lock by removing the command subcarrier modulation on the uplink for a minimum of 10 sec. Operationally the latter technique was used. The command detector lock was reestablished and the emergency command repeated.

Microwave components assembly: The purpose of the MCA was to provide rf band-pass/band-reject filtering, power splitting, rf signal separation, and switching of the DCS. The MCA consisted of a receiver filter, a hybrid junction, an rf circulator switch, and a diplexer. The functions performed by the MCA with its subassemblies interrelated as shown in the block diagram of figure 37 were as follows:

The hybrid assembly coupled the output from either of the two modulator-exciters to drive two TWTA's while isolating both modulator-exciters and TWTA's. The hybrid assembly was a four-port device with an insertion loss of 3.2 dB (tolerance, +0.2 or -0.25), isolation of 25 db, and phase balance of $\leq \pm 2^\circ$. Only one modulator-exciter and one TWTA operated at a time.

The S-band diplexer coupled signals from the HGA to receiver 2, coupled output power of the DCS to the HGA, and isolated the receiver 2 channel from the high transmitted power. Between the transmitter port and the HGA port,
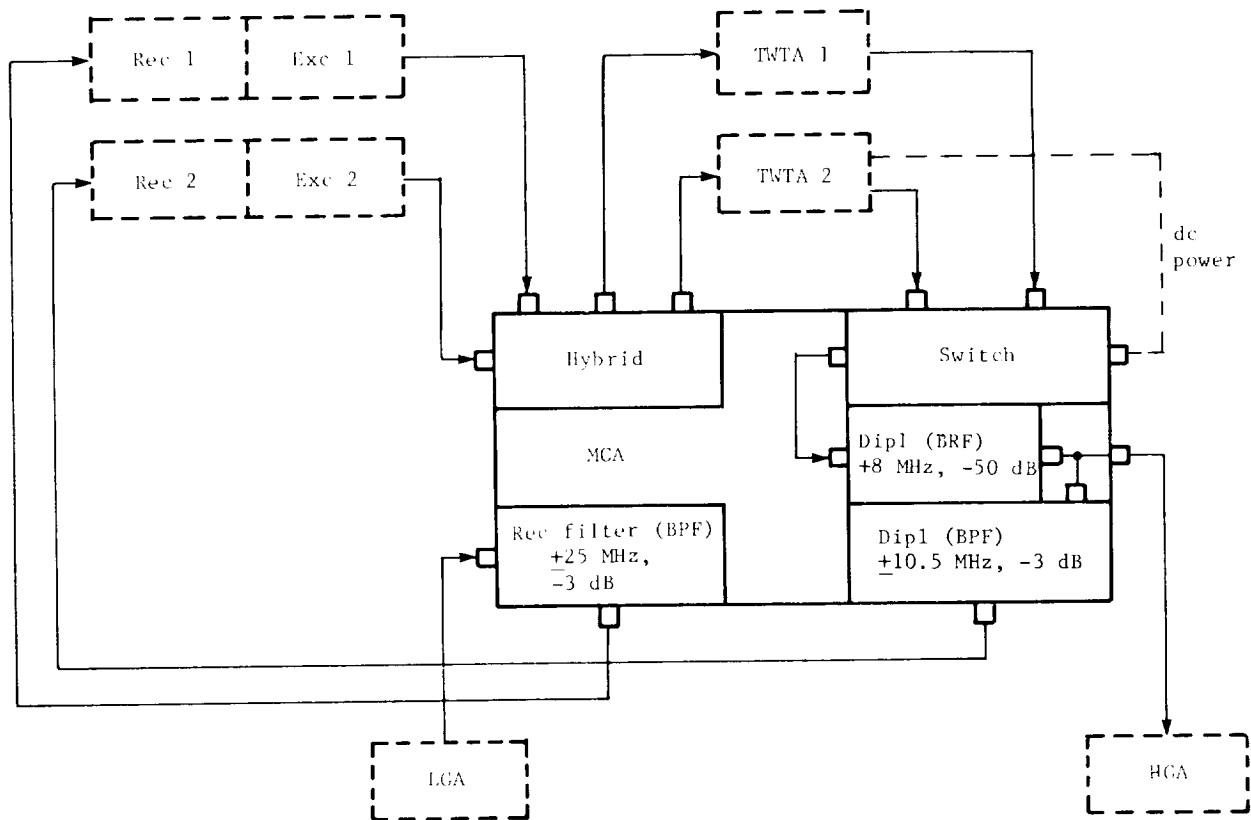
Figure 37.- Functional block diagram of MCA.

the diplexer provided a band reject response with a maximum insertion loss of 0.25 dB at the transmitter frequency and an isolation of 50 dB at the receiver frequency of ±8 MHz. Between the ports of the HGA and receiver 2, the diplexer provided a band-pass response with a maximum insertion loss of 1.2 dB at the receiver frequency and an isolation of 50 dB at the transmitter frequency.

The antenna switch automatically coupled the output power from either of the two TWTA's to the HGA. The switch contained one switchable coil which was powered from TWTA 2 such that the circulation direction was reversed when TWTA 2 was powered. The insertion loss was a maximum of 0.35 dB in either switch direction. The dc power consumption was a maximum of 7 W.

The receiver filter provided isolation from the high transmitted power for receiver 1. The receiver filter provided a band-pass response between its two ports with a maximum insertion loss of 0.4 dB at the receiver frequency and an isolation of 30 dB at the transmitter frequency.

Traveling wave-tube amplifier: The TWTA provided power amplification for the transponder modulator rf output to a level suitable for operation of the DCS downlink. The functions performed by the TWTA with its subassemblies inter-related as shown in the block diagram of figure 38 were as follows:

54

To accept the low-level output of the MCA (transponder modulator-exciter) and to amplify this signal to a nominal of 20 W

To provide signal conditioning of selected critical operating parameters to proper levels for acceptance by the DAPU

To provide operating voltage to switch the circulator switch in the MCA
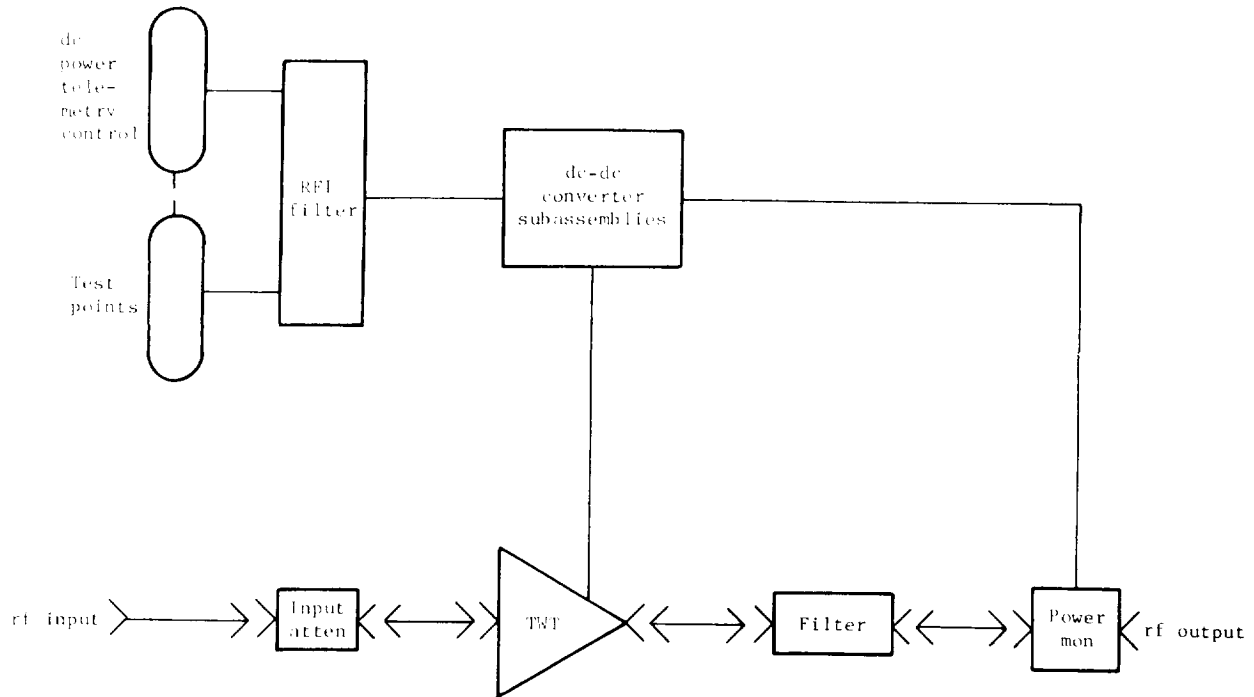
Figure 38.- Functional block diagram of TWTA.

The TWTA contained the following six major subassemblies to accomplish these functions:

Input attenuator: The input attenuator reduced the output of the MCA to the optimum drive levels for proper operation of the TWT and provided input matching of the relatively high VSWR characteristics of the TWT to 1.5:1 during TWTA operation and 1.2:1 when the TWTA is off.

TWT: The TWT provided the necessary power amplification of its input to a level that provided an output of not less than 20 W. This device was a broadband microwave tube which depended upon the interaction between the field of a wave propagated along a waveguide (helix) and a beam of electrons traveling with the wave for its operating characteristics. The electrons in the beam traveled with velocities slightly greater than that of the wave and, on the

average, were slowed by the field of the wave. The loss in kinetic energy of the electrons appeared as increased energy conveyed by the field of the wave and, therefore, acted as an amplifier.

Filter: The filter provided spectral filtering in conjunction with the MCA filtering to insure that unwanted signals were sufficiently attenuated to prevent degradation of the DCS receiver performance. This filter provided a band-reject/low-pass characteristic with an insertion loss of 0.2 dB at the transmitter frequency ±2 MHz and an isolation of 60 dB at the DCS receiver frequency.

Power monitor: The power monitor provided isolation of the TWTA output from high VSWR's and a dc analog voltage proportional to the rf output power of the TWTA.

dc-dc converter: The dc-dc converter provided conditioning of the PCDA undervoltage bus levels to voltages required to operate the TWTA. The converter consisted of an input current limiter/overcurrent protection circuit; a preregulator; a low voltage converter providing a nominal 20 V for operation of low level circuits within the TWTA; TM signal conditioning and drive for the high voltage converter; and a high voltage converter providing the high level cathode, anode, and collector voltages to the TWT. The design used the concept of battery stacking so that the highest current was at the smallest potential (collector current and voltage). The helix operated at a nominal 1600 V with respect to the cathode; the anode, at 2100 V; and the collector, at 1200 V. Included in the low voltage converter was a time delay circuit that prevented application of high voltage to allow sufficient time for TWT warm-up.

Radio frequency interference filter: The RFI filter provided interference filtering of all signals, except rf, which entered or left the TWTA to prevent unwanted signals from degrading the TWTA or DCS performance. The TWTA was sequenced on or off at preprogrammed times by the PCDA in response to commands from the GCSC. At power application, a nominal 90-sec time delay was started within the low voltage converter which inhibited the application of high voltages to the TWT and prevented TWTA power output. Telemetry measurements of TWTA collector temperature, helix currents, and power out were available in TM format 5 for providing an assessment of the functional performance of the TWTA. The switchover to the redundant TWTA, in the event this option was selected, required a ground command update to the sequence.

The application of power to the dc-dc converter was controlled by the PCDA responding to commands from the GCSC. The TWTA's were powered from the PCDA undervoltage bus with a nominal input voltage of 30 V (24 to 37 maximum). Inherent to the design of the dc-dc converter was an active current limiter/ overcurrent protection circuit which disconnected the TWTA from the PCDA bus, except for a nominal holding power, in the event the input current exceeded a nominal 5 A for 50 msec or greater. To reset the overcurrent protection circuit required power removal and reapplication. The input power requirements of the TWTA were as follows:

56

TWTA	Input power, W
1 ON	86
2 ON	87.3
1 or 2 OVERCURRENT	≈9
1 or 2 OFF	0

Transponder: The transponder, in conjunction with the HGA, LGA, and MCA, implemented the VL rf reception, turnaround ranging, and downlink rf frequency generation capability. The transponder consisted of a high-sensitivity, phase tracking, solid-state S-band receiver; a solid-state S-band modulator-exciter which phase-modulated an internally generated signal or a phase-coherent signal from the S-band receiver or a similar receiver in a redundant transponder; circuits for controlling the receiver and modulator-exciter; and integral dc-dc converters, one for the receiver and one for the modulator-exciter. The functions performed by the transponder, with its subassemblies interrelated as shown in figure 39, were as follows:
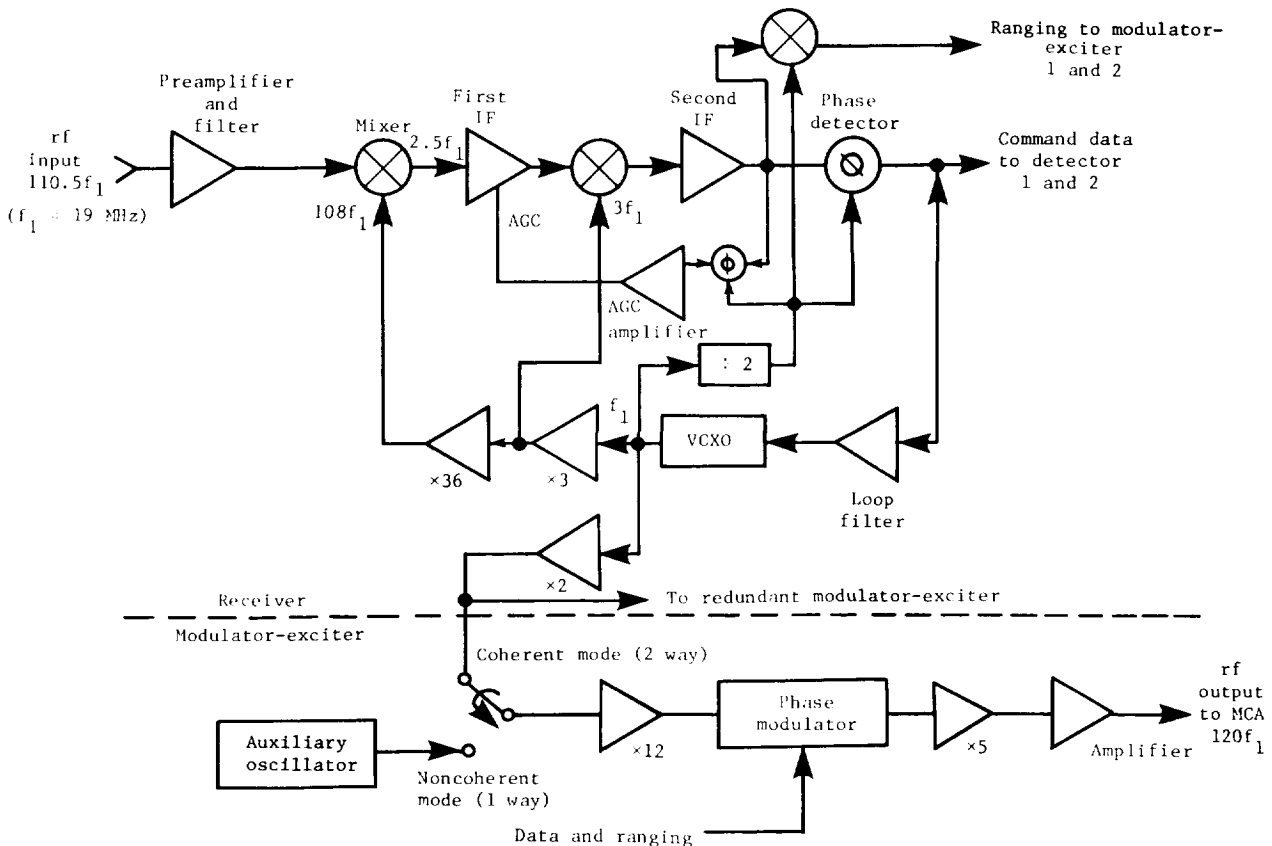

Figure 39.- Block diagram of transponder.

To receive and demodulate S-band command and ranging signals

To generate an S-band signal and to phase-modulate it with composite telemetry

57

To generate an S-band signal coherently translated by precisely 240/221 from the received signal and to phase-modulate it with composite telemetry or telemetry and the recovered ranging signal

To provide status signals to permit monitoring of transponder performance

To provide data for engineering telemetry

The receiver was a dual conversion phase-tracking design. When locked to the incoming signal it furnished the command subcarrier to each of the redundant command detector/decoders, a signal to drive its own and a redundant modulator-exciter coherently with the received carrier, the ranging signal to its own and redundant modulator-exciter, status indications to the CCU TRS and the command detector/decoders, and engineering telemetry signals to the DAPU. The significant specified electrical requirements of the receiver are given in the following table:

Frequency, MHz 2112.971451

Maximum noise figure, dB 6.5

Threshold sensitivity, dBm . . . . −153.5

Frequency stability for −
    FAT . . . . $\pm 1.3 \times 10^{-5}$
    QUAL . . . . $\pm 2.0 \times 10^{-5}$

Acquisition rate, Hz/sec 45

Tracking range from BLF for −
    Strong signal, kHz . . . . ± 126
    SWR = 6 dB, kHz . . . . ± 63

Maximum predetection noise bandwidth, kHz 5

Ranging noise bandwidth, MHz . . . . 1.5 ± 0.3

Maximum ranging delay, nsec 1000

Ranging delay variation, nsec . . . . ± 90

Command modulation index, rad 1.03

Ranging modulator index, rad 1.19

The receiver had seven major subassemblies: preselector filter, S-band preamplifier, IF/video amplifier, IF/frequency divider, VCO module, ×108 multiplier, and signal conditioner. They are discussed as follows.

The preselector filter provided bandwidth limiting and, in conjunction with filtering in the MCA and TWTA's, reduced generated spurs and harmonics to levels

sufficiently low to prevent degradation of receiver performance, primarily phase lock loop threshold.

The S-band preamplifier used high-quality, low-noise-figure, solid-state design to provide necessary amplification of the S-band signal, in conjunction with other IF amplification, to insure that proper levels were available for receiver operation. The preamplifier was the primary controlling factor of the receiver noise figure of 6.5 dB. Also included in this subassembly was the first mixer.

The first IF/video amplifier provided additional amplification of the first IF frequency, provided for AGC to insure a relatively constant input signal level to subsequent circuits over the 83-dB dynamic range of the receiver, converted the signal to approximately 9.5 MHz (second IF), and detected and limited the receiver ranging signal.

The second IF/frequency divider provided the predetection band-pass filtering; amplification, limiting, and phase detection; and division of the 19.1-MHz VCO frequency to 9.5 MHz for the phase detector and AGC coherent references.

The VCO module contained the VCXO which is phase-locked to the incoming rf signal; the phase detector loop filter; telemetry VCXO temperature sensing element; and buffers, amplifiers, and multipliers for conditioning the VCXO output for use by subsequent interval circuits as well as its own and redundant modulator-exciter.

The ×108 multiplier accepted the 19.5-MHz output from the VCXO module and multiplied, filtered, and amplified this signal to provide 2065 MHz and 57.3 MHz references for the first and second mixers, respectively.

The signal conditioner provided the necessary modification of internal signals to make them compatible with the DAPU and the command detectors/decoders. In addition, the signal conditioner provided the ranging on/off interface with the TRS.

The modulator-exciter provided the phase-modulated signals which drive the redundant TWTA's through a hybrid power splitter in the MCA. The modulator-exciter furnished a constant-amplitude S-band signal derived from an internal oscillator and modulated by two PSK square-wave subcarriers from the DAPU. It also provided a constant-amplitude S-band signal derived from either of the redundant phase-locked receivers, modulated by two PSK square-wave subcarriers or a combination of a PSK subcarrier from the DAPU and a ranging signal from redundant receiver 2. The significant specified electrical requirements of the modulator-exciter are as follows:

Frequency, MHz 2294.629630

Power output, dBm . . . . 21 (tolerance, +1.3 or -0)

Frequency stability . . . . ±2.3 × 10^{-5}

59

Modulation sensitivity for -
  Ranging off
    Science, rad . . . . ±0.80 ± 8.4%
    Engineering, rad . . . . ±0.45 ± 8.4%
  Ranging on
    Engineering, rad . . . . ±0.80 ± 8.4%
    Engineering, rad . . . . ±0.45 ± 8.4%

Incidental amplitude modulation . . . . ±2%

The modulator-exciter consisted of three subassemblies: the auxiliary oscillator/×12 multiplier, the phase modulator/×5 multiplier, and the power amplifier. The auxiliary oscillator/×12 multiplier accepted the 38.2-MHz VCXO input from its own or redundant receiver based on the system status; it multiplied, amplified, and filtered this signal and supplied it to the phase modulator/×5 multiplier. This unit also contained an AO that could be used for rf-signal drive to the phase modulator/×5 multiplier during the time periods that the receivers were not in-lock and it contained the necessary logic to select rf drive from its own or redundant receiver based on status signals from the receivers and commands from the TRS. The phase modulator/×5 multiplier phase-modulated the 458.9-MHz signal from the AO/×12 multiplier and amplified and limited the signal to the 2294.6-MHz downlink frequency which drove the S-band power amplifier. This subassembly also contained the logic necessary to inhibit the science subcarrier, to enable ranging modulation from receiver 2, and to change the engineering subcarrier modulation index from 0.45 to 0.80 rad in response to the ranging on control signal from receiver 2. The power amplifier contained a solid-state distributed constant amplifier that generated the 21-dBm output power telemetry interface circuit and a status signal supplied to the TRS that was high as long as the unit output power stayed greater than 18.0 dBm.

The transponder had the capability of selecting its own VCXO/AO or the redundant receivers VCXO, depending on the state of receiver lock, cross-strap, and transfer to VCXO commands. Operation in the AO mode was character-ized as the one-way mode since it did not require an uplink signal and the down-link frequency was not precisely related to the uplink frequency. Operation in the VCXO mode, when the VCXO was phase-locked, was characterized as the two-way mode. The downlink frequency in this mode was precisely related to the uplink frequency and was used for accurate Doppler determination. During ranging mea-surements, the ranging receiver (receiver 2) detected the transmitted ranging signal at base band (two-way operation was required) and modulated the rf down-link with a limited version of this signal. To enter this mode of operation required that receiver 2 be phase-locked to the uplink signal and that receiver 2 and the operating modulator-exciter be sent a ranging on command by the GCSC via the TRS serial command interface. Modulation-exciter 2 supplied a feedback sig-nal to the DAPU via receiver 2; thus, a status indication was provided for telem-etry that ranging was on. If modulator-exciter 1 was on, no indication on telemetry was available to indicate the ranging status. The application of power to the dc-dc converters of the transponder receiver and modulator-exciter was controlled by commands from the GCSC to the PCDA. The receivers were powered by the PCDA equipment bus; modulator-exciters were powered from the undervoltage

60

bus. The nominal input voltage was 30 V (24 to 37 maximum). This voltage was converted to the levels required by the transponder electronics. Inherent in the design of each power supply was an overcurrent protection circuit that would latch the output off if the input current exceeded a predetermined level for 200 msec maximum. The resetting of this latch could only be accomplished by cycling input power. The power consumption levels were as follows:

Receiver	Modulator-exciter	Power, W
Off	Off	0
On, locked	Off	3.4
On, locked, ranging	On	7.6

S-band low-gain antenna.- The S-band LGA was the primary rf uplink path between the VL and the DSN for command purposes. The functions of the LGA were to provide an approximately hemispherical radiation pattern about the negative X-axis of the VL, to receive rf energy transmitted by the DSN stations, and to supply the rf energy to the MCA for subsequent detection by receiver 1. The LGA was a right-hand, circularly polarized, eight-element, crossed dipole above a tuned ground plane. The gain as specified through any planar cut containing the axis of the antenna is plotted in figure 40. The required axial ratio is
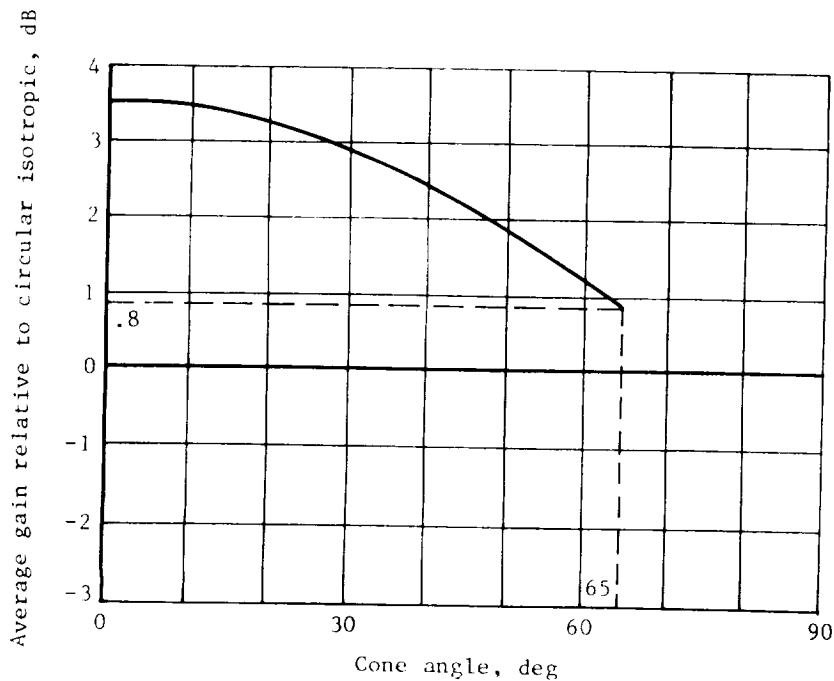
Figure 40.- Free-space radiation pattern of DCS LGA.

shown in figure 41. This mode of radiation pattern could not be obtained with the usual planar arrangement of a turnstile antenna of crossed dipoles over a
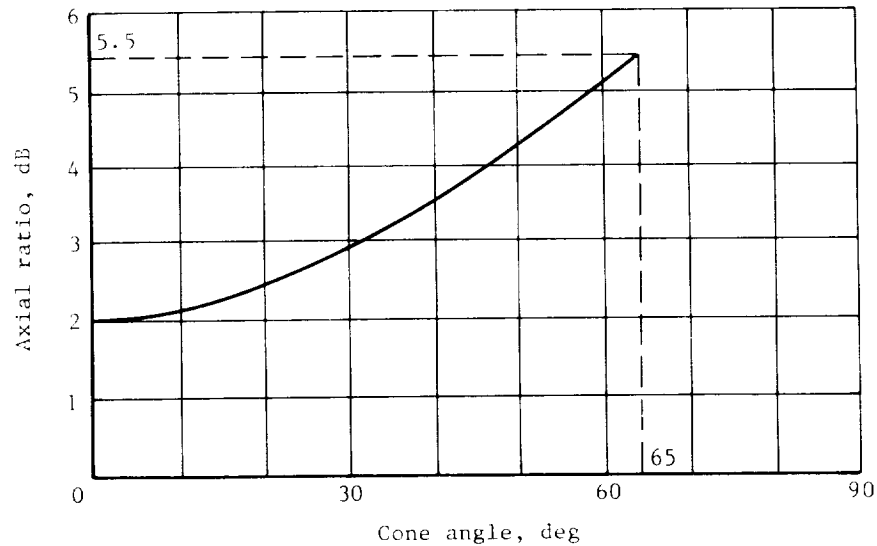

Figure 41.- Free-space axial ratio characteristics of DCS LGA.

ground screen or crossed slots in a conducting plane since they supplied only a radial mode of radiation. An additional mode of radiation was required which basically consisted of a doughnut shape with its null along the axis of symmetry of the antenna. Additional dipole elements depressed by a selected angle below the normal dipole elements were incorporated in the LGA design to obtain these two modes. The desired radiation characteristics in the upper hemisphere were achieved by proper choice of the lengths and inclination angles of the radiating elements and their heights above the ground plane. The geometry and dimensions of the grid wire ground plane configuration, having a maximum size less than 1/2 wavelength, were chosen such that suppression of the backward radiation was greater than would be obtained with a much larger continuous sheet.

S-band high-gain antenna.- The S-band HGA provided a steerable narrow beam radiation pattern characteristic used to transmit S-band VL downlink data and to receive S-band rf energy transmitted by the DSN for ranging and uplink commanding. The functions of the HGA were as follows:

To rotate about two mechanical axes by using an elevation over azimuth mount with the elevation axis parallel to the VL X-Y plane and the azimuth axis perpendicular to the Y-Z plane. Brushless, dc, four-phase stepping motors geared down by 1193.400197:1 in each axis were used to drive these axes. The antenna was prevented from moving when no power was applied to the motors by an integral magnetic detent. The movement capability of the antenna in elevation was from -22° to 92° and in azimuth from -338° to 338° from a point 45° clockwise from leg 1 (negative Z-axis) of the VL. The maximum stepping rate was 0.495823 deg/sec in either axis.

62

To radiate to and receive from the DSN stations by using a nominal 76.2-cm-diameter (30 in.) parabolic reflector with a cup helix phase center feed. The HGA was right-hand circularly polarized dipole with a minimum boresight gain of 21.0 dB at both the receiver and transmitter frequencies. At the transmitter frequency, the axial ratio did not exceed 1.7 dB on boresight and 3.0 dB at 5° off boresight. At the receiver frequency, the axial ratio did not exceed 4.0 dB at up to 5° off boresight.

To provide a nominal 55.88-cm (22.00-in.) mast (referenced from the elevation axis), which was used to mount the HGA on the VL. Integral to the mast was an rf transmission line which was used to provide the rf input interface with the VL cabling at the base of the mast.

To receive from and provide to the CCU resolver signals that were used for telemetry readout of the HGA position. The azimuth resolver was geared down by 1.89401:1 to provide a unique HGA azimuth readout over the 676° of azimuth travel. The azimuth zero reference was the negative Z-axis and the elevation zero reference is parallel to the Y-Z plane (horizontal).

The HGA operated in two modes: slew and holding. In the slew mode, the HGA stepping rate and direction were controlled by commands from the GCSC to the HGAC. The HGAC logic determined the type of command (azimuth or elevation) and its direction and outputted a series of four pulses to the selected axis in the correct sequence to cause clockwise or counterclockwise rotation of the HGA stepping motor. The antenna motor is indexed to a known position at assembly as shown in sketch (a). If the desire was to slew in the clockwise direction the motor phases were energized in a 1-2-3-4 sequence and counterclockwise rotation would be a 3-2-1-4 sequence. The rise/fall times of the current pulses as well as magnitude were controlled by a current limiter in the HGAC to insure proper accelerations of the HGA and proper torque values. The sequence of pulses was selected by motor phase switches. The current pulse width and dwell time between pulses were 55 ± 6 msec to insure reliable stepping and to allow for overshoot settling between pulses. During the dwell time between pulses or when it was not desired to slew the HGA, the pointing position was maintained by a magnetic detent within the motor. The value of magnetic holding torque design was such that it was sufficient to prevent antenna movement with 70 m/sec (230 ft/sec) design surface winds.
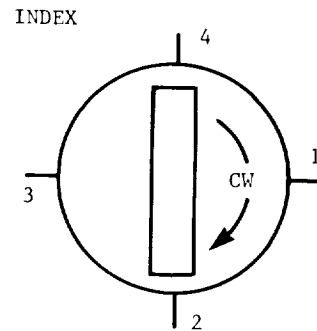
Sketch (a)

Guidance and Control Subsystem

The guidance and control subsystem provided navigation, guidance, and attitude control for the Viking lander from separation of the lander from the orbiter to landing on the surface of Mars. The subsystem is described in two sections; the first section discusses the philosophy, rationale, and implementation of the subsystem design and the second section discusses the subsystem hardware and software. The approach to redundancy is also discussed in the second section.

Subsystem Design Concept

The guidance and control subsystem design concept was strongly influenced by the general requirement to soft-land on the surface of Mars coupled with the environmental constraints derived from the best available pre-Viking Mars data. These data comprised a pre-Viking model of Mars and served as the basis for the derivation of design requirements. The model provided peak values, ranges, and statistics of such G&C critical items as atmosphere, surface slope, craters, and lower atmospheric wind. Obviously, there was a close tie between the trajectory design and the G&C subsystem design. Many of the G&C design requirements were defined by the trajectory design in the process of providing the capability to target the lander to a particular landing site. A statistical approach was used in the G&C design. The probability of meeting each individual requirement had to be at least 0.99; this probability was established in terms of technical feasibility, affordable in terms of dollars, and acceptable in terms of risk. Therefore, numbers presented herein were often referred to as 99-percent numbers as opposed to 3σ or stacked worst-case numbers. The 0.99 probability was equal to 2.58σ for a single dimension probability function. There were a few exceptions to this statistical approach and one of these exceptions was extremely significant. As established by a Project Ground Rule, all atmospheric models were considered equally probable, and, further, each requirement was to meet the 99-percent criterion in the atmosphere that represents the worst case for that particular requirement.

The subsystem design concept is discussed in the order of the descent sequence of events. (Refer to fig. 42.) A few hours prior to separation of the lander from the orbiter, the inertial reference unit (gyroscopes and accelerometers) was calibrated in preparation for the descent. A few seconds prior to lander separation, the lander attitude reference was initialized. After lander separation, the attitude control loops were closed and an attitude maneuver was performed to provide the required orientation for the deorbit impulse. Deorbit velocity steering and thrust modulation guidance was implemented in the celestial frame. The 22-min propulsive burn changed the lander from orbit to the descent trajectory. Attitude hold was maintained during the 2 1/2-hr coast from deorbit to atmospheric entry. At entry (243.8 km (800 000 ft)), navigation was initiated in the Mars local vertical frame. Upon sensing Mars atmosphere encounter, pitch and yaw rate damping control was initiated and the navigator was updated by altimeter data during the aeroshell entry. At an altitude of 6 km (19 500 ft) above the Mars surface, the parachute was deployed and seconds later the aeroshell was jettisoned. The navigator was updated by velocity radar data during the parachute descent. At an altitude of 1.4 km (4600 ft), the terminal engines were ignited and 2 sec later the parachute was released. Gravity turn guidance was implemented during the propulsive descent to the Mars surface.

Inertial reference unit calibration.- The IRU was calibrated at the supplier's plant prior to installation in the lander. Approximately 18 months elapsed between the calibration and the Mars landing. During this period, the IRU was exposed to the high temperatures required for lander sterilization, the launch environment, and the cold-vacuum environment of interplanetary space. Therefore, in-flight calibration of the IRU was necessary to obtain the required accuracy. The first in-flight calibration was performed during interplanetary cruise and a second calibration was performed while orbiting Mars. The first
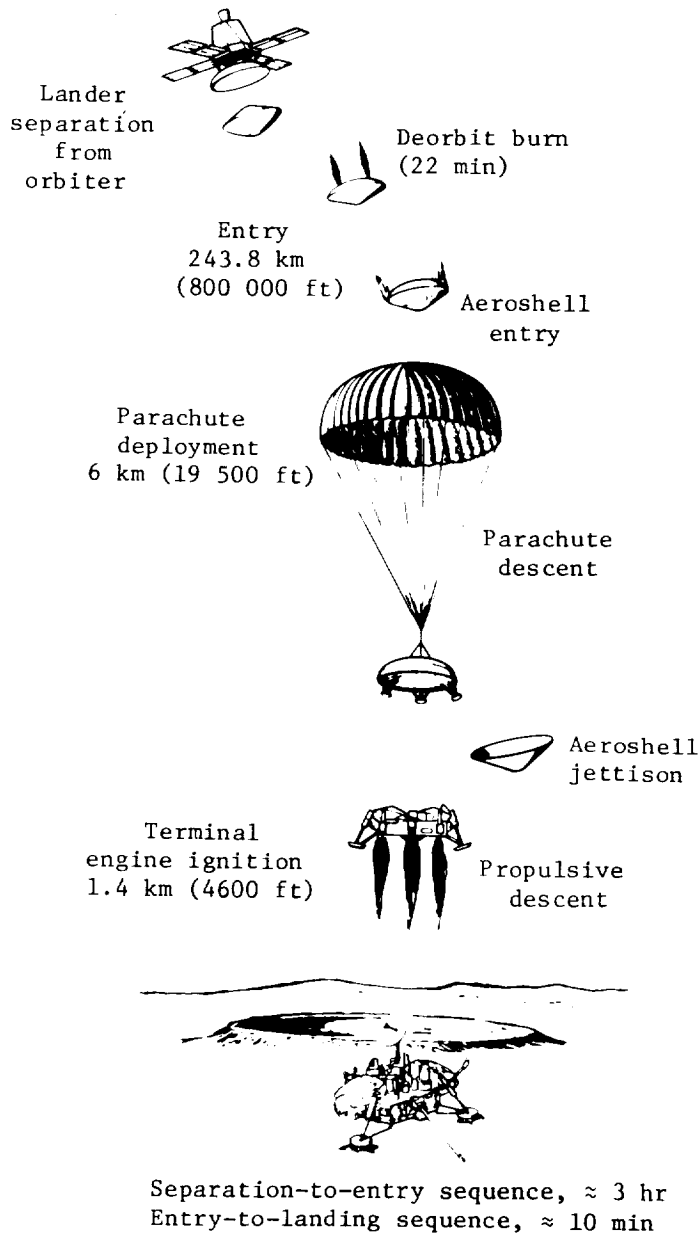
Figure 42.- Lander descent sequence.

calibration provided an in-space reference for the final calibration and also provided a final checkout of the Earth-based calibration software. The parameters provided by the in-flight calibration were gyroscope bias (g-insensitive drift) and accelerometer bias. The flight program residing in the lander's computer (GCSC) compensated the IRU outputs for the known bias errors. Gyroscope and accelerometer scale-factor corrections were also implemented in the flight program. The scale factors used by the computer were obtained from the prelaunch calibration performed at the supplier's facilities. The flight program did not compensate for gyroscope g-sensitive drift and higher order terms

during entry and descent since analyses and simulations showed negligible mission impact; the time from encounter of the Mars atmosphere, and, thus, its aerodynamic vibrational and decelerating environment, to Mars landing was only approximately 10 min. The g-sensitive drifts were corrected by the flight program during postlanded antenna pointing calculations.

Gyroscope in-flight calibration.- The Earth-based calibration software received orbiter celestial sensor data (Sun sensors and star tracker) along with simultaneous lander gyroscope data. The two sets of data were time tagged to permit the calibration software to filter out orbiter angular motions and derive the gyroscope biases. The calibration time was 90 min and the calibration accuracy was approximately 0.9 mrad/hr.

Accelerometer in-flight calibration.- The accelerometers were calibrated during the same time period as the gyroscopes by using Earth-based calibration software. However, unlike the gyroscopes, the accelerometers required an additional calibration after final application of power to the IRU. During development and qualification testing of the accelerometers, it was discovered that significant bias shifts occurred if the accelerometers were allowed to cool from their operating temperature of 71° C (150° F) to the in-orbit ambient temperature of approximately 0° C (32° F). For power management reasons, the in-orbit IRU calibration was scheduled approximately 28 hr prior to separation of the lander from the orbiter. After calibration, IRU power was turned off and the lander batteries were recharged. The IRU cooled to approximately 0° C before power was restored in preparation for lander separation. Thus, an autonomous accelerometer calibration routine was required in the lander computer. Because of flight software design constraints, this calibration was performed immediately after lander separation instead of immediately prior to lander separation. The postseparation accelerometer calibration is described in a later section.

Attitude initialization.- A few seconds prior to separation of the lander from the orbiter, the attitude reference in the GCSC was initialized and attitude computations were initiated. The initial value of the attitude matrix was identity. Thus, lander attitude computations were performed relative to the celestial reference frame defined by the orientation of the orbiter at the time of initialization (nominally the Sun-Canopus reference). The errors associated with initialization of the attitude reference are summarized in table 2 where the uncertainty of the knowledge of the indicated parameters is shown. The known component of errors was accounted for in the trajectory design process. A principal example of the above is as follows. The axes of the gyroscopes in the lander IRU defined the lander body axes. There were alignment errors between the lander gyro reference frame and the VO Sun-Canopus reference frame such as gyro to gyro othogonality, gyro to IRU case misalignments, and IRU case to lander structure misalignments. Each of these misalignments was measured and/or computed at some phase of component or spacecraft assembly. Thus, there was a known value, plus a measurement and/or computation uncertainty. The uncertainty component of the error was considered in the error analyses. The known component of the error could be accounted for in the initial value of the attitude matrix stored in the computer (GCSC) but this required a different initial attitude matrix for each of the two landers and further complicated the configuration control of the critical flight programs. Therefore, the initial attitude matrix was identity and compensation for the

TABLE 2.- ATTITUDE INITIALIZATION UNCERTAINTY

Error source	Distribution statistics	3σ predicted value, mrad	
		Pitch or yaw	Roll
Orbiter celestial sensor alignment, bias, and offset	Normal	5.93	4.19
Orbiter limit cycle	Uniform	8.38	8.73
Orbiter roll gyro drift	Normal	-----	8.20
Lander/orbiter mechnical alignment	Normal	4.36	4.36
Total uncertainties RSS (3σ) 99% (2.58σ)		11.15 9.59	13.42 11.54

known component of the error was provided by the trajectory design. For this example, the specified pointing direction of the deorbit impulse was adjusted to account for the known component of the misalignment errors.

The orbiter roll gyroscope drift shown in table 2 was an error source since the orbiter switched from the star tracker to the gyroscope for roll axis attitude sensing approximately 3 hr prior to separation of the lander from the orbiter. The gyroscope was used to avoid the possibility of the star tracker detecting and tracking a stray light source (e.g., an illuminated particle) and, thus, causing the orbiter to be off the required celestial reference at the time of lander attitude initialization.

Separation.- A few seconds prior to separation of the lander from the orbiter, both attitude and velocity computations were initiated by the lander computer (GCSC). The initial attitude reference was identity and the initial velocities were zero.

The lander/orbiter separation mechanism imparted angular rates and ΔV to the lander. The separation ΔV could be as large as 0.3 m/sec (1.0 ft/sec) on a 0.99-probability basis. This linear motion was sensed by the three accelerometers of the IRU and the velocity routine resident in the flight software accumulated the body axis components of ΔV and transformed them to celestial coordinates. These values of velocity were stored in the computer for use during deorbit.

Since attitude control had not been initiated, the lander rotated slowly at the separation tip-off rate (99-percent tip-off rate is 14 mrad/sec per axis). The angular motion was sensed by the three gyroscopes of the IRU, and the attitude routine of the computer kept track of the lander orientation relative to the celestial reference frame. The attitude routine was an incremental integration of a direction cosine matrix with orthonormality correction terms. The formulation for the second column of the attitude matrix [A] is as follows:

$$
\begin{bmatrix} A_{12} \\ A_{22} \\ A_{32} \end{bmatrix}_n = \begin{bmatrix} 1 & \Delta\theta_Z & -\Delta\theta_Y \\ -\Delta\theta_Z & 1 & \Delta\theta_X \\ \Delta\theta_Y & -\Delta\theta_X & 1 \end{bmatrix} \begin{bmatrix} A_{12} \\ A_{22} \\ A_{32} \end{bmatrix}_{n-1} + E_{c2} \begin{bmatrix} A_{12} \\ A_{22} \\ A_{32} \end{bmatrix}_{n-1} - E_{c23} \begin{bmatrix} A_{13} \\ A_{23} \\ A_{33} \end{bmatrix}_{n-1}
$$

where $\Delta\theta_X$, $\Delta\theta_Y$, and $\Delta\theta_Z$ are the incremental angles obtained directly from the IRU gyroscopes and E_{c2} and E_{c23}, the orthonormality correction coefficients, are

$$
E_{c2} = 0.5\left[1 - \left(A_{12}^2 + A_{22}^2 + A_{32}^2\right)\right]
$$

$$
E_{c23} = 0.5(A_{12}A_{13} + A_{22}A_{23} + A_{32}A_{33})
$$

The third column is computed similarly and the first column is obtained from the cross product of the previously computed elements. The IRU output was sampled every 20 msec and the attitude matrix $[A]$ was also updated every 20 msec. The orthonormality correction coefficients were updated at 1-sec intervals. The 24-bit word length of the computer, coupled with the 20-msec update interval provides an A-matrix drift rate of approximately 1.8 mrad/hr during 99 percent of the descent trajectory. Maximum angular rates prior to parachute deployment were between 18 and 35 mrad/sec (1 to 2 deg/sec). At parachute deployment, angular rates increased significantly but this increase could be accepted due to the short time from this event to touchdown (parachute deployment to touchdown time equaled approximately 2 min).

Postseparation accelerometer calibration.- After separation of the lander from the orbiter and prior to initiation of attitude control thrust disturbances, a quiet period of approximately 4 min was provided for accelerometer bias calibration. The calibration routine simply computed a time average of the accelerometer outputs. The resulting bias coefficients replaced those previously stored in the computer memory and were used to compensate all future accelerometer outputs.

The accuracy of the calibration was approximately $10^{-5}g$ ($1g = 9.8$ m/sec^2) without disturbances. The only significant disturbance was the centripetal acceleration produced by the separation tip-off angular rates. The IRU case was located on the Z-axis of the lander about 0.9 m (3 ft) from the center of gravity. Thus, the centripetal acceleration ($\omega^2 r$) sensed by the Z-axis accelerometer for the 99-percent tip-off rate of 14 mrad/sec equaled 18 $\times$ 10^{-6}g. Similarly, the centripetal acceleration sensed by X- and Y-axis accelerometers was negligible. The potential Z-axis calibration error was small; therefore, the accelerometer calibration routine did not contain a gyroscope feedback loop to remove the centripetal acceleration error from the computation of bias. The error was considered in the error analyses.

Attitude maneuver.- After completion of the accelerometer bias calibration, the attitude control loop was closed and an attitude maneuver was initiated to

68

orient the lander for the forthcoming deorbit impulse. The technique for generating attitude maneuver commands was as follows. An attitude matrix was derived which defined the desired lander orientation relative to the original celestial reference frame. This desired matrix was stored in the computer prior to separation. Given the desired matrix $[A_d]$ and the current value of the true attitude matrix $[A]$, an error matrix $[\Delta A]$ was computed as follows:

$$[\Delta A] = [A][A_d]^T$$

where T indicates matrix transpose. The off-diagonal elements of $[\Delta A]$ represented small angle approximations to roll, pitch, and yaw attitude errors as follows:

Roll error: $\phi_e = 0.5(\Delta A_{23} - \Delta A_{32})$

Pitch error: $\theta_e = 0.5(\Delta A_{31} - \Delta A_{13})$

Yaw error: $\psi_e = 0.5(\Delta A_{12} - \Delta A_{21})$

This technique was used for all attitude maneuvers performed prior to entry into the Mars atmosphere. Each maneuver was defined by a prestored desired matrix $[A_{d,i}]$ and was called at a predesignated time by the sequencing part of the flight software. The technique always commanded a maneuver of less than 180° and the maneuver occurred simultaneously about all three lander body axes; thus, maneuver time was minimized. Also, the lander was allowed to drift in an uncontrolled state as long as the true attitude matrix $[A]$ was computed; the lander returned to the desired orientation $[A_d]$ when the attitude control loop was closed.

Attitude control.- Attitude control commands were generated within the attitude control logic routine. The commands were computed and transmitted to the VDA at 20-msec intervals. The VDA controlled the on/off state of the 24 solenoid valves associated with the 12 monopropellant engines of the RCS. The engines were commanded in pairs and each engine had series solenoid valves. The resulting redundancy insured that attitude control capability was maintained and that the propellant supply was not exhausted for any single engine or solenoid valve failure. (Refer to the sections "Propulsion Subsystem" and the "Valve drive amplifier" for a more detailed description.) The attitude control logic was digital and was implemented as a series of discrete threshold tests within the computer. The logic for a single control axis is sketched in the phase-plane format in figure 43. As stated previously, after completion of the accelerometer bias calibration, attitude control was initiated. Prior to closing the attitude control loops the computer issued an 80-msec command pulse to all 12 engines simultaneously. Thermal soak-back from the 80-msec on pulse warmed the engines above the minimum operating temperature. At the elevated temperature, the chemical transport lag and thrust response time was compatible
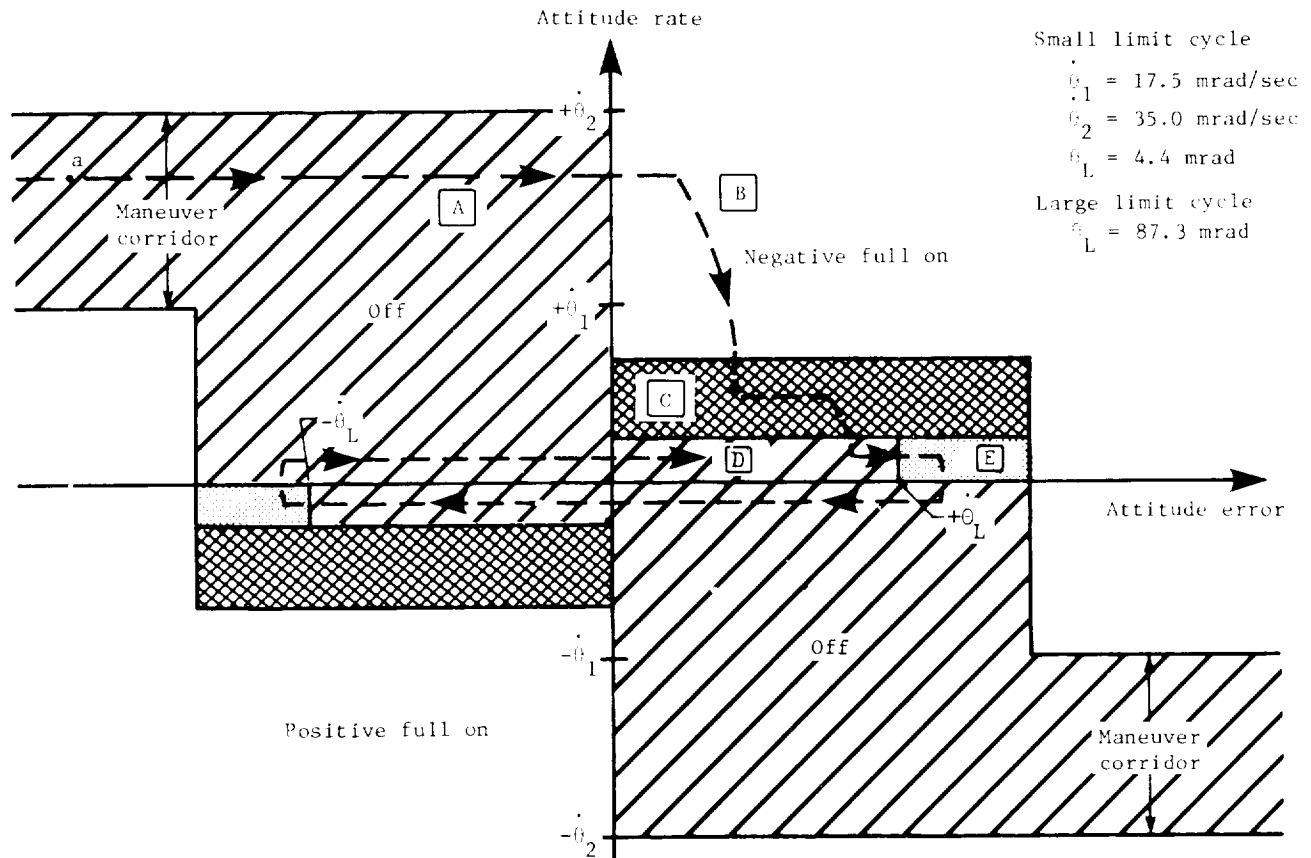
69

Figure 43.- Attitude control logic.

with the switching thresholds of the attitude control logic design. At closure of the attitude control loops, the maneuver to the deorbit orientation was begun by using the attitude errors derived from knowledge of the true attitude matrix and the desired matrix. Thus, all three axes (assuming a three-axis maneuver was being performed) were accelerated into their respective maneuver corridors. The maneuver rate lower boundary is set at 1 deg/sec and the maneuver rate upper boundary is set at 2 deg/sec. The actual maneuver rate may be anywhere between these boundaries due to variation in engine response characteristics and cross coupling between control axes. Thus, a maneuver of 180° required at least 1 1/2 min for completion but was always completed in less than 3 min. While in the maneuver corridor the engines were off and the lander rotated at a constant angular rate. To insure that the engines remained above the minimum operating temperature, the computer kept track of the number of 20-msec pulses issued to each engine. If the number of pulses was less than 4 (4 pulses = 80 msec) in a 70-sec period, the computer issued commands to the engine (and the opposing reaction engine) to make up the deficiency. This pro-

70

cess was called thermal pulsing and was continued until the lander entered the Mars atmosphere.

Figure 43 shows a typical convergence from an attitude maneuver to limit cycle operation for a single axis. At point a in region A, the lander was rotating at a constant rate and the engines were off. Upon entering region B, the engines were commanded full on and, after a response delay, the parabolic deceleration began. Region C was allocated for slowdown. The engines were alternately pulsed on and off. The on-off times were selected to prevent overshoot of region D because of normal transport lag and thrust decay tolerances and thrust level variations due to tank pressure blowdown. Region D was an engines off, constant angular rate, region. Upon entering region E, a single 20-msec pulse was issued. If, after a specified time, the angular rate had not gone through zero, a second 20-msec pulse was issued. This completed convergence. The logic was designed to achieve limit cycle convergence in one phase-plane cycle and to maintain a single pulse limit cycle with no disturbance torques. Limit cycle capability was maintained under 99-percent disturbance torque conditions, but double pulsing occurred.

The attitude control logic had two configurations, one for small limit cycle operation and a second for large limit cycle operation. The only difference between the two configurations was the thresholds of the attitude error switching lines. The small limit cycle had an attitude dead band of $\pm 0.25^\circ$ and the large limit cycle had an attitude dead band of $\pm 5.0^\circ$. The large limit cycle was used during attitude maneuvers to conserve fuel. The small limit cycle was enabled when all three axes had converged to within 10° of the desired attitude. Inertial coupling caused excessive pulsing if the small limit cycle was retained and one or two axes converged faster than the third. The excessive pulsing occurred about the axes that converged first. The large limit cycle was also used during periods where control of orientation was not critical. These periods are discussed later.

Because of structural design and mechanical layout constraints, the RCS control axes were not coincident with the lander body axes. The pitch and yaw engine axes were rotated 45° with respect to the pitch and yaw body axes. The roll axes are coincident. Therefore, a fixed transformation was included in the attitude control routine for the purpose of transforming the angular motion sensed by the IRU and the computed attitude errors from the body axes to the RCS coordinates.

Deorbit.- After completion of the attitude maneuver and at a predesignated time (approximately 7 min after lander separation) the computer enabled the deorbit routine. The deorbit maneuver consisted of a long duration engine burn which provided a lander velocity change ΔV of 156 m/sec (512 ft/sec). The deorbit ΔV established the descent trajectory as illustrated in figure 44. The accuracy with which the burn was performed determined the success of the Mars atmospheric entry and the capability to land at the selected site.
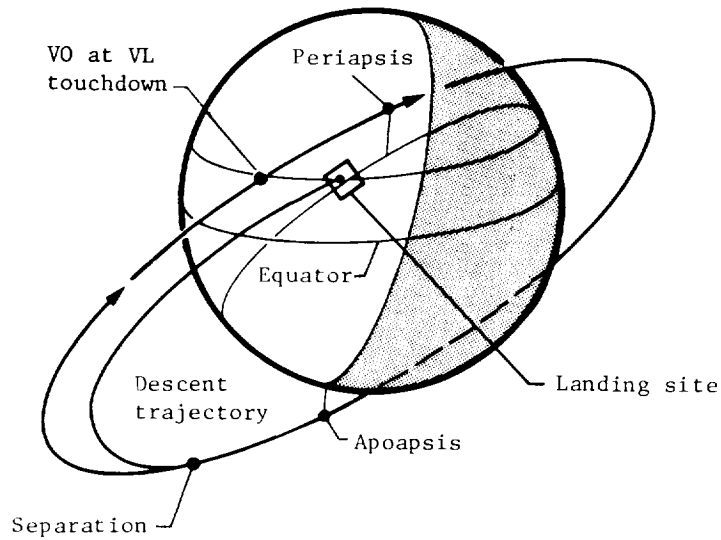
Figure 44.- Deorbit and landing geometry.

A critical parameter in the trajectory design was entry angle γ_E which was defined as the lander flight-path angle at an altitude of 243.8 km (800 000 ft) as shown in figure 45. The allowable range of entry angle was
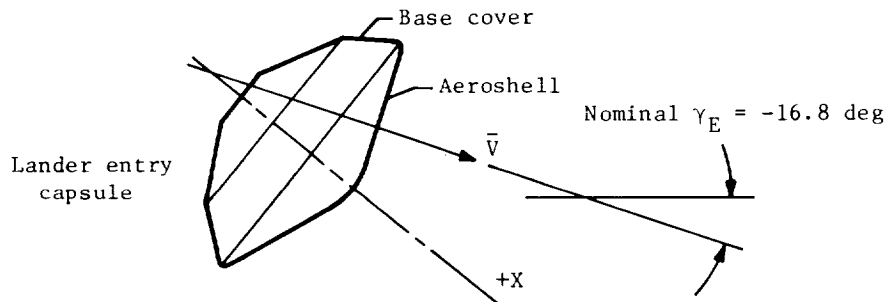
Figure 45.- Definition of entry flight-path angle.

-15.9° to -17.7°; this range was called the entry corridor. Entry angles shallower than -15.9° would create excessive aeroshell dynamic pressure during entry through the Mars atmosphere and would approach the skipout limit (skipout would place the lander back in orbit). Entry angles steeper than -17.7° would create excessive aeroshell thermal stresses and excessive dynamic pressure at parachute deployment.

The portion of the entry corridor that was allocated for targeting the lander to a specified landing site was further constrained by entry-angle dispersions. Entry-angle dispersions due to deorbit execution errors were defined via standard linearized statistical error analysis techniques. There were two

major sources of the deorbit execution error. The first was the attitude initialization error and the second was the IRU performance tolerances. The attitude initialization error was previously discussed and the errors were summarized in table 2. Attitude initialization was the dominant error with respect to ΔV pointing accuracy. The IRU error coefficients are summarized in table 3.

TABLE 3.- IRU ERROR COEFFICIENTS

Parameter	Error coefficients for 0.99 probability
Gyroscopes:	
Bias stability, deg/hr	0.3
g-sensitive drift, deg/hr	2.0
g^2-sensitive drift, deg/hr	0.2
Scale factor,[a] ppm (percent)	400 (0.04)
Axis orthogonality, mrad (arc-min) . . .	0.9 (3)
Accelerometers:	
Bias stability, g units	10^{-4}
Scale factor,[a] ppm (percent)	250 (0.025)
Axis orthogonality, mrad (arc-min) . . .	0.9 (3)

[a]Scale factor is the statistical combination of stability, nonlinearity, and asymmetry.

These IRU performance tolerances contributed to both ΔV magnitude and ΔV pointing errors. However, the dominant parameter was the X-axis accelerometer bias which introduced ΔV magnitude error. The results of the deorbit error analysis in terms of ΔV magnitude error and ΔV pointing error are shown in figure 46 where the 0.99-probability level is a contour on the surface of a 3.4σ error ellipsoid. Propagation of these results along the trajectory to the entry point (243.8 km) yielded a 99-percent entry-angle dispersion of 0.29°. Entry-angle dispersion was also caused by orbit determination error (the orbit from which the lander descended). However, this error propagated to a 99-percent entry-angle error of only 0.026° and was, thus, statistically negligible.

Figure 47 shows the relation *between entry angle and targeting* flexibility in terms of downrange and crossrange angles. The downrange and crossrange targeting angles are defined in figure 48. Thus, if ±0.3° for entry-
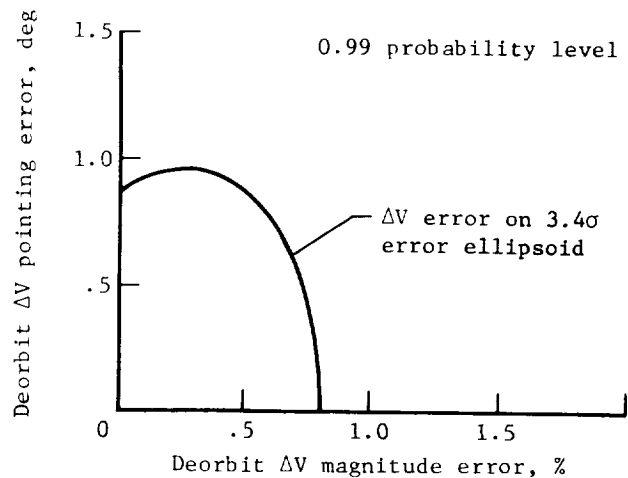
Figure 46.- Results of deorbit error analysis.
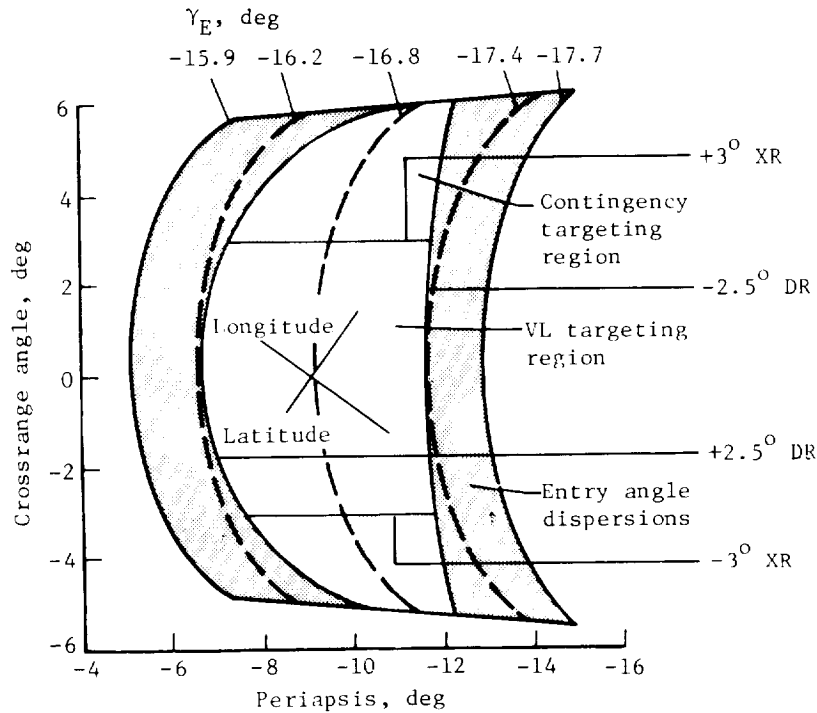
Figure 47.- Entry corridor allocation.

angle dispersions was allowed, the entry-angle corridor that could be used for landing-site targeting is from -16.2° to -17.4°. As shown in figure 47, the shallow entry angle of -16.2° related to a down-range angle or periapsis of -6.5° and the steep entry angle of -17.4° related to a downrange angle or periapsis of -11.5°. The resulting downrange capability of 5° represented 295.6 km (0.97 ft) on the surface of Mars. In addition, crossrange targeting to angles of ±3° was allowed as defined in figure 48 and represented ±177 km (0.58 ft) on the surface of Mars. Crossrange targeting to angles greater than 3° was recommended only as a last resort since the sensitivity of entry-angle dispersions to deorbit execution error increased rapidly beyond this point. The deorbit error analysis did not consider crossranging in excess of 3°.

Figure 48.- Definition of downrange and crossrange targeting angles.

74

Lander targeting was implemented by variation of the start time of the deorbit burn and the lander orientation. The burn start time specified the point in the orbit where the transition to the descent trajectory was begun. Lander orientation determined the ΔV pointing in the celestial frame by using a desi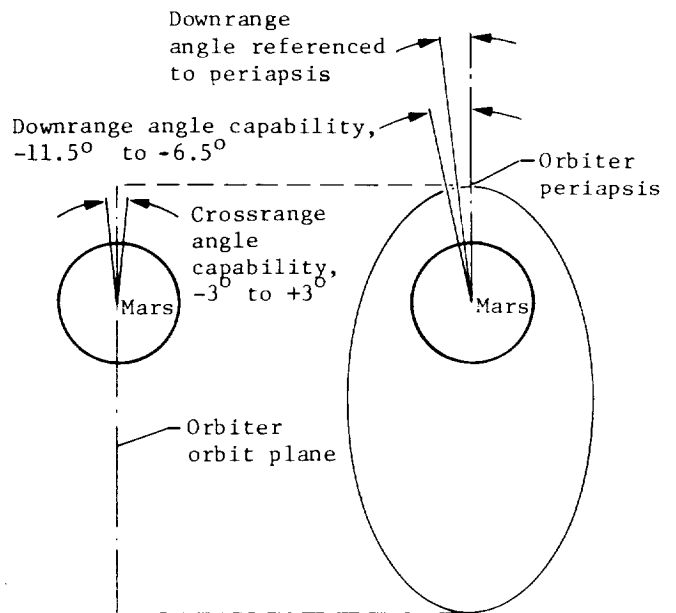red attitude matrix $[A_d]$; thus, the targeted entry angle and crossrange angle were specified. After final orbit determination, the two controllables, start time and $[A_d]$, are defined by an Earth-based trajectory simulation. The deorbit controllables were uplinked to the lander and stored in the computer prior to lander separation. Deorbit ΔV magnitude was not used as a targeting parameter since such use would make the lander weight at atmospheric entry a deterministic variable; entry weight and propellant weight were directly related to burn time and ΔV magnitude. Thus, targeting flexibility was traded for better knowledge of entry weight and more weight for scientific payload.

The deorbit ΔV was obtained from the pitch and yaw RCS engines. The concept was efficient with respect to hardware in that a single propulsion system performed dual functions. However, since the RCS engines were relatively small, a thrust modulation technique was required to control accurately the relatively long burn time (a burn-time error propagated into an entry-angle error). Thus, a ΔV-time contour was stored in the computer as a fourth-order polynomial. The contour design was based on a 2.58σ (0.99-probability level) low thrust from six engines. This design insured that contour tracking capability was maintained with the failure of any single engine. Because of the torque balance constraints of the attitude control logic, a single engine failure automatically removed two of the eight engines from service. During nominal operation with no failures the eight aft-pointed pitch and yaw engines were commanded full on until the current value of true ΔV exceeded the ΔV-time contour by 0.3 m/sec (1.0 ft/sec). At this point all eight engines were commanded off until the time-increasing value of the contour polynomial exceeded the constant value of true ΔV by 0.3 m/sec (1.0 ft/sec). Contour tests were made at 1-sec intervals. The thrust modulation duty cycle, with nominal engine thrust, was 70 percent. During nominal operation (nominal thrust) with a single engine failure, six engines would operate in a 94-percent thrust modulation duty cycle. Under 2.58σ low-thrust conditions, the single engine failure case had a 100-percent duty cycle. During thrust modulation and while the engines were full on, the attitude control logic was inverted so that pitch and yaw engines were pulsed off for attitude control. These thrust modulation techniques eliminated deorbit burn-time errors caused by engine thrust uncertainty due to variations in tank pressure, propellant flow rate, specific impulse, feed line pressure drop, and center-of-gravity offset. The modulation threshold of ±0.3 m/sec (±1.0 ft/sec) and the software sample interval of 1 sec were sized to reduce the burn-time error to a negligible value of ±0.5 percent. The nominal total burn time was 22 min; the total accumulated ΔV was 156 m/sec (512 ft/sec). Propulsion parameters are discussed later in the section "Propulsion Subsystem." Lander mass properties are summarized in table 4.

TABLE 4.- NOMINAL LANDER MASS PROPERTIES

Mission phase	Weight, kg (lbm)	c.g. offset			Moments of inertia			Products of inertia		
		x_{cg}, cm (in.)	y_{cg}, cm (in.)	z_{cg}, cm (in.)	IX, kg-m^2 (slug-ft^2)	IY, kg-m^2 (slug-ft^2)	IZ, kg-m^2 (slug-ft^2)	I_{XY}, kg-m^2 (slug-ft^2)	I_{XZ}, kg-m^2 (slug-ft^2)	I_{YZ}, kg-m^2 (slug-ft^2)
Lander separation	1060 (2340)		-0.99 (-0.39)	-4.60 (-1.81)	909 (670)	521 (384)	563 (415)	-7.5 (-5.5)	-7.9 (-5.8)	+59.4 (+43.8)
Aeroshell entry	977 (2155)		0.00 (0.00)	-4.60 (-1.82)	786 (580)	423 (312)	536 (395)	+1.1 (+0.8)	-3.8 (-2.8)	+6.6 (+4.9)
Parachute descent (aeroshell attached)	931 (2053)		-0.25 (-0.10)	-4.9 (-1.93)	786 (580)	411 (303)	513 (378)	+1.1 (+0.8)	-4.1 (-3.0)	+6.6 (+4.9)
Parachute descent (aeroshell separated)	740 (1632)		-0.61 (-0.24)	-5.21 (-2.05)	490 (361)	217 (160)	366 (270)	-0.7 (-0.5)	-5.4 (-4.0)	-7.9 (-5.8)
Terminal descent (parachute/base-cover separation)	673 (1483)		-0.76 (-0.30)	-5.16 (-2.03)	422 (311)	168 (124)	319 (235)	-0.3 (-0.2)	-5.4 (-4.0)	-7.5 (-5.5)
Landed	603 (1330)		-0.84 (-0.33)	-5.08 (-2.00)	327 (241)	168 (124)	218 (161)	-0.4 (-0.3)	-5.4 (-4.0)	-7.5 (-5.5)

The complete deorbit guidance concept is shown in figure 49. Prior to initiation of the deorbit burn, the lander was oriented via the attitude maneuver routine to the desired attitude $[A_d]$ (within the ±0.25° limit cycle dead band) as described previously. The true attitude matrix, which was the transformation from celestial (inertial) coordinates to lander body coordinates, was available from the previously discussed attitude routine. Therefore, the new inputs were time, which drove the ΔV contour polynomial, and the accelerometer outputs, which measured engine thrust. Refer to figure 49 for the following discussion. The time varying ΔV contour was computed in block 1 and was called the required velocity V_r. The V_r computation interval was 1 sec. In block 2, the changes in body velocity sensed by the accelerometers over a 40-msec interval were transformed to the celestial (inertial) frame and summed with existing celestial velocities. The initial value of celestial velocity was zero at lander separation. At the start of deorbit burn, the value of celestial velocity was the measured velocity imparted to the lander by the lander-orbiter separation mechanism. Block 2 was updated at 40-msec intervals. In block 3, velocity to be gained V_g was computed by subtracting the measured accumulated inertial velocity V_I from the required velocity V_r in the celestial frame and then transforming these differences to the body frame. The X-axis component of velocity to be gained $V_{g,Xb}$ was used in block 4 to control thrust modulation. The Y- and Z-axis velocities to be gained were used in block 5 to generate velocity steering commands for pitch and yaw attitude control. This velocity steering technique resulted in the Y and Z body axis velocities (and thus the lateral accelerometer outputs) being driven to zero by the attitude control logic.
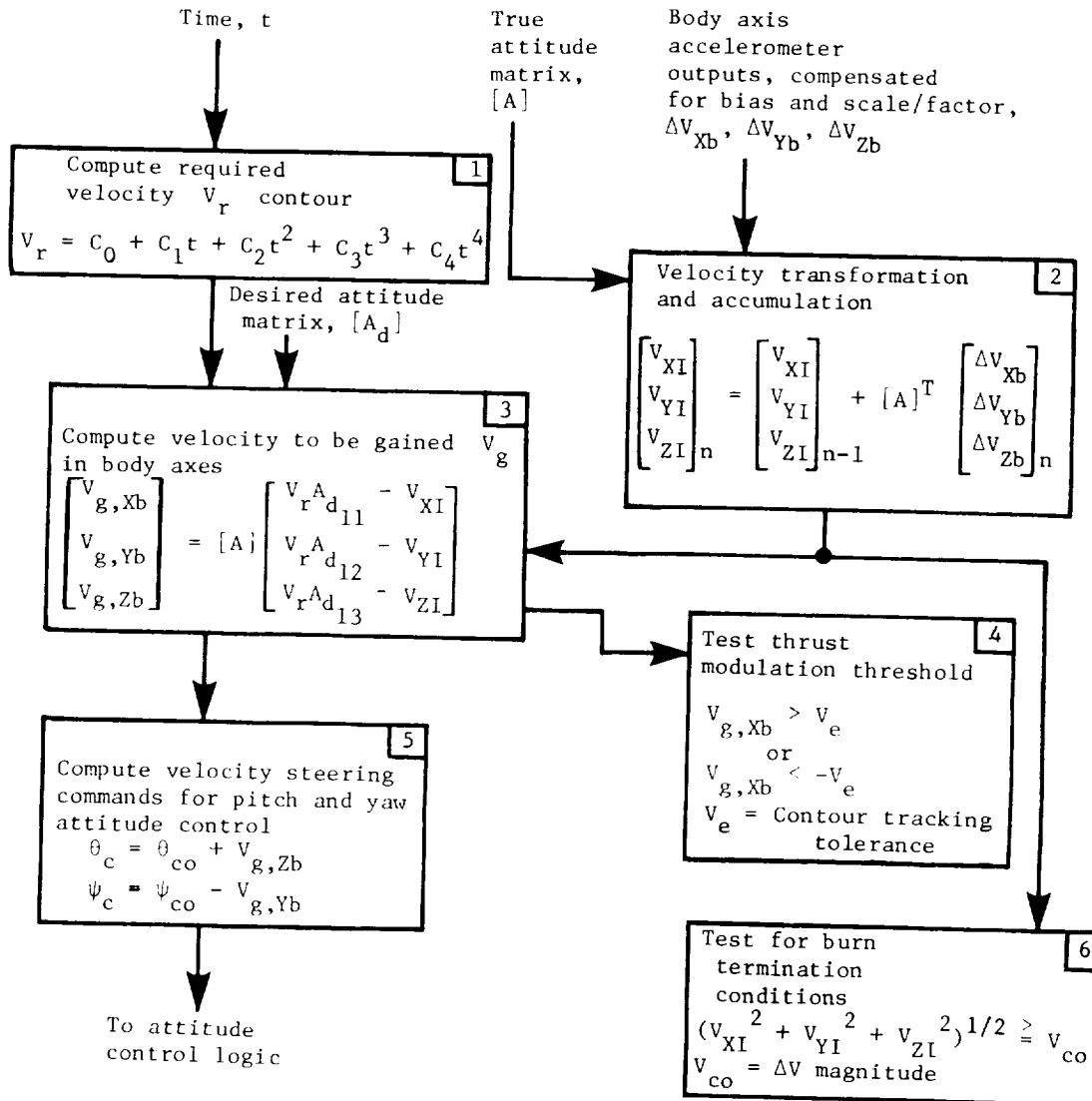
Time, t

True
attitude
matrix,
[A]

Body axis
accelerometer
outputs, compensated
for bias and scale/factor,
ΔV_{Xb}, ΔV_{Yb}, ΔV_{Zb}

1 Compute required
velocity V_r contour

$$V_r = C_0 + C_1 t + C_2 t^2 + C_3 t^3 + C_4 t^4$$

Desired attitude
matrix, $[A_d]$

2 Velocity transformation
and accumulation

$$\begin{bmatrix} V_{XI} \\ V_{YI} \\ V_{ZI} \end{bmatrix}_n = \begin{bmatrix} V_{XI} \\ V_{YI} \\ V_{ZI} \end{bmatrix}_{n-1} + [A]^T \begin{bmatrix} \Delta V_{Xb} \\ \Delta V_{Yb} \\ \Delta V_{Zb} \end{bmatrix}_n$$

3 Compute velocity to be gained V_g
in body axes

$$\begin{bmatrix} V_{g,Xb} \\ V_{g,Yb} \\ V_{g,Zb} \end{bmatrix} = [A] \begin{bmatrix} V_r A_{d_{11}} - V_{XI} \\ V_r A_{d_{12}} - V_{YI} \\ V_r A_{d_{13}} - V_{ZI} \end{bmatrix}$$

4 Test thrust
modulation threshold

$V_{g,Xb} > V_e$
or
$V_{g,Xb} < -V_e$
V_e = Contour tracking
tolerance

5 Compute velocity steering
commands for pitch and yaw
attitude control

$\theta_c = \theta_{co} + V_{g,Zb}$

$\psi_c = \psi_{co} - V_{g,Yb}$

To attitude
control logic

6 Test for burn
termination
conditions

$(V_{XI}^2 + V_{YI}^2 + V_{ZI}^2)^{1/2} \geq V_{co}$
V_{co} = ΔV magnitude

Figure 49.- Deorbit guidance.

Therefore, deorbit ΔV pointing errors due to RCS engine thrust vector mis-alignment and attitude control limit cycle error was removed (steered out). Lateral accelerometer (Y- and Z-axes) bias and misalignment uncertainties were introduced by the velocity steering technique; these errors were relatively small compared with attitude initialization errors and were better defined than engine thrust vector alignment error, that is, misalignment between thrust vector and the nozzle center line and misalignment caused by the lander structural deformation resulting from thermal sterilization. Block 6 provided the test that terminated the deorbit burn when $V_I = V_{co} = \Delta V = 156$ m/sec (512 ft/sec). Blocks 3, 4, 5, and 6 were updated at 1-sec intervals.

Most of the fuel contained in the RCS propellant tanks was used during the deorbit burn to minimize atmospheric entry weight. The RCS attitude control

function remained active until parachute deployment and aeroshell separation. The fuel allocation is summarized in table 5.

TABLE 5.- DEORBIT-ENTRY FUEL ALLOCATION

Item	Fuel allocation	
	kg	lbm
Deorbit ΔV	72.85	160.6
Attitude control (maneuvers and limit cycle)	5.72	12.6
Trapped in feedlines	1.00	2.2
Propulsion/guidance and control subsystem tolerances	.95	2.1
Unallocated margin	4.31	9.5
Total	84.83	187.0

Coast.- The deorbit maneuver established the descent trajectory. The lander reached an arbitrarily defined entry point (nominally 243.8 km (800 000 ft) above the Mars surface) approximately 2 1/2 hr after completion of the deorbit burn. This 2 1/2-hr period was called the coast phase. Immediately after completion of the deorbit burn, the computer scheduled an attitude maneuver. The attitude maneuver was implemented as described previously in section "Attitude maneuver." The desired attitude matrix $[A_d]$ defined the lander orientation required to meet the constraints of lander to orbiter communication relay link geometry, lander thermal control system, and lander ultraviolet sterilization. Thermal control constraints prevented direct solar radiation of the aeroshell heat shield to avoid establishing thermal gradients prior to atmospheric entry. Ultraviolet radiation of the base cover was required to kill organisms that had found their way from the unsterilized orbiter to the lander.

After completion of the attitude maneuver, a three-axis attitude hold was established. Since attitude control requirements were only ±10° during the coast phase, the attitude control logic (fig. 43) was switched from the small limit cycle mode to the large limit cycle mode to conserve RCS fuel. The large limit cycle dead band was ±5.0° and the coast phase attitude control fuel usage was typically 0.5 to 1.0 kg (1.0 to 2.0 lbm). During the long coast phase, the GCSC was programmed to place itself in a sleep mode to conserve power and reduce internal lander heating. While in the sleep mode, the attitude matrix was updated at 200-msec intervals instead of 20-msec intervals. (Velocity computations were not made during the coast phase.) If the attitude control dead band was exceeded in any axis, the computer automatically awakened

78

and stayed awake until all axes were within the dead band. When awake, the attitude matrix was updated at the normal 20-msec interval. The computer also awakened if thermal pulsing was required to keep the RCS engines above the minimum operating temperature. The sequencing routine continued to run in the sleep mode so that the computer awakened to perform scheduled housekeeping and scientific functions.

Approximately halfway through the coast phase, a 180° roll maneuver was performed for thermal equalization and ultraviolet sterilization of the part of the base cover that had been previously shaded. The lander-orbiter communications geometry was unchanged by the roll maneuver.

Attitude hold in the large limit cycle mode continued until approximately 9 min prior to the entry point. At this time, an attitude maneuver was performed to orient the lander for entry. The lander was a lifting body during atmospheric entry (as opposed to a ballistic body); therefore, this attitude maneuver adjusted the roll orientation to place the built-in center-of-gravity offset, and thus, the lift vector, in the plane of the descent trajectory. This same roll attitude adjustment properly oriented the fan-shaped altimeter antenna pattern relative to Mars. The aeroshell face was a 20° cone; therefore, the attitude maneuver also adjusted the pitch angle of attack to facilitate data collection by upper atmosphere science instruments. The total orientation was defined by a desired matrix $[A_d]$ and is illustrated in figure 50.
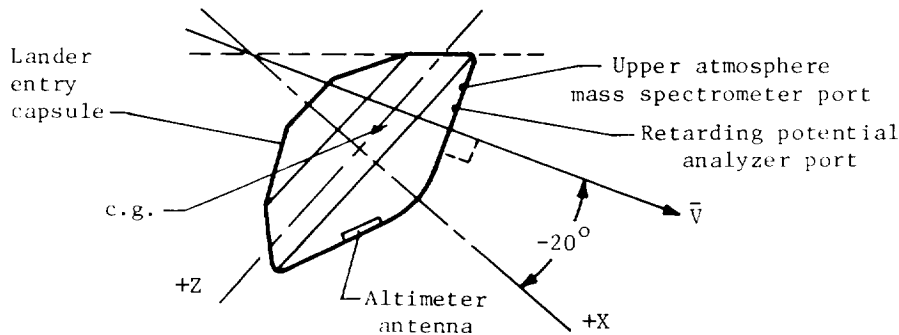

Figure 50.- Lander orientation 6 min before entry. X-Z body plane lies in plane of trajectory.

After allowing 3 min for completion of the entry attitude maneuver, the computer initiated a preprogrammed pitch-over rate to maintain the angle of attack at -20°. The pitch-over was stored as a second-order polynomial and was superimposed on the pitch attitude command.

Entry.- Entry was defined as the predicted time at which the altitude above the Mars mean surface level was 243.8 km (800 000 ft). At the prestored entry time, the computer performed the following functions:

(1) A pitch-up attitude maneuver was initiated by changing the constant term of the pitch-over polynomial. This maneuver adjusted the pitch angle of attack to the predicted aerodynamic trim angle of attack in preparation for the

aerodynamic entry. The predicted trim angle of attack was -11,1°; the pitch-over rate was continued to maintain the desired angle of attack.

(2) The lander reference was changed from the celestial frame established at lander-orbiter separation to a Mars surface, local vertical frame at the projected landing site. A prestored transformation matrix was used to transform the true attitude matrix from the celestial frame to the local vertical frame. Entry navigation was begun in the new local vertical frame with outputs from the IRU gyroscopes and accelerometers. Position, velocity, altitude, and rate of change of altitude were initialized to targeted values stored in the computer prior to lander separation. The initial value of total velocity was about 4570 m/sec (15 000 ft/sec). Since attitude was not updated at entry, attitude errors that have accumulated during the long coast phase must be considered in the entry error analyses. The targeting uncertainty of the other states were used in the error analyses.

(3) The RA was powered on at entry and was commanded to the search mode. The computer was programmed to switch from the prime RA to the backup RA, back to the prime RA, etc., at 30-sec intervals until one of the altimeters locked. Typically, a nonambiguous lock on the surface of Mars occurred between 137 km (450 000 ft) and 122 km (400 000 ft).

The computer monitored accelerometer output to detect entry into the sensible atmosphere. A deceleration threshold of 0.05g (Earth) was selected because it was well within the accelerometer detection capability and it occurred before aerodynamic forces overcame RCS attitude control forces and caused excessive fuel usage. A deceleration of 0.05g was normally detected about 2 min after entry. Once 0.05g was detected, the attitude control logic was reconfigured to provide only angular rate damping about the pitch and yaw axes. Pitch attitude and yaw attitude were determined by the balance of aerodynamic forces on the aerodynamically stable aeroshell configuration during entry. The RCS was used to keep pitch and yaw angular rates below 1.0 deg/sec. Roll attitude hold is maintained for proper orientation of the entry lift vector and the altimeter antenna pattern.

Starting at 0.05g, RA measurements of altitude were used to update the navigator's estimate of altitude. The nominal altitude at 0.05g was roughly 77 km (250 000 ft). The entry navigation concept is shown in figure 51. Block 1 transformed body-axis ΔV's to the local vertical inertial frame using the current value of the attitude matrix. Block 1 also computed the effect of gravity on inertial velocity and the total accumulated inertial velocity. The symbols ΔV_{Xb}, ΔV_{Yb}, and ΔV_{Zb} represented the change in body velocities over a 40-msec interval as measured by the IRU accelerometers. The attitude matrix $[A]$ was updated at 20-msec intervals and was computed with the same attitude routine described previously. The A-matrix now represented the transformation from the local vertical inertial frame to the body frame. A Δt of 40 msec was used in the computation of the effect of gravity on inertial velocity (accelerometers do not sense gravity). In block 2 (fig. 51), the inertial velocities were integrated to obtain the components of position R along the local vertical coordinates. Block 3 computed altitude rate of change $\dot{H}$ and integrated the result to obtain the navigator's estimate of altitude H. The term $V_{XI}(R_X/R)$, for example, represented the component of V_{XI} along the position

80

To 1.1 km/sec (3609 ft/sec) test logic

Body axis accelerometer outputs, compensated for bias and scale factor error, ΔV_{Xb}, ΔV_{Yb}, ΔV_{Zb}

Attitude matrix, $[A]$

V_R

Compute velocity relative to Mars surface 6

$V_{R,X} = V_{XI} - V_{s,X}$

$V_{R,Y} = V_{YI} - V_{s,Y}$

$V_{R,Z} = V_{ZI} - V_{s,Z}$

V_I

Velocity transformation, accumulation, and gravity correction 1

$$\begin{bmatrix} V_{XI} \\ V_{YI} \\ V_{ZI} \end{bmatrix}_n = \begin{bmatrix} V_{XI} \\ V_{YI} \\ V_{ZI} \end{bmatrix}_{n-1} + [A]^T \begin{bmatrix} \Delta V_{Xb} \\ \Delta V_{Yb} \\ \Delta V_{Zb} \end{bmatrix}_n + \Delta t \begin{bmatrix} g_{XI} \\ g_{YI} \\ g_{ZI} \end{bmatrix}_n$$

g

V_I

To parachute deployment logic

H

Estimate of position, R 2

$R_n = r + H_{n-1}$

$R_{X,n} = R_{X,n-1} + \Delta t \left[\dfrac{3\left(V_{XI}\right)_n - \left(V_{XI}\right)_{n-1}}{2} \right]$

$R_{Y,n}$ and $R_{Z,n}$, similarly

V_I

Estimate of altitude, H 3

$\dot{H}_n = \left(V_{XI}\right)_n \dfrac{R_{X,n}}{R_n} + \left(V_{YI}\right)_n \dfrac{R_{Y,n}}{R_n} + \left(V_{ZI}\right)_n \dfrac{R_{Z,n}}{R_n} + K\,\varepsilon H$

$H_n = H_{n-1} + \Delta t \left[\dfrac{3\dot{H}_n - \dot{H}_{n-1}}{2} \right]$

R

εH

H

Navigator error relative to RA measurement 4

$\varepsilon H = H_{RA} - H_{n-t}$

$t = 100$ msec

Estimate of gravity, g 5

$g_n = g_0 + K_g H_{n-1}$

$g_{XI,n} = g_n \dfrac{R_{X,n-1}}{R_{n-1}}$

$g_{YI,n}$ and $g_{ZI,n}$, similarly

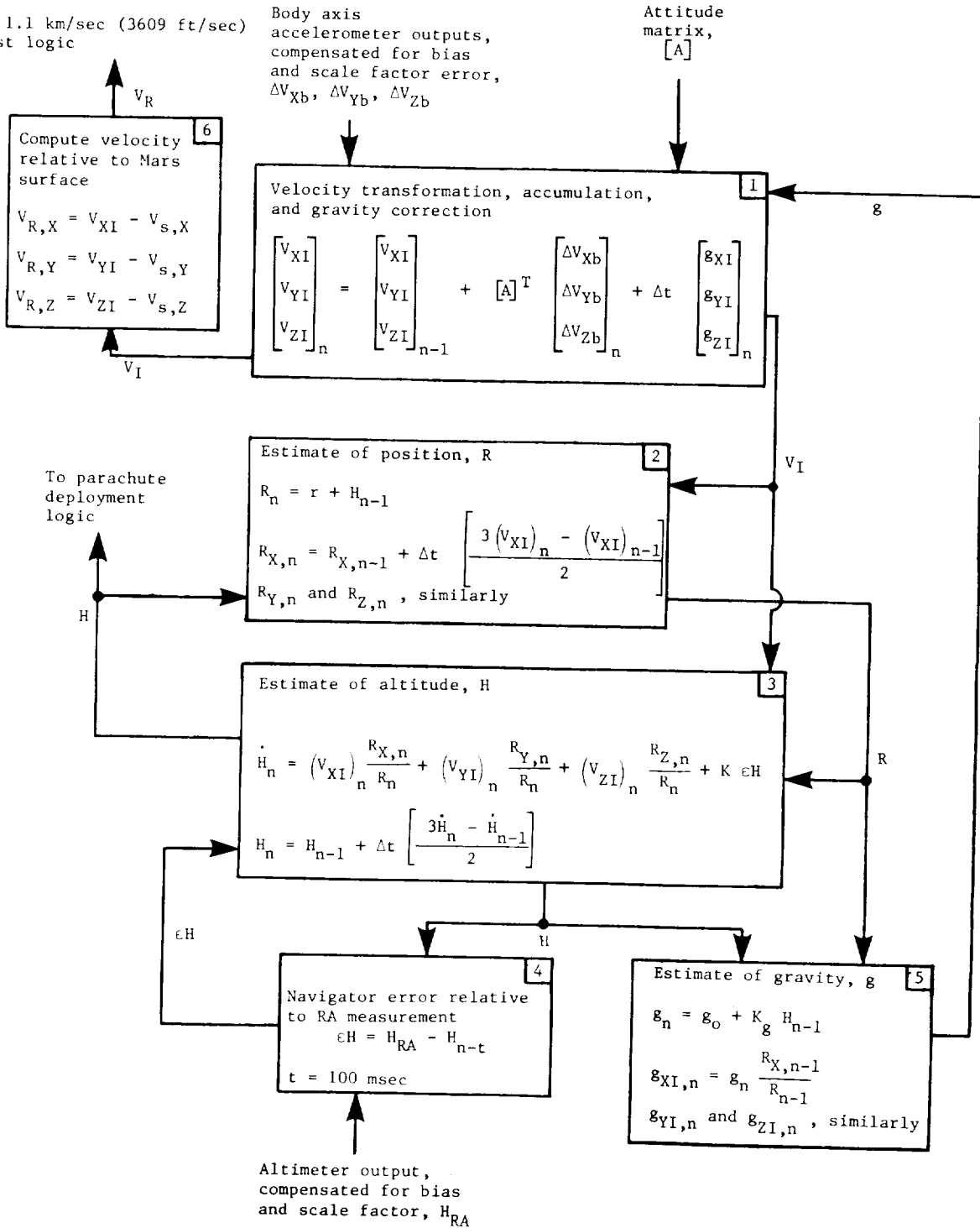Altimeter output, compensated for bias and scale factor, H_{RA}

Figure 51.- Entry navigation.

vector R as shown by the simplified geometry of figure 52. The navigator's estimate was updated by RA measurements with the term K εH. The error was
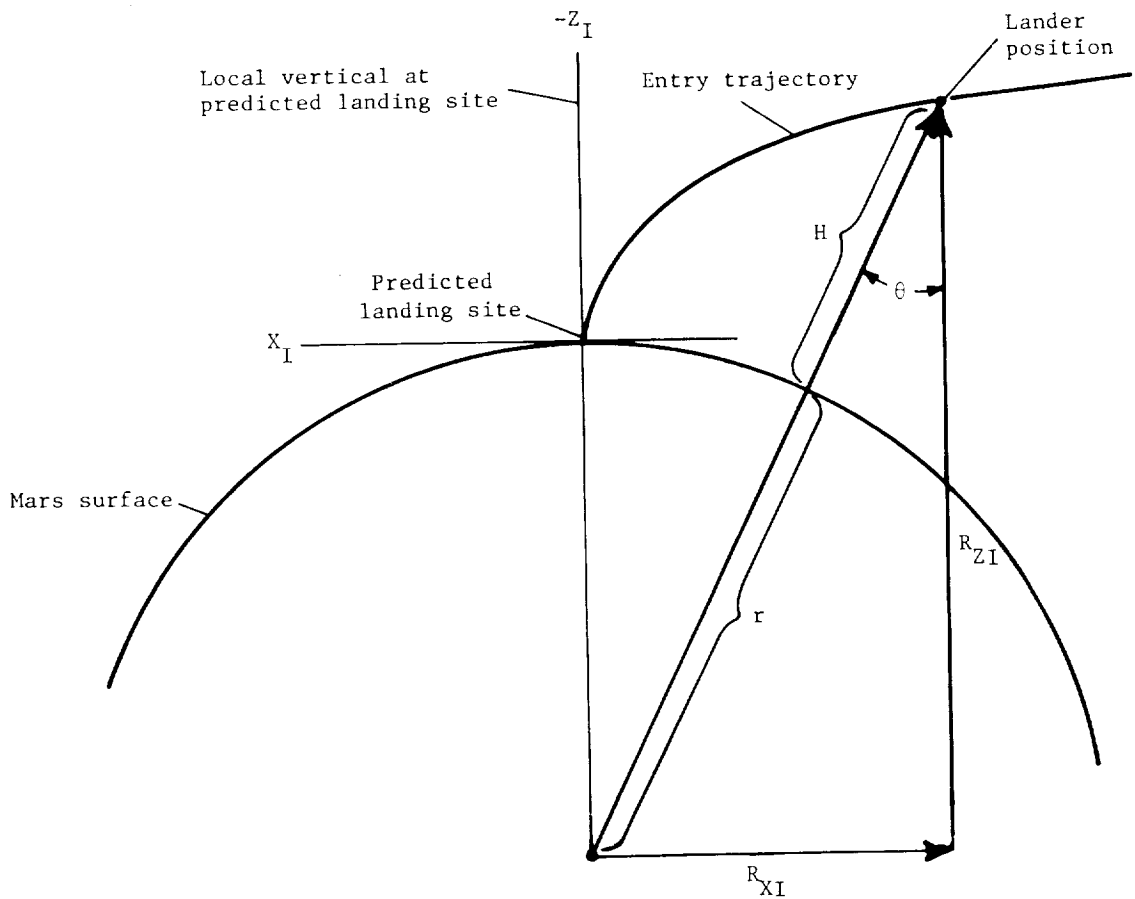
Figure 52.- Entry navigation geometry.

computed in block 4 (fig. 51) as the difference between measured and estimated altitude. The constant K was 0 prior to 0.05g and was nominally 1 after 0.05g provided that the RA tracker lock and data good flags were positive.   If the RA signal-noise ratio dropped below the data good threshold or the RA lost lock on the Mars surface, K was set to zero, RA data were disregarded, and the inertial navigator was not updated by altimeter measurements.

Blocks 1, 2, 3, and 5 (fig. 51) were updated at 40-msec intervals. The RA output was sampled at 200-msec intervals and block 4 was updated at 200-msec intervals. The comparison of RA output and navigator's estimate occurred at the same mission time. Since the RA output was averaged over a 200-msec period, the output represented the measured altitude 100 msec prior to transfer of data from the RA to the GCSC. Back values of the navigator's estimates at 40 msec were stored in GCSC and subsequently used to compute an estimated altitude which was 100 msec old (H_{n-t} where $t = 100$ msec) and was therefore comparable with the RA measurement. In addition, figure 51 does not provide visiblity of software timing. Continuing with the same example, the altitude error εH computed on a 200-msec time boundary by block 4 was not passed to block 3 until the next 200-msec time boundary. Therefore, the navigator's estimate was updated with

an error εH that was the true error approximately 300 msec in past mission time. Performance and stability analyses and simulations were used to define the allowable limits of transport lags caused by computational time delays.

Approximately 4 min after entry, the lander GCSC issued commands for deployment of the aeroshell stagnation temperature and pressure probes in support of the science subsystem. The probe deployment occurred when the lander velocity relative to the rotating Mars atmosphere was 1.1 km/sec (3600 ft/sec). Relative velocity V_R was computed by block 6 of figure 51 by subtracting Mars surface velocity from the inertial velocities computed in block 1 of figure 51 and then comparing the result with 1.1 km/sec (0.0004 ft/sec). The 99-percent error in probe deployment was mission dependent but was typically less than 50 m/sec (164 ft/sec). Simultaneous with the probe deployment, the computer issued commands to the propulsion subsystem to open the terminal descent system propellant bleed-in valves. This bleed-in avoided water-hammer shock at engine ignition.

The primary objective of the entry navigator was to converge on an accurate estimate of altitude relative to the local Mars surface prior to parachute deployment at approximately 6.0 km (19 500 ft). It was proven by analysis and simulation that sufficient time for navigator convergence existed while allowing for rf blackout which could occur as early as 0.05g and last for as much as 60 sec, time required to switch to the backup RA if the prime unit failed to relock after blackout, and time required for navigator convergence after receipt of good RA data. Maintenance of parachute structural integrity and attainment of the required decelerating drag dictated deployment of the parachute at the prestored altitude with an error no greater than 168 m (550 ft). The error analysis results are shown in table 6. Altitude errors caused by computer computational delays, terrain bias, RA electronic bias, antenna cable delays, and pyrotechnic deployment delays were removed by the flight software design.

TABLE 6.- ERROR ANALYSIS RESULTS AT PARACHUTE DEPLOYMENT

Error source	Value
Random:	
Altitude rate initialization error at entry (3σ value), m (ft)	40 (131)
Navigator velocity error (initial and accumulated) (3σ value), m (ft)	68 (223)
Radar altimeter measurement error (3σ value), m (ft)	74 (243)
Total random error:	
RSS (3σ), m (ft)	108 (355)
99% (2.58σ), m (ft)	93 (305)
Deterministic:	
Altimeter bias error, m (ft)	12 (39)
Total 99% error, m (ft)	105 (344)

Approximately 7 min after entry, the parachute deployment altitude of 6 km (19 500 ft) was encountered. The computer issued commands to fire the mortar that deployed the parachute. The dynamic response to the mortar fire shock and the parachute opening transient produced 99-percent angular rates of ±83 deg/sec about the lander body axes. Therefore, the IRU gyroscopes had a high torque mode capable of tracking angular rates of 100 deg/sec. This high-rate mode prevented gyroscope saturation and, thus, loss of the attitude reference required for terminal descent and landing. The high-rate mode was automatically activated by the IRU electronics when angular rates exceeded 12.5 deg/sec. The gyroscope drift rates increased in the high-rate mode but this performance degradation was tolerable because of the short time the IRU was in the high-rate mode (<30 sec) and also because lander touchdown occurred within 2 min after parachute deployment.

The RA transmitter was inhibited 6 sec after parachute deployment; the aeroshell was jettisoned 7 sec after parachute deployment. At this point the RA was switched from the aeroshell antenna to the lander body antenna, and roll attitude control was switched from the aeroshell RCS to the terminal descent propulsion system. Pitch and yaw attitude was not controlled during parachute descent. The RA transmitter inhibit command was removed and the RA began searching for the Mars surface target with the lander body antenna 10 sec after parachute deployment. Also the TDLR was powered on and each of its four Doppler velocity beams began searching for Mars surface returns. Based on path-loss-capability analyses, the probability of obtaining both RA and TDLR lock, prior to initiation of terminal descent navigation at 19 sec after parachute deployment, was greater than 0.99. The angular dynamics produced by the parachute opening transient, local atmospheric winds, and Mars radar cross section were parametrically considered in the statistical path-loss-capability analyses.

Terminal descent.- Terminal descent navigation was initiated and a roll attitude maneuver was performed 19 sec after parachute deployment. The purpose of the roll maneuver was to establish the optimum postlanding orientation to facilitate interpretation of data obtained from the various surface science experiments. A major concern was the lighting conditions for optimum photographic coverage of the surface area where samples were collected. The four small TDS on/off roll engines were used for this maneuver and the subsequent roll attitude hold mode. (See later section "Propulsion System.") The roll-axis attitude control logic was identical to that used by the RCS. (See fig. 43.) The small limit cycle of ±0.25° was used. The roll maneuver was completed about 30 sec prior to releasing the parachute; this was made possible by a swivel-type coupler in the parachute bridle that provided rotational isolation between the lander and the deployed parachute. After completion of the roll maneuver, the desired roll orientation was maintained until touchdown.

The terminal descent navigator was a radar-aided inertial navigator in the sense that the basic navigation algorithms were driven by inertial measurements made by the IRU and were then updated by radar altitude and velocity measurements. The inertial navigator, with updates of 40-msec intervals, smoothed and extrapolated the radar data between the 200-msec updates. The radar measurements were the navigator's true reference. The navigator computations were made in the lander body frame and radar measurements were made relative to the Mars surface. Therefore, the navigator was more accurately described as a relative

84

navigator. The navigator was initialized 19 sec after parachute deployment by transforming the relative velocities (computed in block 6 of fig. 51) from the inertial frame into the body frame as shown by the following equation:

$$\begin{bmatrix} u_0 \\ v_0 \\ w_0 \end{bmatrix} = [A] \begin{bmatrix} V_{R,X} \\ V_{R,Y} \\ V_{R,Z} \end{bmatrix}$$

The terminal descent navigation concept is shown in figure 53. Only three elements of the attitude matrix were required for this navigator implementation. The three local vertical elements were computed in block 1; the update interval is 20 msec. The basic body velocity equation is

$$u = \int \left[a_X + (-qw + rv) + gA_{13} + K_u(u_R - u_{nav}) \right] dt$$

and similarly for v and w. The incremental form of the basic velocity equations were solved in block 2. The altitude estimate was computed in block 3 by integrating the altitude rate $\dot{H}$. The computation of $\dot{H}$ used the three direction cosines to compute the component of body velocities lying along the local vertical. The update interval for blocks 2 and 3 was 40 msec ($\Delta t = 40$ msec). The navigator errors relative to radar measurements were computed in block 5 at 200-msec intervals; the RA and TDLR outputs were sampled at 200-msec intervals. Therefore, as for the entry navigator, past values of the navigator 40-msec estimates were stored in the computer and used to compute values of navigator estimates which were valid 100 msec in past mission time to be comparable with the radar measurements.

The body axis velocities (u_R, v_R, w_R) of block 5 were derived from the Doppler frequency shift along the four beams of the TDLR. Conversion of Doppler counts to beam velocity was based on the transmitter frequency and the sample interval. Transformation from TDLR beam axes to lander body axes is defined by the geometry shown in the section "Terminal descent and landing radar." The geometric relationship was such that when all four beams were locked, the velocity along each body axis could be computed by two independent equations. The functional equations in terms of beam velocities are

$$u_1 = f(v_{B1} + v_{B3}) \qquad\qquad v_1 = f(v_{B1} - v_{B2})$$

$$u_2 = f(v_{B2} + v_{B4}) \qquad\qquad v_2 = f(v_{B4} - v_{B3})$$

$$w_1 = f(v_{B2} - v_{B3})$$

$$w_2 = f(v_{B1} - v_{B4})$$

IRU outputs,
compensated for
bias and scale factor

To terminal
descent
control
laws

1 Local vertical elements
of attitude matrix

$$\begin{bmatrix} A_{13} \\ A_{23} \\ A_{33} \end{bmatrix}_n = \begin{bmatrix} 1 & \Delta\theta_Z & -\Delta\theta_Y \\ -\Delta\theta_Z & 1 & \Delta\theta_X \\ \Delta\theta_Y & -\Delta\theta_X & 1 \end{bmatrix} \begin{bmatrix} A_{13} \\ A_{23} \\ A_{33} \end{bmatrix}_{n-1}$$

$\Delta\theta_X$
$\Delta\theta_Y$
$\Delta\theta_Z$

ΔV_X
ΔV_Y
ΔV_Z

A_{13}
A_{23}
A_{33}

u
v
w

2 Estimate body velocity

$$\Delta u = \Delta V_X - (\Delta\theta_Y\ w) + (\Delta\theta_Z\ v) + \Delta t\ (g\ A_{13} + K_u\ \varepsilon u)$$

$$\Delta v = \Delta V_Y + (\Delta\theta_X\ w) + (\Delta\theta_Z\ u) + \Delta t\ (g\ A_{23} + K_v\ \varepsilon v)$$

$$\Delta w = \Delta V_Z - (\Delta\theta_X\ v) + (\Delta\theta_Y\ u) + \Delta t\ (g\ A_{33} + K_w\ \varepsilon w)$$

$$u_n = u_{n-1} + \Delta u$$

$$v_n = v_{n-1} + \Delta v$$

$$w_n = w_{n-1} + \Delta w$$

H

εu
εv
εw

3 Estimate altitude

$$\dot{H} = \left[-(A_{13}\ u) - (A_{23}\ v) - (A_{33}\ w) \right] + K_H\ \varepsilon H$$

$$H_n = H_{n-1} + \Delta t\ \left[\frac{3\dot{H}_n - \dot{H}_{n-1}}{2} \right]$$

g

H

εH

5 Navigator error relative
to radar measurements

$$\varepsilon H = H_{RA} - H_{n-t}$$

$$\varepsilon u = u_R - u_{n-t}$$

$$\varepsilon v = v_R - v_{n-t}$$

$$\varepsilon w = w_R - w_{n-t}$$

$$t = 100\ msec$$

4 Gravity

$$g_n = g_o + K_g\ H_{n-1}$$

Altimeter and
velocity radar
outputs, H_{RA}, u_R, v_R, w_R

Figure 53.- Block diagram of terminal descent navigation.

When all four TDLR beams had positive tracker lock and data good flags, the radar data coefficients (K_u, K_v, K_w) of block 2 were all equal to 1 and the radar body velocities (u_R, v_R, w_R) were obtained from the average of the two computational methods. For example: $u_R = (u_1 + u_2)/2$. If one of the four TDLR beams failed or lost tracker lock, the redundancy configuration allowed continued computation of all three body velocities. For example, if beam 1 unlocked $u_R = u_2$, $v_R = v_2$, and $w_R = w_1$ since u_2, v_2, and w_1 were not functions of v_{B1}. If two TDLR beams failed or unlocked, only one body velocity could be computed and the appropriate radar data coefficients were set equal to 0. For example, if beams 3 and 4 unlocked, $v_R = v_1$, $K_u = 0$, $K_v = 1$, and $K_w = 0$. This logic was implemented in the flight software and was executed based on the status of the tracker lock and data good flags. The flags were generated by the TDLR electronics and were passed to the computer at 200-msec intervals.

In addition to the beam usage logic discussed, the computer was programmed to detect TDLR false locks on the image lobe or third harmonic. Since the image lobe of beam 1 lay along the primary lobe of beam 3 (the diagonally opposite beam) and similarly for the other three beams, it was possible to formulate tests for reasonability. These reasonability tests were valid only if all four beams were locked (three beams locked on the primary lobe Mars surface return). The technique had false lock detection but not isolation. Therefore, if a false lock was detected, all velocity radar data were disregarded until the false lock cleared. Analyses showed that false locks were improbable (<3 percent) and those that would occur cleared within 6 sec. Because of the extrapolating nature of the inertial navigator, operation within specifications for 6 sec was possible without radar updates. The false lock test logic was required to avoid accumulation of large navigator errors while receiving erroneous radar updates for as much as 6 sec.

The RA electronics generated tracker lock and data good flags which were similar to those generated by the TDLR. The computer logic monitored these RA flags and set the data coefficient K_H of block 3 (fig. 53) accordingly.

The radar-aided navigation concept allowed effective isolation of radar noise and tracker lags from the control loops and, as previously stated, allowed continuation of the basic navigation process during radar dropouts. Also, closure of the radar update loops reduced inertial navigation errors to biases; thus, growth of the error with time was prevented. Refer to block 2 of figure 53, and, as an example, an error of 5° in the knowledge of the inertial direction of the local vertial (A-matrix error) produced a lateral velocity drift equal to $g_{Mars} \sin \epsilon\theta$ or 0.34 m/sec^2 (1.1 ft/sec^2). The error grew with time at a rate of 0.34 m/sec^2 if the navigator was in the inertial mode; the error was reduced to a velocity bias of 0.34 m/sec if the velocity radar update loops were closed. This discussion also applied to errors in the IRU gyroscope and accelerometer measurements. The bias errors in u, v, and w, passed from block 2 to block 3, were likewise reduced to altitude bias errors by closure of the radar altimeter update loop.

A Kalman filter implementation of the terminal descent navigator was analyzed but was never seriously considered because performance requirements could be met by the relatively simple navigation scheme described and because the

Kalman filter was costly in terms of GCSC memory size. However, one loop of the Kalman filter was developed as a contingency. This loop used TDLR data to update the attitude matrix during terminal descent. This contingency algorithm was developed since the lander attitude reference was obtained from the orbiter celestial reference prior to lander separation and was not updated thereafter and also to protect against IRU error accumulation in excess of requirements during the aerodynamic entry and parachute deployment transient. Attitude matrix algorithm development and IRU development satisfied the requirements, and the attitude update algorithm was not required.

At an altitude of approximately 1.4 km (4600 ft) above the local Mars surface, the three terminal descent engines were ignited. These engines operated in a blowdown mode. The initial thrust range of each engine was from 400 to 2700 N (90 to 610 lbf). The thrust was varied by throttle valves. A throttle setting of 0 percent was fully closed and the engine produced a thrust of 15 percent; a throttle setting of 100 percent was fully open and the engine produced 100 percent thrust. The blowdown mode simplified the propulsion hardware but required more complicated analyses and flight software design. (Refer to the later section "Propulsion Subsystem.")

After ignition, the terminal descent engines were warmed up for 2 sec at 10 percent throttle (23.5 percent thrust); thrust chambers had to be hot to insure responsiveness to throttle commands. The parachute was released 1.4 sec after engine ignition, and the pitch and yaw attitude control loops were closed 2 sec after engine ignition. Parachute drag provided the primary force required to separate the parachute from the lander. Control loop closure was delayed 0.6 sec to allow the parachute canister and base cover to clear the separation guide rails prior to applying attitude maneuver torques.

Pitch and yaw attitude control was provided by differential throttling of the terminal descent engines. The attitude control laws were designed to drive lateral body velocities to zero; thus, at loop closure, a tip-up maneuver was automatically performed to align the lander longitudinal axis (X-axis) with the total relative velocity vector. The axial velocity control loop was closed 5 sec after engine ignition and the engines were throttled up to provide the terminal descent propulsive deceleration. Axial thrust was adjusted to track a prestored velocity-altitude contour. Pitch and yaw attitude control maintained the thrust vector in alignment with and opposed to the total relative velocity vector; thus, horizontal and vertical relative velocity components were reduced simultaneously and at a rate determined by the velocity-altitude contour. The resulting gravity turn guidance was the fuel-optimum control law and converged to a vertical descent as the lander approached touchdown on the Mars surface. Touchdown occurred approximately 30 sec after engine ignition.

A simplified block diagram of the terminal descent guidance and control system is shown in figure 54. The terminal descent navigator was the focal point for information flow within the system. The navigator processed sensor data and computed the parameters required by the control laws. The navigation concept was described previously and the sensors are described in the section "Components." Navigator estimates of the body axis velocities were used to compute pitch and yaw commands for the attitude control loop. Pitch and yaw
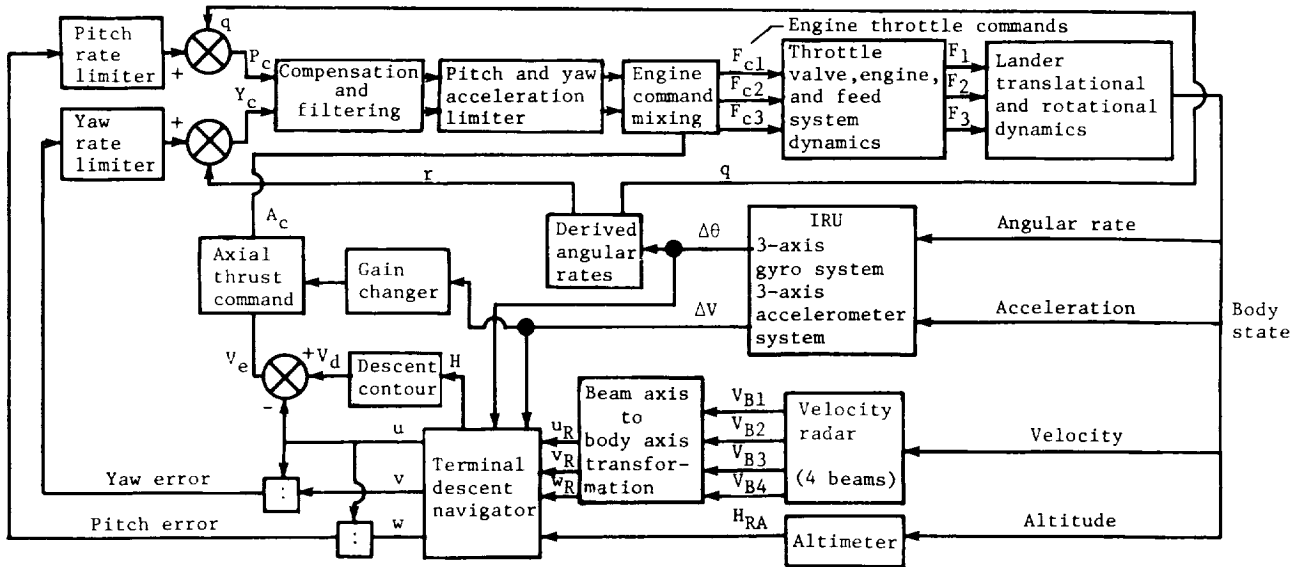
Figure 54.- Block diagram of terminal descent G&C system.

errors were derived by dividing the lateral body velocities v and w by the axial velocity u; that is,

$$\text{Pitch error} = \frac{w}{u}$$

$$\text{Yaw error} = \frac{v}{u}$$

Misalignment of the terminal engines produced undesired lateral body velocities. Accumulation of these undesired velocities was sensed by the lateral accelerometers and the velocity radar and was reflected in the navigator estimates of v and w. Control of the pitch and yaw errors to 0 cancelled the effect of terminal engine misalignment and insured that the engine thrust vector was aligned with the total relative velocity vector. Terminal engine misalignments were also the dominant disturbance torque on the roll attitude control system. Roll control was independent of pitch and yaw control and was described previously. The roll control system was sized such that failure of one of the four small roll engines did not cause loss of control capability when operating under 99-percent disturbance torques. Alignment of the geometric center line of each terminal engine relative to the body axes was measured during lander assembly and verified to be within the specification of ±1.0°. The measured misalignment and measurement uncertainties were used in conjunction with analytical estimates of misalignment between the engine thrust vector and the geometric center line to establish roll control torque margins. Technical feasibility studies showed

that actual measurement of thrust vector to geometric center-line alignment during terminal engine firing tests was not practical.

The derived pitch and yaw errors were rate limited to 30 deg/sec for general system stability and to prevent TDLR drop lock during the tip-up maneuver. (See fig. 54.) Angular rates were derived from IRU outputs to provide inner loop rate damping. The resulting pitch and yaw commands were filtered to provide stability compensation, and acceleration was limited to prevent excitation of fuel slosh modes that might allow pressurant to escape through the propellant outlet ports in the fuel tanks. The pitch and yaw commands were then processed by the engine command mixing equations. These equations transformed the attitude commands from the body axes to the terminal engine axes defined in later section "Propulsion Subsystem" and superimposed the attitude commands on the axial velocity command.

The navigator estimate of altitude H was related to a desired axial velocity V_d by the terminal descent contour, as shown in figure 54. The dual contours are sketched in figure 54 and represent the critical performance boundaries for terminal descent. Contour 1 was required for maximum fuel usage (fuel boundary) and countour 2 was required for maximum thrust (thrust-weight ratio boundary). The initial velocity for contour 1 was obtained by vectorially adding the 99-percent high velocity at parachute release and a 99-percent wind velocity. (See sketch (b).) The parachute terminal velocity was approximately
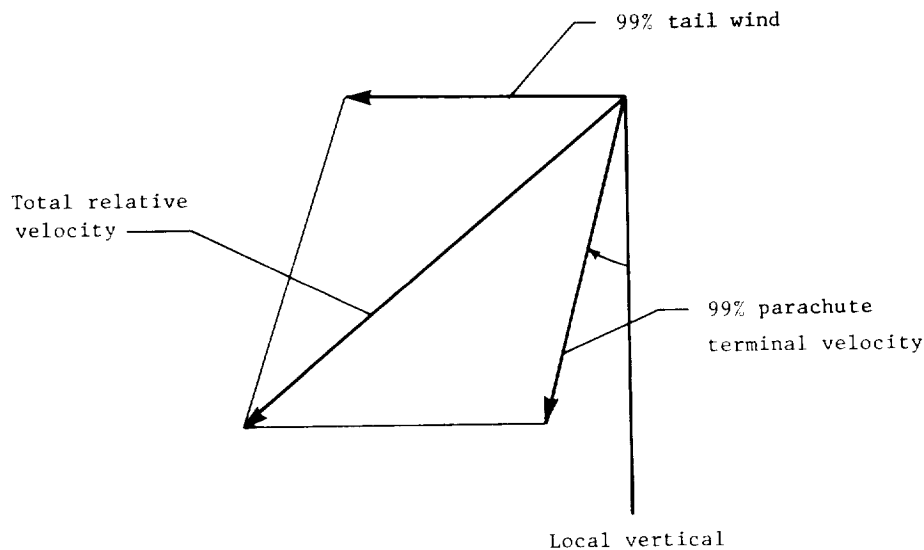
Sketch (b)

80.5 m/sec (264 ft/sec) at a flight-patch angle of 6.9°, that is, 21° from vertical. Horizontal velocity was accumulated during the parachute phase due to atmosphere winds. The 99-percent value of wind velocity was 51 m/sec

90

(167 ft/sec); it was considered as a tail wind to maximize total velocity and, thus, maximize amount of decelerating fuel required.

The contour was generated by a ground computer simulation containing a detailed model of the propulsion subsystem. The simulation considered a statistical combination of propulsion tolerances (propellant flow rate, specific impulse, etc.) and navigator errors (velocity, altitude, A-matrix, etc.) that tended to contribute to maximum fuel usage. In addition, the program simulated a continuous and constant 99-percent surface slope of $9°$; the simulated lander flew downslope to maximize flight time and, thus, fuel usage. The program iteratively solved for engine ignition altitude and fuel load while being constrained to a predetermined throttle position and a terminal velocity of 2.44 m/sec (8.0 ft/sec) at an altitude of 16.5 m (55 ft). This technique resulted in a total fuel load of 75.0 kg (165.3 lbm) at a nominal throttle position of 76.5 percent.

The nominal throttle position was established by separate analyses and six-degree-of-freedom simulations. Throttle tolerances were caused by uncertainties in propulsion and guidance and control parameters, for example, propellant tank pressure, propellant flow rate, engine thrust calibration, altimeter error, velocity radar error, throttle valve driver error, moment arm error, and center-of-gravity error. The 99-percent throttle tolerance for axial velocity control was ±7.3 percent. Thus, the 99-percent high throttle position was 76.5 percent + 7.3 percent or 83.8 percent. Therefore, a limit of 84 percent was established for axial velocity commands. This limit was an average of the three throttle positions. The three terminal engines were located symetrically about the lander geometric center; they were not symetrical about the center of gravity. This center-of-gravity offset caused the throttle positions of engines 1 and 3 to be higher than the 84-percent average limit and the throttle position for engine 2 to be lower than the 84-percent average limit for maximum deceleration and without disturbing the lander attitude. The throttle variance of engines 1 and 3 was 5.7 percent greater than the nominal; therefore, the 99-percent high throttle limit for engines 1 and 3 was 84 percent + 5.7 percent or 89.7 percent. A throttle limit was applied to the velocity control channel to prevent coupling between the axial velocity loop and the attitude loop; throttle travel above the 84-percent average limit (89.7 percent for engines 1 and 3) was reserved for attitude control with differential throttling of the engines. The 99-percent throttle tolerance for attitude control was ±6.3 percent due to parameter uncertainties. This left 4.0 percent throttle travel for nominal attitude control, 100 percent - (89.7 percent + 6.3 percent) equals 4.0 percent. Results of six-dimensional simulations established the requirement of 4.0 percent throttle travel for nominal attitude control and limit cycle functions.

Contour 2 of figure 55 represents the thrust-weight ratio boundary. The initial velocity for contour 2 was obtained by vectorially adding the 99-percent high velocity at parachute release and a head-wind component as shown in sketch (c). Since the head-wind magnitude was selected to cancel the horizontal component of the parachute terminal velocity, the initial velocity was
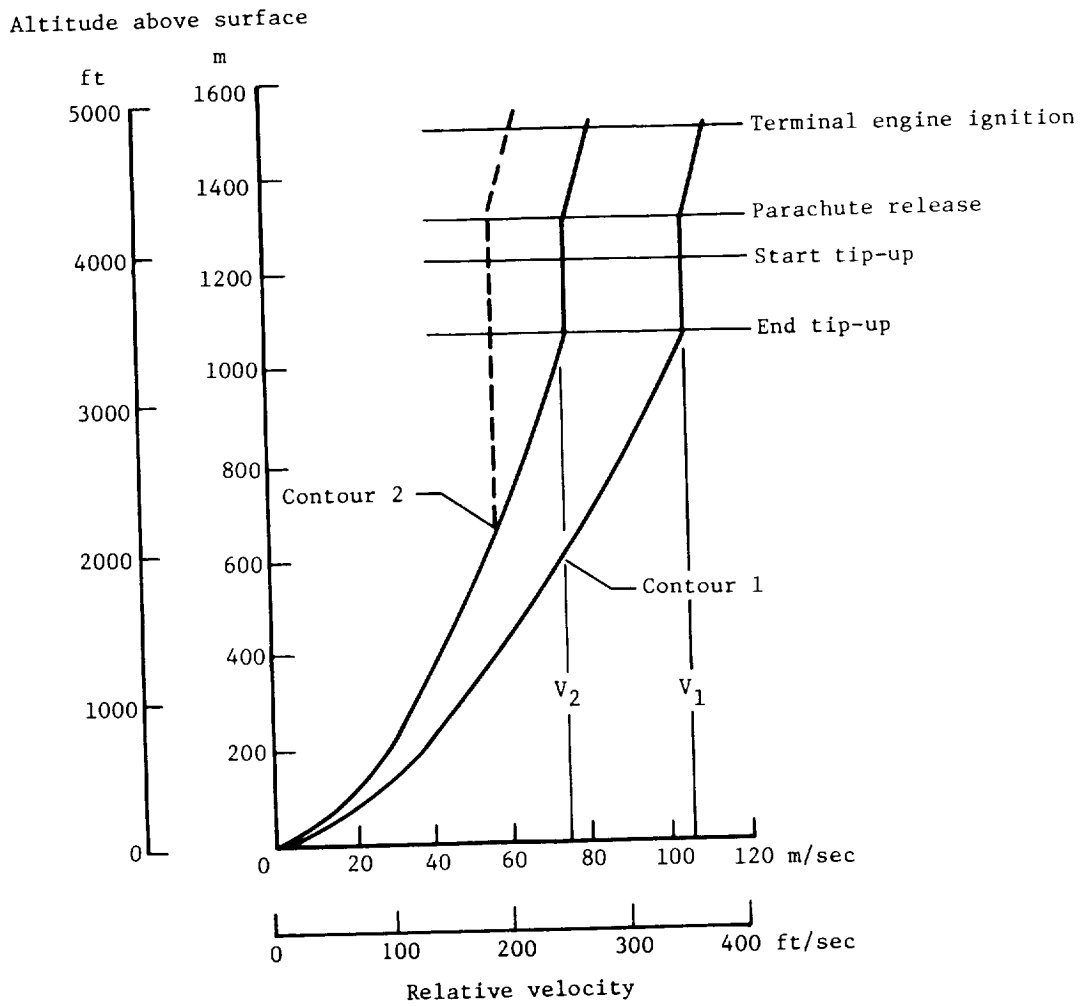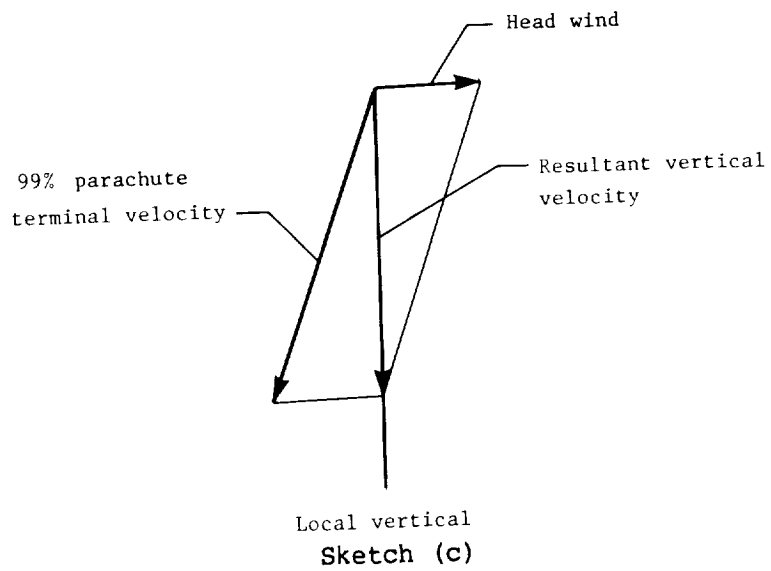
Figure 55.- Terminal descent contours.

Sketch (c)

the maximum vertical velocity. This high vertical velocity caused the lander to descend to the Mars surface in minimum time. Thus, if such conditions had been encountered, the engines would operate at high thrust for sufficient time to reduce the lander velocity to a terminal value of 2.44 m/sec (8.0 ft/sec). Contour 2 caused the engines to throttle up earlier; thus, sufficient time at high thrust was provided. Without contour 2, the lander dropped in altitude until contour 1 was encountered. At this point the engines throttled up to the axial limit (84 percent average) and remained at this limit, but terminal velocity was not achieved. The average throttle position required to track contour 2 was 55 percent under nominal conditions. The axial velocity command limit remained at 84 percent. Surface slope was not a factor in the design of contour 2; that is, a vertical descent had no downrange travel.

Design of the dual contours was based on worst-case combination of 99 percent parachute terminal velocity, 99 percent wind, and 99 percent surface slope. This was a justified departure from the statistical design concept. As stated earlier, the various atmospheric models were, by project management definition, not treated statistically. The worst-case atmosphere for contour design was the minimum density atmosphere. This atmosphere was the dominant factor in producing the 99-percent high parachute terminal velocity used in the design of both contours. Since the parachute terminal velocity was directly related to an atmospheric model, it was not treated statistically. Combining the 99-percent wind velocity with the 99-percent long-term surface slope was justified since surface slopes had insignificant effect on terminal descent unless such slopes occurred in combination with wind; that is, the downrange travel produced by the wind increased the lander's sensitivity to surface slope. This contour design approach evolved over a period of years and was strongly influenced by analyses coupled with exhaustive parametric six-dimensional simulations of terminal descent. These parametric simulations were deterministic in nature and were designed to explore the various boundary conditions. Results of analyses and corresponding parametric simulations indicated the necessity of deterministically defining wind direction for the worst case (tail wind) and defining surface slope direction for the worst case (downslope) if an overall probability of success of 0.99 was to be achieved. Verification of the contour design approach was provided by Monte Carlo simulations. A set of Monte Carlo statistics was generated for each of the atmospheric models. The Monte Carlo runs were initialized at the entry point (243.8 km (800 ft)) to evaluate the effect of entry parameters (e.g., entry angle dispersions and aeroshell lift-drag ratio tolerances) on parachute terminal velocity and landing success. The initial Monte Carlo results showed that soft-landing failures did exist and that most of the failures occurred in the minimum density atmosphere. Since each set of statistics was based on only 500 runs, 5 additional Monte Carlo sets were run with the minimum density atmosphere model. The number of failures varied from set to set; the minimum number of failures was 2 out of 500 (0.4 percent), the maximum number of failures was 12 out of 500 (2.4 percent), and the average number of failures for all sets was 5 out of 500 (1.0 percent). An error analysis of the Monte Carlo program established the simulation accuracy at ±2 percent. Therefore, it was possible to conclude that the contour design approach produced a probability of successful landing that was very close to the desired probability and, since failures occurred in all sets, the design approach was not overly conservative.

During the design and test phases of the lander, entry weight was tightly controlled and weight allocations were limited to the minimum necessary to meet mission requirements. Thus, the fuel load allocated for terminal descent was 74.98 kg (165.3 lbm) as justified by the described design approach. After completion of the test program, aeroshell and parachute entry performance capabilities were known and after assembly of the flight landers, entry weight was accurately known. This allowed computation of the final entry weight margin. Because of the criticality of terminal descent, a sizable part of the entry weight margin was reallocated to terminal descent fuel contingency. The terminal propellant was increased to the tank load limit of 83.91 kg (185.0 lbm). One-half of the additional 8.94 kg (19.7 lbm) of propellant was allocated to fuel margin and one-half was allocated to throttle margin. The fuel margin provided contingency for errors in the atmospheric model that would produce higher parachute terminal velocity and also provided contingency for surface features that would produce longer flight time, for example, flying into valleys or into craters. The throttle margin provided contingency for surface features that tended to reduce flight time and required additional thrust to compensate for rapid changes in measured altitude, for example, flying upslope or landing near the high edge of a large crater or valley. The terminal descent fuel allocation is shown in table 7 for both the computed load required to provide a high prob-

TABLE 7.- TERMINAL DESCENT FUEL ALLOCATION

Item	Fuel allocation for -			
	99% load[a] (Nominal throttle = 76.5%)		Flight load[b] (Nominal throttle = 70.0%)	
	kg	lbm	kg	lbm
Nominal usage on maximum velocity contour (contour 1)	65.32	144.0	69.85	154.0
Engine warm-up	2.31	5.1	2.31	5.1
Trapped in feed lines	2.22	4.9	2.22	4.9
Usage for mean roll attitude control	.32	.7	.32	.7
99% propulsion, guidance, and control tolerances	4.81	10.6	4.81	10.6
Fuel margin	.0	.0	4.40	9.7
Total	74.98	165.3	83.91	185.0

[a]Computed load to provide 99-percent landing success.

[b]Flight load is tank load limit and provides 6.5-percent throttle contingency and 4.40-kg (9.7 lbm) fuel contingency.

94

ability of successful landing (approximately 99 percent) and for the flight load (tank load limit). Monte Carlo analysis of the final flight load was not performed.

Prior to closing the axial velocity control loop, the flight software selected a descent contour based on the navigator's estimate of total relative velocity. Contours 1 and 2 were stored in polynomial form in the computer. If the total relative velocity was greater than V_1, contour 1 was used. (See fig. 55.) If the initial velocity was less than V_2, contour 2 was used. If the relative velocity was less than V_1 and greater than V_2, an interpolation routine was used to generate a contour that lay between contour 1 and contour 2. Since contour 1 was based on the maximum expected total velocity, it was unlikely that V_1 would be exceeded. However, if V_1 was exceeded, the lander had to recover and converge on contour 1 prior to touchdown. The throttle and fuel margins provided limited recovery capability as discussed previously.

If the mean density atmosphere and zero wind velocity were assumed to be the most probable, then the most probable initial relative velocity was about 60 m/sec (200 ft/sec); therefore, contour 2 was used in most cases. The dashed line shown in figure 55 is representative of the path the lander followed in the altitude-velocity domain. The lander maintained a nominal engine throttle setting of 10 percent after completion of tip-up maneuver and dropped in altitude at near constant velocity (slight acceleration) until contour 2 was encountered. Upon sensing contour intercept, the calculation of axial velocity error V_e was enabled. The velocity error V_e was computed by subtracting the desired velocity V_d obtained from the velocity-altitude contour from the navigator's estimate of axial velocity u as shown in figure 54.

An alternate to the velocity-altitude contour approach just described was considered in early design analyses. These analyses indicated that a multibeam slant-range radar implementation of the terminal descent contour was technically feasible for the Viking mission and would offer performance comparable with the broad-beam altimeter approach. The decision to use the altimeter was based primarily on hardware considerations.

The X-axis accelerometer output was used to change the gain of the axial command loop to compensate for propellant tank pressure blowdown. (See fig. 54.) The X-axis ΔV accumulated after parachute release was roughly proportional to the change in engine thrust due to tank pressure decay. The resulting axial velocity command A_c was superimposed on the pitch and yaw attitude commands by the engine mixing equations. Appropriate axial command gains were used in the engine mixing equations to compensate for the known center-of-gravity offset when computing engine throttle commands. This center-of-gravity compensation minimized the transient disturbances that couple into the attitude channels when large axial thrust changes were commanded. The largest axial thrust command changes occurred at contour intercept and at the transition to the constant velocity descent phase.

At an altitude of 99 m (325 ft), as estimated by the navigator, the TDLR was switched to the low power mode; beam width was reduced to enhance accuracy. At altitudes below 41 m (135 ft), the RA measurements were disregarded by the navigator, and altitude was computed from IRU and TDLR data only. The RA cut-

off was necessary to avoid possible false lock on rf signal returns from the lander structure. The cut-off limit of 41 m (135 ft) was established by analysis of data obtained from special rf tests that were conducted with the proof test lander and a flight-type RA.

Under nominal conditions, the lander reached a terminal velocity of 2.44 m/sec (8.0 ft/sec) at an altitude of 16.8 m (55.0 ft) and maintained this terminal velocity during a constant velocity descent to the surface of Mars. Trajectory perturbations generally prevented the occurrance of the two terminal conditions simultaneously. Therefore, the sequencing module of the GCSC initiated the constant velocity phase when either the navigator estimate of axial velocity reached 2.44 m/sec (8.0 ft/sec) or when the navigator estimate of altitude reached 16.8 m (55.0 ft). At initiation of constant velocity descent, the engines were throttled back to provide 1g (Mars) of decelerating force, and various control system gains were changed to enhance stability.

Series-parallel touchdown switches were mounted in each of the three landing legs. The design was such that a single failure cannot produce a false indication of touchdown or prevent the computer from receiving an indication of true touchdown. At touchdown, pyrotechnic valves were fired to seal the propulsion subsystem feedlines, all control loops were opened, and navigator computations were terminated. The dynamic touchdown requirements shown in table 8

TABLE 8.- LANDING CONDITIONS AT TOUCHDOWN

Item	Requirement[a]	99% value (b)
Velocity: Vertical, u, m/sec (ft/sec) . . . . Lateral, v and w, m/sec (ft/sec) . .	2.44 ± 0.91 (8.0 $\pm$ 3) 0 ± 1.22 (0 $\pm$ 4)	2.44 ± 0.46 (8.0 $\pm$ 1.5) 0 ± 0.61 (0 $\pm$ 2)
Attitude: Pitch and yaw, deg . . . . Roll, deg	0 ± 5 $c_{AZ} \pm 10$	0 ± 1.8 $c_{AZ} \pm 10$
Angular rate: Pitch and yaw, deg/sec . . . . Roll, deg/sec	0 ± 7 0 ± 3	0 ± 1.8 0 ± 1.0

[a]Requirement for stable landing based on landing leg design and Mars surface models.
[b]99-percent error analysis results.
[c]AZ refers to desired landed azimuth.

insured a 99-percent probability of stable landing, based on the structural landing system capabilities and Mars surface models. The error analysis results at touchdown were also given in table 8. The primary error contributors were navigator error, wind forces, and terminal engine misalignment.

Terminal descent stability was most critical during constant velocity descent when gain and phase margins reached minimum values. Figure 56 presents
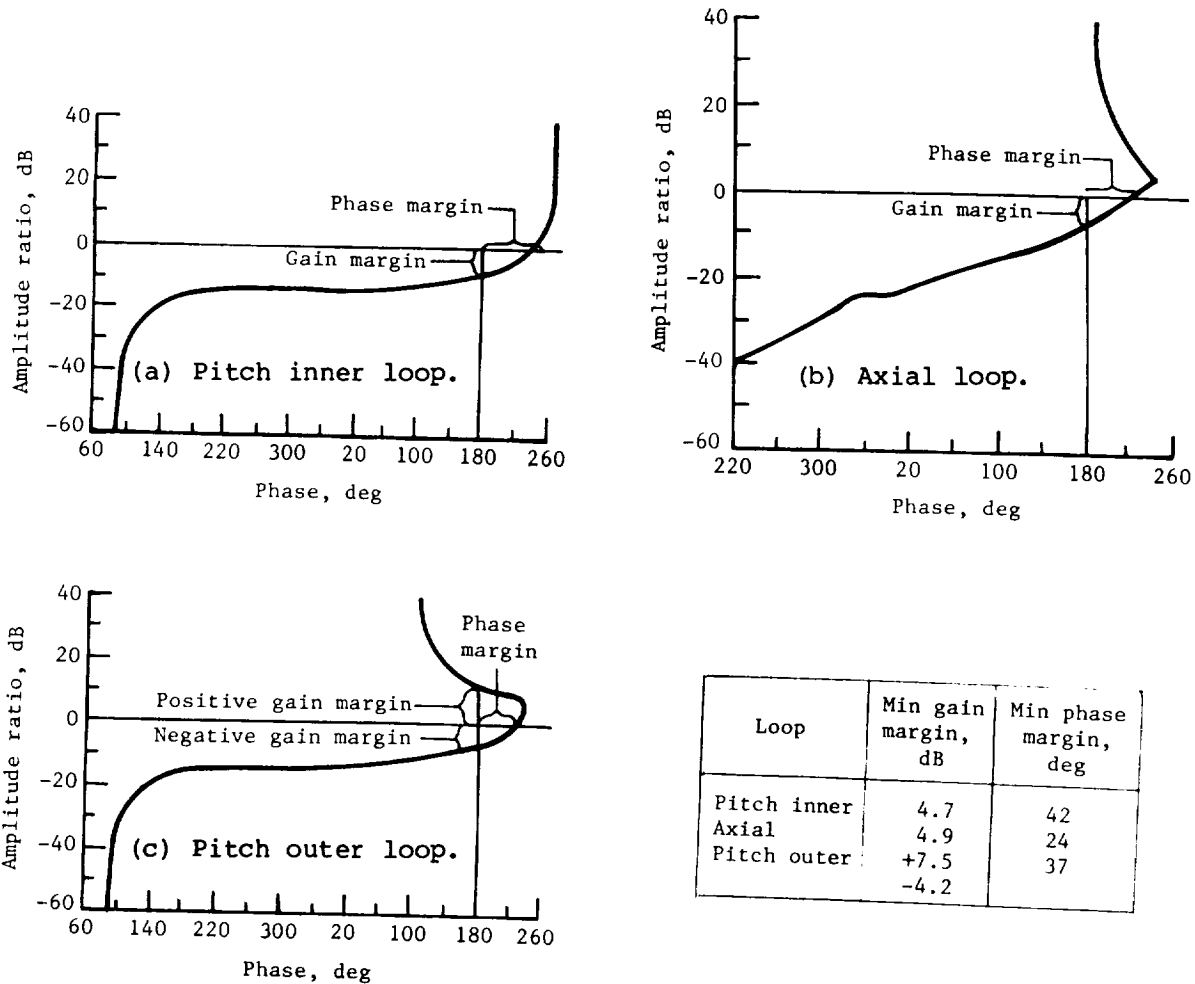
96

Figure 56.- Open-loop frequency response during constant velocity
descent. Axial velocity, 2.44 m/sec (8.0 ft/sec); TDLR locked
and tracking; RA disabled.

open-loop gain-phase plots for the three control loops. The three control loops
are shown in figure 54. The pitch and yaw attitude controls had an inner loop
and an outer loop. The inner attitude loop was updated at 20-msec intervals by
using rate feedback derived from the IRU gyroscope outputs; engine throttle com-
mands were issued at 20-msec intervals. The outer attitude loop was closed
through the navigator and was updated at 40-msec intervals. The axial velocity
loop was closed through the navigator and was updated at 40-msec intervals.
Radar data were processed by the navigator at 200-msec intervals. The plots
shown in figure 56 were generated by a sampled data stability analysis program
which evaluated the effect of software sample intervals and computational trans-
port lags on stability.

The total system was designed to have a minimum gain margin of 6 dB and
a minimum phase margin of 25° over the range of deterministic gain variation.
The deterministic gain variation occurred because the axial loop gain changer

97

(fig. 54) only partially compensated for the engine thrust variation due to tank pressure blowdown. Without the gain changer, the blowdown gain ratio was 2.60:1. The gain changer reduced the ratio to 1.56:1 or 3.8 dB. This deterministic gain variation was present in all three control loops. The plots of figure 56 show the gain margin and phase margin for nominal gains. These margins were degraded to the values given by random gain variations produced by uncertainties in engine location, inertia, IRU gain, throttle value position, and propellant flow linearity. Propellant flow linearity was the dominant random uncertainty. The degraded gain and phase margins were thus shown to be adequate for terminal descent stability.

Components

A brief description of each of the components of the guidance and control subsystem is presented in this section.

Guidance, control, and sequencing computer.- The GCSC (also referred to as the lander computer) was a random-access, stored-program, general-purpose digital computer system with the following characteristics: 18 432 words (approximately 6000 were required for guidance and control related functions), 0.05-mm (2-mil) plated-wire memory, 25-bit word length (24 data + 1 parity), NRZ-L serial transfers, direct and indirect addressing, 3 levels of indexing, two's complement arithmetic, 8-level priority interrupt system, memory and I/O parity checking, 4-serial data registers, 3 discrete registers, an error status register, a power control register, a cycle complete register, and a programmable timer register. Master clock frequency was 2.304 MHz. Execution times were as follows: bit time, 868 nsec; cycle time, 4.34 μsec; add, 8.68 μsec; multiply, 81.6 μsec; and divide, 128.5 μsec. The GCSC incorporated selectable block redundancy as shown in figure 57. Each memory contained a complete flight program. If hardware failures or software errors were detected during in-flight checkouts prior to separation of the lander from the orbiter, the redundant string was selected via commands transmitted from Earth. Only one of the redundant strings was powered on at any given time; there was no communication between the redundant strings and no antonomous switchover was allowed during descent to the Mars surface. In addition to the interfaces with G&C components described in the section "Subsystem Design Concept," the GCSC also interfaced with other lander subsystems in the process of controlling the mission sequence of events. These interfaces provided software control of pyrotechnic events such as parachute deployment and terminal engine ignition; data collection, storage, and playback by the telemetry subsystem; transmission and receipt of data (downlinks and uplinks) by the communication subsystem; and deployment mechanisms and power distribution to various subsystem components, including the science subsystem, by interface with the power subsystem.

Flight program.- The flight computer program was divided into four subprograms: executive, prelaunch and preseparation checkout, descent (separation to landing), and postlanded. The executive was based on an interrupt priority structure. The driving functions were prioritized such that a logical progression of events occurred when several interrupts occurred simultaneously. The executive contained a self-test routine designed to detect single point hardware failures within the GCSC. The self-test routine included an instrument self-
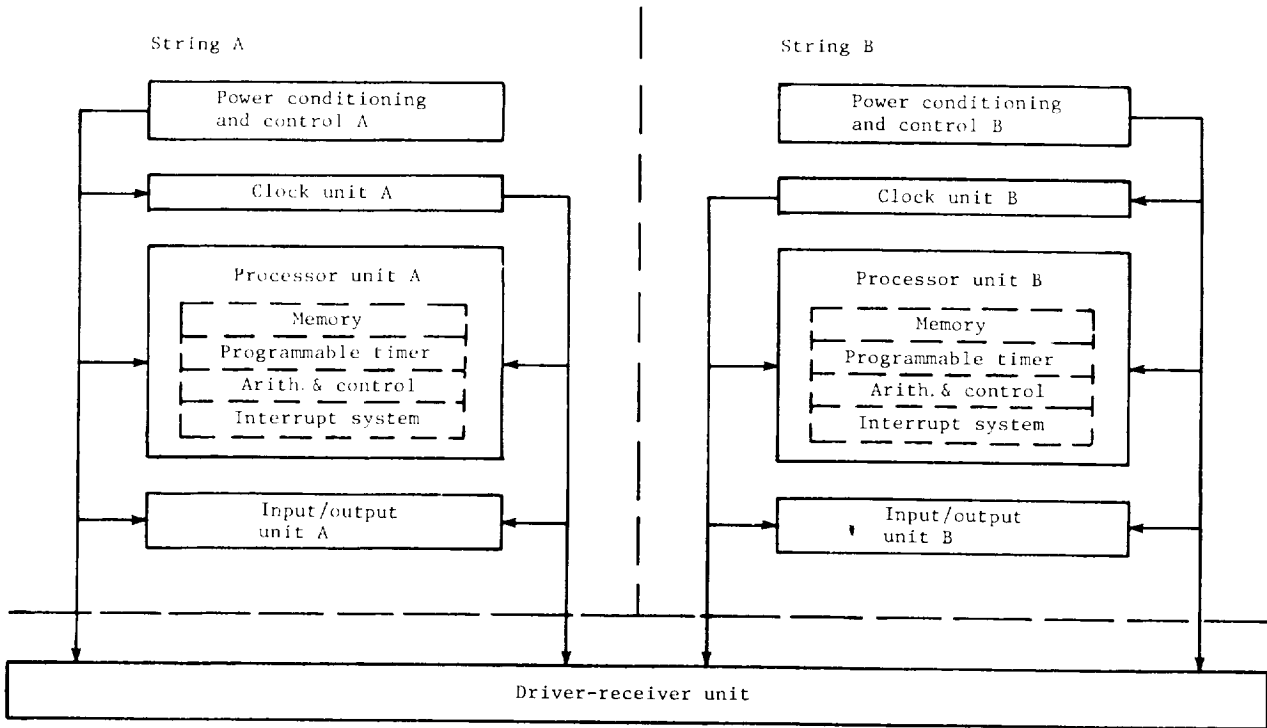
```
┌──────────────────────┐                    ┌──────────────────────┐
│  Power conditioning   │                    │  Power conditioning   │
│  and control A        │                    │  and control B        │
└──────────────────────┘                    └──────────────────────┘

┌──────────────────────┐                    ┌──────────────────────┐
│    Clock unit A       │                    │    Clock unit B       │
└──────────────────────┘                    └──────────────────────┘

┌──────────────────────┐                    ┌──────────────────────┐
│   Processor unit A    │                    │   Processor unit B    │
│  ┌─────────────────┐  │                    │  ┌─────────────────┐  │
│  │     Memory      │  │                    │  │     Memory      │  │
│  │ Programmable timer│ │                    │  │ Programmable timer│ │
│  │  Arith. & control │ │                    │  │  Arith. & control │ │
│  │ Interrupt system  │ │                    │  │ Interrupt system  │ │
│  └─────────────────┘  │                    │  └─────────────────┘  │
└──────────────────────┘                    └──────────────────────┘

┌──────────────────────┐                    ┌──────────────────────┐
│   Input/output        │                    │   Input/output        │
│   unit A              │                    │   unit B              │
└──────────────────────┘                    └──────────────────────┘

┌────────────────────────────────────────────────────────────────────┐
│                      Driver-receiver unit                            │
└────────────────────────────────────────────────────────────────────┘
```

Figure 57.- Redundancy in GCSC.

test, a memory test, and an input/output test. The prelaunch and preseparation routines provided for checkout of the various lander subsystems and components. Preseparation checkout is described in reference 1. The descent routines included the G&C algorithms as described in the section "Subsystem Design Concept." These routines also provided program sequencing and control of data processing, storage, and telemetry. All descent calculations for navigation, guidance, and control occurred during particular calculation periods. The calculation periods occurred at four defined rates based on the GCSC real-time interrupt which interrupts processing once every 10 msec and are given as follows:

(1) A-rate calculation period occurred once for every two RTI's (20-msec period)

(2) B-rate calculation period occurred once for every two A-rate calculation periods (40-msec period)

(3) C-rate calculation period occurred once for every five B-rate calculation periods (200-msec period)

(4) D-rate calculation period occurred once for every five C-rate calculation periods (1000-msec period)

Six descent modules are therefore designed to perform the following descent tasks:

99

(1) The A-rate module performed the 20-msec frequency tasks

(2) The B-rate module performed the 40-msec frequency tasks

(3) The C-rate module performed the 200-msec frequency tasks

(4) The D-rate module performed the 1000-msec frequency tasks

(5) The sequencing module was a subroutine of the A-rate module which performed the sequencing tasks

(6) The telemetry module performed the formats 2, 2A, 2P, and 3 telemetry tasks

The postlanded routines controlled sequencing, operation, and data gathering in support of the landed scientific payload. A routine was also required for control of the high-gain antenna pointing; pointing data were obtained from the gyroscopes and accelerometers.

Inertial reference unit.- The IRU provided a continuous measurement of three orthogonal (pitch, yaw, and roll) components of lander attitude and velocity motion with respect to the inertial reference. The IRU utilized rate integrating gyroscopes and pendulous integrating accelerometers as the sensing devices for making these measurements. Since these devices had a single degree of freedom, one was required for each axis requiring motion sensing. The IRU included four gyroscopes, three in an orthogonal triad and the fourth skewed at equal angles with respect to the triad for backup redundancy. The IRU also included four accelerometers, three in an orthogonal triad and the fourth parallel and redundant to the critical roll axis (X-axis) accelerometer. These sensing devices were used in the strap-down mode in that they were effectively hardmounted directly to the lander structure and thereby are physically subjected to the identical dynamic motions experienced by the lander. The gyroscope and accelerometer orthogonal triads were precisely aligned and defined the lander pitch, yaw, and roll axes by the IRU mounting structure. The IRU incorporated selectable block redundancy in a common enclosure. If failures were detected during in-flight checkouts prior to separation of the lander from the orbiter, block redundancy was selected by flight software changes transmitted from Earth. The available block redundancy included electronics, thermal controls, and power supplies as well as the sensors mentioned previously. The IRU sensors were operated in a torque rebalance mode. Thus, the current required to hold each sensor at its null position was a measure of the motion encountered. The bandwidth of the sensor pulse rebalance servo loops was approximately 20 Hz. The gyroscopes had a low torque rebalance range of 12.5 deg/sec. This low range was used for all mission phases except the parachute phase and the terminal descent phase where predicted angular rates necessitated a high torque rebalance range of 100 deg/sec. The accelerometers had single torque rebalance ranges of 20g along the roll axis (entry deceleration axis) and 5g along the pitch and yaw axes. Gyroscope short term bias stability was typically 0.1 deg/hr, and accelerometer short term bias stability was typically less than $5 \times 10^{-5}g$. The IRU error coefficients are summarized in table 3. These coefficients were used in the subsystem error analysis. The

IRU was thermally controlled during cruise to Mars to maintain gyroscope temperature above $-11°$ C ($12°$ F) to avoid predicted thermal stress failures. The IRU was thermally controlled during operation to maintain the gyroscopes and electronics at $71°$ C ($160°$ F) and the accelerometers at $65.5°$ C ($150°$ F). The IRU interfaced with the GCSC to perform its guidance and control subsystem functions. The IRU also interfaced with the power subsystem for operating and thermal control power and with the telemetry subsystem to provide data for both science and engineering.

Radar altimeter.- The RA measured lander altitude relative to the surface of Mars. The total RA system was composed of two identical and independent sets of RAE housed in separate boxes, an antenna mounted on the aeroshell, an antenna mounted on the bottom of the lander, and an antenna switch. The RA was a noncoherent pulse-type altimeter with a leading-edge tracker. The operating frequency was 1 GHz and the operating range was 137 km (450 000 ft) to 41 m (135 ft). The altitude range was divided into four modes to enhance accuracy over the large dynamic range and to provide false target discrimination; the tracker searched only the altitude range indicated for each mode. These four modes are

Mode 1:   3 to 137 km (10 000 to 450 000 ft)

Mode 2:   1.2 to 7.6 km (4000 to 25 000 ft)

Mode 3:   0.46 to 1.8 km (1500 to 6000 ft)

Mode 4:   0 to 0.76 km (0 to 2500 ft)

The accuracy of the altitude measurement was 1.5 percent or 152 m (500 ft) in mode 1. In modes 2, 3, and 4, the accuracy was 4.5 percent + 1.5 m (5 ft). Additional false target discrimination was provided by a variable, return signal strength threshold which was a function of altitude and provided graduated attenuation for receiver desensitization to false targets. (False targets were any radar reflectors other than the surface of Mars, e.g., the aeroshell and parachute canister after they separated from the lander, see fig. 58.) The antenna mounted on the aeroshell had a broad-beam fan-shaped pattern approximately $20°$ by $80°$. The smaller dimension was maintained in the plane of the trajectory. (See fig. 59.) The antenna mounted on the lander was used after separation of the aeroshell and had a broad-beam hemispherical pattern. With either of these broad-beam antennas, the RA operated in a first-return mode; that is, the RA responded to surface slopes and features and measured the distance to the nearest point on the surface. The antenna switch, in response to software commands, allowed operation of either RAE with either antenna. As stated previously, the electronics of the RA system were block redundant. If a failure was detected in one RAE during in-flight checkout prior to separation of the lander from the orbiter, the failed RAE could be permanently disabled by flight software changes transmitted from Earth. In addition, the flight program stored in the GCSC autonomously switched to the backup RAE if the prime RAE failed to lock-on the Mars surface during entry. The RA interfaced with the GCSC to perform its guidance and control subsystem functions. The RA also interfaced with the power subsystem for operating power and with the telemetry subsystem to provide data for both science and engineering.
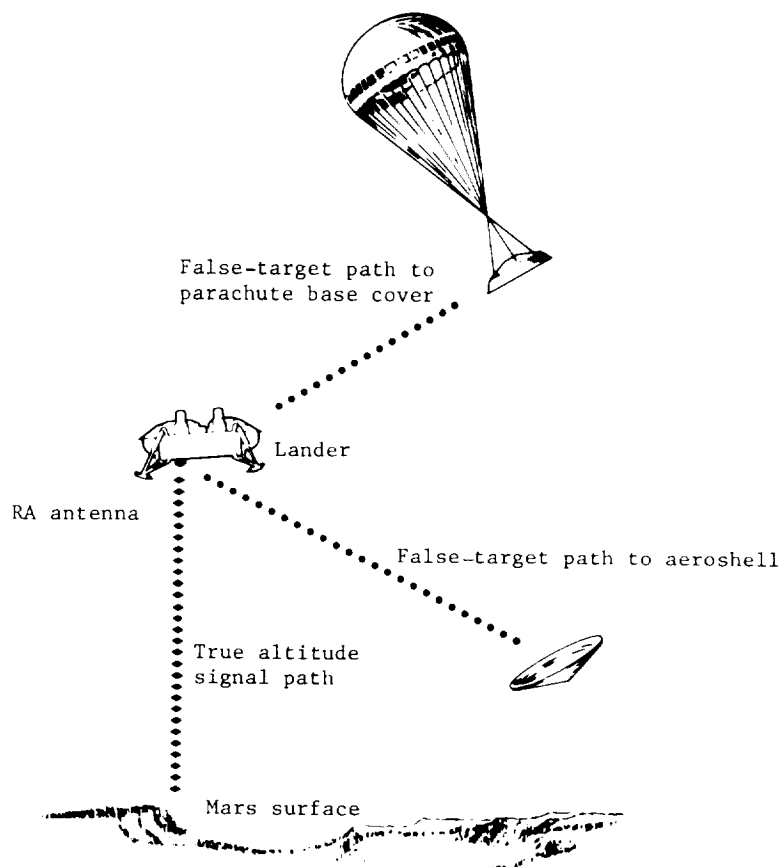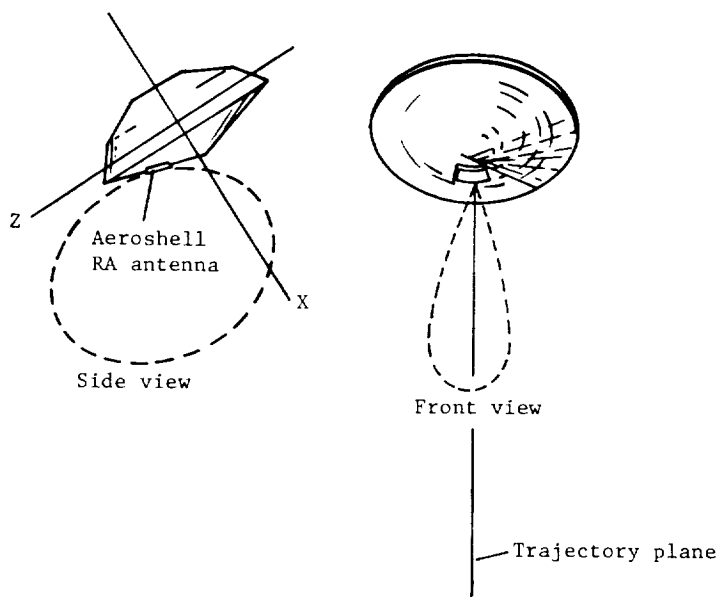
Figure 58.- Altimeter false-target geometry.

Figure 59.- Radar altimeter aeroshell antenna pattern.

Terminal descent and landing radar.- The TDLR, which was a continuous wave, four-beam Doppler radar, measured lander velocity relative to the surface of Mars. The antenna phased arrays were an integral part of the component structure; thus, the TDLR was mounted on the bottom of the lander for proper field of view. As shown in figure 60, the four beams were symmetrical about the lander
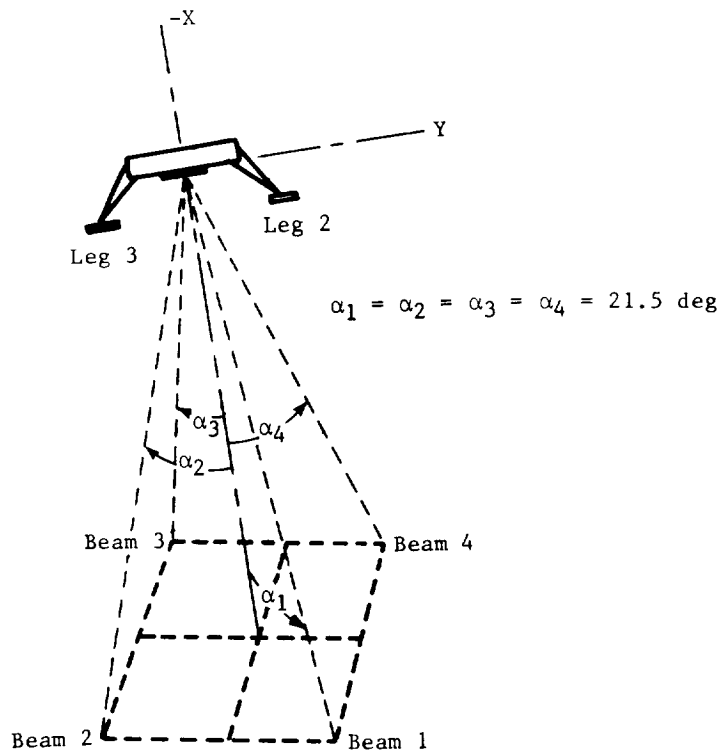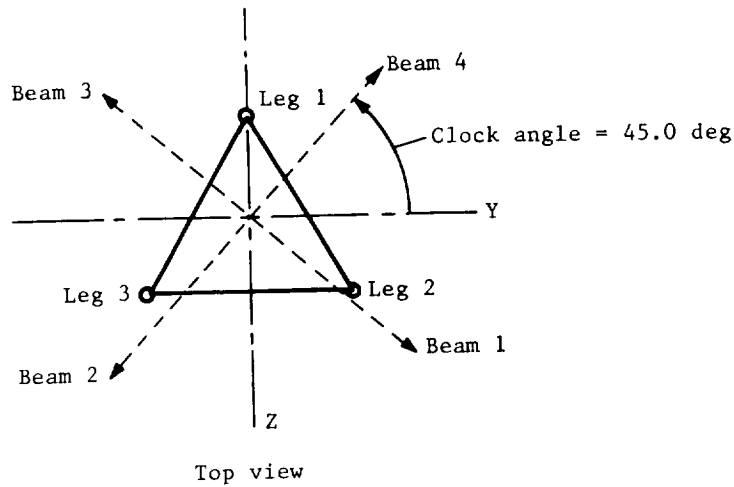

Figure 60.- TDLR beam geometry.

roll axis and were rotated 45° with respect to the lander pitch and yaw axes. The four splay angles were equal at 21.5°. The gain of each beam was approximately 29 dB and the beam width was less than 3.5°. The output of the IMPATT diode transmitters is 150 mW at a nominal frequency of 13.3 GHz. However, each beam has a separate frequency to avoid cross coupling due to side-lobe return and coupling between radiators; the frequency separation was nominally 12 MHz. The velocity range of each beam was approximately 1 to 225 m/sec (3 to 738 ft/sec) with an accuracy of 1.5 percent or 0.3 m/sec (1.0 ft/sec), whichever was greater. The second-order receiver servos were designed to track positive Doppler only (closing range rate) to provide false-target discrimination.

Since each of the four beams was completely independent and, as explained in the section "Subsystem Design Concept," only three of the four beams were required for a safe landing, redundancy was thus provided. If a beam failure was detected during in-flight checkout prior to separation of the lander from the orbiter, use of the failed beam data could be deleted in the flight software by changes transmitted from Earth. In addition, the flight program stored in the GCSC disregarded velocity data from a beam that failed to display positive tracker lock and data good flags and autonomously flew the mission with the remaining three beams. (See fig. 61.) The flags were generated by the TDLR electronics and passed to the computer. The tracker lock flag indicated lock-on the Mars surface return and the data good flag indicated a signal-noise ratio adequate to meet accuracy requirements.

One beam illuminating aeroshell

Three beams illuminating Martian surface
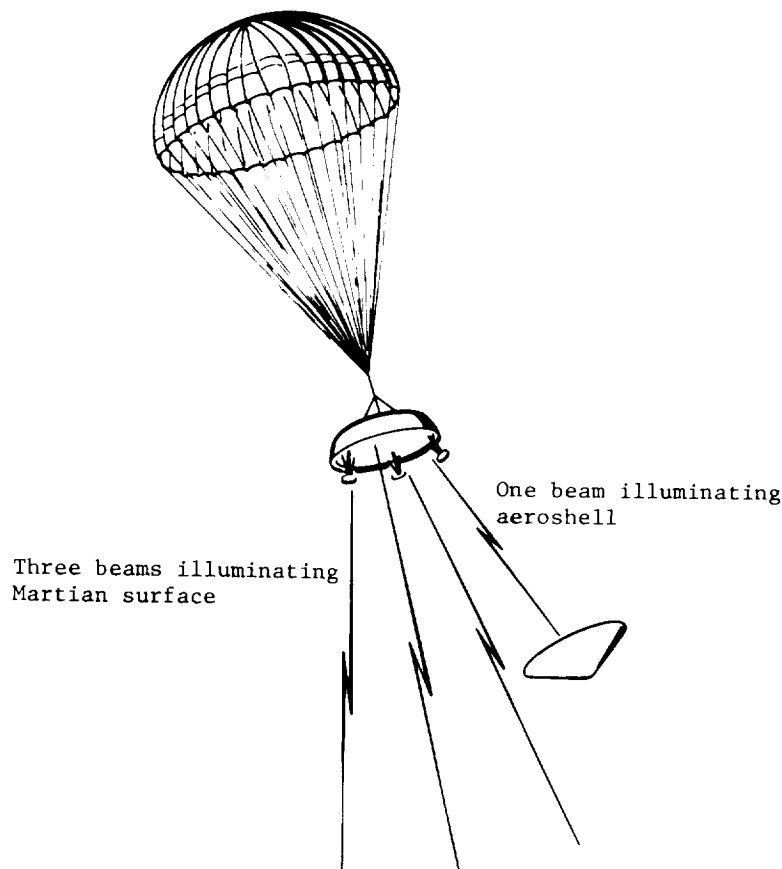
Figure 61.- TDLR false-target geometry.

The TDLR interfaced with the GCSC to perform its guidance and control sub-
system functions. The TDLR also interfaced with the power subsystem for operat-
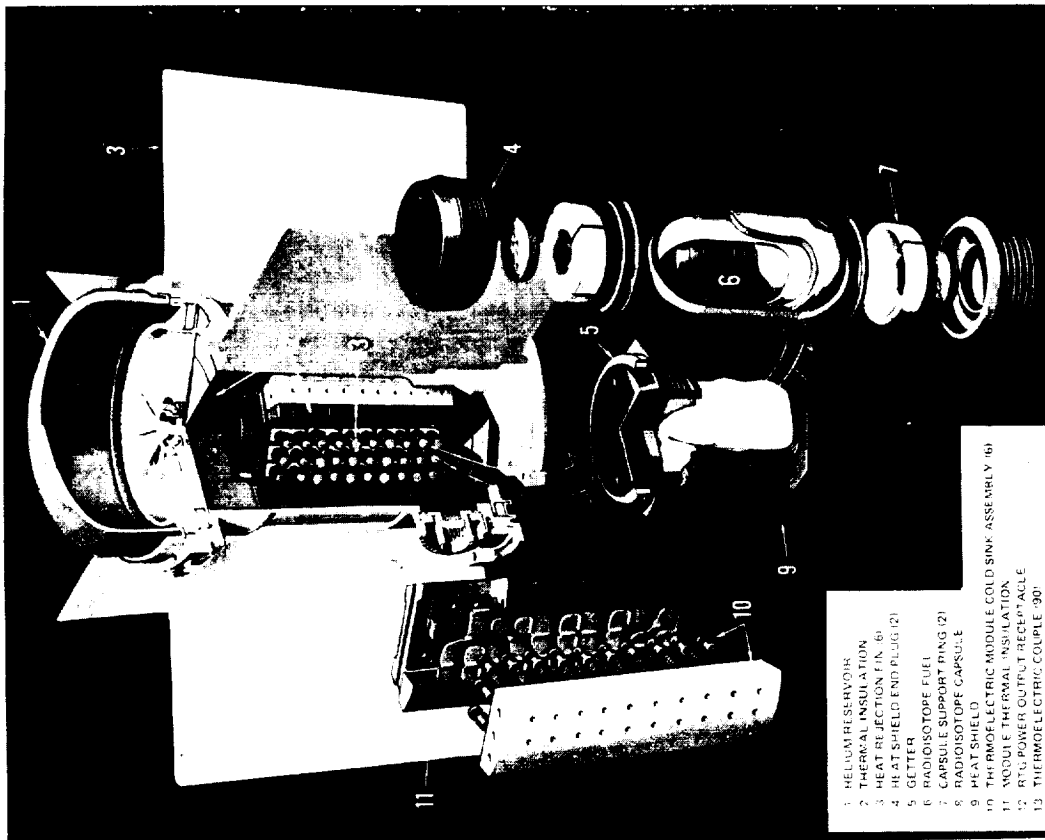ing power and with the telemetry subsystem to provide data for both science and
engineering.

Valve drive amplifier.- The VDA was the interface component between the
G&C and propulsion subsystems and contained the drivers for both the solenoid
valves (reaction control engines) and the throttle valves (terminal descent
engines). All propulsion valve commands were generated in the GCSC for both
the RCS and the TDS. The RCS and TDS are discussed in a later section "Propul-
sion Subsystem." The RCS section of the VDA received digital RCS commands from
the GCSC. The commands were decoded, and appropriate on or off valve drivers
were actuated. The RCS section of the VDA contained passive quad-redundancy
for compatibility with RCS valve and engine redundancy. The redundancy was
passive in that nominal performance was maintained without issuing commands to
clear the failure. The TD portion of the VDA received digital commands from
the GCSC. The commands were decoded and the current output of the pulse-width-
modulation amplifiers was appropriately adjusted. The TD portion of the VDA
also received analog feedback from the terminal descent engine throttle valve
position transducers. The TD portion of the VDA provided both forward loop and
feedback loop compensation to maintain required stability margins. The VDA
interfaced with the power subsystem for operating power and with the telemetry
subsystem to provide data for both science and engineering.

Power Subsystem

Radioisotope Thermoelectric Generator

The required electrical power for the VLC after separation from the VO was
supplied by two RTG's (SNAP 19/Viking). The RTG was 53 cm (23 in.) from fin
tip to fin tip and 41 cm (16 in.) high and weighed 15.4 kg (34 lbm). Each RTG
produced a minimum electrical power output of 35 W during the 90 days of mission
operations on the Mars surface. The RTG, shown in figure 62, had a thermoelec-
tric couple array which converted thermal energy produced by a radioisotopic
heat source directly into electrical power. The radioactive decay of the
plutonium-238 fuel resulted in a nominal heat generation rate of 682 W(t) at
the time of capsule fuel loading. This initial thermal inventory decayed
exponentially with time at a rate related to the plutonium-238 half-life. The
waste heat was rejected through a housing-radiator assembly.

The four main functional elements of the RTG - housing-radiator assembly,
thermoelectric converter assembly, radioisotopic heat source assembly, and
telemetry instrumentation - are described as follows.

The RTG housing-radiator assembly consisted of a six-finned cylinderical
housing, two ribbed end covers, two U-channel seal-weld rings, and a dome res-
ervoir. All components were fabricated from a magnesium-thorium alloy. The RTG
was installed on the lower end cap cooler of the VLC with six mounting legs; the
upper end cooler-radiator assembly of the VLC is mounted on a flange with six
holes at the top of the housing. The end cap coolers provided auxiliary ground
cooling before launch and supplemented the RTG radiator area after launch.

Power, W	35
Voltage, V	4.4
Weight, kg (lbm)	15.4 (34)
Fuel	Plutonium-238
Fuel form	Plutonium-molybdenum cermet (PMC)
Thermal loading, W	682
Hot junction temperature, °C (°F)	571 (1060)
Fin root temperature, °C (°F)	171 (340)
Thermoelectric couples	TAGS-85/2N
Number of thermoelectric couples	90
Emmissivity	0.85
Solar absorptivity	0.3

1. HELIUM RESERVOIR
2. THERMAL INSULATION
3. HEAT REJECTION FIN (6)
4. HEAT SHIELD END PLUG (2)
5. GETTER
6. RADIOISOTOPE FUEL
7. CAPSULE SUPPORT RING (2)
8. RADIOISOTOPE CAPSULE
9. HEAT SHIELD
10. THERMOELECTRIC MODULE COLD SINK ASSEMBLY (6)
11. MODULE THERMAL INSULATION
12. RTG POWER OUTPUT RECEPTACLE
13. THERMOELECTRIC COUPLE (90)

Figure 62.- Radioisotope thermoelectric generator.

The thermoelectric converter assembly consisted of six thermoelectric modules surrounding the hexagonally shaped heat source; each module had an associated cold-end hardware assembly (springs, pistons, alignment buttons, and heat sink bar). The thermoelectric converter materials were Teledyne isotopes TAGS-85 with a thin SnTe segment at the hot side (P-leg) and 3M Company 3M-TAGS-2M(M) PbTe (N-leg). Each thermoelectric module contained 15 P-N couples for a total of 90 couples per generator. The couples were electrically connected in a parallel-series configuration (couples were connected in paralleled pairs and the resulting 45 couple pairs were connected in series). Electrical power generated in the thermoelectric circuit was withdrawn through a 26-pin electrical receptacle in the side of the housing. The generator power circuit incorporated a magnetic compensation loop at the mounting end of the generator (end nearest the power output receptacle) to minimize the external magnet field caused by the electrical current flow in the thermoelectric circuit. A ring-shaped zirconium getter assembly for removing any hydrogen gas which might be generated by remaining moisture within the generator components was nested in a recess at each end of the heat shield.

The radioisotopic heat source assembly was a four-layer, vented capsule enclosed in a right hexagonal prism graphite reentry body. The design provided for intact reentry through aerothermal heating and fuel retention on Earth impact. To prevent pressure buildup, a pressure release device vented the helium gas generated by the fuel decay to the thermoelectric converter volume.

Telemetry instrumentation monitored the operating conditions within the RTG by means of leads through the 26-pin electrical receptacle. A platinum RTD, metal oxide thermistor, and resistance (voltage divider) pressure transducer monitored the hot junction temperature, fin root temperature, and internal pressure, respectively.

The two operating modes of the RTG were shorted and on load. In the shorted mode the RTG output voltage was less than 1.0 V dc with a short-curcuit current of approximately 20 A. In this nonoperating mode, the degradation of the RTG thermoelectric couples was minimized due to the reduced operating temperature of the hot junction. When the RTG was on load the PCDA maintained the RTG output voltage at 4.4 ± 0.1 V dc. In this configuration, the RTG could supply power from 35 to 47 W depending on fin root temperature and RTG age.

The RTG's interfaced with the lander subsystems and components as follows:

Thermal: The RTG's, in addition to supplying electrical power, also supplied the VLC with thermal energy which was used to maintain the VLC at operational temperatures. The RTG's were mounted on the VLC body and separated from the equipment plate by a thermostatically controlled thermal switch. When the switch was closed, the waste heat from the RTG was channeled into the VLC body; when the switch was open, the majority of the heat was rejected by radiation and convection. In addition to the lander thermal control system, an active cooling system was provided for prelaunch thermal control. This system interfaced with the RTG via an upper and lower end cap cooler mounted to the respective RTG flanges. Chilled water flowed through these end cap coolers as well

as the VLC equipment plate to remove waste heat from the VLC during prelaunch operations. The system was disconnected and purged at launch.

PCDA: The two series-connected RTG's were connected to the PCDA via the VLC harness. The PCDA maintained the RTG's in either of the two operating modes. In the short-circuit mode the RTG series output was shorted internal to the PCDA by using series redundant motor driven switches. In the on-load operating mode, the PDCA converter maintained the RTG series output at 8.8 ± 0.2 V dc.

Telemetry: The two RTG temperature sensors were signal conditioned in the DAPU and the output was low-level signals. The pressure transducer was a high-level telemetry signal stimulated by a 5 V dc input from the DAPU.

At delivery the RTG's were required to supply a minimum of 40.5 W and a maximum of 47.0 W at a fin root temperature of $166^\circ \pm 3^\circ$ C ($330^\circ \pm 5^\circ$ F) and an output voltage of 4.4 ± 0.1 V dc. Two series-connected RTG's were required to supply a minimum of 81.0 W and a maximum of 94.0 W at 8.8 ± 0.2 V dc at a fin root temperature of $166^\circ \pm 3^\circ$ C ($330^\circ \pm 5^\circ$ F). The power output at the EOM was a minimum of 35 W for each RTG under the same voltage and temperature conditions. The anticipated RTG power output as a function of load voltage is shown in figure 63. From an operational viewpoint, the RTG's remained in the short-circuit mode except when they were required to supply power. This minimized the exposure of the thermoelectric couples to high temperature; thus, RTG degradation was also minimized. RTG temperatures (fin root and hot junction) varied considerably throughout the mission depending upon environmental conditions, operating mode, and spacecraft configuration. The hot junction temperature ranged from 371° to 582° C (700° to 1080° F) and the fin root ranged from 38° to 182° C (100° to 360° F). RTG internal pressures ranged from 89.6 to 131 kPa (13 to 19 psia) at delivery depending upon temperature. The pressure was expected to increase to as high as 179.3 kPa (26 psia) during RTG life due to helium buildup within the RTG.

Batteries

During the various Viking Mission phases, from launch through the post-landed scientific data acquisition periods, electrical power requirements frequently exceeded the capabilities of either the VO power system during cruise or the VL RTG's. The in-flight checkout test sequence required battery power during the subsystem checkouts. During entry and landing operations, the electrical power requirements exceeded the RTG capabilities by a considerable margin. Several of the scientific experiments and the rf transmitters also required battery power during their operation. During other periods of the mission sequences, the electrical power demands were well below the capabilities of the VO power subsystem or the VL RTG's, and, since the RTG's operated at a constant power level, the excess energy must be dumped into load banks and dissipated as heat. Rechargeable batteries were used to store this excess energy until needed during periods of peak power demand. Nickel-cadmium batteries were well suited for this application since they could withstand the VLC sterilization requirements and the space environment and were capable of many charge-discharge cycles. Each VLC required two battery assemblies. Each assembly contained two 30-V nominal, 24-cell, nickel-cadmium batteries. Each battery had

Equivalent thermal input, 682 W
Average fin root temperature, 166° C (330° F)

——— Predicted ETG/RTG beginning of life
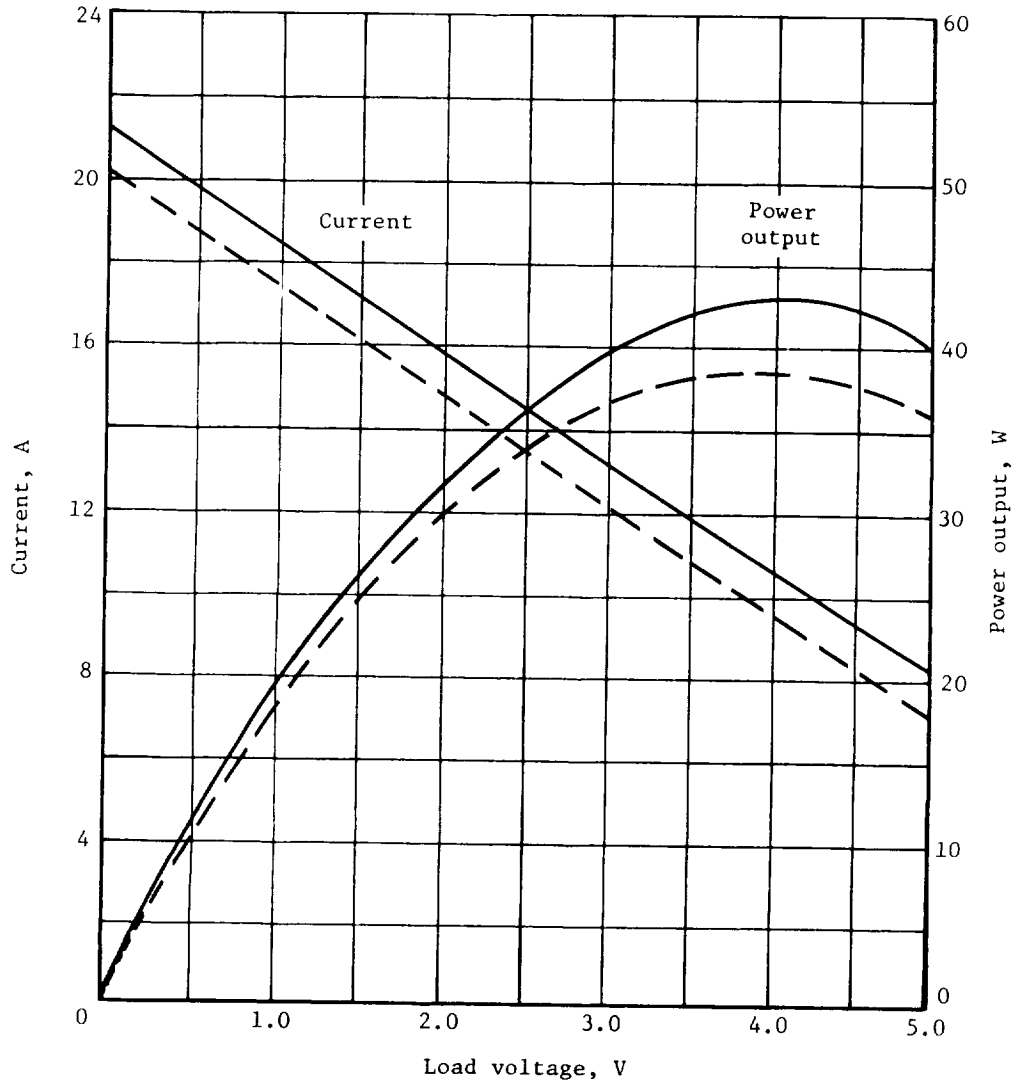——— Predicted RTG end of mission

Figure 63.- Nominal steady-state generator voltage-current power relationships.

a name plate capacity of 8 A-hr. The cells were assembled with their bases resting against a center plate which separated the two batteries within the assembly and served as a heat sink to transfer the heat from the cells to the mounting plate. The cells used in the batteries were 8 A-hr (at end of life) sealed nickel-cadmium cells. Each cell contained 11 positive plates and 12 negative plates. The cell plate design used a perforated steel sheet as a substrate. This steel substrate was nickel plated, then loaded with a nickel powder which was sintered. The plates, which were 80 percent porous, were then

loaded with active material (cadmium on the negative plates and nickel on the positive plates). The cell plates were stamped from the steel sheet substrate after loading. The plate edges were coined to prevent flaking. Polypropylene was selected for the separator material over the more conventional nylon due to the high temperature sterilization requirements of the Viking program. The separators were fabricated into bags with welded edges and then slipped over the positive plates. An additional layer of separator was wrapped around the assembled plate pack. A solid sheet of polypropylene was placed between the cell case and the plate pack to insulate the plates from the case. The cell case was fabricated from type 304L stainless steel. The bottom and top headers were electron beam welded to the case sides. The top header contained the two cell terminals and the fill tube. Both the positive and negative terminals were insulated from the cell case with ceramic insulator seals. The fill tube was sealed off during the final stages of assembly and test. An aluminum strip was fastened with epoxy to the recessed bottom of each cell base to a heat-transfer surface between the cells and the center plate. A thermally conductive, electrical insulating, potting compound was applied to the heat-transfer plate during assembly to provide a low thermal impedance path from the cell bases to the plate; thus, the heat-transfer rate was improved. The cells were electrically insulated from each other by a 0.1-mm-thick (5 mil) sheet of Kapton wrapped around the sides of each cell. The mechanical structure of the battery served as a restraint for the cell sides to prevent bulging during charging. Oxygen gas was generated, as a normal process, during the latter stages of charging and when the battery was overcharged. This pressure buildup caused the cell cases to bulge unless restrained. The pressure gradually decreased as the oxygen was chemically recombined at the negative plates. A temperature sensor, consisting of a platinum resistance element, was placed between the fourth and fifth cell in each row of cells. Two of the sensors had a nominal resistance of 1600 Ω and were used to provide data relative to the battery temperature to the VLC battery charge logic. The third sensor was a 160-Ω unit and interfaced with the telemetry subsystem to provide data on battery operation during the mission. The battery assembly detail parts were fabricated from magnesium-thorium alloy. These parts received an anodic treatment during fabrication to inhibit corrosion of the magnesium alloy.

The batteries were operated in five modes throughout the Viking Mission. These modes were (1) discharged, (2) condition charging, (3) float charging, (4) recharging, and (5) discharging. During the early phases of the mission from lift-off to the in-flight checkout period, the batteries were discharged. Just prior to the in-flight checkout period, the batteries were condition charged. Condition charging consisted of charging at a low rate (0.53 A) for 24 hr. This low rate was used whenever the batteries had been left in a completely discharged condition for extended periods of time. Float charging was a low-rate trickle charge applied to a charged battery to maintain it in a charged condition over a period of time. A C/160 charge rate was used for float charging. Recharging was required after the batteries had been utilized to supply energy to the VLC subsystem. Recharge rates varied from as low as C/40 up to a C/6 rate. The recharge rate was dependent upon the available energy from the RTG's. The batteries were discharged by switching them to a 19.3-Ω load bank or by switching them to the VLC buses and using them to power the subsystems.

The four batteries were switched between the battery charge and the equipment bus by the PCDA. Connections to the equipment bus were made through isolation diodes. The two battery assemblies were installed in the VLC side by side on the equipment mounting plate. Close contact between the battery base and the mounting surfaces was required to provide a low thermal impedance for the transfer of heat between the battery and the VLC structure. Power requirements of the batteries were limited to those required to recharge the batteries after they were discharged. This charging power was obtained from the VO via the BPA when the VLC and VO were mated. After VO and VLC separation, the charging power was supplied by the RTG's. The quantity of power was determined by the depth of discharge of the batteries and the charging efficiency. The charging efficiency was a function of the depth of discharge, the charge rate, and the battery temperature during charging.

Because of the decrease in charge efficiency as the temperature increased, thermal constraints were imposed to prevent subjecting the batteries to excessive temperatures during charging. Charging was not initiated if the battery temperature was greater than 21° C (70° F) because the temperature during charge should not exceed 22° C (90° F). Starting the charge at 27° C (80° F) was allowable if the upper temperature limit was monitored to prevent the temperature from reaching 38° C (100° F) which was the maximum allowable temperature at end of charge. The relationship between the battery load voltage and depth of discharge for different load currents is shown in figure 64. The voltage data were representative of steady-state values for a battery temperature of 21° C (70° F). The W-hr efficiency at 21° C (70° F) for the flight batteries during the charge-discharge cycle of the acceptance test was 76 to 77 percent; the A-hr efficiency was 85 to 85.9 percent.

Bioshield Power Assembly

The BPA provided the power interface between the VLC and the VO and was the primary power and command source during the cruise portion of the mission. It was mounted external to the bioshield and remained attached to the VO at separation. (See fig. 65.) The BPA isolated and conditioned VO power for use by VLC loads; supported VLC loads for cruise, maintenance, and Mars orbit; provided charge capability for the VLC batteries; provided signal power to the VO for initiation of VO commands; provided signals and power as required to switch preselected VLC loads; provided mode signals to the GCSC; limited inrush current on the VO buses during regulator power application; and provided fault protection by monitoring the BPA equipment bus for undervoltage or overvoltage conditions, by disabling the converter when either condition existed, by monitoring the converter power output, by disabling the converter when an overload existed, and by fusing selected thermal loads. The BPA regulated the VO power with redundant regulators. The output was 33 V dc ± 5 percent with a steady-state load capability of 0 to 750 W with peak transients of 780 W. The redundant chargers included two constant-current outputs of C/15 and C/40 (C = 8 A). The available rates to the batteries were C/15, C/7.5, and C/160. The C/7.5 rate was obtained by operating the two chargers in parallel. The C/160 rate, used for float charging, was obtained through a divider network connected to the four batteries with one charger operating at the C/40 rate.
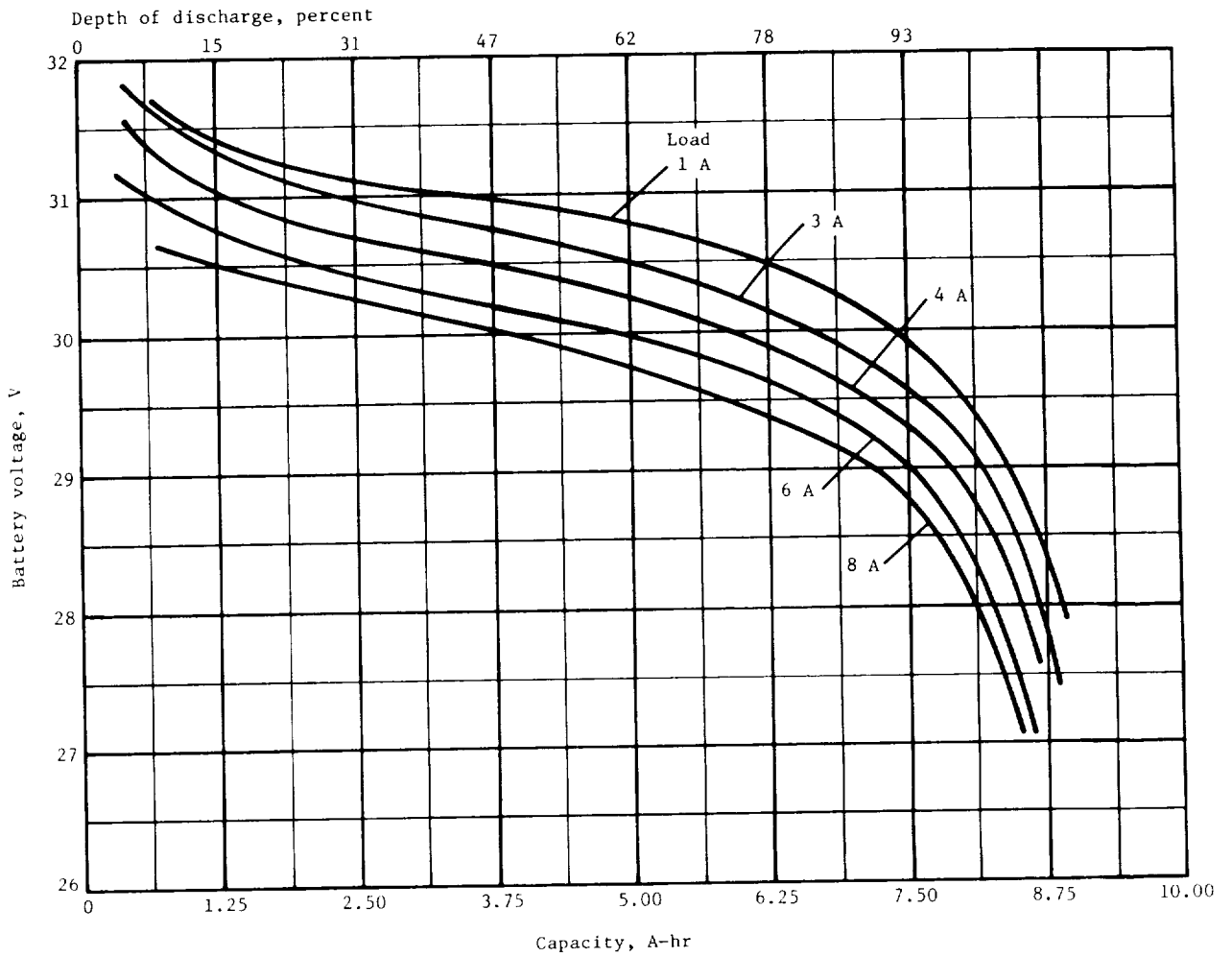
Depth of discharge, percent

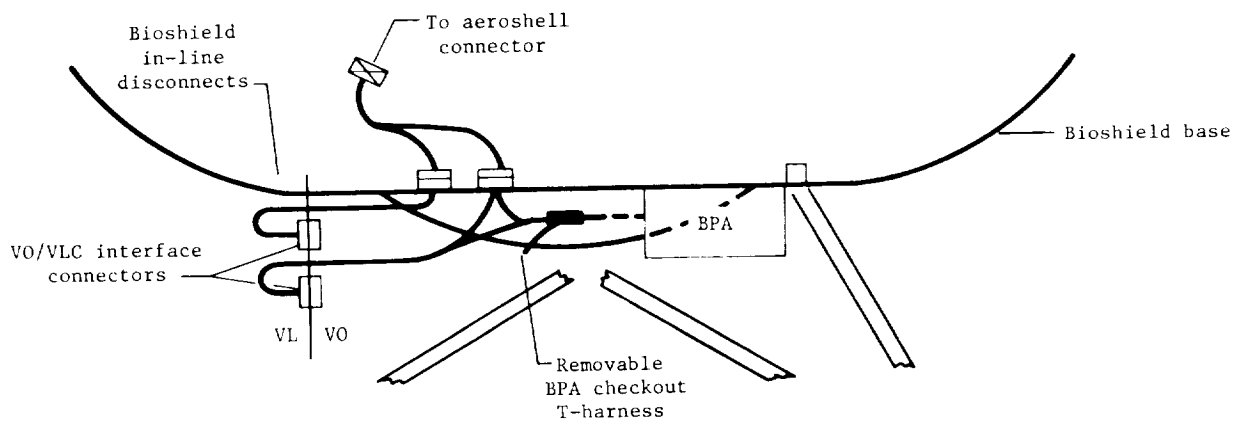Figure 64.- Battery capacity for cruise phase.

Figure 65.- Location of BPA.

112

A functional description of the major circuits in the BPA is as follows:

The BPA converters were duty cycled and frequency modulated dc-dc converters rated at a steady-rate output of 150 W. The output voltage was 33 V dc ± 5 percent over an input voltage range of 25 to 50 V dc and a case temperature range of -37° to 71° C (-35° to 160° F). Each converter contained a battery charge circuit that provided high and low battery charge rate currents. A block diagram of the BPA converter is shown in figure 66. Each BPA
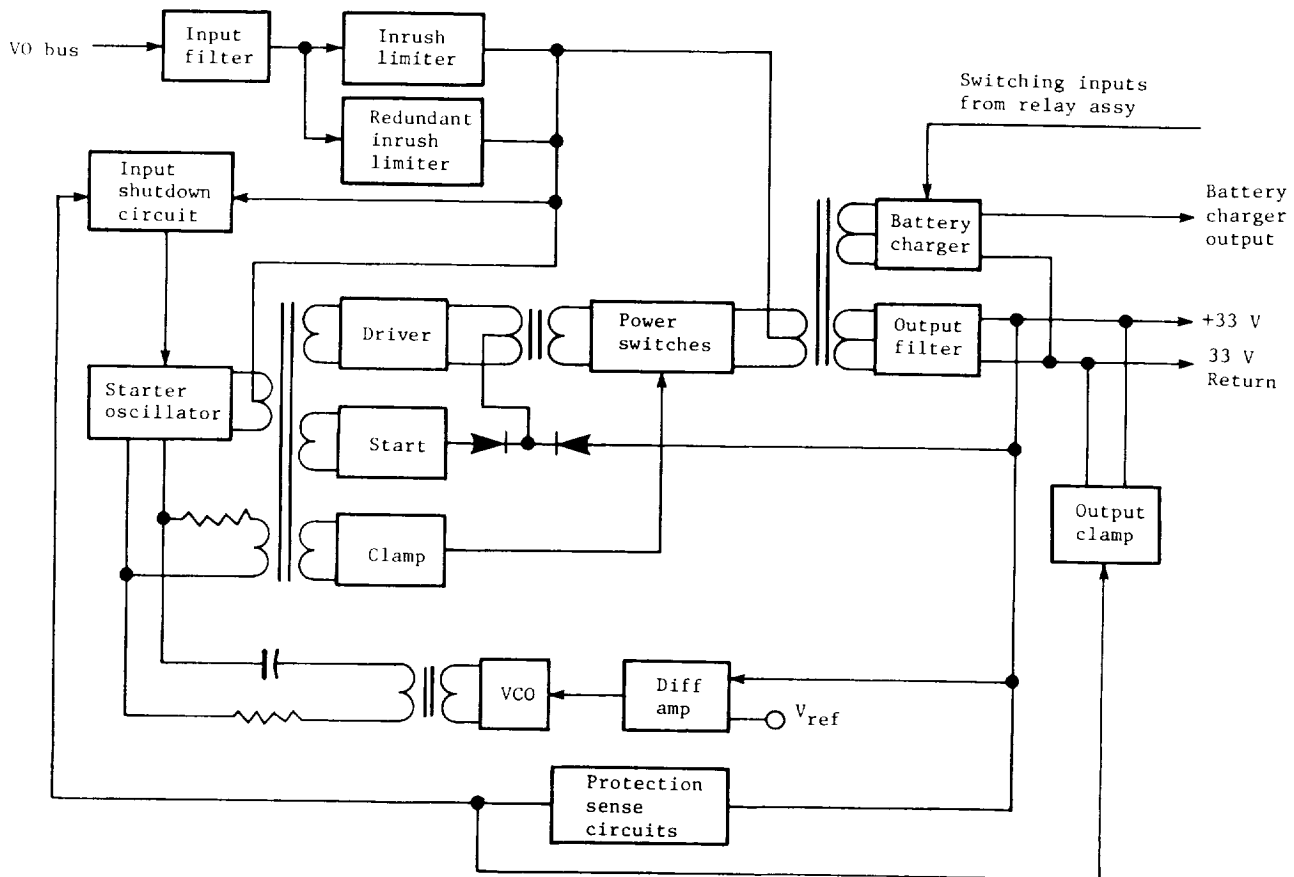
Figure 66.- Block diagram of BPA converter/charger.

converter contained circuitry to protect against output overvoltage, undervoltage, and overload. The overvoltage and undervoltage circuits functioned analogously except that no time delay was included in the overvoltage circuit, whereas the undervoltage circuit had a time delay on its output of 2 to 3 sec. The converter shut down when the output voltage exceeded 37 V dc or the output dropped below 22.5 V dc for more than 2 sec. The overload sensor detected loads in the range of 160 to 180 W (165 ± 7.7 W actual) and disabled the converter in 150 to 500 nsec. In the event of a BPA converter trip because of overload, undervoltage, or overvoltage condition, the VO input power was removed for at

least 1 min to reset the regulator. Then VO power was reapplied. The output of each of the fault protection sense circuits was fed into a driver circuit that fired an SCR crowbar on the input of the converter and an SCR shutdown circuit on the input of the converter which clamped the bases of the starter oscillator transistors. The inrush current to the converter at turn-on was limited to a maximum of 72 A by a 4.22-Ω resistor in series with the input filter. This resistor was bypassed by a saturated transistor when the primary current in the converter power transformer had reached a predetermined threshold (nominally 10 nsec from application of the input voltage).

In addition to the 33 V dc output to the BPA equipment bus, each BPA converter contained a battery charger circuit whose output was a selectable constant current of either 200 mA ± 15 percent (low rate: C/40) or 533 mA ± 10 percent (high rate: C/15). The low-rate output was further divided to provide float charge capability to four batteries simultaneously at a rate of C/160 each. When batteries were float charged, all batteries were on the battery bus to preclude damage to the BPA float charge divider networks, float charging was accomplished only when the charger was in the low rate, and the float charge enable relay was not closed unless it was intended to immediately initiate float charge. The voltage on the battery charger output bus was limited to a maximum of 90 V dc by an overvoltage clamp circuit whose output reset the on/off and rate (set to high rate) relays. The output voltage attempted to maintain the output current level by increasing the output voltage to the full secondary voltage of the power transformer. If the output was open-circuited, the voltage rose to 75 ± 15 V at which time the sensing circuit turned the charger off. If either charger output was open-circuited, it was reenabled prior to attempting to charge batteries. This was adopted as the primary mode of charger shutdown.

The buffer relay assembly provided load switching and signal buffering upon command from the VO and from the power subsystem. The buffer was designed such that no single piece part failure resulted in the issuance of an inadvertent output. The output circuits were capable of delivering 2 A at 40 V dc. The BPA buffers were designed for nonentry operation. VO commands or simulated VO commands could not remain high for longer than 150 msec. The BPA was operational while the VLC was attached to the VO. The normal mode of operation during cruise was for one BPA regulator to be powered from the VO. For special tests, system checkouts, or battery charging, both regulators and chargers could be operated. For VL tests or checkouts that exceeded the total VO input power available or the maximum load of the two regulators, the VLC was switched to internal power with the BPA supplying only signal power for VO-initiated commands and power for IRU operation. Power from BPA regulator 2 was required for IRU warm-up when that component was being tested. In addition, power would be required from the BPA regulators for heaters during the periods when the VLC was on internal power. Input power to the BPA regulators could be turned off by the VO during maneuvers or other critical events when the VO could not supply the minimum power required by the VLC.

The BPA interfaced with the VO, LCE, PCDA, GCSC, LPCA, and DAPU. A summary of the functions in each of these interfaces is as follows.

Three separate inputs were provided to the VLC for VO unregulated dc. Two of these unregulated inputs supplied power to the BPA regulators and were desig-

nated as VO bus 1 and VO bus 2. The third unregulated input supplied power to the D-feedline tertiary heaters. VO bus 1 supplied unregulated VO power to BPA regulator 1, and VO bus 2 supplied power to BPA regulator 2. The VO was capable of supplying the following steady-state power to the VLC: VO bus 1, a minimum of 250 W; VO bus 2, a minimum of 250 W; VO unregulated dc heater bus, a maximum of 30 W; and VO buses 1 and 2 and VO unregulated dc heater bus, a total of 300 W.

The BPA supplied two signal power inputs of 33 V dc from a single BPA signal bus to supply the power for VO-initiated discrete commands. The signal bus was diode isolated from both BPA power regulators and could be powered from either or both BPA regulators. The VO supplied 24 relay switch closures, supplied from the VO signal buses 1 and 2, to generate discrete commands for VLC switching.

The BPA contained four 10-A relays that controlled the application of power to one staging connector at the staging plane to arm and initiate connector separation upon command from the LCE. The connector had two pin pullers to which power was applied, either of which initiated connector separation. The commands to actuate the relays were also supplied by the LCE. The LCE provided the commands to the BPA to perform the following functions: pyrotechnic safety; power system reset; arm launch pyrotechnic devices; fire launch pyrotechnic devices; and safety launch pyrotechnic devices.

The BPA provided control signals to the PCDA to initiate load switching. Many of these signals required currents in excess of the VO capability. In order to supply the required current, the BPA contained buffers to amplify the VO (signal bus) current. The BPA provided power to the PCDA equipment bus during cruise. The electrical bus which distributed dc regulated power from the VO and VLC regulators was designated the BPA equipment bus. This bus was normally supplied by regulator 1 in the BPA. If a failure occurred, the bus was transferred to regulator 2 by VO command. The IRU bus was supplied directly from regulator 2. The dc steady-state output voltage was 33.0 V dc ± 5 percent. The maximum output noise and ripple did not exceed 0.25 V peak to peak. During normal load switching or VLC reset loads conditions, the dc voltage could exceed the dc regulation envelope specified but could not exceed an envelope of 25 to 40 V dc and could return to within steady-state output limits within 50 msec. The BPA provided two battery chargers for support of battery conditioning and charging prior to Mars orbit insertion. These charger outputs were provided to the PCDA charge bus. One charger received power from regulator 1 and the other received power from regulator 2. Because the two chargers were redundant to each other, no redundancy within an individual charger was required; however, no single BPA failure resulted in loss of any function for both chargers. If one regulator or charger failed, the C/7.5 charge rate would be lost and the charge cycle would be performed at a C/15 rate with an optional topping charge from the RTG/PCDA converter. The charger was designed as an integral part of the regulator and not as a load on the dc output. Each charger provides the following outputs:

High charge rate: constant current C/15 ± 10 percent

Low charge rate: constant current C/40 ± 15 percent

Float charge rate: accomplished with the C/40 charge rate charging all four batteries simultaneously; constant current C/160 per battery with series resistance added to effect sharing to each battery; for battery charge voltages matched within ±0.125 V dc, the current balance was within ±25 percent; for a shorted cell in one battery, the current unbalance ratio was less than 4:1

Load sharing: both chargers were capable of operating in parallel at either the high or low rate to charge one battery at a time

Output voltage: 24 V dc minimum to 40 V dc maximum for C/15 or C/40 charge rates

Charge rate control: charger was in the high charge rate unless commanded to low charge rate by the PCDA; when the charger was commanded off, the charge rate was reset to high

Charger output at no load: 90 V dc maximum; sense and switch circuit was incorporated to turn the charger off within 100 msec when the output voltage reached 75 ± 15 V dc.

The PCDA, in response to GCSC commands, controlled specified switches in the BPA. The PCDA supplied sufficient current to drive the relays so that buffer circuits were not required in the BPA. Voltage for these functions was 31 V dc maximum and 21.8 V dc minimum and was applied for 50 msec minimum to 180 msec maximum. Diode isolation was provided in the PCDA such that a voltage applied from the BPA would not damage the driver circuitry.

The BPA provided mode signals to the GCSC for the prelaunch C/O mode, pre-separation C/O mode, and separation mode. The GCSC provided a signal ground return which was switched through contact closure in the BPA. The proper VO command or PCDA signal closed the switch contact, resulting in a mode signal to the GCSC. The GCSC detected the leading edge of the BPA inputs, processed them as interrupts, and tested the signal 20 to 60 msec later. If the input was in the set position when tested, the GCSC entered the routine called for by the BPA mode signal.

The BPA provided control signals to the LPCA to initiate pyrotechnic events.

The BPA provided two bilevel outputs to the DAPU to indicate on or off status of the BPA float charge enable relay and BPA regulator 2. The signals were -0.5 to 1.0 V dc in the off condition or 2.5 to 10 V dc in the on condition. The VO provided two separate input power lines to the BPA. These two lines supplied power to the redundant converter/battery chargers in the BPA. The dc steady-state voltage varied from 25 to 50 V dc. The power input required to the BPA depended on the lander loads during each phase of the mission. The converter/charger efficiency was approximately 70 percent when the load was higher than 50 W.

116

Power Conditioning and Distribution Assembly

The PCDA was mounted internal to the VLC body in the center of the equipment plate. (See fig. 21(b).) The PCDA provided the interface with the batteries and the BPA and was the primary power interface with all VLC components. The principal functions of the PCDA were as follows:

To convert RTG power for VLC loads and battery charging

To provide charge control logic for sensing and switching batteries as a function of battery voltage and temperature

To provide the interface with the BPA for power distribution and control of selected functions within the BPA

To provide power transfer from external to internal power

To provide load switching in response to GCSC digital signals, LCE discrete signals, and VO discrete signals via BPA

To provide fault sensing and overload protection for selected VLC loads (fuses or active overload sensors)

To provide undervoltage sensing and protection to assure batteries are not discharged to the point of cell reversal (postlanded function)

To provide sensing and control against improper GCSC operation via the sentry timer (postlanded function)

To provide a sequencer to take proper switching action when sensing an undervoltage, GCSC failure, or GCSC overload

To provide interface to decode S-band decoder signals for GCSC transfer

Major subassemblies and functional circuits of the PCDA are shown in the diagram of figure 67. The following paragraphs contain functional descriptions:

Converter/charger: The converter and battery charger were contained in a single unit. The converter provided voltage regulation of the RTG output and drew a constant amount of power from the RTG source. The power drawn from the RTG's ranged from 70 to 94 W depending on the age of the RTG's. Maximum power transfer from the RTG to the equipment was assured for all variations in output voltage. The converter had two modes of operation: the equipment mode and the charge mode. In either mode all required power was fed to the VLC equipment bus. When the equipment bus voltage increased above 34.8 V, implying there was more power than the equipment bus needed, the converter/charger was switched to the charge mode. In this mode, power not required by the equipment bus was used for battery charging. When the battery charging was completed, no current
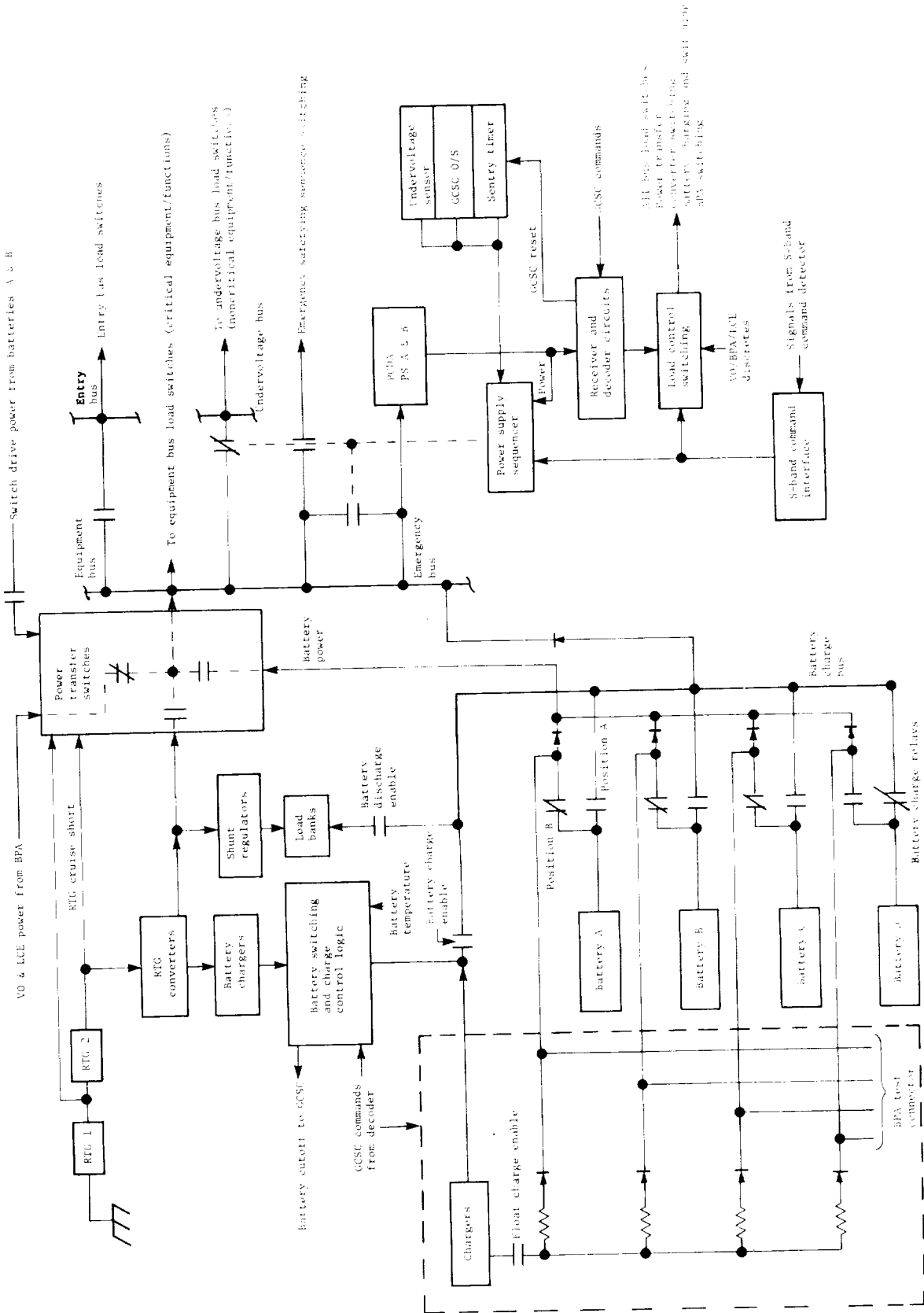
Figure 67.— Block diagram of PCDA.

118

flowed to the charge bus and the equipment bus voltage rose until limited by the shunt regulator. When the equipment bus voltage dropped, implying an RTG power deficiency, the batteries began to supply the necessary power. The charger supplied current to the batteries at rates up to C/6.

Shunt regulator: The shunt regulator contained four differential amplifier circuits that compared the equipment bus voltage to four independent zener diode references. When the equipment bus voltage exceeded the zener diode reference threshold, the power transistors started conduction and diverted the excess power to the load banks to be dissipated. The quad-redundant configuration prevented any single failure from affecting operation of the shunt regulator/load bank system. The shunt regulator limited the equipment bus voltage to 36.4 ± 0.25 V dc.

Charge control: The charge control logic sensed charge bus voltage and battery temperature and controlled the charge enable and discharge enable relays to prevent damage to the batteries and to optimize the utilization of power. The PCDA used redundant charge control circuits to prevent a single failure from causing loss of charge control capabilities. Each charge control circuit had four temperature-sensing channels, one channel for each battery. As a battery was connected to the charge bus, the appropriate temperature-sensing channel was activated. The output of the temperature-sensing channels was utilized for two functions: maximum temperature cutoff and full charge cutoff.

Maximum temperature cutoff was used only when full charge cutoff failed. The output of the temperature sensor, which was proportional to the battery temperature, was provided to a comparator circuit where it was compared to a reference voltage. If this voltage comparison indicated that the battery being charged exceeded its maximum allowable temperature limits for a battery connected to the charge bus of 53° C (127° F), the charge control initiated a signal to open the charge enable relays. It also initiated a bilevel telemetry signal to the DAPU to indicate which charge control took action and sent a battery cutoff signal to the GCSC to indicate that action had been taken. This cutoff signal was used for charge control backup only since the summary method of charging and controlling batteries was accomplished through the use of predetermined and timed sequences.

The charge control utilized a temperature-compensated battery cutoff voltage concept during normal charging activities to determine when a battery was fully charged. This concept insured that the battery was not overcharged or undercharged for a wide range of battery temperatures. This was accomplished by ORing the temperature sensor output with the output of an amplifier which was monitoring the charge bus voltage. This signal was provided to a comparator circuit where it was compared with a reference voltage. If this comparison indicated that the battery being charged had reached its temperature-compensated cutoff voltage, the charge control initiated a signal to accomplish these same functions.

The charge control also contained circuitry to monitor the battery during the discharge cycle to prevent the battery from discharging to the point of cell reversal. This circuitry consisted of a comparator which compared the charge bus voltage with a reference voltage. If this comparison indicated that the

battery voltage had reached its minimum discharge voltage cutoff of
27.2 ± 0.25 V dc, the discharge control initiated a signal to open the dis-
charge enable relays. It also initiated a bilevel telemetry signal to the
DAPU to indicate which discharge control took action and it sent a battery
cutoff signal to the GCSC to indicate that action had been taken. The battery
cutoff signal was used as the primary method of timing the discharge cycle
with a timed end of discharge used as a backup. The only method of opening
the discharge enable relays once they had been closed was by the output signal
from the discharge control. The charge control and discharge control telemetry
utilized latching bilevel signals to indicate which unit last interrupted charge
or discharge. At initial application of power to the charge control circuitry,
these signals were in either a high or low state. The initial state remained
until the charge control or discharge control took action to remove a battery.
At this time, the signal indicated which charge control took action and then
remained in that state until the other charge control or discharge control took
action.

Digital interface: The function of the digital interface circuit was to
decode computer commands from the GCSC and to generate output command signals
for the control of power supply outputs and for the activation of relay coils
and pin-puller circuits. The major portion of this circuit was powered down
until the GCSC commanded it to power up. The digital system interfaced with
the GCSC through line receivers, one for an enable line, one for a data line,
and one for a shift pulse line. The command words were 9 bits transferred at
a rate of 96 000 bps. The command words used an NRZ-L format. The command
words were separated by at least 75 msec. The circuitry remained powered up
until a particular power-down word was issued. The circuitry controlled the
power-up sequence, with the 28-V line turned on last and turned off first to pre-
vent inadvertent outputs during power up. The PCDA internal power supplies pro-
vided other signals to the digital interface to insure that inadvertent commands
were not issued and to insure that the digital interface was disabled if the
power supply of 5 V dc dropped below acceptable limits (4.5 V dc). These sig-
nals included the delay signal which insured that the power supply was above
4.5 V dc before 28 V dc was allowed to turn on; the undervoltage sensor which
monitored the 5 V dc supply and disabled the digital interface if this voltage
dropped below 4.5 V dc; and the 28 V dc sensor which insured that 28 V dc was
off before 5 V dc was allowed to turn off.

Pin-puller circuit: The pin-puller circuit contained switching, current
limiting, and gating necessary to apply battery power to the pin pullers of an
electrically actuated staging connector, seismometer uncaging mechanism, and
the GCMS power and PDA mechanism. There are six pin-puller circuits - a primary
and backup for each of the signals described in the previous paragraph.

Power load switching: The digital driver assemblies accepted decoded digi-
tal commands from the digital interface and translated them into drive signals
to the appropriate relays. The digital interface commands were received in the
form of two bilevel signals. These bilevel signals were ANDed with the enable
pulse in the first stage of the hybrid driver. If the two digital interface
bilevels to any particular driver were high at the time of the enable pulse,
the driver output was high and the associated relay was transferred. The relay
driver was also turned on without the bilevel input commands by means of the

120

reset input. If the reset input was low, the output was high regardless of the state of the input logic. The reset input was used to command relays from the charge control, failure monitor, and overload sensor circuits. The relays were connected in three different configurations depending upon requirements. These configurations were series redundant, parallel redundant, and nonredundant.

Sentry timer: THE PCDA contained two sentry timers which monitored GCSC operation by timing the period between GCSC reset commands. Upon failure to receive a reset signal within the specified time of 65 to 360 sec, the timers initiated operation of the emergency mode sequencer. The sentry timers were disabled during cruise and entry and were enabled by GCSC command for preseparation checkout and after landing. The design philosophy implemented for sentry timer operation was that no single failure within the sentry timer or its associated circuitry would cause a premature or false output. This was accomplished by using two identical sentry timer circuits powered from different power supplies and interconnected in a configuration that required an output from both sentry timers before action was taken.

Undervoltage sensors: The PCDA contained two undervoltage sensors which monitored the power subsystem condition by monitoring the equipment bus voltage. Upon sensing a low voltage condition of 26.5 ± 0.25 V dc, the undervoltage sensors initiated operation of the emergency mode sequencer. The voltage remained below the limits for 50 to 100 msec before an output was generated by the undervoltage sensor. As for the sentry timers, the design philosophy implemented for undervoltage sensor operation was that no single failure within the undervoltage sensor or its associated circuitry would cause a premature or false output. This was accomplished in the same manner as that described for the sentry timer.

Overload sensors: The overload sensor was a resettable electronic fuse. Current was measured by monitoring the voltage across a current sense resistor in series with the load being sensed. This voltage was provided as the input to the OS circuitry. When an overload or fault was sensed, the OS generated an output signal to indicate an overload. When this signal was generated, the OS took action that ultimately resulted in removing the load being sensed from the bus by opening its power relays. A total of five VLC loads were sensed by OS circuits: DAPU, GCSC, tape recorder, PCDA power supply A, and PCDA power supply B. The design implementation included both redundant and nonredundant circuits. The definition of each type of circuit is given as follows:

Redundant OS: The GCSC and DAPU were sensed with a redundant OS. The design philosophy implemented for redundant OS operation was that no single failure within the OS or its associated circuitry would cause a premature or false output. This was accomplished by using two identical OS circuits powered from different power supplies and interconnected in a configuration that required an output from both OS circuits before action was taken. In addition, no single failure (sense resistors) caused permanent loss of the load. These criteria were met by using parallel sense resistors so that if one resistor opened, the load could still operate through the other resistor. The DAPU OS actually opened all four DAPU load relays for an overload, whereas the GCSC OS initiated operation of the emergency mode sequencer for an overload. The redundant OS detected an overload and reset the appropriate load switches within

121

5 sec when the load current exceeded the normal load peak current by more than 600 percent normally or 300 percent with a single PCDA failure.

Nonredundant OS: The tape recorder and PCDA power supplies A and B were sensed with nonredundant OS. This design concept contained failure modes that could result in premature removal of the load; hence, this concept was not used in mission-critical applications. All nonredundant overload sensors actually opened the appropriate relay in the event of an overload. The OS detected an overload and reset the load switch within 5 sec when the load current exceeded the normal load peak current by more than 300 percent.

Emergency mode sequencer: The emergency mode sequencer performed two functions: (1) the sequencer provided an interface with the S-band detectors to provide the capability of switching computers via ground control and (2) when both signals were received from the sentry timers or the undervoltage sensors or the GCSC overload sensors, the sequencer initiated a hardware implemented sequence that placed the VLC in an emergency mode by placing the VLC loads in a safe configuration ready for ground update. The redundancy philosphy implemented in the sequencer design was identical to that for the sentry timers, undervoltage sensors, and the GCSC overload sensors; that is, no single failure would result in an output signal. The sequencer provided the interface between the PCDA and the command detectors. The sequencer received signals from the two command detectors and decoded them to pulse the appropriate GCSC transfer relays. The interface consisted of four line-driver, line-receiver interface circuits. Each command detector provided a GCSC A ON/B OFF command and a GCSC B ON/A OFF command. Upon detecting the same instruction from both command detectors, the PCDA performed that command. The PCDA did not transfer the GCSC if one transfer command was received from one detector and the alternate command was received from the other detector. These commands were performed by the PCDA regardless of the status of the PCDA emergency mode sequencer or the GCSC transfer inhibit relay. The PCDA provided the capability to disable the S-band command interface to protect against command detector outputs which occurred during detector power down. The PCDA provided redundancy so that no single failure resulted in transfer of any GCSC load relay. The commands from the S-band command detector were 250 ± 30 msec. The two corresponding transfer commands had a minimum time coincidence of 75 msec. The PCDA S-band command interface did not respond to spurious outputs from the S-band command interface which occurred at power up. The spurious output pulse width was not greater than 100 μsec at the 10-percent points.

Failure monitor: The failure monitor provided fault protection for the VLC power subsystem by monitoring RTG converter/charger operation. If the failure monitor detected a failure, it took action to switch from the on-line converter/charger to the backup converter/charger. The criteria established for determination of a failure were as follows:

RTG input voltage high: Any failure within the converter/charger that caused the RTG input voltage to rise toward its open-circuit voltage. When the RTG rose to 11 V maximum, the failure monitor transferred to the backup converter/charger.

122

RTG input voltage low: Any failure within the converter/charger that caused the RTG input voltage to drop toward its short-circuit voltage. When the RTG dropped to 6.0 V minimum, the failure monitor transferred to the backup converter/charger.

Charge bus failure: Any failure within the converter/charger which caused the charge output to drop more than 2 V less than the equipment bus voltage when there was excess energy available from the RTG. Excess energy available was determined by monitoring the shunt regulator (i.e., if the shunt regulator was off, there was no excess energy being supplied to the equipment bus; if the shunt regulator was on, excess energy was being dumped into the load bank). When this condition existed, the failure monitor switched to the backup converter/charger.

Telemetry: The PCDA provided telemetry signals from various loads and buses in the PCDA to the DAPU. There were four types of telemetry circuits used in the PCDA: voltage dividers for bilevel signals, voltage dividers for high-level analog signals, shunts for low-level analog signals and active current monitors for monitoring the bus currents in the PCDA. There were 13 bilevel telemetry signals in the PCDA. The bilevel signals were used to monitor relay closures applying power to the various loads and for status indications. There were four shunts used in the return sides of the four batteries. These monitors were used to measure the charge and discharge current of the batteries. The shunts are 10-A, 50-mV shunts and therefore require a voltage divider across each shunt to give the 0 to 40 mV output to DAPU. There were 6 high-level single-end analog telemetry monitors. These monitors provided a 0 to 5 V signal proportional to 0 to 40 V dc for voltage monitors and proportional to 0 to 3 A for the shunt regulator output current monitors. The three active current monitors sensed the equipment bus, charge bus, and RTG bus currents. The current monitor used two saturable reactors driven by a buffered square-wave generator to perform as a dc transformer.

PCDA power supplies: The PCDA contained two power supplies to provide required voltages and power to the PCDA internal circuitry. The power supply received input power from the PCDA emergency bus. The input power source was protected by an overload sense circuit which detected an overload condition on the power input line and opened the input circuit. The PCDA had two identical power supplies to provide the required redundancy. The power supply was made up of an input filter, preregulator, converter, and an output circuit for distributing and controlling power to the PCDA loads.

Operating modes of the PCDA for specific mission phases are given as follows:

Cruise: The PCDA electronics were inactive during launch and most of cruise. The switching logic responded to 28-V discrete commands from the LCE prior to launch (tape recorder on, LPCA 1 on, and LPCA 2 on) and from the VO during cruise. The PCDA also responded to GCSC digital commands during cruise. When these commands were required, the VO issued commands to power up the PCDA supplies. The GCSC then issued a decoder power-up command which applied voltage to the digital interface enabling it to receive and decode digital commands. The sequences in which digital command control was required include

GCMS vent sequences, battery conditioning, GCSC A and B cruise checkout, GCMS bakeout sequences, battery recharge, battery discharge, battery precharge, initiate float charge, terminate float charge, and pre-preseparation update. In addition to the switching function performed by the PCDA during cruise, periods of time existed when peak power demands exceeded the capabilities of the BPA. During these time periods, power was transferred from the VO to the VLC. In this configuration, power was supplied to the VLC loads from the RTG's through the PCDA converters and from the four VLC batteries. At the completion of these sequences, power was transferred back to the VO and the VLC loads were supplied from the BPA.

Battery conditioning: Major battery-related functions of charging, discharging, and float charging occurred during cruise. During these battery operations, the PCDA provided switch control and charge control based on GCSC digital inputs and internal logic. The battery conditioning was accomplished by sending VO commands through the BPA to place the GCSC in an update mode. Flight operations then issued VL command message segments implementing the real time input/output GCSC software to accomplish PCDA and BPA switching.

Preseparation and separation: During preseparation and separation activities the VLC was on internal power. The PCDA provided the command interface with the GCSC for switching loads to determine the health of the lander prior to separation. The PCDA also provided power from the RTG's and the batteries except for IRU warm-up and some heater loads. The undervoltage sensors, overload sensors, sentry timers, and charge control logic were enabled during the preseparation period but were disabled just prior to separation and were not reestablished until after landing. After the preseparation checkout of VLC was complete, all four batteries were recharged in preparation for entry.

Entry: The entry phase began with orientation of the VL for the deorbit burn and ended at touchdown on the planet's surface. During this phase, the PCDA provided power from the batteries and the RTG's and provided load switching under command from the GCSC. All overload, undervoltage, sentry timer, and battery charging functions were suspended during this period.

Postlanded: During the postlanded phase of operation, which extended from touchdown on the surface of Mars until the end of the Viking Mission, the PCDA operated continuously. All fault protection devices and battery charging circuitry were enabled. Both PCDA power supplies were energized, but one converter and charger were used with automatic switching to the redundant ones if a converter failed. For a GCSC failure or an equipment bus undervoltage condition, the emergency mode sequencer was triggered. This sequence switched loads to put the lander in a safe operating mode. The current operating sequence was interrupted by switching to the backup GCSC and a mode command was sent to the GCSC to initiate a periodic sequence to transmit data over the UHF link to the VO. In addition, the uplink components were energized to provide command capability from the Earth.

The PCDA provided the interface with the RTG, the batteries, and the BPA and was the primary interface with all VLC components. A summary of the PCDA interface functions is given in the following paragraphs.

124

The series connected RTG's were controlled by the PCDA through the VLC cabling in two modes: on load and shorted. For the on load mode, the PCDA converter controlled the RTG voltage by regulating it to 8.8 ± 0.2 V dc at the RTG connector. When the RTG's were in the shorted condition, the resistance of the cabling and the PCDA was low enough to insure that the RTG voltage was much less than 1.0 V dc.

The PCDA provided the interface with all four lander batteries. Each battery provided a temperature sensor for use by the PCDA power conditioning circuitry for charge termination when an overtemperature condition existed and for temperature-compensated charge control. The PCDA contained switching logic which placed each battery on charge or discharge in response to GCSC digital commands. The PCDA provided redundant circuitry to monitor battery charge and discharge operations to prevent battery damage and to optimize the utilization of power.

The BPA provided control signals to the PCDA to initiate load switching. The BPA provided power to the PCDA equipment bus during cruise from the VO/VLC regulators utilizing the BPA equipment bus. The BPA provided two battery chargers for support of battery conditioning and charging prior to MOI. These charger outputs are provided to the PCDA charge bus.

The PCDA contained active redundant GCSC/PCDA digital interfaces, either of which could perform the required switching functions. The GCSC issued digital commands to the PCDA. All command words were outputted simultaneously to each PCDA decoder. The transfer of digital command words was at the rate of 95 000 bps ± 0.1 percent with a total of 9 bits transferred per command word with an NRZ-L format. The three inputs for each word consisted of an enable signal, shift pulse, and a data signal. An enable signal set the receiving logic to receive command data. The trailing edge of the enable signal acted as the execute command. The shift pulse signal was used to shift data into the PCDA shift registers. The shift signal provided by the GCSC used an RZ format. One or more commands were contained in a sequence. The first word transferred in any sequence was the power-up word to the PCDA followed by the command word or words to accomplish the switching function. A sequence was terminated by the power-down word to the PCDA. The selection of digital words included a 2-bit separation (odd parity). The total number of distinct command words which the GCSC was capable of transferring to the PCDA can be as many as 196. The PCDA provided two discrete signals to the GCSC. These signals were provided over a standard line driver, line receiver interface. These signals were as follows. Battery cutoff signal was used as a backup to charge control if charging based on time became inadequate. The GCSC required an update in order to use this signal. Initiate emergency update sequence signal was provided to the GCSC as part of the emergency mode sequence initiated by the emergency mode sequencer. The switches which transferred IRU power from the BPA IRU bus to the PCDA entry bus provided a switch position indication to the GCSC when the switches were in the PCDA bus position. The GCSC sampled this switch position prior to separation to verify IRU power transfer.

When the ability to reset the overload protection device was required, as for the tape recorder and PCDA power supplies, overload sense circuits were used. These sense circuits had the following characteristics.

The sensor detected an overload and reset the load switch within 5 sec when the load current exceeded 300 percent of the normal power of the unit.

The sensor did not detect an overload if the load was less than 150 percent of the normal peak power of the unit.

The sensor did not detect an overload during the turn-on inrush defined for these loads.

The sensing element in combination with the power system source and distribution impedances limited fault current to a maximum of 50 A. The sensing element resistance was not less than 0.5 Ω. Voltage drop across the tape recorder sensing element did not exceed 0.5 V at peak current. When the reset capability and fail-safe redundancy were required, as for the GCSC and DAPU overload protection, parallel sensing elements and sensing circuitry with series outputs were used. The DAPU overload sensor trip limit was based on the sum of the peak powers or inrush energies for the DAPU and data storage memory. These overload sensors had the following characteristics:

The sensor detected an overload and reset the load switch within 5 sec when the load current exceeded the unit's normal peak power by 600 percent normally or 300 percent with a single PCDA failure.

The sensor did not detect an overload when the load was less than 150 percent of the unit's normal peak power including the effect of any PCDA single failure.

The sensor did not detect an overload during the turn-on inrush defined for these loads.

The sensing element in combination with the power system source and distribution impedances limited the fault current to 50 A maximum. The sensing element resistance is approximately 0.5 Ω normally or 1.0 Ω with a single failure.

Redundancy was such that no single failure caused removal of power from the load or loss of the ability to turn the load on.

Upon sensing an overload, the GCSC overload sensor provided two commands to the power supply sequencer to initiate its switching sequence which opened the GCSC power switch.

The GCSC overload sensor was disabled by bypassing its sensing element during entry.

The PCDA provided circuitry to accept GSCS transfer commands from the S-band detectors to provide GCSC transfer capability when one GCSC failed.

The PCDA provided six pin-puller circuits, each switching power from an individual battery. Two circuits were utilized to initiate staging connector separation by applying power to redundant pin pullers on the staging connector. Two circuits were used to uncage the seismometer. The other two circuits were used to open the GCMS PDA.

126

The PCDA switched power to all VLC components by means of 2-A or 10-A relays. These relays were controlled by digital commands from the GCSC, by discrete commands from the VO or LCE, and by discrete commands generated internal to the PCDA.

The PCDA provided 34 telemetry measurements to the DAPU. These measurements fell into three signal types as follows:

High-level single-end analog signals with full-scale open-circuit range of 0 to 5 V dc with respect to single-point structure ground: Source impedance should not exceed 2500 Ω.

Low-level double-end analog signals with full-scale open-circuit unipolar differential mode data range of 0 to 40 mV dc: All spectral components of any common mode voltage, with respect to single-point structure ground, should not exceed 5 V peak from dc to 10 Hz and 1 V peak to peak from 10 Hz to 1000 Hz. The maximum common mode source impedance should be 10 000 Ω. Signal source impedance (differential mode) should not be greater than 1000 Ω and should not be unbalanced with respect to single-point structure ground by more than 100 Ω.

Bilevel signals where OFF equaled -0.5 to 1.0 V dc and ON equaled 2.5 to 10.0 V dc: Signal input should be sensed with respect to single-point structure ground. Signal source impedance should not be greater than 10 000 Ω. The PCDA received power from the BPA during cruise and from the RTG's and batteries when in a postlanded configuration. The power provided by the RTG ranged from 70 to 94 W at all times when the RTG's were not shorted. The power drawn from the BPA and the batteries were a function of the equipment bus load and varied as a result of the mission configurations. The output power provided by the PCDA also varied as a function of the equipment bus load. The conversion efficiency at which power was provided to the batteries and VLC load from the RTG's varied between 78 and 90 depending on whether the VLC was in a charging or discharging mode. In addition to these converter/charger losses, the PCDA internal electronic equipment did not dissipate more than 5.28 W when the PCDA power supplies were in standby and less than 29.6 W peak (100 msec). The PCDA equipment bus voltage varied as a function of the operating mode. The voltage ranges for each operating mode are given in the following table:

Operating mode	Voltage range, V dc
VO (BPA)	33.5 ± 5%
Battery discharge	26 to 32
Battery charge (PCDA charger)	34.8 ± 0.4
Shunt regulator	36.25 to 37

Propulsion Subsystem

The propulsion subsystem consisted of two major subassemblies: the reaction control system and the terminal descent system. The RCS provided three-axis attitude-control thrust from shortly after the lander separated from the orbiter until the aeroshell was jettisoned. The RCS also provided the deorbit impulse required to alter the lander trajectory for Mars encounter. The RCS was composed of 12 engines, 24 on/off solenoid valves, and 2 propellant tanks plus the necessary feed lines and pyrotechnic valves. All components of the RCS were mounted on the aeroshell as shown in figure 68. The engines were the
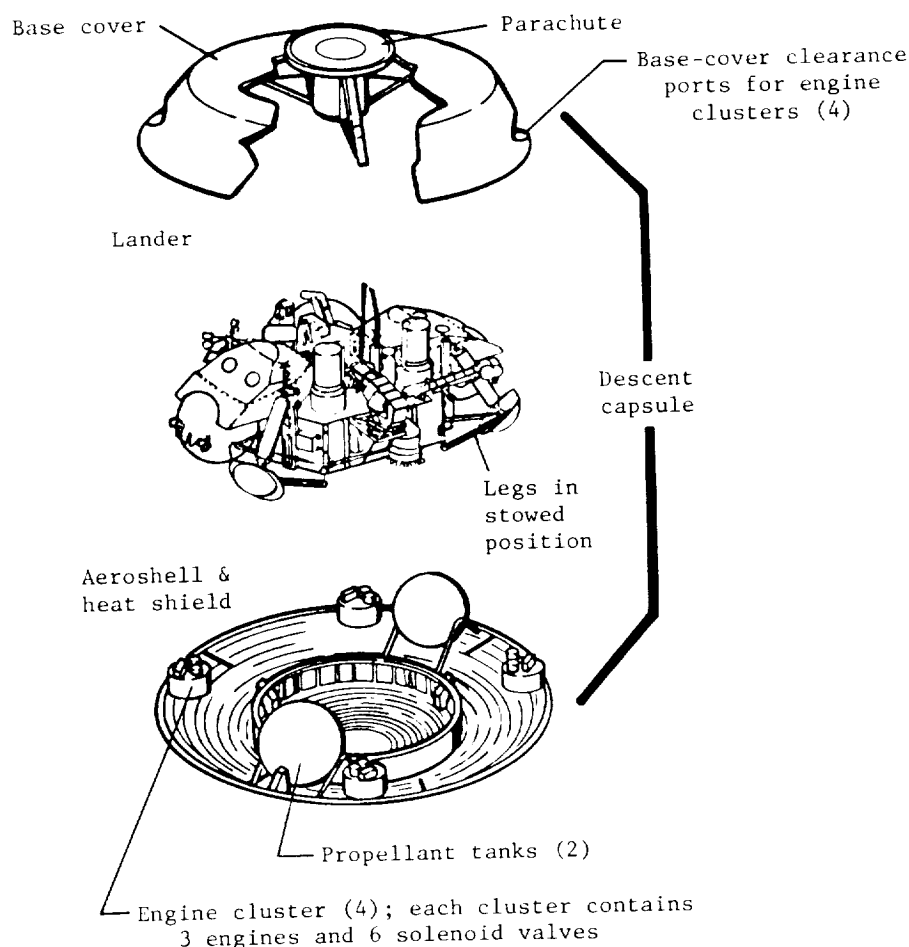
Figure 68.- Location of reaction control system components.

spontaneous catalytic monopropellant type; the propellant was purified hydrazine. The thrust of each engine was approximately 36 N (8 lbf) at the initial tank pressure of approximately 2.40 MPa (348 psia). The four roll engines formed CW and CCW couples. However, the thrust vector of all eight pitch and yaw engines was aligned with the negative X-axis to provide the deorbit impulse.

128

(See fig. 69.) The engine/valve configuration for each engine pair (for example, the two CW roll engines) is shown in figure 70. This configuration allowed

⊗ Thrust vector into paper
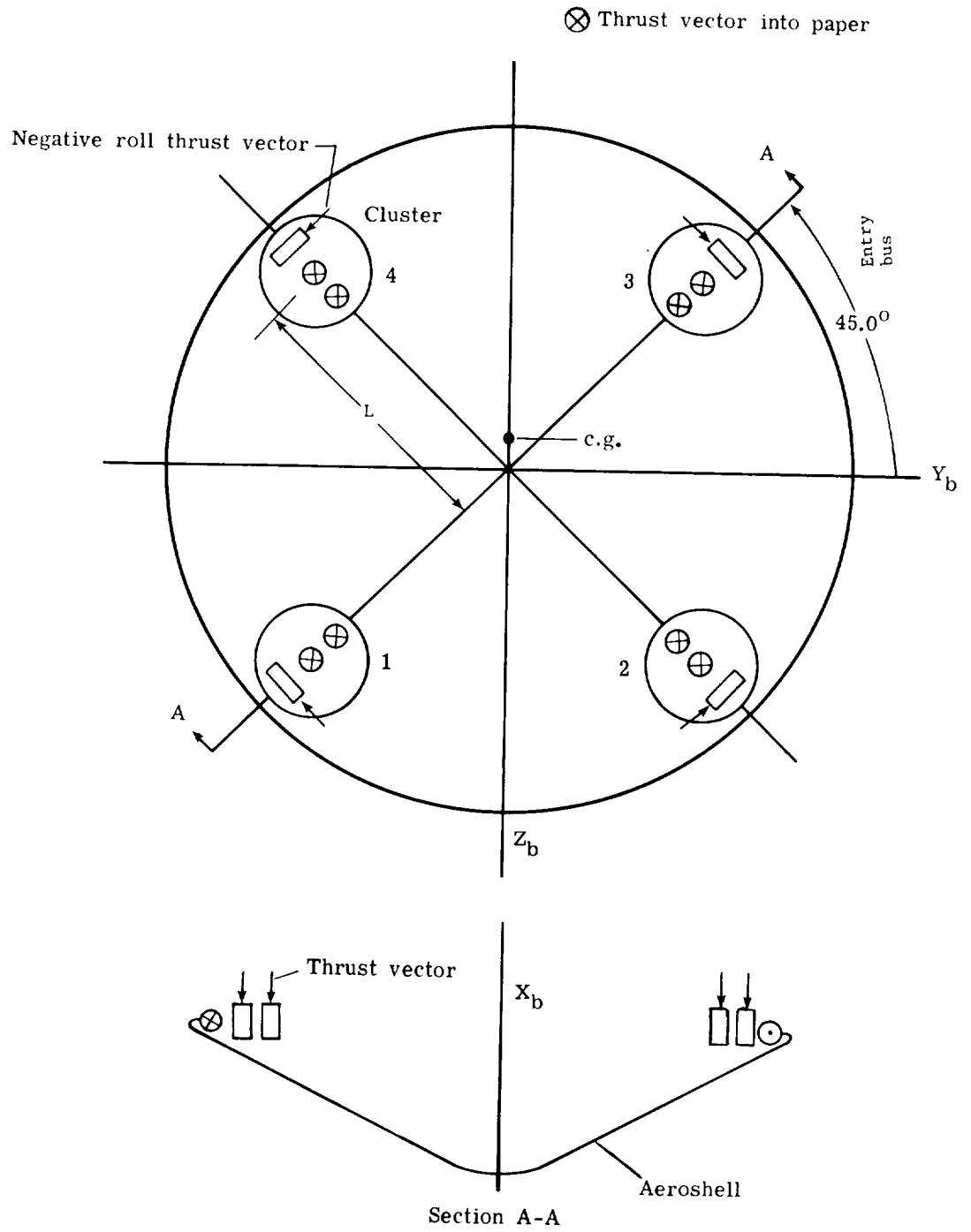
Figure 69.- Geometry of RCS. L ≈ 1.5 m (5 ft); c.g. offset, 4.65 cm (1.83 in.) along $-Z_b$ axis; each cluster contains 2 pitch/yaw engines and 1 roll engine.
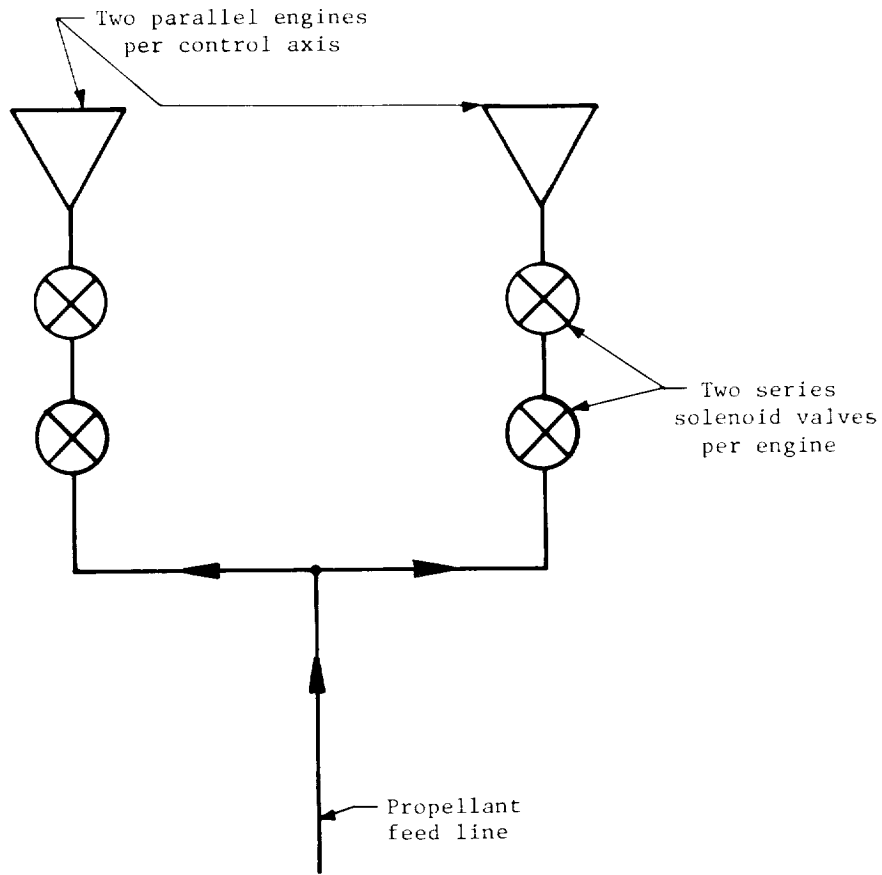
Figure 70.- RCS engine/valve configuration.

failure of any single engine or single solenoid valve (either open or closed) without loss of control capability. The propellant tanks were titanium spheres with an inside diameter of 56.2 cm (22.14 in.). Each tank contained a pressurant/propellant isolation diaphragm for positive expulsion, as shown in figure 71; the pressurant was nitrogen and the propellant was hydrazine. The RCS operated in a blowdown mode (no pressure regulation). The initial tank pressure was approximately 2.40 MPa (348 psia) and the total RCS propellant load was 84.8 kg (187 lbm). The RCS propellant tanks, feed lines, and engines were thermally insulated and thermally controlled by heaters to prevent propellant freeze-up during cruise to Mars and/or at engine ignition. The RCS interfaced with the G&S subsystem via the VDA to perform its primary functions, with the power subsystem for thermal control power, and with the telemetry subsystem to provide engineering data.

The TDS provided three-axis attitude control and the impulse required to reduce the lander velocity to approximately 2.4 m/sec (8 ft/sec) at touchdown. The TDS was activated at aeroshell separation. The TDS was composed of three large (high-thrust) terminal descent engines, four small roll engines, and two propellant tanks along with the necessary feed lines and pyrotechnic valves. All components of the TDS were mounted on the lander. (See figure 72.) The decelerating impulse was provided by three terminal descent engines. These
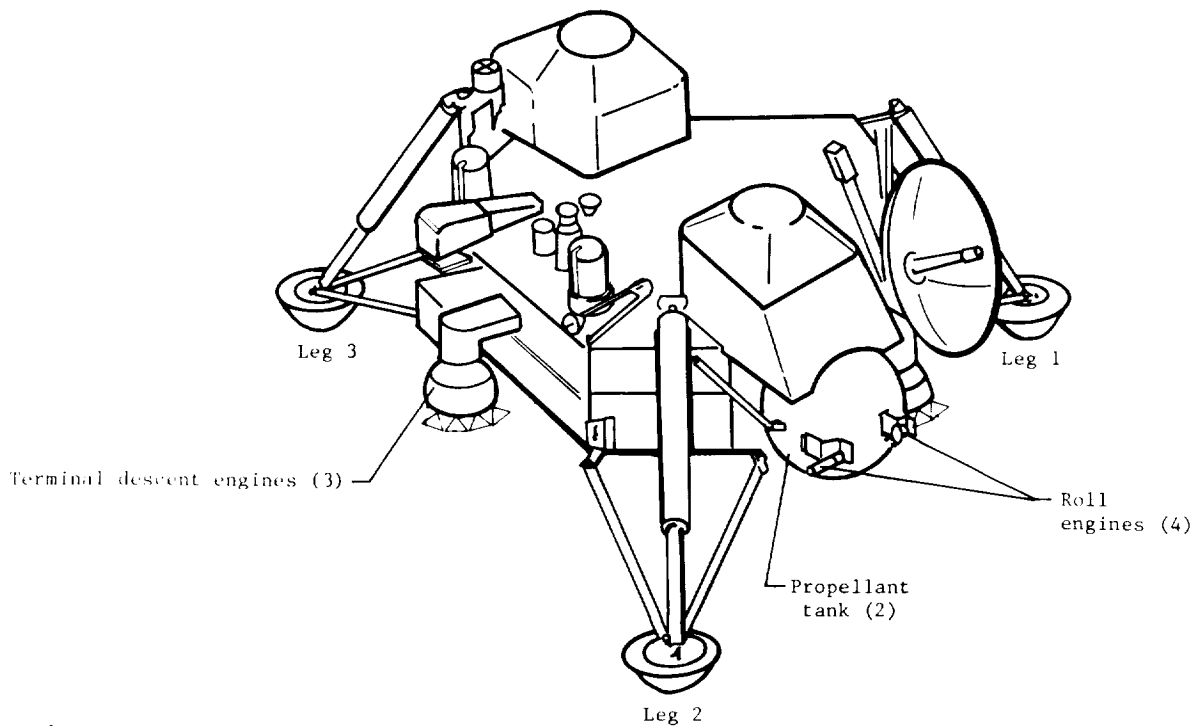
130
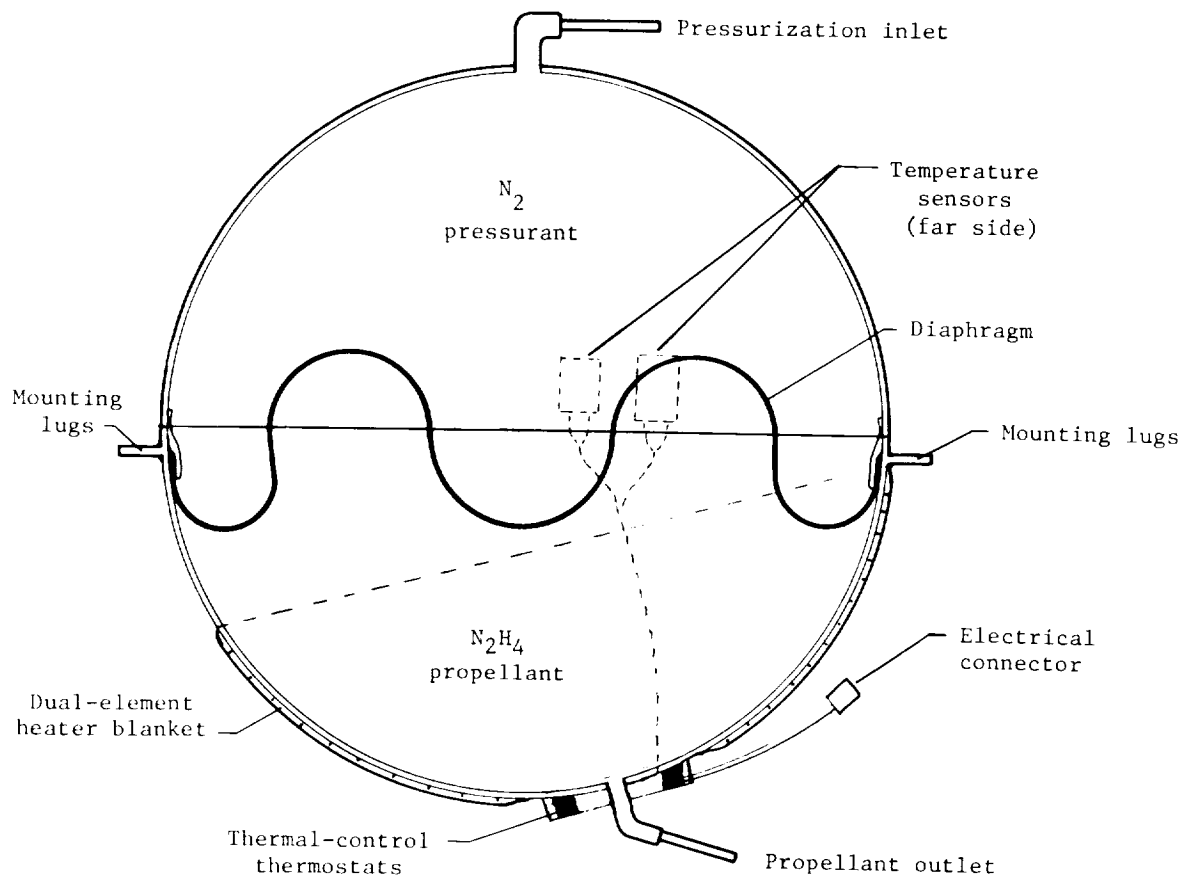
Figure 71.- RCS propellant tank.

Figure 72.- Location of components of terminal descent propulsion system.

engines were the spontaneous catalytic monopropellant type. The variable thrust
was controlled by a motor-driven throttle valve which controlled the flow rate
of the hydrazine propellant. The thrust of each engine was approximately 2700 N
(600 lbf) at an engine inlet pressure of 3.31 MPa (480 psi) and with the
throttle valve fully open. The exhaust of each engine exited through 18 small
nozzles (fig. 73) to minimize alteration of the landing site by engine plume
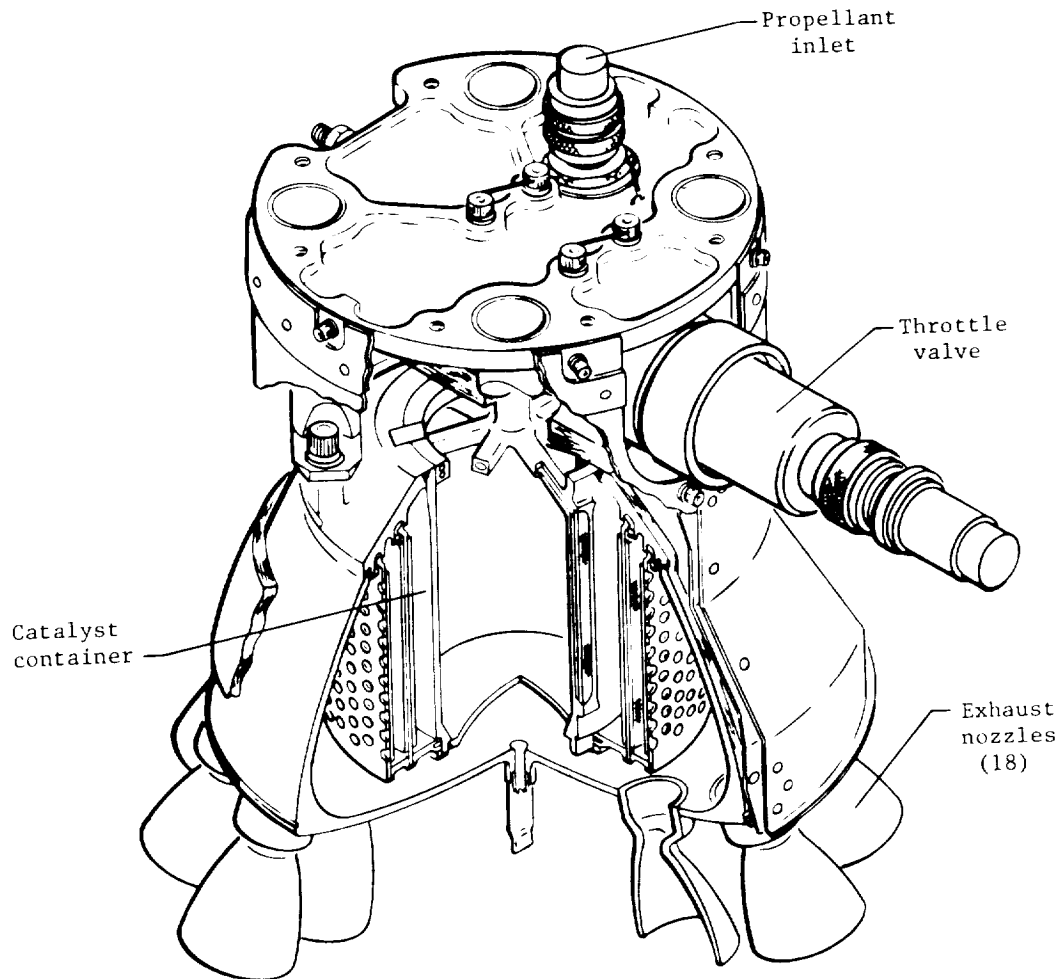
Figure 73.- Terminal descent engine.

impingement. The three engines were equally spaced around the lander body, 120°,
between each engine (fig. 74). The terminal descent engines were single string;
there were no redundant engines or throttle valves. Pitch and yaw control was
obtained with differential throttling of the three large terminal descent
engines; roll control was obtained with four separate smaller engines. These
roll engines formed CW and CCW couples and were identical to the RCS engines.
Also, the design provided the same redundancy configuration as the RCS. The
thrust of each engine was approximately 44.5 N (10 lbf) at the initial tank
pressure of 3.65 MPA (530 psia). The propellant tanks were titanium spheres
with an inside diameter of 57.9 cm (23.5 in.). Pressurant/propellant isolation
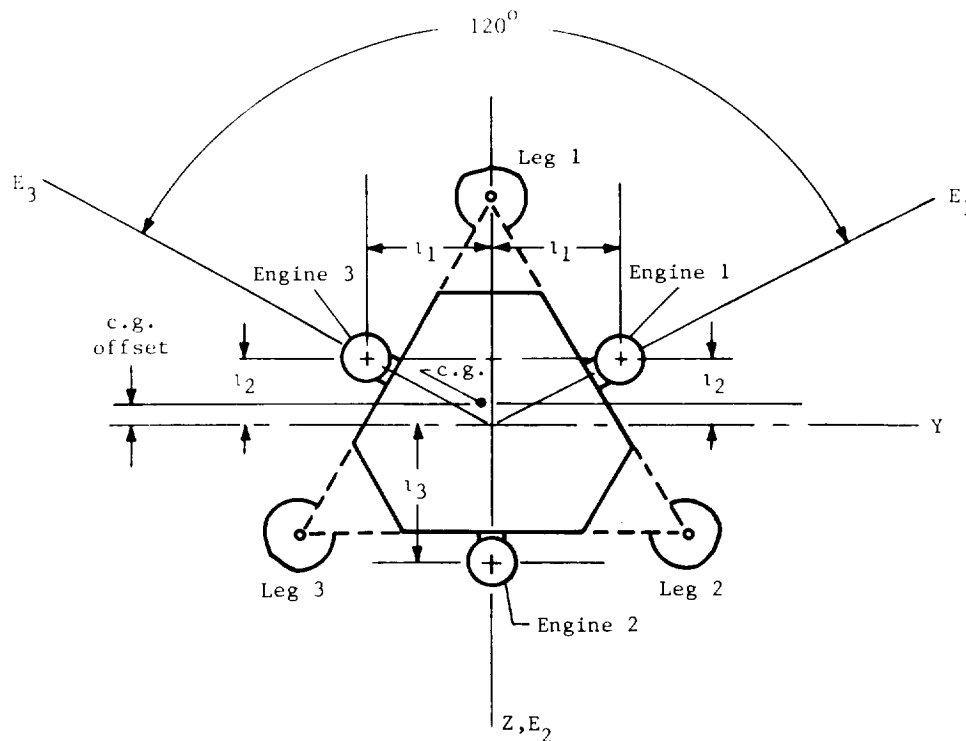
132

Figure 74.- Geometry of terminal descent engine. l_1 = 83.6 cm (32.9 in.);
l_2 = 48.3 cm (19.0 in.); l_3 = 96.5 cm (38.0 in.); c.g. offset along
-Z axis, 4.95 cm (1.95 in.); Y,Z are lander body axes; E_1,E_2,E_3 are
terminal descent engine axes.

diaphragms were not required since the deceleration associated with the Mars
atmospheric entry forced the propellant to the bottom of the tanks. Slosh baf-
fles and antivortex baffles were used to prevent escape of pressurant through
the propellant outlet ports. The TDS operated in a blowdown mode (no pressure
regulation). The initial nitrogen pressure was approximately 3.65 MPa
(530 psia) and the total TDS propellant load was 83.9 kg (185 lbm) of hydrazine.
The TDS propellant tanks and engines were thermally insulated and thermally con-
trolled by heaters to prevent propellant freeze-up during cruise to Mars and/or
at engine ignition. The TDS interfaced with the G&C subsystem via the VDA; roll
solenoid valve on/off commands and throttle valve position commands were
received from the VDA; and throttle valve position transducer outputs were sup-
plied to the VDA. Thermal control power was obtained from the power subsystem
and engineering data were supplied to the telemetry subsystem.

Pyrotechnics Subsystem

The pyrotechnics subsystem consisted of pyrotechnic and pyromechanical
devices and the pyrotechnic control circuitry required to perform prelaunch and
postlaunch operational sequence functions. The pyrotechnic subsystem accepted
pyrotechnic firing power directly from the AGE or from the LPCA. The VLC pyro-
technics subsystem, shown in the functional block diagram of figure 75, con-
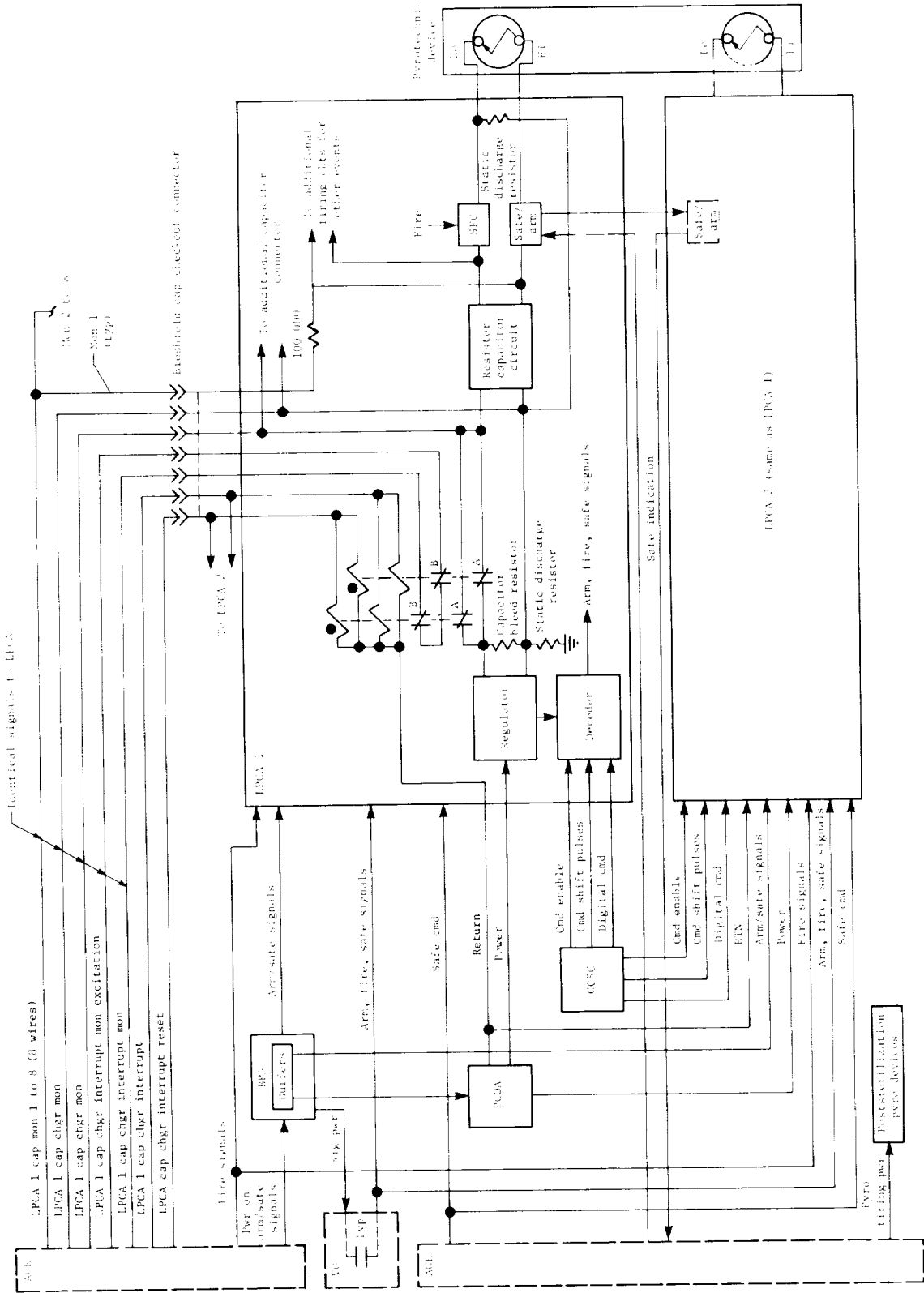sisted of the following components:

133

Figure 75.- Functional block diagram of pyrotechnics control subsystem.

LPCA

Pyrotechnic devices
  Viking standard initiators
  Pressure cartridges
  Parachute mortar cartridge

Pyromechanical devices
  Separation nuts
  Pin pullers
  Cutters
    Bolt cutter
    Cable cutter
    Rotary cutter
    Tube cutter
  Valves
    6 mm (1/4 in.) normally open
    6 mm (1/4 in.) normally closed
    19 mm (3/4 in.) normally open
    19 mm (3/4 in.) normally closed
  Decelerator mortar assembly

Lander Pyrotechnic Control Assembly

The LPCA circuitry performed the safety, arm, and fire control for all
pyrotechnic and pyromechanical devices on the Viking lander. Capacitor energy
storage was used with the firing circuits isolated from all other landed power
lines. The pyrotechnic control circuitry accepted discrete signals from the
LCE and the VO as well as digital signals from the lander GCSC. The energy
required to fire the pyrotechnic device was stored in capacitor banks in the
LPCA. Energy storage was compatible with the Viking standard initiator, a 1-A,
1-W, no-fire initiator. Safe monitors and automatic safe command were main-
tained until launch. Two LPCA's were used on each VL to provide redundancy.
Both LPCA's were mounted external to the equipment plate on side beam 3 near
lander leg 1. The LPCA's were interconnected as shown in figure 75. Each LPCA
fired one bridge wire of each pyrotechnic device so that failure of one LPCA did
not affect the mission. A functional block diagram of the LPCA is shown in fig-
ure 76 and a functional description of the LPCA circuitry is contained in the
following paragraphs.

All power utilized inside the LPCA was supplied by its own power supply
which drew up to 2.0 W steady-state power from the lander equipment bus (28 V
nominal). The power supply was made up of an input filter, preregulator, con-
verter, and an output circuit for distributing power to the LPCA loads.

The relay assembly contains the arm/safe relays and the diodes used for
suppression and blocking. Forty-five relays were used in the LPCA. These
relays were double-pole, double-throw, 2-A, magnetic latching relays. Forty-
three of the relays were used to arm and safety the Viking initiators, one set
of contacts for each relay was used for each initiator. The second set of con-
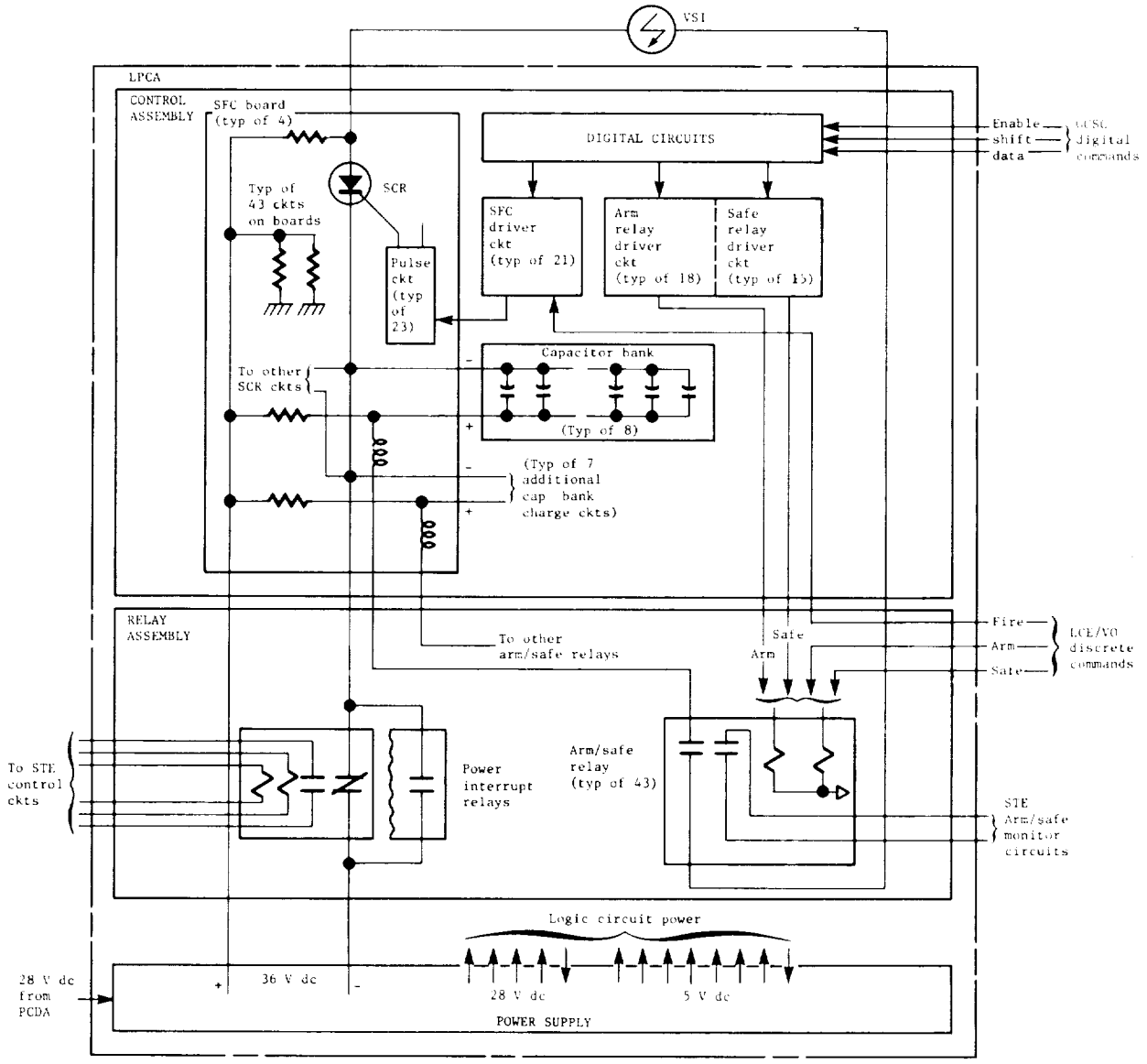tacts of each relay was connected in series with the contacts of all other

135

Figure 76.- Functional block diagram of LPCA.

relays to provide the "safe all relays" indication. The remaining two relays were used to interrupt the 36 V dc power to the capacitor banks. Two boards were used to mount hybrid diodes and discrete diodes. These diodes were used for relay coil suppression and for signal blocking applications when a relay was operated from more than one source.

The LPCA contained eight capacitor banks to provide the energy required to fire the initiators. Each capacitor bank consisted of twelve 82-μF wet slug capacitors. The capacitor banks were charged from the LPCA power supply 36-V output through a 3.4-kΩ resistor. Each capacitor bank charged to 36 V in 12 sec or less. Several initiators (6 to 7) were connected to each capacitor bank via the arming relays. The arming relays and mission sequence of events insured

136

that only one initiator at any given time was fired from a capacitor bank. The capacitor banks were capable of supplying nominally 300 mJ (150 mJ worst case) to each initiator.

The function of the digital system was to decode computer commands from the GCSC and to provide output command signals for the control of power supply outputs and for the activation of relay coils and squib fire circuits.

The digital driver assemblies accepted decoded digital commands from the digital interface and translated them into drive signals to the appropriate relays and squib fire circuits. The digital interface commands were received in the form of two bilevel signals. These bilevel signals were ANDed with the enable pulse in the first stage of the hybrid driver. If the two digital inter- face bilevel signals to any particular driver were high at the time of the enable pulse, the driver output was high and the associated relay or squib fire circuit was activated.

The LPCA contained squib fire circuits to apply the required energy to the initiators. These circuits contained pulse transformers whose outputs drove one or more SCR trigger gates. The SCR's were connected in series with the initiators and were used to perform the firing function when they were turned on and their associated arm relay was enabled. One SCR was used for each ini- tiator with the exception of the terminal engine shutdown valve initiator where series redundant SCR's were used.

There are two operating modes for the LPCA: discrete signal mode and digi- tal control mode. The LPCA responded to discrete arm, safety, and fire commands generated by either the VO or the LCE. These commands could come directly from the LCE and VO in the form of 28 V dc signals or they could be transmitted through the BPA buffers. The arm and safety commands went to relay coils to close or open contacts in series with the pyrotechnic devices. The fire com- mands went to the squib fire circuits which turned on a silicon-controlled rectifier in series with the pyrotechnic device. In the digital control mode the LPCA responded to arm, fire, and safety commands from the GCSC. These com- mands consisted of an enable pulse, shift pulses, and serial data pulses. The LPCA decoded the GCSC commands and energized the appropriate relay driver or squib fire circuit driver.

Pyrotechnic Devices

The VSI, shown in figure 77, consisted of an Inconel 718 body, threaded at the output end to mate with pyromechanical device sockets (ports) and equipped at the input end with an integral two-pin electrical connector receptacle. Near the center, a hexogonal wrenching surface was provided. At the receptacle end, two gold-plated electrical contact pins passed through glass/metal seals through a bulkhead to the interior of the body. The pins passed through the bottom of a ceramic cup which was bonded by epoxy to the inside of the body and ball- checked. A single 0.05-mm-diameter (0.002 in.) stainless-steel bridge wire was welded across the inner ends of the pins, which were machined flush with the bottom of the ceramic cup. An explosive charge was pressed into the ceramic cup, in contact with the bridge wire. Insulating dishes were placed over the

137

CIRCUIT DIAGRAM

0.95 to 1.15 Ω

Bridge wire

Initiation charge

2.22 cm (7/8 in.)

Serial no.

1.91 cm (3/4 in.)

A

0.48 cm (3/16 in.)
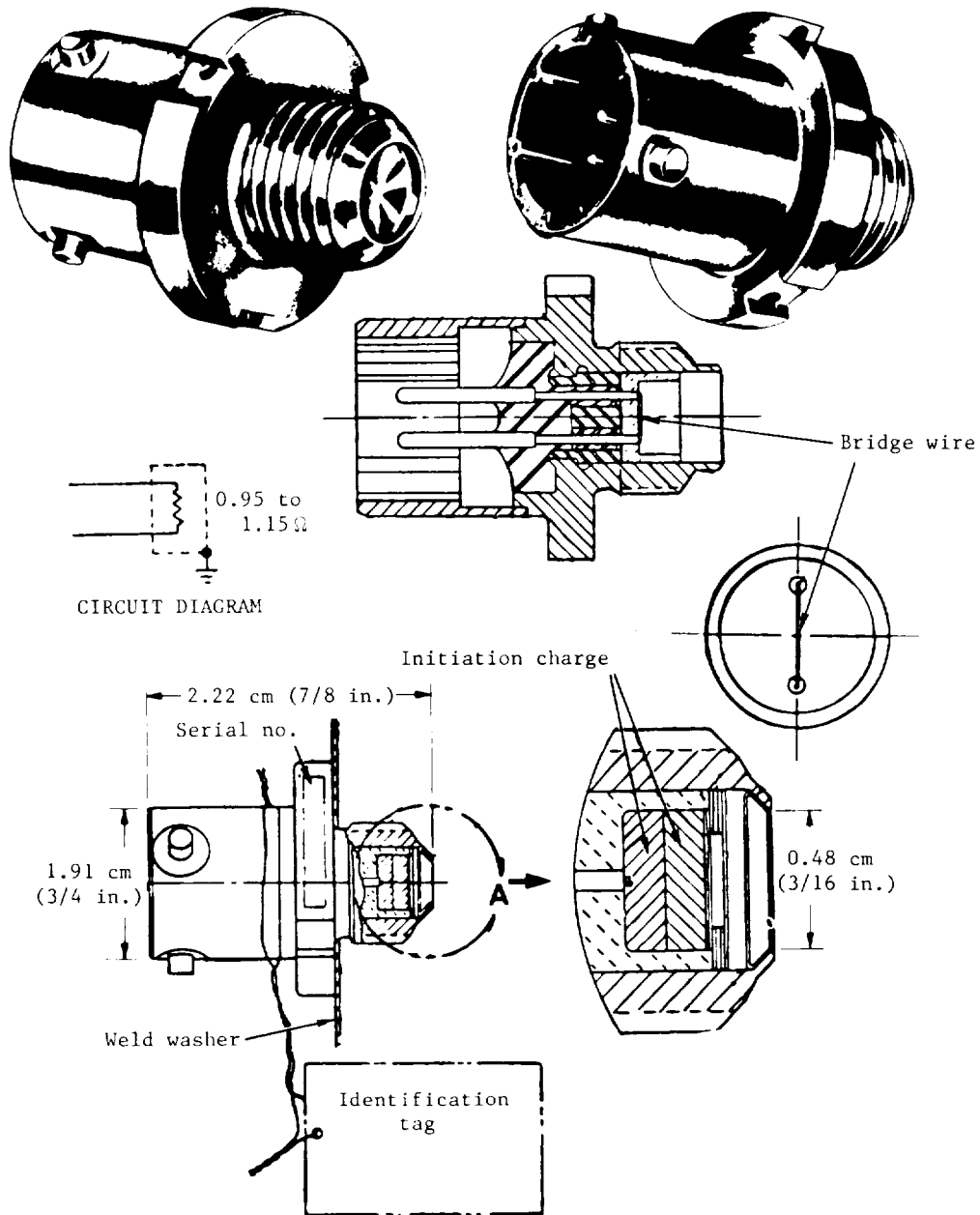
Weld washer

Identification tag

Figure 77.- Viking standard initiator.

loaded ceramic cup and bonded with epoxy, then a steel cup, mouth out, was pressed into the body and welded in place. When power was applied to the VSI, the bridge wire heated to incandescence (resistive heating) and ignited the explosive charge in contact with it. The gases resulting from the explosive reaction ruptured the steel cup and flowed into the pyromechanical device. The bridge wire was placed in contact with the bottom of the ceramic cup to provide

138

a heat sink so that electrical excitation less than that required for firing would not damage the unit; the heat sink pulled the heat away from the charge and wire. VSI usage is shown in figure 78.
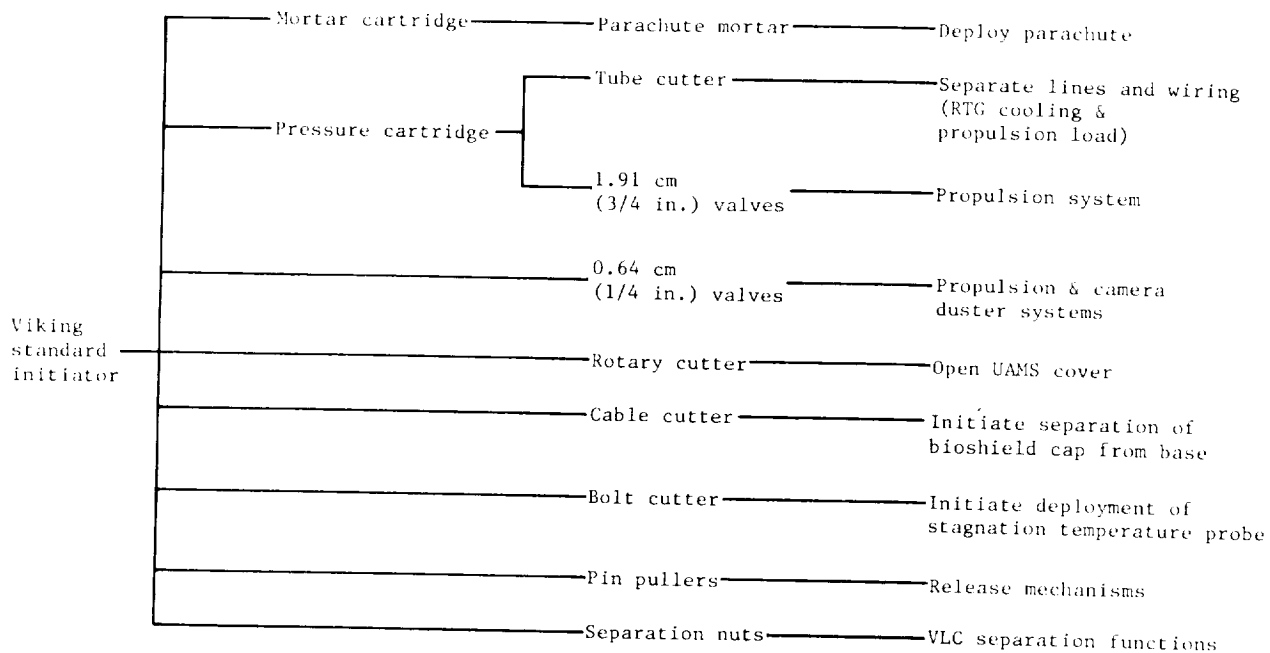
```
                    ┌──── Mortar cartridge ──────── Parachute mortar ──────────── Deploy parachute
                    │
                    │                            ┌── Tube cutter ──────────────── Separate lines and wiring
                    │                            │                                (RTG cooling &
                    ├──── Pressure cartridge ────┤                                propulsion load)
                    │                            │
                    │                            └── 1.91 cm
                    │                                (3/4 in.) valves ──────────── Propulsion system
                    │
                    │                               0.64 cm
Viking              ├─────────────────────────────  (1/4 in.) valves ──────────── Propulsion & camera
standard ───────────┤                                                             duster systems
initiator           │
                    ├───────────────────────────── Rotary cutter ──────────────── Open UAMS cover
                    │
                    ├───────────────────────────── Cable cutter ───────────────── Initiate separation of
                    │                                                             bioshield cap from base
                    │
                    ├───────────────────────────── Bolt cutter ────────────────── Initiate deployment of
                    │                                                             stagnation temperature probe
                    │
                    ├───────────────────────────── Pin pullers ────────────────── Release mechanisms
                    │
                    └───────────────────────────── Separation nuts ────────────── VLC separation functions
```

Figure 78.- Pyrotechnic and pyromechanical devices powered by VSI.

The VPC of figure 79 consisted of a hollow Inconel 718 body, with external screw threads on the output end to match the cartridge parts provided in the pyromechanical devices, and a VSI which was mounted in the body by its screw threads and welded at the input end. Inside was an explosive charge sandwiched between two thin aluminum dishes by a function ring at one end of the charge and an internal shoulder at the VSI end. The output end of the cartridge was closed by a metal cup, pressed in place, and welded to the body. When the VSI in the cartridge fired, the blast of hot gases ignited the explosive charge and the combined gases ruptured the closure cup, releasing the gas into the pyro-mechanical device.

The parachute mortar cartridge assembly, shown in figure 80, provided the energy to eject the aerodecelerator system parachute. The mortar cartridge consisted of 65 grams of potassium perchlorate type propellant divided into a booster charge and a main charge. Two VSI's were mounted on the cartridge assembly and were used to actuate the device. The cartridge assembly was threaded and was installed into a steel breech. When the VSI's in the cartridge fired, the hot gases ignited the booster charge and then the main charge. The combined gases ruptured the closure disk and released the gas into the breech. The gases left the breech through a hybrid orifice into the aerodecelerator mortar assembly to expel the parachute.
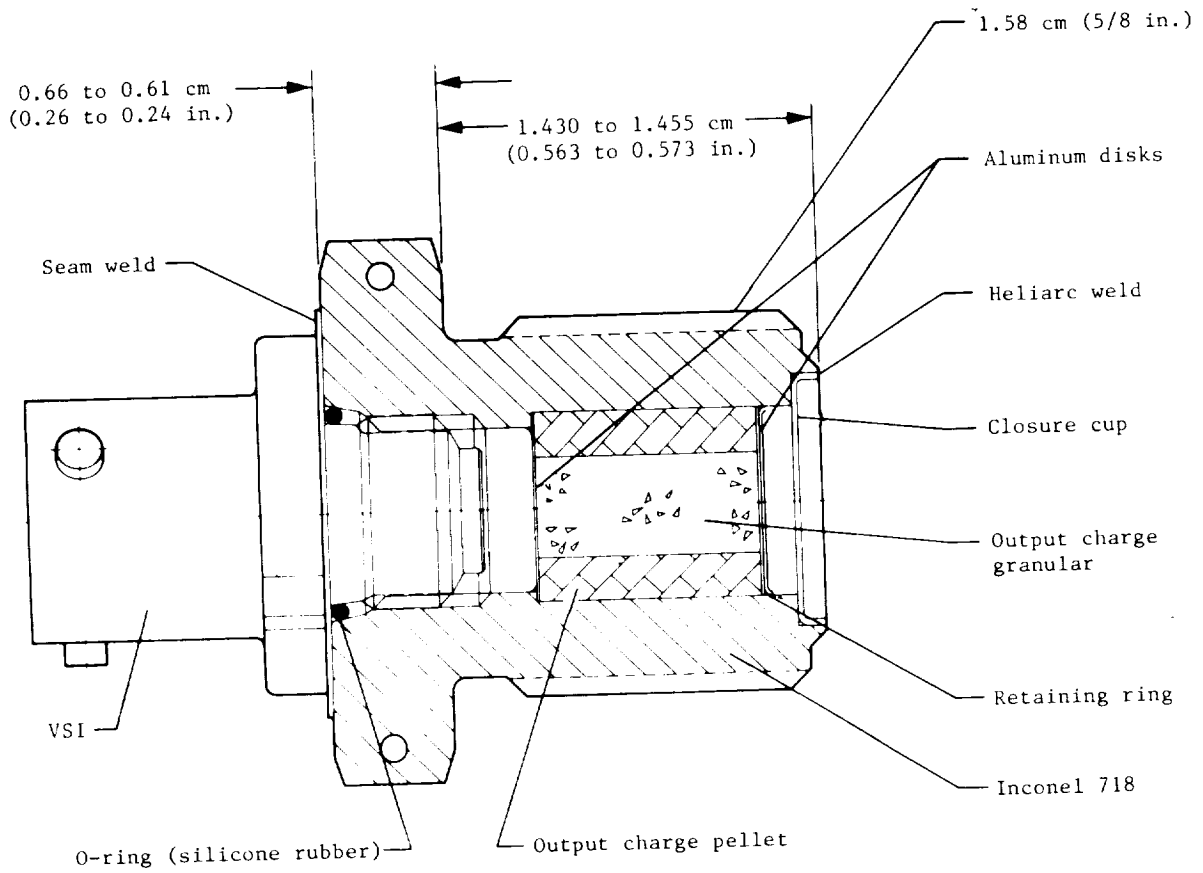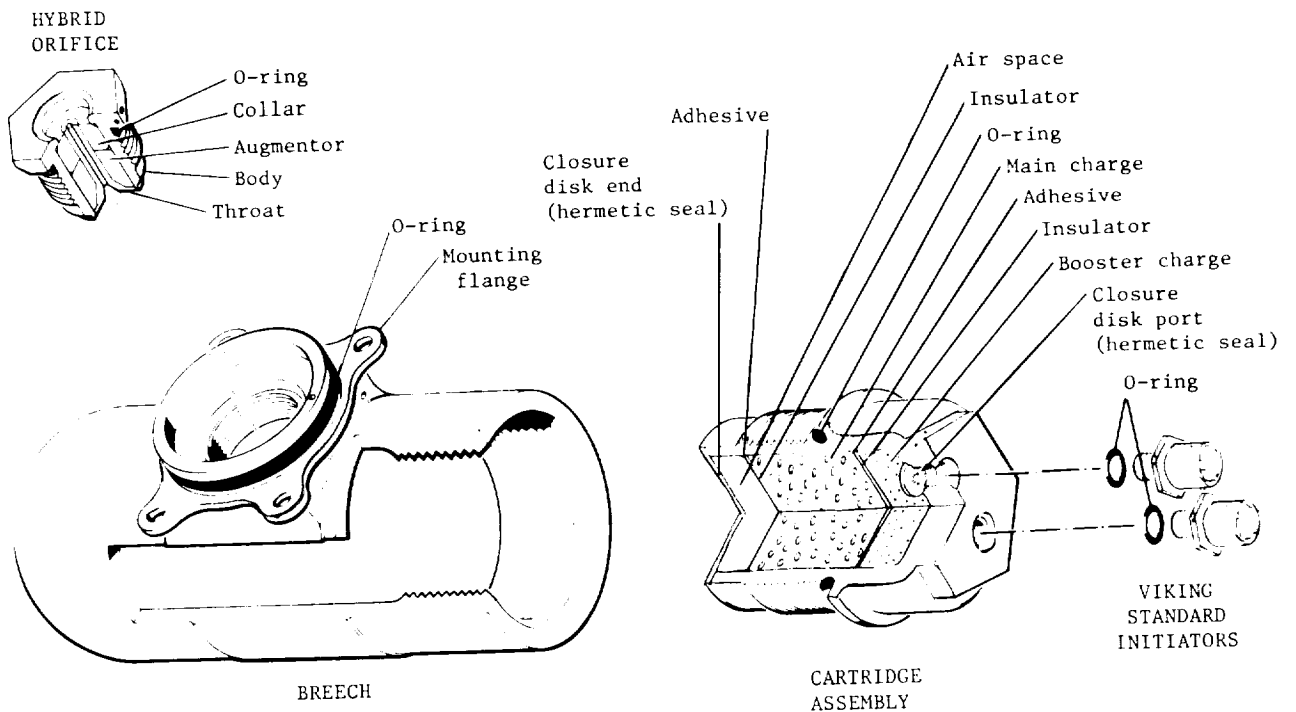
0.66 to 0.61 cm
(0.26 to 0.24 in.)

1.430 to 1.455 cm
(0.563 to 0.573 in.)

1.58 cm (5/8 in.)

Seam weld

Aluminum disks

Heliarc weld

Closure cup

Output charge
granular

VSI

Retaining ring

Inconel 718

O-ring (silicone rubber)

Output charge pellet

Figure 79.- Pressure cartridge.

HYBRID
ORIFICE

O-ring
Collar
Augmentor
Body
Throat

O-ring
Mounting
flange

Adhesive

Closure
disk end
(hermetic seal)

Air space
Insulator
O-ring
Main charge
Adhesive
Insulator
Booster charge
Closure
disk port
(hermetic seal)

O-ring

VIKING
STANDARD
INITIATORS

BREECH

CARTRIDGE
ASSEMBLY

Figure 80.- Mortar power unit.

The cartridge-actuated separation nut, shown in figure 81, had a threaded steel collet on the inside, slit nearly through, lengthwise, in four places.
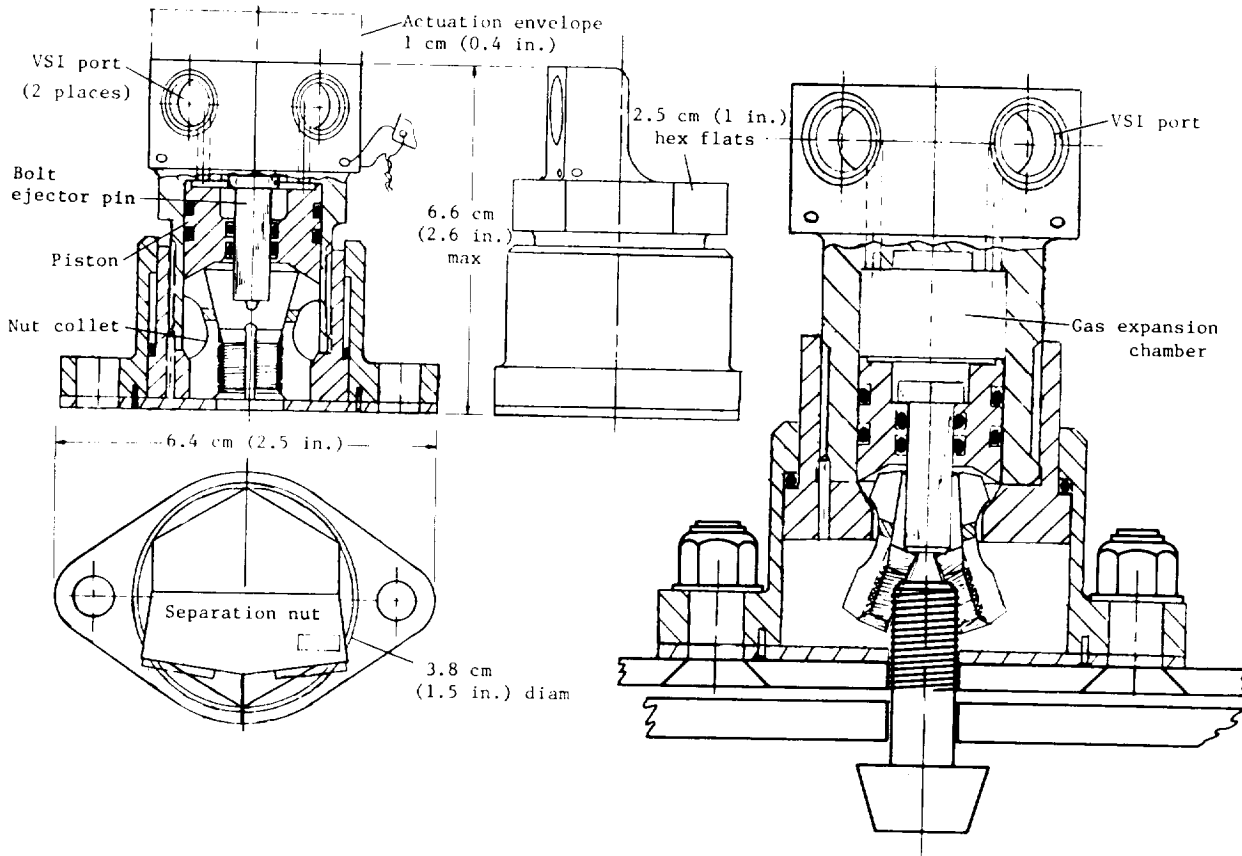
Figure 81.- Cartridge-actuated separation nut.

The closed end of the body was equipped with two ports for the power cartridges (VSI's) which were connected by passage to the inside of the body. Between the end of the collet and the blank end of the body was a piston, sealed against the body by sealing rings. Surrounding the entire assembly was a base by which the separation unit could be secured to the structure of the vehicle. When the load bearing bolt was installed in the nut, the bolt engaged the internal threads in the collet. When the power cartridges were fired, the resulting gas pressurized the space between the closed end of the body and the piston. Since the piston could not move, the body moved and disengaged the ring from the collet. At the end of the body stroke, the threaded portions of the segments petaled outward and disengaged the bolts. The 0.08-mm (5/16 in.) bolt size was used for VL/VO, aeroshell, and bioshield cap separation, and the 0.11-mm (7/16 in.) bolt size was used for parachute truss and base cover separation.

The cartridge-actuated pin pullers, shown in figure 82, consisted of a hollow aluminum body with screw threads for mounting the devices at one end and

PYRO OPERATED PIN PULLER USED FOR ALL INSTALLATIONS EXCEPT HGA
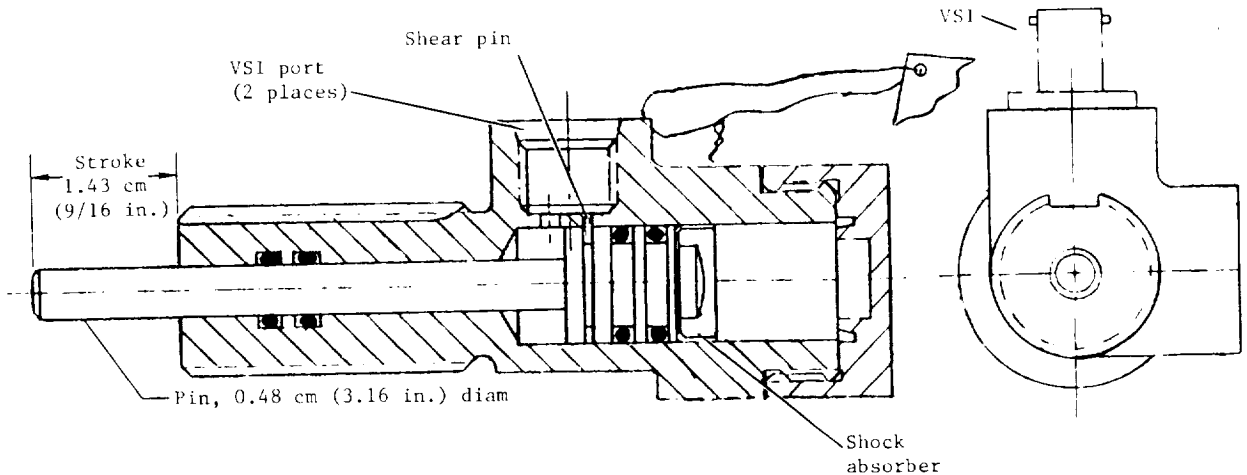
PYRO OPERATED PIN PULLER USED FOR HGA ONLY
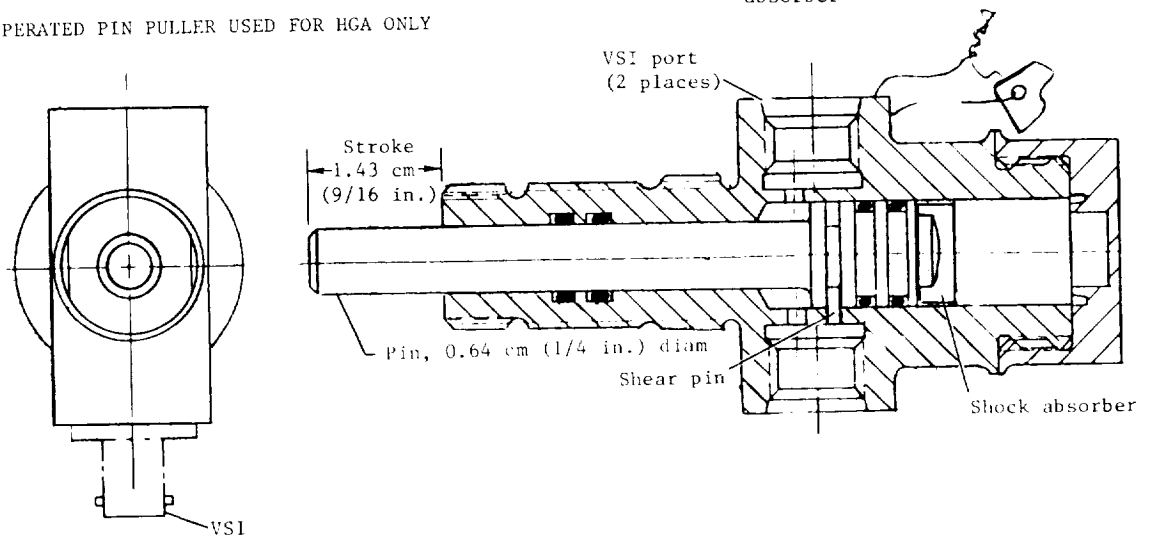
Figure 82.- Cartridge-actuated pin pullers.

a threaded welded cap at the other end. Two cartridge ports (VSI ports) were provided near the center, arranged so that the gas passages permitted the gas pressure to be applied under the head of a steel pin. When the actuating cartridges were fired, the resulting gas pressure was applied to the bottom of the piston head to force the piston head to pull the portion of the pin extending beyond the body threads into the body; this released the load by pulling the pin from a clevis joint. At the end of its stroke, the steel cup engaged the circular groove in the end cap. Deformation of the steel cup absorbed some of the shock of the impact and locked the pin in the retracted position. The 0.05-mm (3/16 in.) diameter size was used for landing leg release, meteorology

142

boom release, biology PDA cover release, and vent valve release, and the 0.06-mm (1/4 in.) diameter size was used for HGA release.

Two kinds of cartridge-actuated cutters were used: tube, bolt, and cable cutter and rotary cutter. A typical cutter is shown in figure 83. The cutter
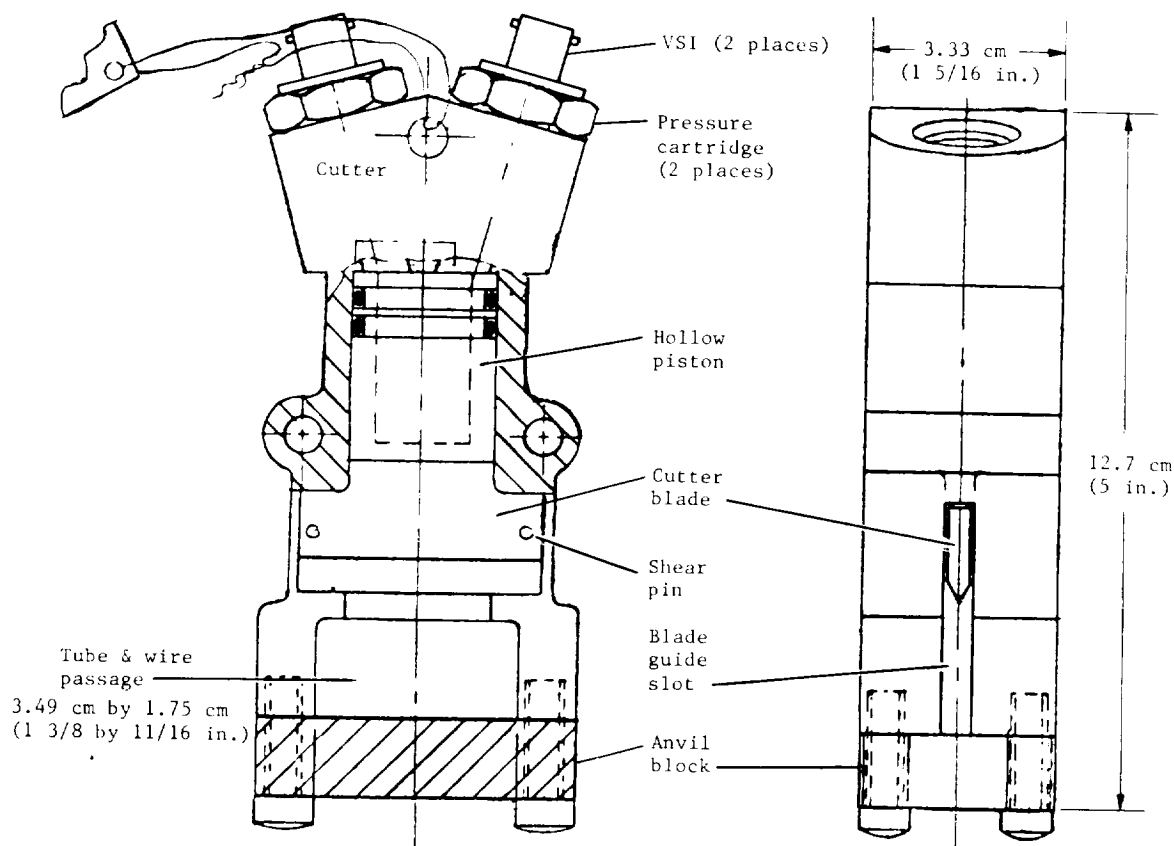
Figure 83.- Typical cutter.

consisted of a hollow aluminum body closed at one end with provisions for mounting an anvil to close the hollow, at the other end. At the anvil end of the body, a transverse hole was provided. The target to be attacked by the cutter passed through this hole. In the body was the steel blade with a sharp cutting edge on one end; the other end was round and equipped with sealing rings. The closed end of the body had machined actuating cartridge ports connected to the hollow by passages. The blade was retained in the cocked or unfired position by shear pins. When the pressure cartridges or VSI's were fired in the ports, the resulting gas pressure forced the blade toward the target and sheared the retaining pins. The blade built up significant kinetic energy before it struck the target. The sharp edge of the blade cut the target and sank into the anvil. The tube cutter was used to cut propulsion fill lines (2 places) and RTG coolant lines, and the cable and bolt cutters were used to cut the bioshield cap latch

cable (3 places) and the stagnation temperature probe retaining bolt. The rotary cutter shown in figure 84 was used to release the outward portion of
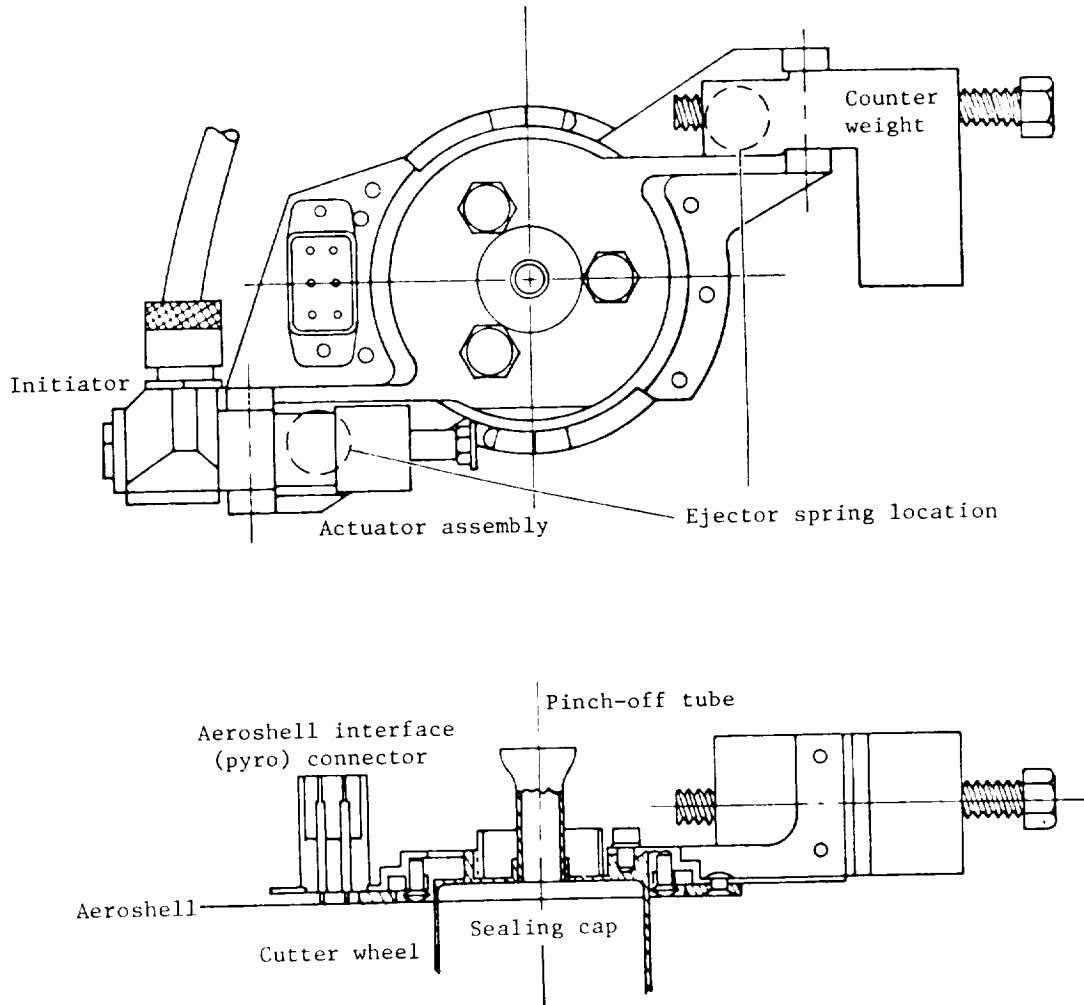
Figure 84.- Rotary cutter (UAMS).

the sealed instrument cap on the UAMS. The rotary cutter was a 12 cutting wheel mechanism driven by a pyrotechnic actuator and powered by two VSI's. Positive release of the sealing cap was assured by firing either or both VSI's. The cutter was mounted to the removable portion of the UAMS cover so that the cutter was jettisoned along with the removed portion of the cover.

The cartridge-actuated valves were either normally closed valves or normally opened valves. The inlet tubes of the NC cartridge-actuated valves as seen in figure 85 consisted of a single machined port, formed to provide a blind or blank-ended hole. Provisions were made at the blank end for a thin, short section that could be sheared off. This tube was welded into the valve body

VPC/VSI port (2)

NC valve

Tension screw

Piston

Ported ram

Shear spool

Bleed-in valve port

Shear wedge

Drain valve port

Piston

Shear plugs

Tension screw

NO valve

VPC/VSI port (2)
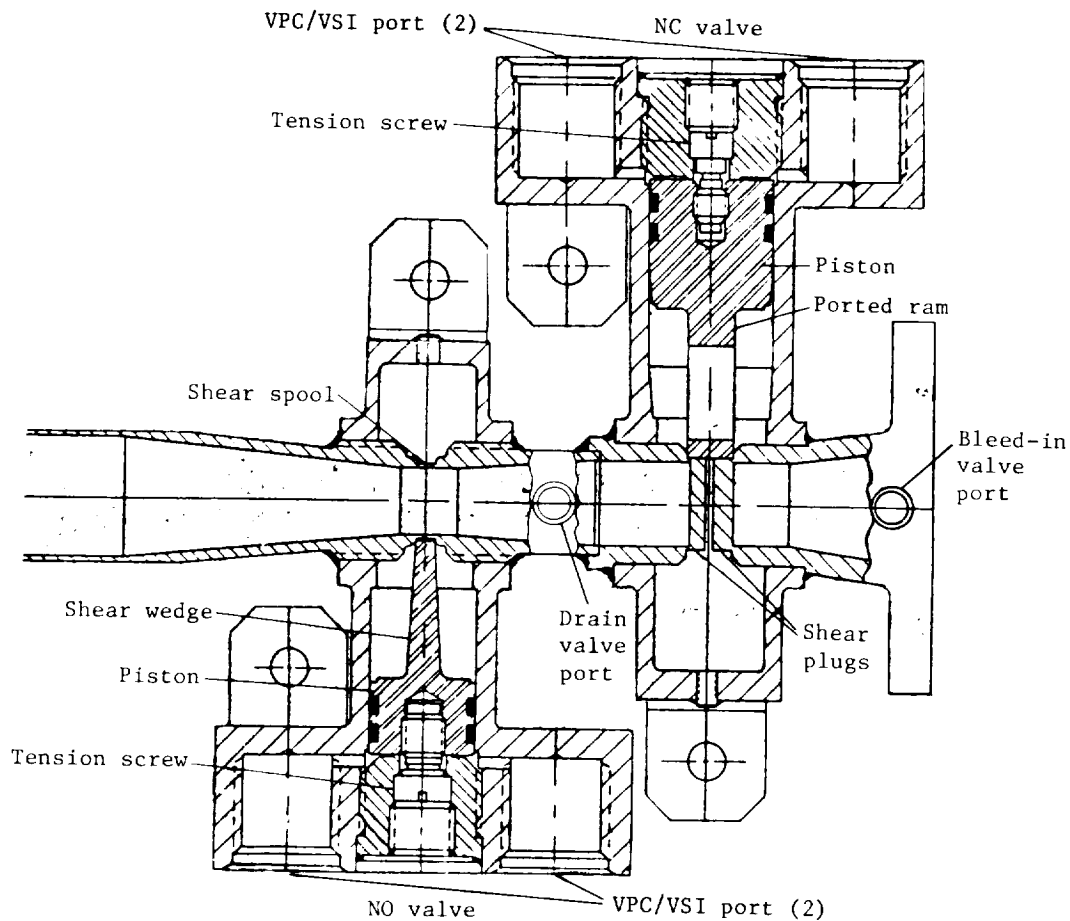
Figure 85.- Cartridge-actuated valve.

and was opposed by a similar tube at the outlet. A ram and piston in the body were driven by the cartridge gases against the shear section of both tubes. When the ram sheared the ends of the inlet and outlet tubes, it continued to pass between the sheared-off tubes until a port in the ram was aligned with the inlet and outlet tubes. At that instant the ram struck a built-in stop in the body and remained aligned between the inlet and outlet. Thus, after firing, a relatively clear unobstructed flow passage was provided between the inlet and outlet. The inlet and outlet tubes of the NO valve, as seen in figure 85, were made as one piece so that a clear unobstructed flow passage between the inlet and outlet was provided. At the center, a thin-wall section was provided by machining the outside of the tube. The valve body was a closed-end cylinder locally formed to accept the tubes and the actuating cartridges. A ram slid in the body driven by the cartridge gases. When so driven, the thin end of a cutter wedge on the ram was driven against the thin shear section of the shear tube to cut the thin section out. The wedge continued to move between the two tube ends until the wedge was firmly jammed between the tube ends and the wedge. The 0.19-mm-diameter (3/4 in.) tube with NC valve was used for terminal engine (main) start; the 0.19-mm-diameter (3/4 in.) tube with NC/NO valve was used for

terminal system enable (NC portion) and terminal system shutdown (NO portion);
the 0.06-mm-diameter (1/4 in.) tube with NC valve was used for deorbit terminal
system bleed-in, deorbit system start, and deorbit system fill transfer; the
0.06-mm-diameter (1/4 in.) tube with NO valve was used for deorbit and terminal
system fill isolation; the 0.06-mm-diameter (1/4 in.) tube with NC valve
(threaded outlet) was used for deorbit and terminal system drain; and the
0.06-mm-diameter (1/4 in.) tube with NC valve (high pressure) was used for
camera duster enable.

The aerodecelerator mortar assembly of figure 86 was an aluminum cylinder
3.8 mm (15 in.) in diameter and 6.6 mm (26 in.) long. Packed inside was a
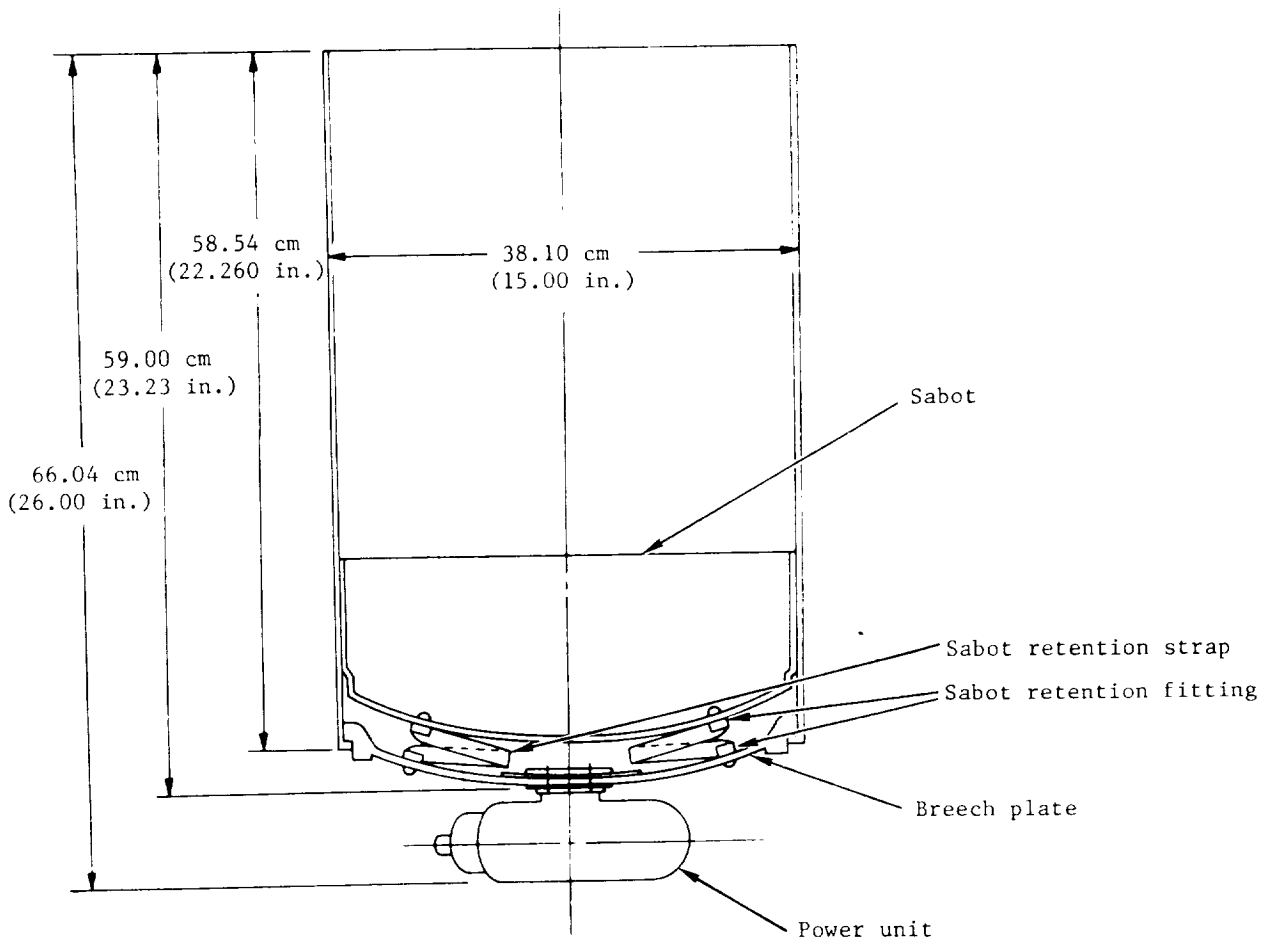
Figure 86.- Aerodecelerator mortar assembly.

parachute bridle assembly. The mortar ejected the parachute (approximately
45.4 kg (100 lb) ejected weight) at a muzzle velocity of about 35 m/sec
(115 ft/sec) into the wake of the entry vehicle. The parachute then deployed
to decelerate the entry vehicle's descent to the Martian surface. The VSI

initiated mortar cartridge, located on the breech that was attached to the breech plate at the base of the mortar, provided the gas pressure that accelerated the sabot and ejected the parachute. The mortar was mounted such that it reacted through the vehicle center of gravity to avoid disturbing torques.

Pyrotechnics Subsystem Interfaces

The pyrotechnic subsystem interfaced with the VO, BPA, GCSC, PCDA, and VLC AGE. Discrete signals were received by the LPCA directly from the VO to arm RTG coolant line cutters and to fire the bioshield latch cable cutter and the bioshield cap separation nuts. Discrete signals from the BPA were initiated by the VO or the lander LCE. Signals were initated by the VO to arm the bioshield latch cable cutters, to arm the bioshield cap separation nuts and fire RTG coolant line cutters, and to reset all safe/arm relays in LPCA 1 and 2. Signals were initiated by the LCE to fire the enable bioshield vent valve, separate the RTG and preflight makeup pressurization line, seal the RTG cooling loop, and energize the bioshield cap to parachute canister staging connecter pin puller and to safety these four functions. Discrete signals directly from the LCE were used to arm relays for enabling bioshield vent valve, separating RTG and preflight makeup pressurization lines, sealing the RTG cooling loop and the bioshield cap to the parachute canister staging connector. Each LPCA responded to digital arm, fire, and safety commands generated by the GCSC. These commands were used for separating the lander from the orbiter and other functions during deorbit, entry, and initialization of the lander immediately following landing. Three inputs required for each command were an enable signal, shift pulses, and serial command data. The PCDA switched power to the LPCA on command from the LCE or GCSC. The LPCA received input power from the equipment bus through a PCDA switch. The voltage at the LPCA interface was 24 V dc to 37 V dc. The power consumed by each LPCA was 2 W maximum average or 25 W peak excluding turn-on inrush.

Telemetry and Data Handling Subsystem

The telemetry and data handling subsystem acquired, processed, stored, and modulated for transmission all VLC science and engineering data during prelaunch checkout and throughout the launch, cruise, preseparation checkout, entry, and postlanded phases of the mission. A summary of the data handling capability is shown in table 9. The telemetry subsystem consisted of a DAPU, a DSM, and a TR along with engineering pressure and temperature transducers. The relationship of the components of the telemetry and data handling subsystem is shown in figure 87.

The DAPU acquired data from 120 low-level analog (0 to 40 mV) differential (including 26 resistance bridge channels), 64 high-level analog (0 to 5 V) single-end, 48 bilevel (0 or 5 V), and 15 serial digital sources. These data were sequenced and formatted for storage in the 196 608-bit plated-wire DSM or the 40 million bit serial digital TR, were forwarded to the VO for storage/transmission through direct lines or the UHF transmitter or were transmitted directly to Earth through an S-band transmitter. The telemetry and data handling subsystem design was redundant/fail-safe so that no single failure caused

the loss of more than one science interface, of more than 64 low-level or 32 high-level analog channels, of both the DSM and TR, or of both the UHF and S-band interfaces.

TABLE 9.- VL TM DATA HANDLING REQUIREMENTS

Mission phase	Output to	Data description	Modes	Data rate, bps	Coding	Symbol rate, bps	Subcarrier	Remarks
Cruise	Hardline to orbiter	Engineering status monitors format 1	CR-1	(1)	None	(1)	None	(1)
	None	None	CR-2	None	None	None	None	(2)
Preseparation checkout	Hardline to orbiter	GCSC mem readout via format 3	CR-3	2 000	None	2 000	(3)	
		GCSC mem readout, direct	DT-7	1 000	None	1 000	(3)	(4)
		Science calib. & format 2 checkout	RT-1A	(5)	None	(5)	(3)	(5)
		Science calib. & format 2A checkout	CR-6	2 000	None	2 000	(3)	(6)
		Tape playback	DT-1A to 1H	1 000	None	1 000	(3)	(4)
		DSM readout	DT-4/CR-9	1 000/2 000	None	1 000/2 000	(3)	(4)
		Real-time eng format 5	CR-7	2 000	None	2 000	(3)	
Separation to deorbit burn	UHF	Entry science & eng format 2	RT-1A,-1C,-1D,-1E,-1F	4 000	Split-phase	8 000	None	(7)
Deorbit burn to 0.1g	UHF	Entry science & eng format 2A	RT-12A to RT-2E	4 000	Split-phase	8 000	None	
0.1g to chute deployment	UHF	Entry science & eng format 2	RT-1A,-1C,-1D,-1E,-1F	4 000	Split-phase	8 000	None	(7)
Chute deployment to landing	UHF	Entry science & eng format 3	RT-2A,-2C,-2D,-2E,-2F	4 000	Split-phase	8 000	None	
Landed (relay link trans-mission)	UHF	Tape playback	RT-5A to RT-5H	16 000	Split-phase	32 000	None	
		Tape playback	RT-8A to RT-8H	4 000	Split-phase	8 000	None	
		DSM readout	RT-6	16 000	Split-phase	32 000	None	
		DSM readout	RT-9	4 000	Split-phase	8 000	None	
		Real-time imaging	RT-4, RT-13	16 000	Split-phase	32 000	None	
		GCSC memory readout	RT-10	16 000	Split-phase	32 000	None	
		GCSC memory readout	RT-11	4 000	Split-phase	8 000	None	
		Real-time eng format 5	RT-3	4 000	Split-phase	32 000	None	(8)
		Real-time eng format 5	RT-7	4 000	Split-phase	8 000	None	
Landed (direct link trans-mission)	S-band	Tape playback	DT-1A to DT-1H	1 000	Block code	5 333 1/3	A	
		Tape playback	DT-2A to DT-2H	500	Block code	2 666 2/3	A	
		Tape playback	DT-3A to DT-3H	250	Block code	1 333 1/3	A	(9)
		DSM readout	DT-4	1 000	Block code	5 333 1/3	A	
		DSM readout	DT-5	500	Block code	2 666 2/3	A	
		DSM readout	DT-6	250	Block code	1 333 1/3	A	
		Real-time imaging	DT-10,-12,-13,-14	250	Block code	1 333 1/3	A	
		GCSC memory readout	DT-7	1 000	Block code	5 333 1/3	A	
		GCSC memory readout	DT-8	500	Block code	2 666 2/3	A	
		GCSC memory readout	DT-9	250	Block code	1 333 1/3	A	
		Real-time eng format 5	All DT modes	8 1/3	None	8 1/3	B	(10)
Landed (data storage)	Tape	Imaging data	ST-1A to ST-1H and ST-10A to ST-10H	16 000	None	16 000	None	
	Tape	DSM data transfer	ST-2A to ST-2H	16 000	None	16 000	None	
	DSM	Eng format 4	SC-1	4 000	None	4 000	None	Preferred mode
	DSM	Eng format 5	SC-3	4 000	None	4 000	None	
	DSM	Eng format 5	DT-12,-14	8 1/3	None	8 1/3	None	
	Tape	Eng format 4	ST-3A to ST-3H	4 000	None	4 000	None	Backup to SC-1
	DSM	Formatted science data	SC-2B to SC-2F	16 000	None	16 000	None	Preferred mode
	Tape	Formatted science data	ST-5 to ST-9	16 000	None	16 000	None	Backup to SC-2B to SC-2F
	DSM	Imaging data	SC-4 and SC-5	250	None	250	None	
	DSM	GCMS data	SC-2A	4 000	None	4 000	None	
	Tape	GCMS data	ST-4	4 000	None	4 000	None	

[1]Orbiter dependent.
[2]This mode (CR-2) used for tape-recorder maintenance during cruise.
[3]VL TM output signal modulates VO telemetry subcarrier directly.
[4]In preseparation checkout phase, the data is delivered to VO interface before block coding.
[5]Data rate at preseparation interface is 2000 bps and consists of real-time data only.
[6]These modes available for use in preseparation checkout.
[7]Format 2 data collection rate, 2000 bps; transmitted data, 2000 bps of this real-time data, interleaved bit by bit with the same data delayed 60 sec.
[8]Each data bit (at 4000 bps) treated as one undefined bit followed by three identical sequential bits (at 16 000 bps), then split-phase coded.
[9]Channel A subcarrier frequency, 72 kHz; biphase modulated at symbol rate.
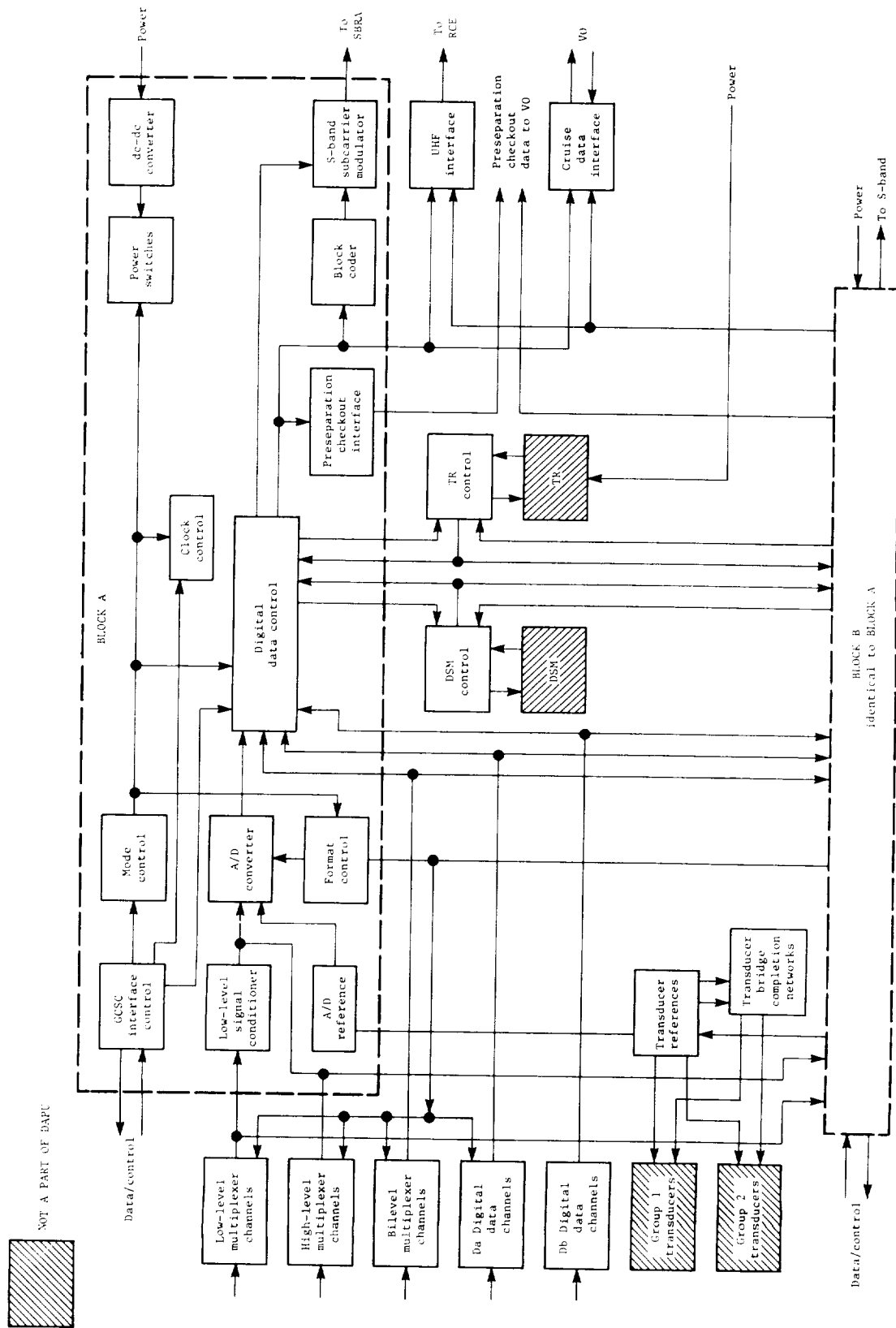[10]Channel B subcarrier frequency, 12.0 kHz coherent; biphase modulated at symbol rate.

148

Figure 87.- Block diagram of telemetry and data handling subsystem.

The low-level analog channels measured the differential voltage between each input signal pair. A total of 120 channels were sampled and were arranged into groups of 8 channels. Each group of eight channels was protected against positive overvoltage by a Zener diode, followed by a secondary gate which prevented propagation of the failure. Each gate was an MOSFET switch which resulted in open inputs when the DAPU was powered down or in standby mode. The low-level signal conditioner had a gain of 125 which amplified the 0 to 40 mV differential input into a 0 to 5 V signal compatible with the 8-bit analog-to-digital converter.

Twenty-six of the low-level channel inputs were derived from bridge completion networks included in the DAPU.

The high-level analog channels measured the voltage between the signal and ground. A total of 64 channels were arranged in a manner similar to that of the low-level channels except that the signal was single ended and not amplified prior to the analog-to-digital converter input. The multiplexer consisted of eight groups of eight channels switched through block switching gates to the block redundant analog-to-digital converter in a manner which limited any single failure to 32 channels.

The analog-to-digital converter was a dual slope converter in which the input voltage from either the low-level signal conditioner or a high-level channel was applied to yield a count of 255 for a 5 V or greater input and a proportionally lower count for input voltages below 5 V.

The total conversion time, including initialization and settling times, was 1.972 msec permitting a maximum bit rate for analog data of 4000 bps.

The DAPU provided 5-V excitation to transducers requiring a precision reference through two separate supplies in which no single-point failure, including a load short, caused the loss of both supplies. The supplies were power switched to save power and are on for 1 msec during each analog channel sample.

The bilevel channels measured the voltage between the signal and ground and the associated bit for each channel was a 0 for voltages of -0.5 to 1.0 V and a 1 for voltage of 2.5 to 10.0 V. A total of 48 channels were arranged in a manner similar to that of the low-level multiplexer except that the signal was single ended and the level determined by a level detector without block switching gates. The most probable failure mode was the same as in the low-level multiplexer but some failure modes exist which caused the loss of all bilevel channels.

The Da serial digital channels were provided for collecting serial digital data on a time-shared basis with the analog and bilevel channels. The interface with each component, except the GCSC, consisted of a continuous shift clock operating at the selected data collection bit rate, an enable line that was high during the data transfer bit periods, and a data line that was set to the data level following the trailing edge of each shift pulse when the enable was high.

150

The Da1 (memory readout (MRO)) and DA4 (time/segment count) channels from the GCSC operated in a similar manner except that no enable line existed and only 24 shift pulses were sent for each transfer over a command/data line.

The telemetry and data handling subsystem operated in seven formats under control of the DAPU. The formats are described as follows:

Format 1 contained engineering data monitored during cruise from Earth to Mars. These data were transferred to the VO telemetry for insertion in the VO format for transmission to Earth. The format 1 data cycle consisted of 64 words. One 7-bit word was transferred to the VO upon receiving an enable signal from the VO. The minimum interrogation period was 10 msec except during TR maintenance (mode CR-2) when it was 1.5 sec.

Format 2 contained engineering and GCSC data from separation through deorbit burn and from sensing of 0.05g plus 7 sec to parachute deployment plus 6.5 sec. Collected data were transmitted in real time and also were delayed through the DSM for 60 sec and interleaved bit by bit with real-time data; this resulted in the same data being transmitted twice with a 60-sec time diversity. The format 2 major frame consisted of four minor frames. Each minor frame consisted of 250 8-bit words collected at a rate of 2000 bps. Transmission was performed in real time at a rate of 4000 bps.

Format 2A contained engineering, GCSC, and entry science data from completion of deorbit burn to sensing of 0.05g plus 7 sec. The format 2A major frame consisted of 2 minor frames and each minor frame consisted of 250 8-bit words collected at a rate of 4000 bps. Data were transmitted in real time at a rate of 4000 bps.

Format 2P was used for VLC data during the IRU calibration portion of pre-separation checkout. Formats 2 and 2P were identical except for the GCSC data measurements.

Format 3 contained engineering and GCSC data from parachute deployment plus 6.5 sec to landing. The format 3 major frame consisted of 4 minor frames and each minor frame consisted of 250 8-bit words collected at a rate of 4000 bps. Data were transmitted in real time at a rate of 4000 bps.

Format 4 was used for periodic collection and storage of engineering and science status monitors during the postlanded phase. The format 4 frame consisted of 96 8-bit words collected at a rate of 4000 bps; 1 frame was sampled following each GCSC command. Channel Da4 contained only time in format 4.

Format 5 was used for real-time collection and transmission of engineering data during postlanded operations. The format 5 frame consisted of 96 8-bit words collected and transmitted in real time or stored in the DSM at a rate of 8 1/3 bps for S-band direct link and at a rate of 4000 or 16 000 bps for the UHF relay link. Channel Da4 alternated time and segment count in format 5.

Format control was accomplished through four ROM's, one each for formats 2, 2A, and 3 plus one for formats 1, 4, and 5. Each ROM contained 256 10-bit words with the ROM's for formats 2, 2A, and 3 utilizing 250 words and the remaining

ROM using 1 word for each word in each of the 3 formats (64 words for format 1 and 96 words each for formats 4 and 5).

Science Data Collection

Science data were collected by two methods:

(1) Time sharing with engineering data on the previously described analog or Da channels, with most of the time-shared science data on Da 2 UAMS and Da 3 RPA

(2) Dedicating the data collection to a science instrument on a Db channel where each Db channel consisted of a data message that was formatted by the instrument and each instrument included sync and identification in the format

There were nine Db channels with one for each landed-science instrument and one each for the surface sampler and the GCSC memory data. The data source provided a data-ready signal to indicate that a fully formatted digital message was available for transfer. The data-ready signal remained high until the complete message was transferred. When the data-ready signal was high, the GCSC commanded the DAPU into a mode to service that Db channel; when the data-ready signal was low, the DAPU reverted to standby. The imaging and GCSC channels did not have data-ready signals and the DAPU continued in the commanded mode until the GCSC issued a new command or the DAPU reverted to standby because of cycling of power or a full DSM.

Data Storage

The VLC telemetry and data handling subsystem included two storage devices: the DSM and the TR. The DSM was a 8192-word by 24-bit plated-wire memory and the TR was a four-channel serial digital recorder with a 10 million bit storage capability on each channel. The normal data storage strategy was to store post-landed science and engineering data in the DSM. When the DSM was nearly filled, its contents were dumped on the TR. Imaging, GCMS mass scan, and entry data were stored on the TR directly because of the large amount of data. The telemetry subsystem was designed so that no single failure caused the loss of both the DSM and the TR. If the DSM was lost, all data could be stored in the TR but with interrecord gaps approximately equal to 1 sec at the recording bit rate. These interrecord gaps made recording of short messages extremely inefficient. The loss of the TR required a drastic reduction in mission data storage because a maximum of 196 000 bits of data could be stored between transmissions.

Data Storage Memory

All interfaces with the DSM were through the DAPU as shown in figure 87. The DAPU provided raw power to the DSM plus an operate mode enable signal. The DSM was powered through a DPDT magnetic latching relay controlled in a manner

to minimize relay switching cycles by switching the relay only when a GCSC command was different from the previous command. The operate mode enable signal was provided by the DAPU main power supply so that the DSM was off when the DAPU was in standby although the relay was providing raw power to the DSM. When the DAPU was commanded into a DSM mode, the DAPU recovered the 13-bit address stored in word 0 of the DSM as soon as the DSM ready line was high. Data were transferred between the DAPU and DSM as follows:

Read cycle: The DAPU read the contents of the DSM in consecutive order, starting with word 1 until commanded by the GCSC to terminate that mode of operation. Upon termination, address 1 was written into word 0 of the DSM.

Write cycle: The DAPU wrote data into the DSM into consecutive words, starting with the address recovered from word 0 of the DSM. The write operation continued until the data-ready signal became low, one frame of format 4 had been stored, address 8191 had been written into memory, or the GCSC commanded mode termination. Upon completion of a write mode, the address was incremented by one and written into word 0. If word 7936 was reached during the write cycle a transfer request was issued to the GCSC upon the completion of that mode. The transfer request notified the GCSC that the DSM might not have sufficient storage remaining for the next message and it must be read, normally, into the TR.

Write-read cycle: The DAPU wrote word 1, incremented the address by one and read word 2, then wrote word 2 in a continuing sequence until word 5000 was reached. The sequence then reset to read word 1, write into word 1, and repeat the cycle. This sequence was used to temporarily store 120 000 bits for a 1-min delay of data transmission during entry format 2.

Tape Recorder

All TR interfaces were controlled by the DAPU with the exception of the input power from the PCDA. When a record command was received by the DAPU, the control lines to the recorder assumed the commanded states. When the TR issued a ready signal, data were shifted into the TR. Operation continued until a new mode command was received or a TES was received wherein the recorder transferred to a standby mode and the DAPU informed the GCSC of this status. When a tape reproduce mode was commanded, the control lines to the TR assumed the commanded states. The DAPU began data transmission immediately. Operation continued until a new mode command was received or a TES was received wherein the TR went to a standby mode, the DAPU informed the GCSC of this status. When the DAPU was in the cruise mode and power was applied to the TR, the TR maintenance mode was initiated by the TR logic supply going high. The purpose of the tape maintenance mode was to move the tape during launch vibration and periodically during cruise. During the maintenance mode the TR was commanded into a reproduce mode at 1000 ± 100 bps. The initial direction was forward. The direction was reversed each time a cruise enable occurred while the TR logic supply was high and the TR ready line was low. This reversed the tape direction when either end of the tape was reached.

Data were transmitted from the VL on a UHF link to the VO for relay to Earth and on an S-band link for direct transmission to Earth. In addition, while the VLC was mated with the VO, the data were hard wired to the VO for transmission to Earth. The DAPU provided data at a rate of 4000 bps or 16 000 bps to the UHF transmitter for data transmission to the VO. All data were alternate-bit-complemented so that long strings of 1's or 0's that were probable in some modes of operation were changed into an alternating 1-0 code at the UHF interface to minimize bit synchronization ambiguity. After alternate-bit-complementing, the data were split-phase-modulated. Format 5 data were generated at a maximum rate of 4000 bps. Since it was impractical to interrupt a 16 000-bps UHF transmission with a 4000-bps transmission, a quasi 16 000-bps mode (RT-3) was generated in which each data bit was repeated four times following synchronization, identification, and 32 don't care bits. The DAPU provided preseparation data to the VO on hard lines through block redundant MOSFET gates. The preseparation interface provided alternate-bit-complemented data to the VO at 1000 or 2000 bps. The DAPU provided two cross-wired redundant subcarrier outputs to the S-band modulator as shown in figure 87. Subcarrier A data were generated at a rate of 250, 500, or 1000 bps and block-coded into a Reed-Mueller 32:6 bi-orthoganal code with comma freedom. The block-coded data at a rate of 1333 1/3, 2666 2/3, or 5333 1/3 symbols/sec biphase modulated a 72-kHz subcarrier generated from the 576-kHz GCSC clock. Subcarrier B was modulated by format 5 real-time data generated at a rate of 8 1/3 bps. These data biphase modulated a 12-kHz subcarrier generated from the 576-kHz GCSC clock. When operating in the ranging mode, only subcarrier B operated. The DAPU provided cruise data to the VO on nonredundant hard lines. The VO provided continuous shift pulses at a rate of 20 kHz or less and enable pulses that were 7 shift pulses wide at a repetition rate of 100 PPS or less. The DAPU responded to each enable with 7 bits of data.

Science Subsystem

Entry Science

The overall objective of the entry-science investigations was to define the physical and chemical state of the Martian atmosphere and its interaction with the solar wind. In the upper atmosphere, the composition and abundance of neutral species were determined by the UAMS. The ion concentration and ion and electron energy distributions were determined by the RPA. In the lower atmosphere, pressure, temperature, density, and mean molecular weight were determined by pressure and temperature measurements together with data from the VL guidance system. The location of the entry-science instruments is depicted in figure 88.

Upper atmosphere mass spectrometer.- The UAMS was used to determine the neutral components in the upper atmosphere of Mars and the variations in their relative abundances as a function of altitude.

The UAMS was mounted on the V S/C aeroshell and was operated during the descent phase of the mission. The instrument sealing cap was severed after the
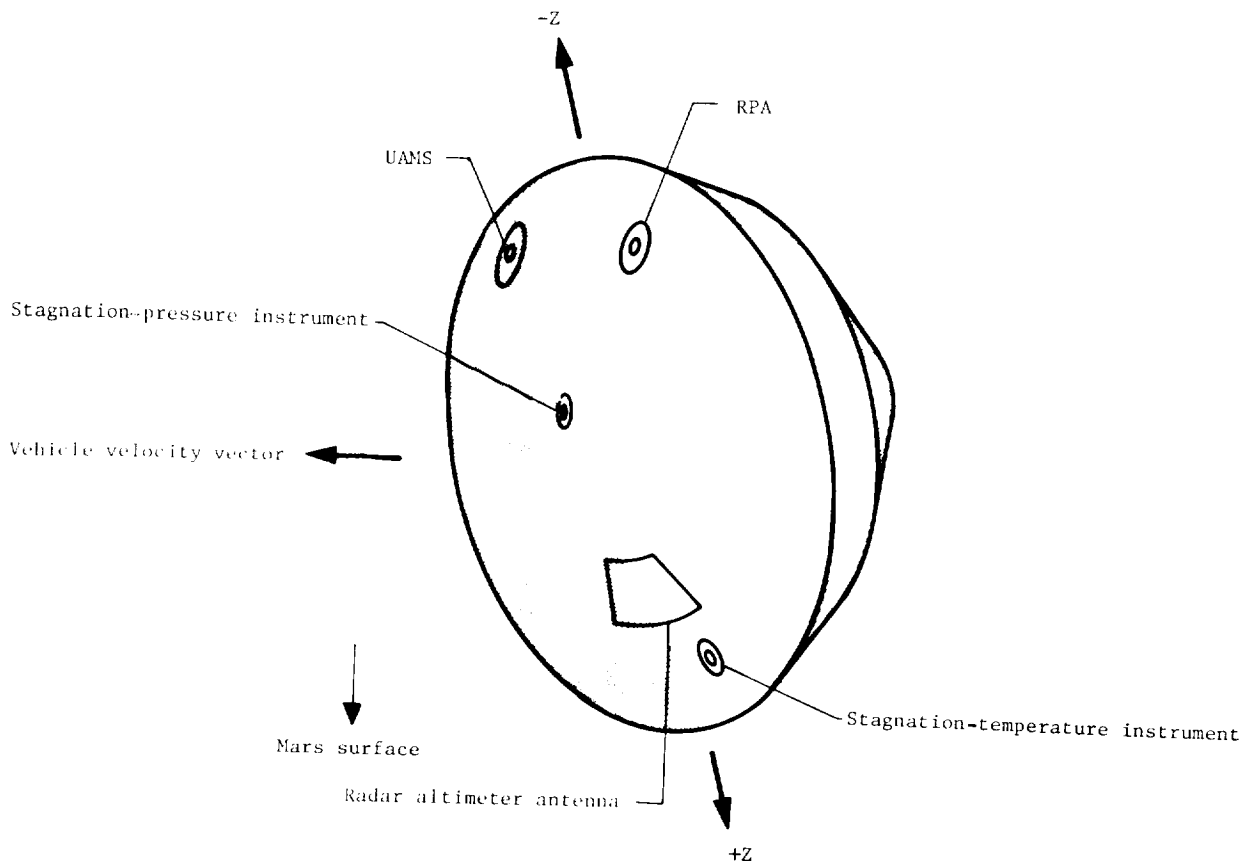
154

Figure 88.- Location of entry-science instruments.

termination of deorbit burn. Data gathering on a continuous basis was initiated at Entry - 40 min (approximately 5000-km altitude) and terminated at sensing 0.05g + 7 sec (approximately 100-km altitude). The UAMS scanned through the mass range from ≈0.9 to ≈50 m/e every 5 sec.

The UAMS consisted of three major functional assemblies: sensor assembly, electronics assembly, and the cutter assembly. The sensor assembly was a double-focusing mass spectrometer of the Mattauch-Herzog geometry with a semi-open ion source and two Faraday cup ion collectors. The basic geometry is shown in figure 89. Once the sealing cap had been cut off, the ion source was exposed at the front of the aeroshell and neutral particles in the Mars atmosphere entered the ion source (ion box). Electrons were prevented from entering the source by the potential on the electron repeller grid, and ions were prevented from entering the source by the potential on the ion box. A narrow beam of electrons passed through the ion source in front of the ion exit slit and this electron beam ionized a small fraction of the neutral particles in the ion source. The potential gradients in the ion source were such that the ions formed in the electron beam were drawn through the ion exit slit and then accelerated into the analyzer section of the sensor by the potential difference between the ion box and the grounded object slit plate. Ion transmission through the object slit was optimized by the voltage trimming on the J-plates

155
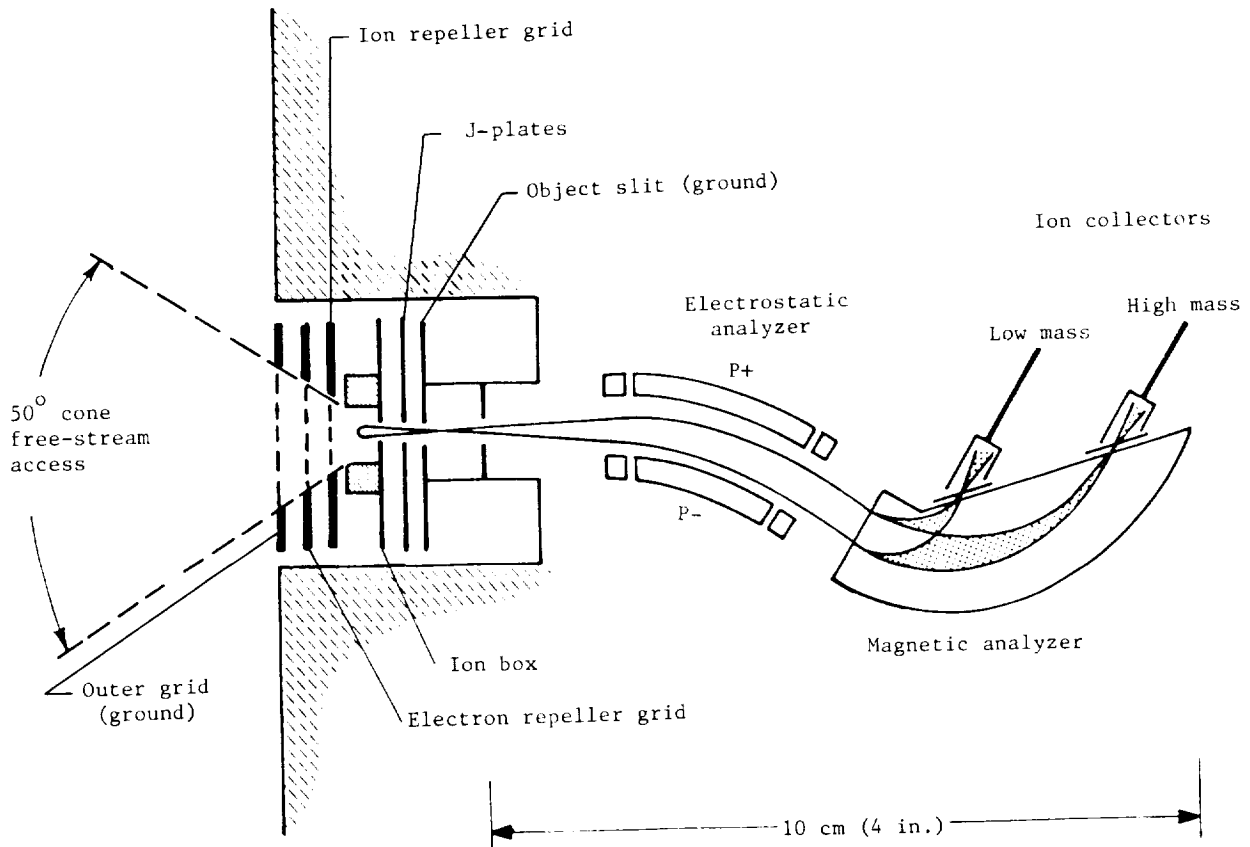
Figure 89.- Ion source and analyzer section.

which were used to focus the ions and obtain optimum ion transmission through the analyzer. The electronics assembly consisted of three major functional elements: data acquisition, data processing, and power conversion. These functional elements provided the power conditioning and distribution necessary to operate the UAMS functions and the data manipulation required to transfer the output data. The cutter assembly had the task of cutting the sealing cap which vacuum sealed the sensor. In order to prevent contamination of the sensor and also allow the filaments to be powered-up for testing in the Earth environment, the sensor internal pressure was kept in the pressure range of 10^{-9} to 10^{-5} torr (1 torr = 133.3 Pa). This pressure was maintained by periodic use of an ion pump.

Retarding potential analyzer.- The RPA was used to measure the concentrations and energy distributions of ions and electrons in the Mars upper atmosphere. The measurements made during the descent of the V S/C determined ionic species and ion concentration profiles as a function of altitude, ion and electron temperature profiles as a function of altitude, and the characteristics of the interaction of the solar wind and the Mars atmosphere.

The RPA operated from shortly after the termination of the deorbit burn until 7 sec after the sensing of 0.05g, at which time power was permanently removed from the instrument. During the deorbit coast period, data were

156

gathered on a periodic basis (every 10 percent altitude change or less) and transmitted to the VO. At Entry - 40 min, data gathering became continuous; all data gathered between Entry - 6 min and power removal were stored on the VL tape recorder as well as being transmitted in real time.

The RPA consisted of two functional assemblies, both mounted in the same housing. These assemblies were the sensor assembly and the electronics assembly. The sensor assembly was composed of seven wire grids. (See fig. 90.) As the voltages on the grids were swept through a range of positive and negative
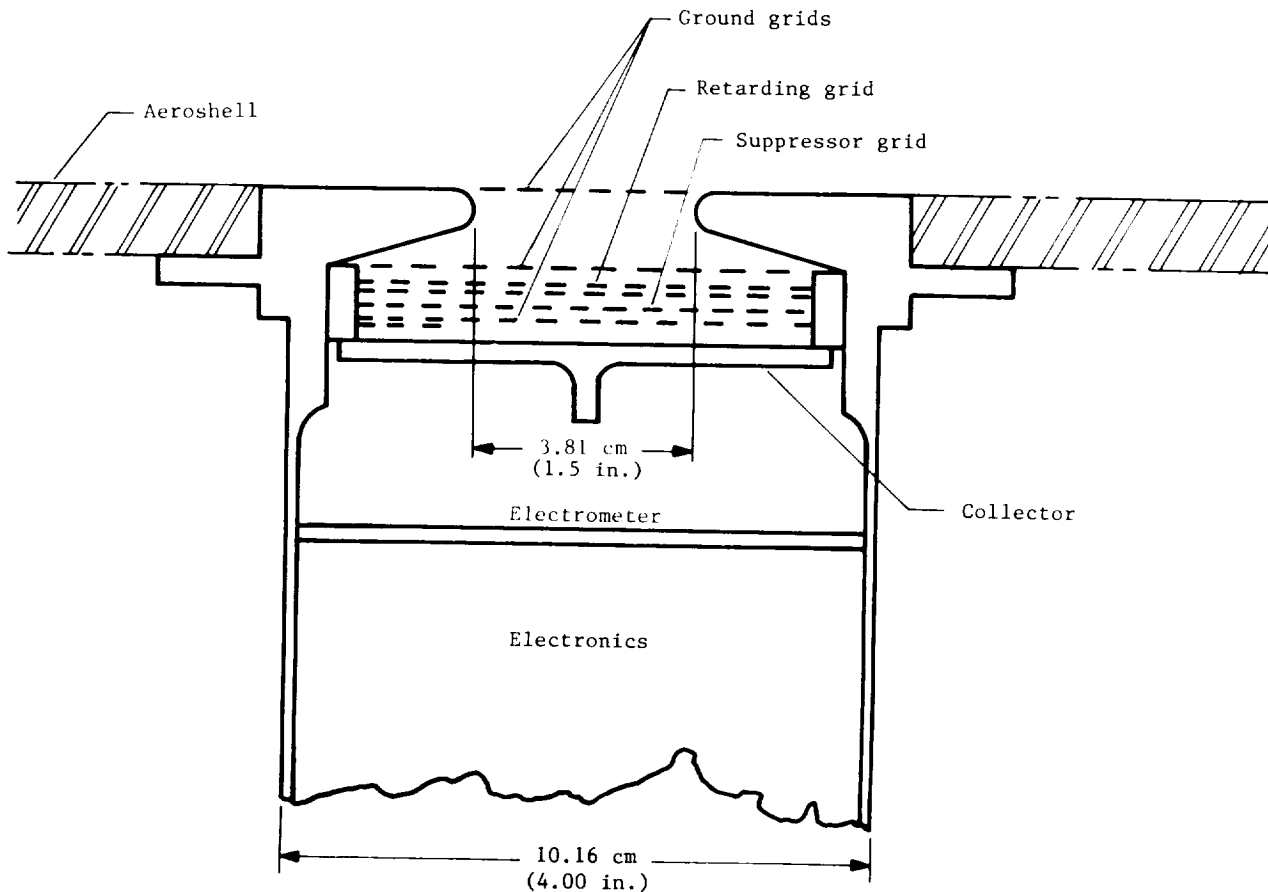
Figure 90.- RPA sensor assembly.

potentials, varying portions of the population of the ions and electrons in the Mars atmosphere penetrated the grid structure. Those charged particles which traversed all seven grids were collected by a "collector." This produced a current which flowed into an electrometer that provided amplification. In essence, the seven grids acted as an electrical filter, which admitted only those particles possessing selected ranges of energies and electrical charge. The electronics assembly consisted of three major functional elements: data acquisition, data processing, and power conversion. These functional elements provided the power conditioning and distribution necessary to operate the RPA functions and the data manipulation required to transfer the output data to the lander system.

<u>Stagnation-pressure instrument</u>.- The stagnation-pressure instrument was used to provide data from which the vertical pressure profile of the Martian atmosphere could be determined from as high an altitude as possible down to the point of aeroshell separation (an altitude of approximately 5.5 km (18 000 ft)).

The instrument was mounted on the inside of the aeroshell with a sampling port on the front of the aeroshell at the stagnation point at the trim angle of attack. Due to the high velocity of the VLC during this phase of the mission, the stagnation pressure was significantly higher than the ambient pressure; therefore, VLC velocity and orientation data were required to correct the instrument measurements.

The input pressure in the stagnation-pressure transducer acted on one side of a thin stretched diaphragm. The other side of the diaphragm was referenced to a hard vacuum chamber. In this chamber there was a capacitance electrode parallel to the diaphragm. At zero absolute pressure, the diaphragm was flat and the sensor capacitance was minimum. The tension of the diaphragm was set so that under full-scale pressure, the capacitance doubled. At twice full-scale pressure, the diaphragm contacted the backplate; thus, an overpressure stop was provided. A cross section of the sensor subassembly is shown in figure 91.
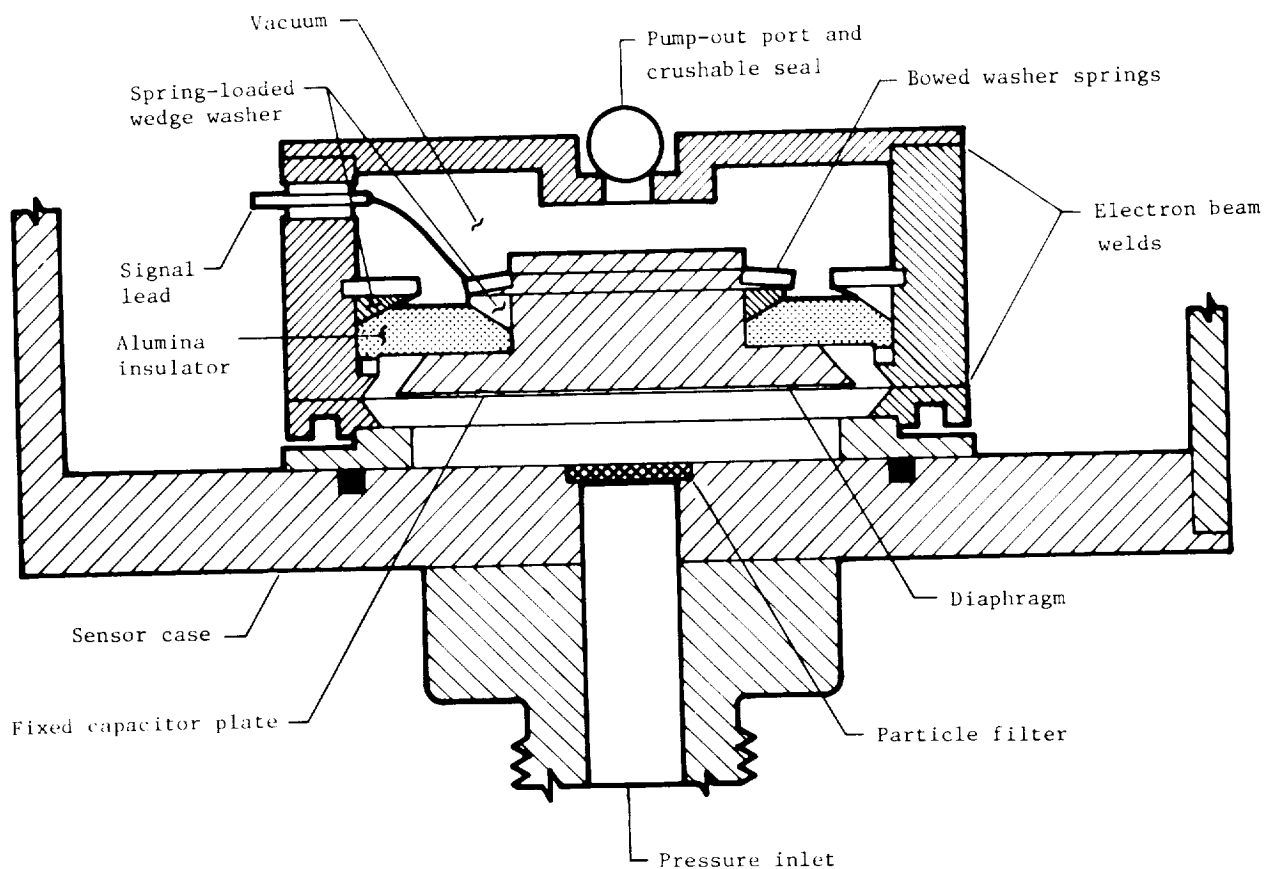
Figure 91.- Stagnation-pressure instrument sensor subassembly.

Ambient-pressure instrument.- The ambient-pressure instrument was used to provide data from which the vertical pressure profile of the Martian atmosphere could be determined during the parachute and terminal phases of descent to the Martian surface. In addition, it was used to measure atmospheric pressure during the postlanded portion of the mission.

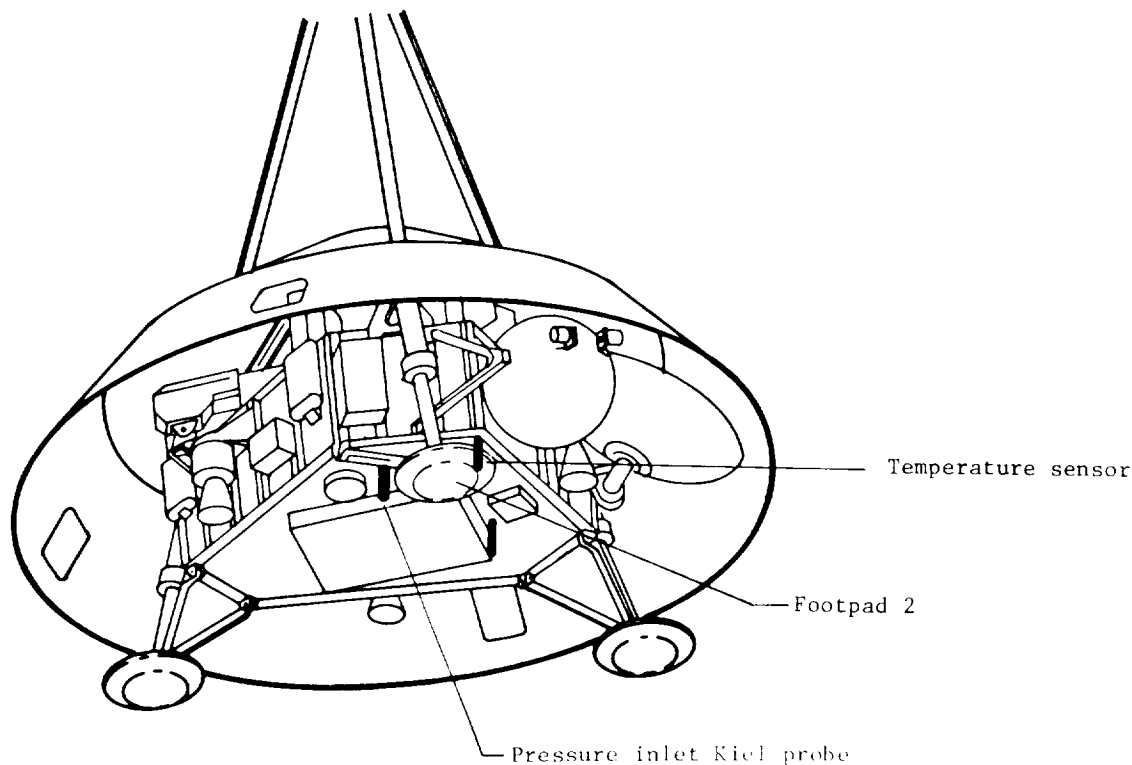The ambient-pressure instrument which was located inside the equipment compartment and the inlet on the VLC are both shown in figure 92. The instrument

Figure 92.- Ambient-pressure instrument inlet.

was designed to measure ambient pressure over the range of 0 to 1.79 kPa (0 to 18 millibars) and was attached to a Kiel probe near footpad 2.

The instrument was the same as the low-range engineering pressure sensors except for more extensive screening. It was a variable reluctance type with all signal conditioning and power circuitry contained within the sensor case. The variable element in the sensor was a thin metal diaphragm positioned between two magnetic inductance coils. The metal diaphragm separated a chamber connected to the external pressure port and a sealed reference chamber. Deflection of the diaphragm produced a decrease in the magnetic flux of one coil while simultaneously increasing the magnetic flux of the other coil. The output voltage was proportional to the ratio between the two inductances. The sensor required 24 to 37 V dc with 6 mA input and provided 4 V dc output for a full range of 1.79 kPa (18 millibars). The sensor was 12.7 cm in length, 3.8 cm in

diameter, and 5.08 cm in height (including the mounting feet) and weighed 454 g.
The sensor required a six-pin plug for its electrical connection and 0.06-mm
(1/4 in.) flared tubing for its pressure connection.

Temperature sensors.- The entry-science temperature sensors were used to
measure the vertical temperature profile of the Martian atmosphere over as large
an altitude range as possible.

Two instruments were employed to accomplish the required measurements.
One instrument, the stagnation-temperature instrument, was mounted on the aero-
shell and took measurements during the latter part of the ballistic entry. The
other instrument, the ambient-temperature instrument, was mounted on footpad 2
and took measurements after the aeroshell had been jettisoned and the landing
legs were deployed. The stagnation-temperature instrument was designed to mea-
sure temperatures over the range of 100 K to 750 K, with an accuracy of
± 3.5 K + 1 percent of reading. The ambient-temperature instrument was designed
to measure temperatures over the range of 100 K to 400 K, with an accuracy of
± 1.3 K + 2.1 percent of reading.

Both instruments were essentially similar in basic design concept, being
based upon multiple thermocouples. The major outputs were derived from the out-
put of three thermocouple elements in series. In order to provide redundancy
against breakage, each of the three thermocouples had two other thermocouples
in parallel with it. The electronics associated with each instrument were essen-
tially passive, being merely resistance bridge networks which used the 5 V dc
DAPU transducer excitation voltage as reference.

Landed Science

The primary emphasis of the Viking Mission was on gathering information
on biological, chemical, and environmental characteristics most relevant to the
search for extraterrestrial life. In addition, investigations of the interior,
surface, and meteorology of Mars were carried out. The general location of the
science instrumentation on the VL is shown in figure 93. The scientific goals
and the investigations performed by instrumentation of the VL are given in the
following table:

| Scientific goal	Investigation	Instrument
Visually examine landing site	Lander imaging	2 cameras
Search for evidence of life	Direct biology	3 metabolism and growth detectors
Determine atmospheric composition and its variations with time; search for and study organic compounds	Molecular analysis	GCMS
Determine elemental abundance	Inorganic chemical analyses	X-ray spectrometer
Determine temporal variations of pres- sure, temperature, and wind velocity	Meteorology	Pressure, temperature, and wind sensors
Determine seismological characteristics	Seismology	3-axis seismometer
Determine magnetic properties of surface	Magnetic properties	2 magnet arrays and magnifying mirror in conjunction with VL imaging system
Determine physical properties of surface	Physical properties	Surface sampler system in conjunction with VL imaging system

160
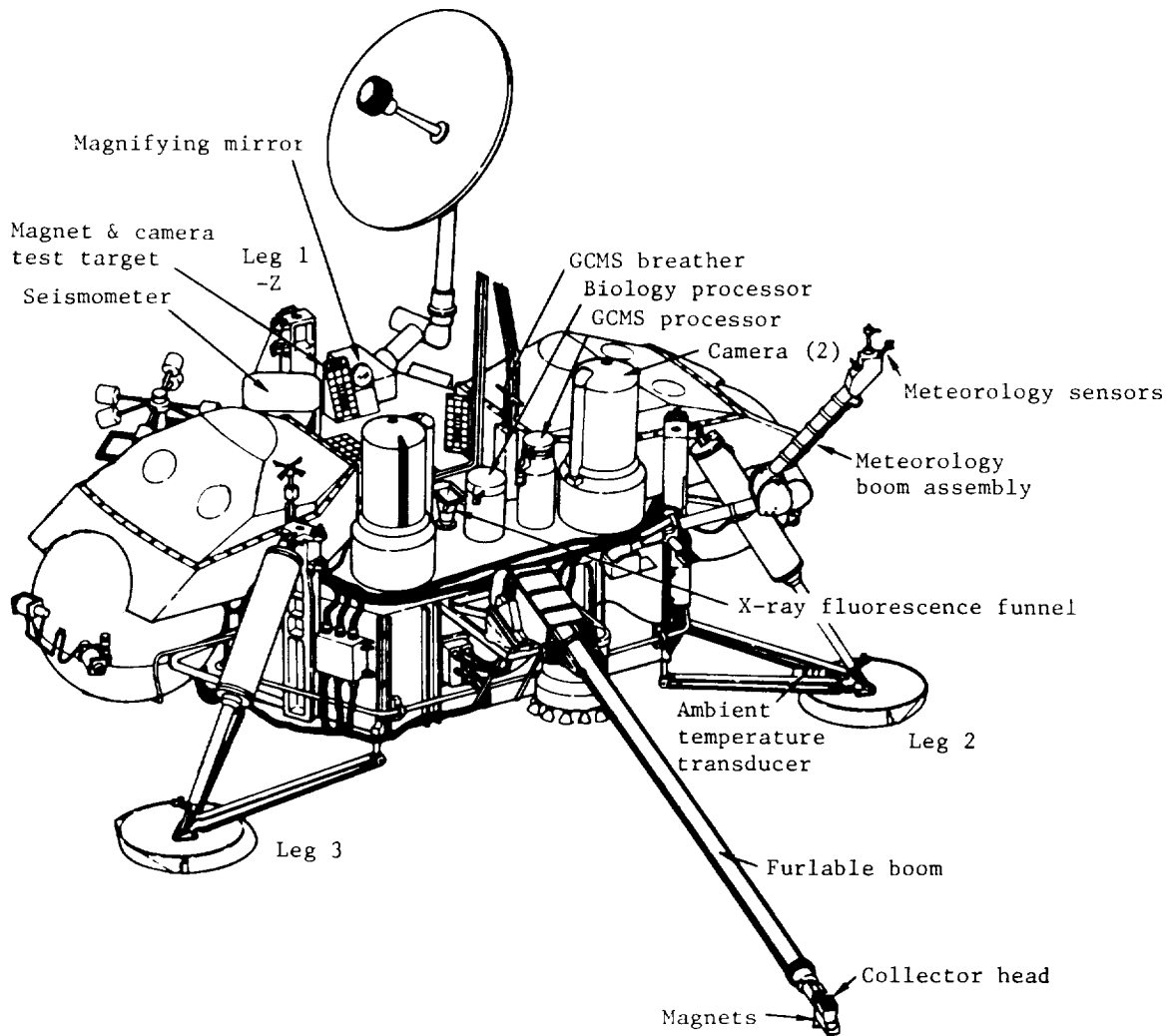
Figure 93.- VL instrument location.

Biology investigation.- The objective of the biology investigation was to measure for evidence or conversely lack of evidence for metabolism of microorganisms that were present in samples of the Martian surface.

The biology instrument provided a test chamber environment that was conducive to metabolism and/or growth of life forms. The instrument contained three complete biological experiments, each operating on a different principle, along with the electronics to operate them and to record their findings for transmission to Earth. These experiments were the gas exchange experiment, the labeled-release experiment, and the pyrolytic release experiment. The GEX experiment operated on a simple principle: living organisms alter their gaseous environment as they live, respire, eat, and reproduce. Gaseous changes could indicate that life processes were going on. In this experiment, a Mars surface sample inside a sealed cup was either humidified with water vapor or was partially sub-

merged in a complex aqueous nutrient medium. The general functioning of the
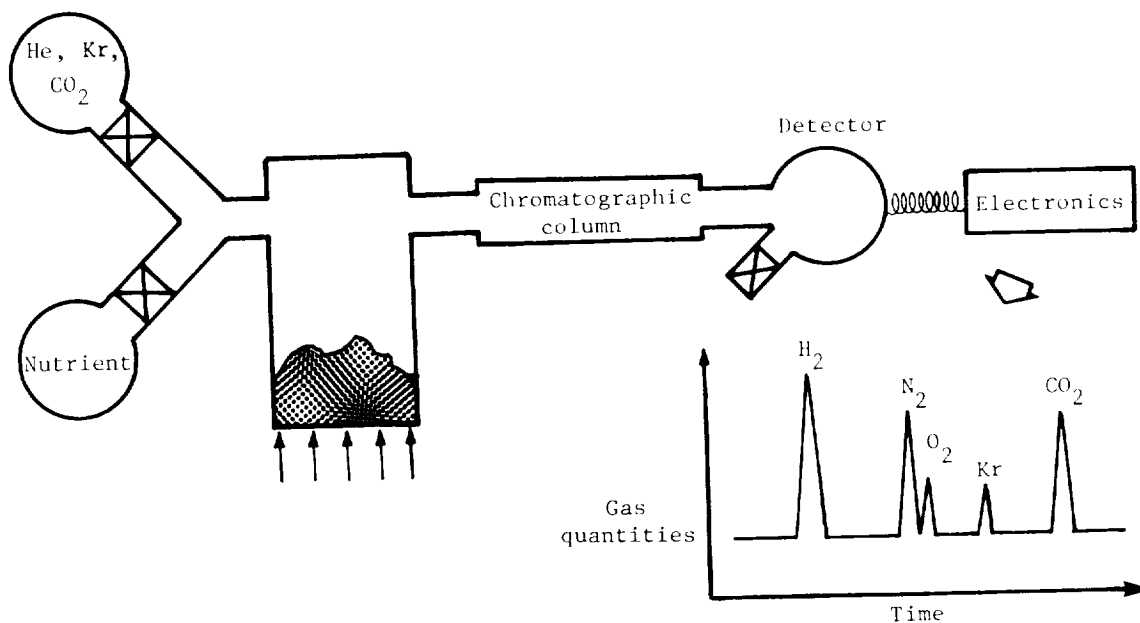GEX experiment is shown in figure 94.

Figure 94.- GEX experiment.

The LR experiment also searched for signs of metabolic activity in the Mars
surface sample. A sample of the Martian surface was loaded into a test cell,
barely moistened by a nutrient labeled with radioactive carbon-14, and allowed
to incubate at 8.3° C (47° F) for up to 11 days. If there were any microorgan-
isms which consumed the nutrient they would release gases that contained radio-
actively labeled wastes (carbon-14). The LR experiment detected any volatile
radioactive carbon products such as carbon-14 dioxide ($^{14}CO_2$), carbon-14 monox-
ide (^{14}CO) or methane ($^{14}CH_4$). The general functioning of the LR experiment
is shown in figure 95.

The PR experiment had a primary goal of detecting photosynthetic organisms
under normal, arid Martian conditions. The experiment detected the presence of
organisms capable of assimilating and forming organic material from $^{14}CO_2$ and
^{14}CO. A $1/4$-cm^3 surface sample was incubated in a test cell with a mixture of
$^{14}CO_2$ and ^{14}CO under simulated Martian sunlight for a period of 5 days. After
the removal of the incubation atmosphere, the surface sample was pyrolyzed by
heating to 625° C. During this process, the unincorporated $^{14}CO_2/^{14}CO$ gas
released from the sample was passed through an OVT, collected at a radiation
detector, and counted as the first peak. The heavier organic molecules iden-
tified with organisms were collected in the OVT. After the collection of the
first peak, this organic material was eluted from the OVT by heating to 650° C,
collected in the detector, and counted as the second peak. The general func-
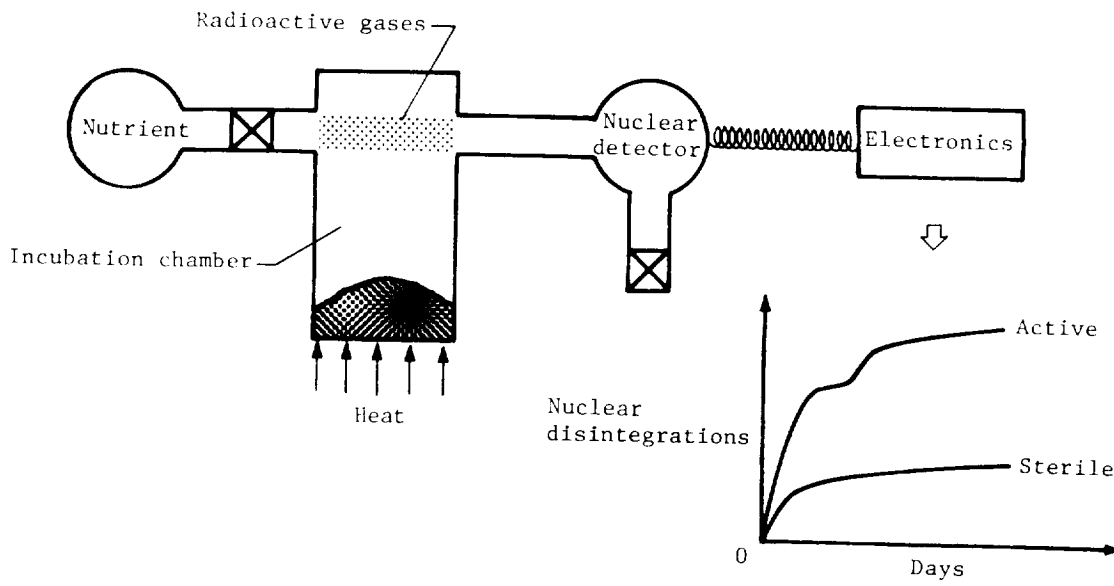tioning of the PR experiment is shown in figure 96.
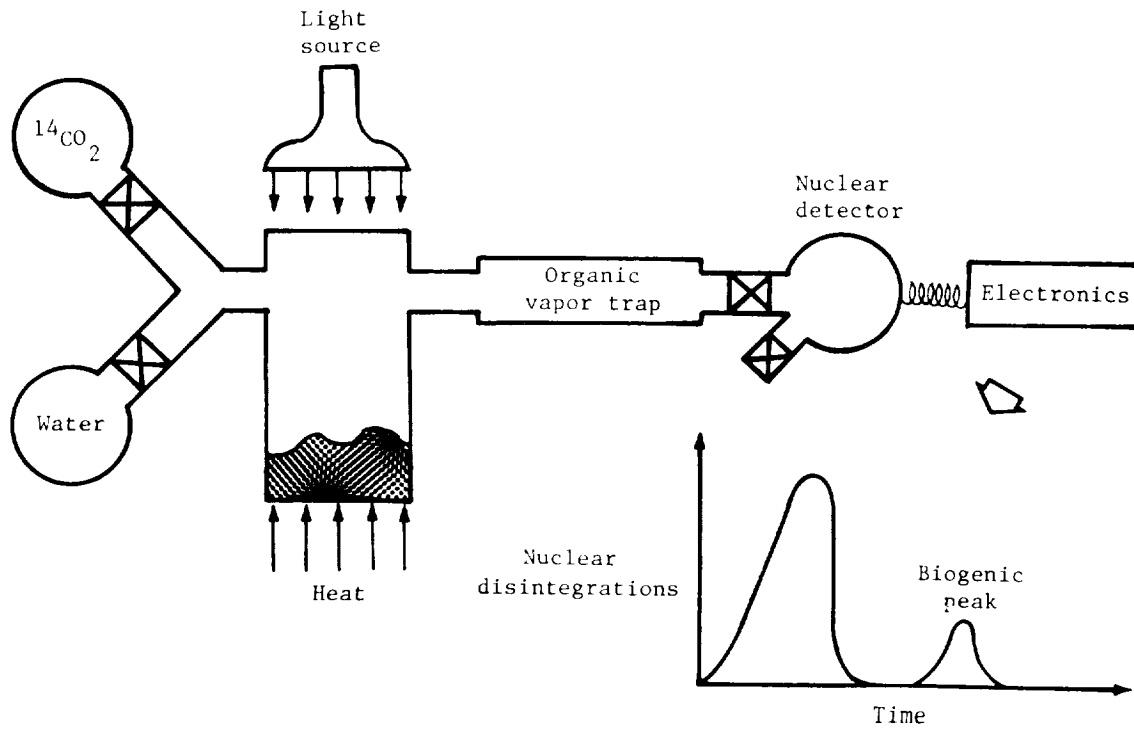
Figure 95.- LR experiment.

Figure 96.- PR experiment.

An initial understanding of the VBI may be gained in a broad sense from examination of the VBI operational system block diagram shown in figure 97.
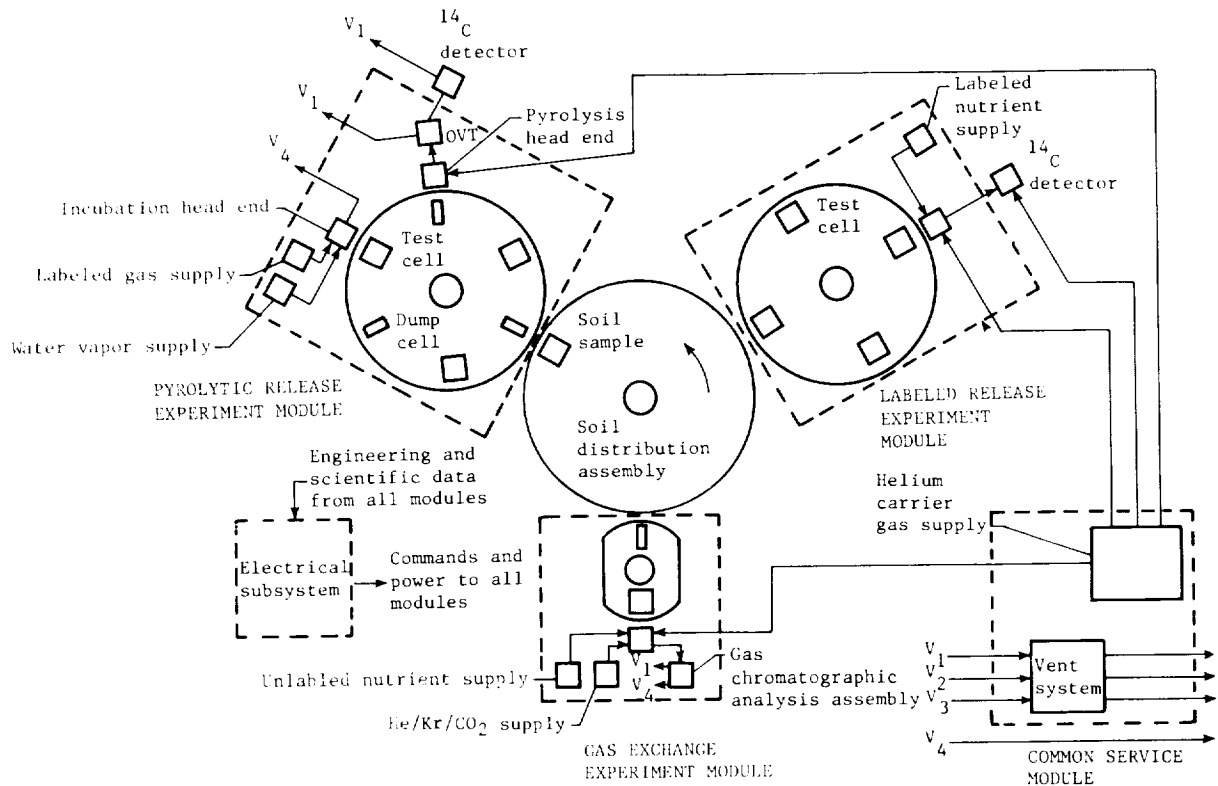

Figure 97.- Operational block diagram of VBI system.

Operationally, the VBI functioned through its interface for commands and power from the VL while providing both engineering and scientific data to the VL for transmission to Earth. This interface was carried out within the VBI in the electrical subsystem. The other significant operational interface between the VBI and the VL provided for a supply of Martian surface sample to the VBI from the VL SSCA. This interface was implemented in the VBI soil distribution assembly for distribution to the three experiment modules. Internal functions of the VBI were performed through a complex system of pneumatics which provided for the use of pressurized helium as a working medium, storage of certain nutrients for biological experiment functions, and a waste management system which insured removal of spent fluids and gases from the working areas. Brief descriptions of the three experiment modules are given in the following paragraphs.

The GEX module consisted primarily of two cells (one for receiving surface samples for analysis and one for receiving surplus surface sample), a head-end assembly for incubation, a nutrient reservoir containing the liquid nutrient

164

supply, another reservoir for the incubation and internal standard gas, a gas sample valve assembly for metering and injecting a sample of head-space gas into the chromatograph column, the duplex chromatographic column assembly consisting of matched active and reference columns, and a duplex thermal conductivity detector for measuring the separate gas components as they emerged from the active and reference columns. Also part of the GEX system was a reservoir of $He/CO_2/O_2$ gas which was used to precondition the active column prior to the experimental sequences.

The LR module consisted primarily of four test cells for receiving surface samples, a head-end assembly for maintaining the environment for incubation of organisms in the surface sample and injecting the nutrient into the test cell, a detector for measuring the results of incubation, and a supply of labeled nutrient for injection into the surface sample.

The PR module consisted primarily of test and dump cells and two head-end assemblies, one for incubating the surface samples and one for pyrolyzing them. A water vapor supply, a labeled gas supply, and a lamp were ancillary to the incubation head end while an organic vapor trap and ^{14}C detector assembly provided the equipment needed for the pyrolysis, elution, and measurement functions of the experiment. The surface sample was loaded into the cells from an SDA, and helium gas was provided by the CSM.

Gas chromatograph mass spectrometer.- The GCMS performed atmospheric and organic analyses on the Martian surface. The primary purpose of the atmospheric analysis was the identification of constituents of the Martian atmosphere and the determination of their abundances, including possible variations, that were not detectable with remote optical spectroscopy. The purpose of the organic analysis investigation was to analyze samples of the Martian surface and subsurface for its organic content through gas chromatographic and mass spectral methods. The molecular analysis system was capable of analyzing compounds which constituted between 0.1 ppm and 2500 ppm by weight of the samples.

An initial understanding of the GCMS functions can be obtained by referring to figures 98 and 99. One of the two prime functions of the GCMS was to analyze the Martian atmosphere. The instrument first acquired an atmospheric sample by opening an atmospheric inlet valve (V9) for some finite period of time and allowing the Martian atmosphere to equilibrate in the GCMS AFA equilibration volume, after which an atmospheric analysis would be commanded. CO/CO_2 filtration was commanded prior to initiation of the atmospheric analysis to permit investigation of minor constituents in the Martian atmosphere. The other prime function of the GCMS was to perform molecular analyses of Martian surface samples. Finely ground samples of Martian surface material were delivered to the GCMS by the PDA which was affixed to the GCMS LPA. Upon command, the LPA was sequenced to load a portion of the sample into one of three ovens contained within the LPA. During an organic analysis, a selected sample oven was heated to drive off organic vapors contained in the sample within the oven. The vapors were injected into the gas chromatographic column in the GCA. During the remainder of the organic analysis, molecular compounds which had been injected into the column were separated and carried to the mass spectrometer where mass spectra were generated.
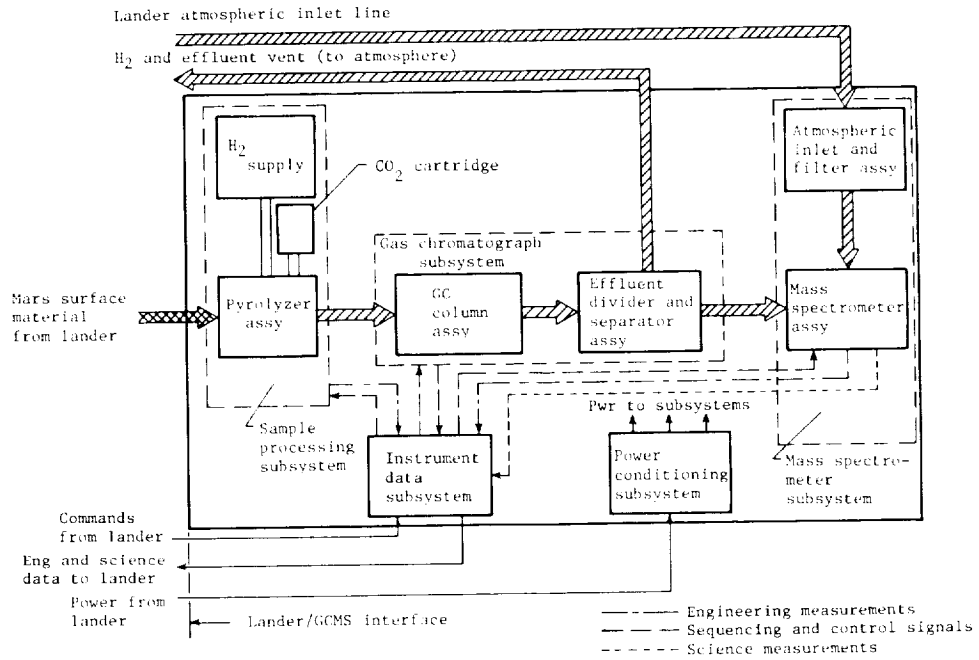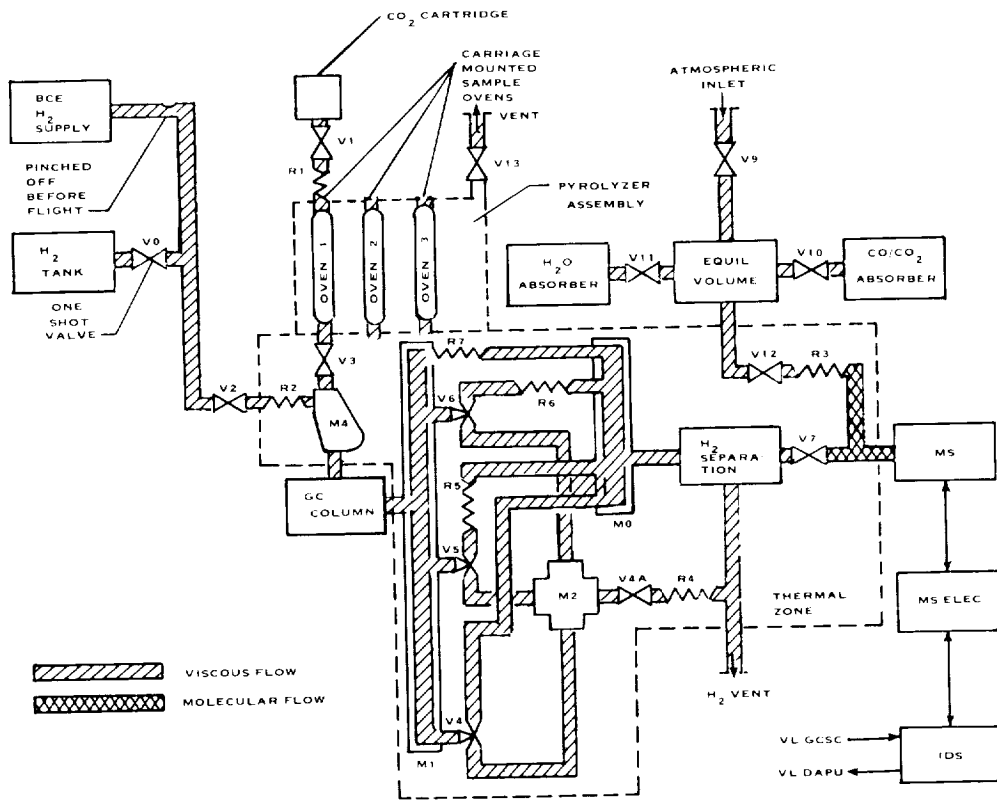
Figure 98.- Block diagram of GCMS instruments.

Figure 99.- Block diagram of GCMS gas flow.

The GCMS consisted of two major assemblies: the sensor subset and the instrument data system assembly. The sensor subset contained five subassemblies: hydrogen supply assembly, loading and pyrolyzing assembly, gas chromatograph assembly, atmospheric filter assembly, and mass spectrometer assembly. The HSA consisted of a hydrogen tank containing H_2 at a pressure of approximately 5.2 MPa (750 psig), a one-shot valve (V0), a pressure transducer, and two high-pressure valves (V1 and V2). Associated with the HSA was the CO_2 cartridge which provided pressurant for a pyrolyzed sample. After pyrolysis, the hydrogen carrier gas was provided through valve V2. The one-shot valve contained the hydrogen within the tank until such time as carrier gas was required. The LPA received a portion of a surface sample from the integrated PDA. The LPA then loaded the sample into one of three ovens in response to command and control by the IDS and IEA. During an organic analysis, the sample oven was heated to one of four selectable temperatures in order to drive off the organic compounds within the sample. The GCA served to control and separate the flow of the vapor products of the sample of interest as they travel from the pyrolysis oven to the mass spectrometer. The GCA was made up of the GC column and a heated assembly (thermal zone) which contained valves and restrictors (effluent divider) and a hydrogen separator. The AFA consisted of an atmospheric inlet valve (V9), an equilibration volume (approximately 10 cm^3), a CO/CO_2 filtration chamber and valve (V10), and an H_2O absorber chamber and valve (V11). An atmospheric sample was admitted to the GCMS through V9 and allowed to equilibrate in the storage chamber. It was then analyzed by the mass spectrometer either before or after filtration. The MSA was the assembly wherein analysis took place and mass spectra were generated. During an atmospheric or organic analysis, the sample of interest entered the ionizing chamber of the mass spectrometer ion source. The ions, which were produced in the electron beam column, were extracted from the ionizing region by an electric field and were focused on the exit aperture of the ion source, that is, the object slit. The electric sector focused the ions in energy along its image plane. This plane became the object plane for the magnetic sector. Ions from the magnetic sector object plane were focused to second order in angle at the magnetic sector image plane. As the scan voltage was continuously decreased, ions of increasing mass were swept across the resolving slit and a mass spectrum was generated, which was characteristic of the gas in the ion source. The ion currents through the resolving slit were amplified by an electron multiplier to increase the currents to a level suitable for an electrometer amplifier. The electrometer amplifier amplified the current output from the electron mulitplier and converted it to a voltage signal. The IDA received commands from the VL GCSC, initiated and controlled GCMS sequences in response to commands, and digitized both engineering and mass spectral data and transmitted these data to the VL data acquisition system.

Lander camera system.- Each lander had two identical LCS's which were used to geologically characterize the Martian landscape, to look for macroscopic evidence of life, to support surface sample acquisition, to support the magnetic properties and physical properties investigations, and for atmospheric characterization.

Figure 100 presents a view of the VL. The two cameras were separated by 0.8 m and viewed the surrounding terrain from a nominal height of 1.3 m. The primary function of the cameras was to visually examine the characteristics of
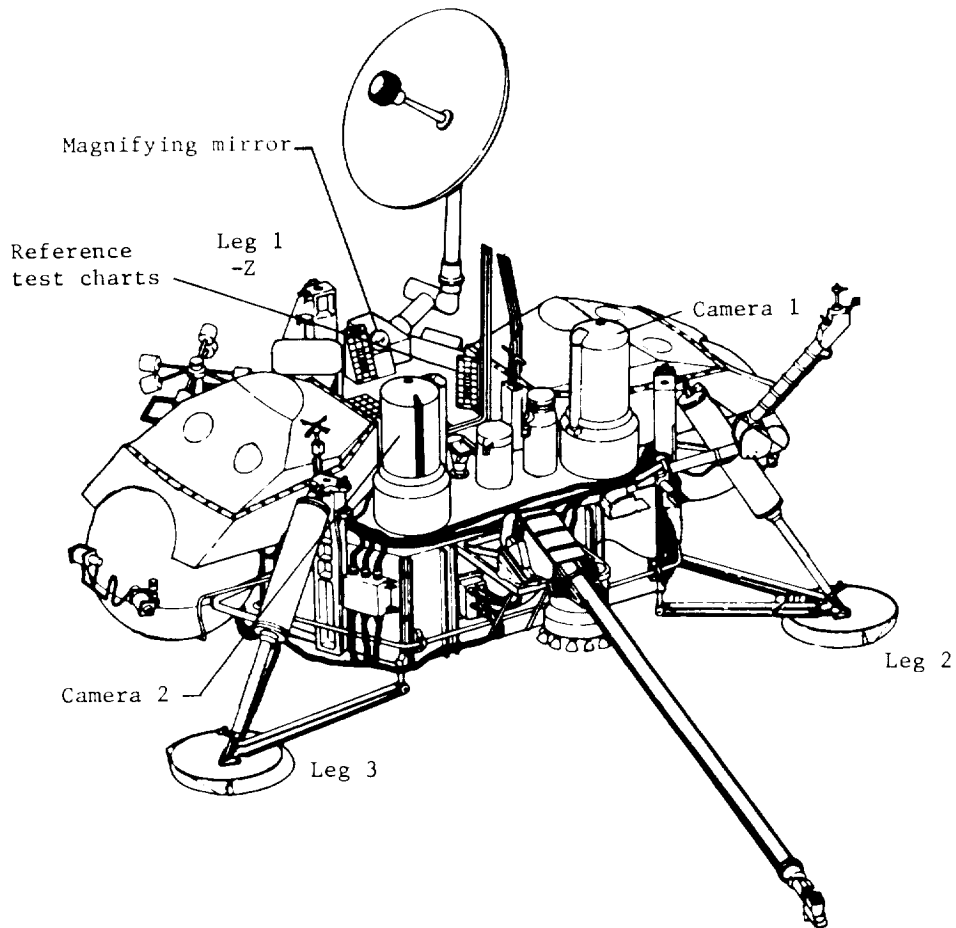
Figure 100.- Lander camera locations.

the landing site. In addition to the visual examination of the surface features, the cameras were able to measure the optical density of the atmosphere. The primary support function of the cameras was to obtain stereo imaging of the surface sampler area. An important constraint on VL orientation was to avoid shadowing the surface sampler area at favorable Sun elevations. A general goal was to obtain morning and afternoon lighting of the sampler area, first from one direction and then from the other, to insure that all features in this area could be viewed at one time or another out of shadow. A roll maneuver, that is, a rotation about an axis parallel to the camera major axis, was executed during the final VL descent phase to achieve this function.

Figure 101 presents a simplified cutaway view of the camera. The upper elevation assembly rotated in azimuth during operation, and the lower azimuth assembly was bolted to the VL. The thin camera housing and the major support structure were made of beryllium to provide lightness, stiffness, and low thermal expansion and contraction. The inner surfaces of the housing were treated with a matte black finish to reduce internal light reflections, and the outer matting surfaces were gold plated to suppress electromagnetic interference.
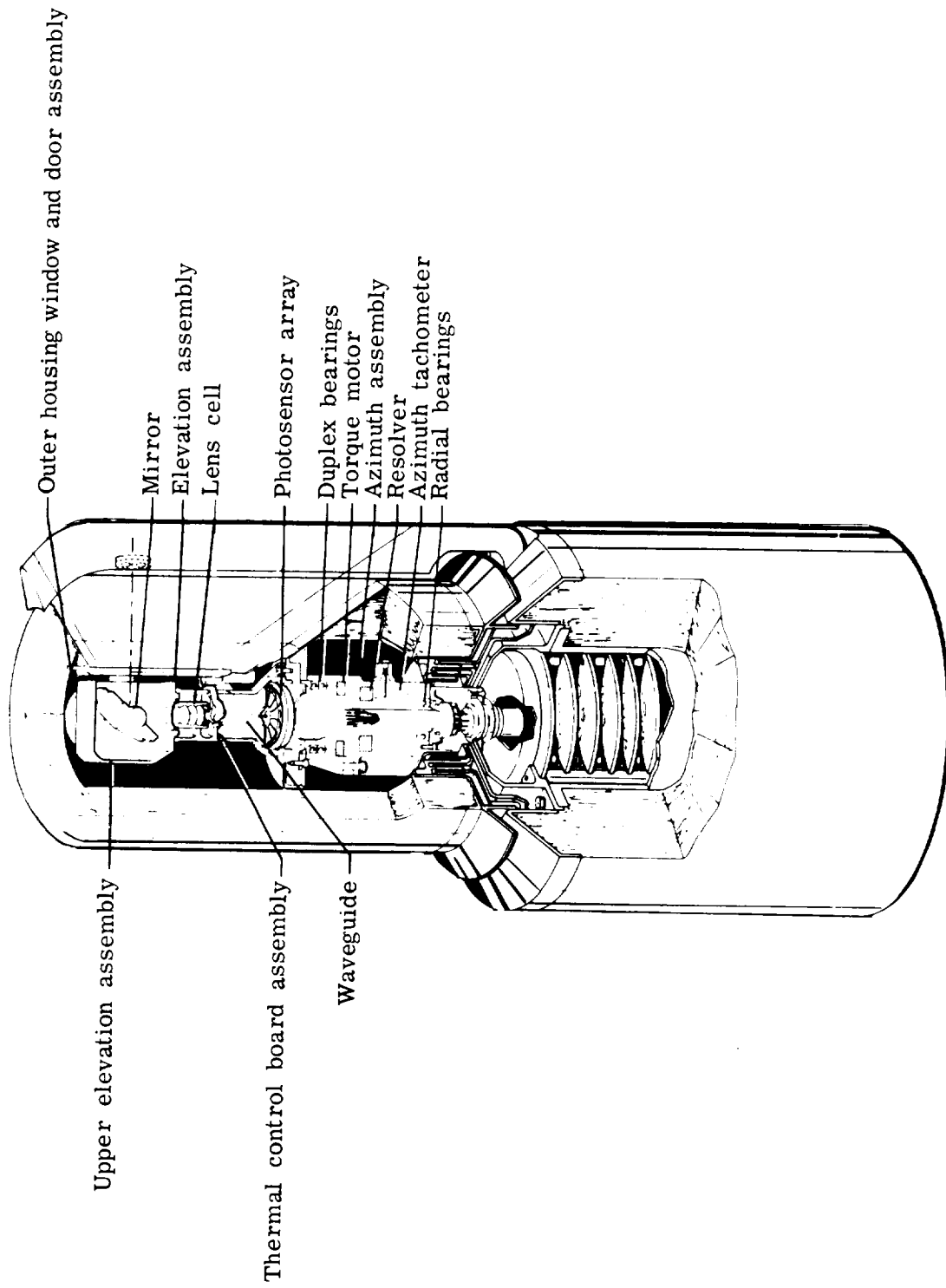
168

Outer housing window and door assembly

Mirror
Elevation assembly
Lens cell

Photosensor array

Duplex bearings
Torque motor
Azimuth assembly
Resolver
Azimuth tachometer
Radial bearings

Upper elevation assembly

Thermal control board assembly

Waveguide

Figure 101.- Simplified cutaway view of Viking lander camera.

169

A 3- to 5-cm-thick blanket of fiberglass and aluminum foil insulated the entire camera to reduce radiative and convective transfer to the cold Martian atmosphere. In addition, thermostatically controlled heaters were located in the vicinity of critical components to maintain their temperature above -40° C. The elevation assembly was hermetically sealed and filled with argon gas at a pressure of nearly 10^5 Pa (1 bar). The azimuth assembly was exposed to the Martian atmosphere. Dust was prevented from entering by a labyrinth seal between the rotating and stationary parts of the camera. The camera had two windows. The outer window, referred to as the contamination cover, was hinged on one side and spring loaded. By rotating the camera nearly 360° in a rapid slew mode, a lever could be forced against the side of the dust post with sufficient impact to release a catch on the contamination cover which then permitted a spring to move it out of the optical path. This cover protected the inner window from gaseous condensation during the VL heat sterilization process prior to flight and from dust contamination during operation on Mars. The narrow window entrance was usually stored behind a post to avoid unnecessary exposure to dust. The post contained two small tungsten filament light sources that permitted the camera performance to be checked when the VL was stored inside the aeroshell during the flight to Mars. CO_2 carried under pressure in a container inside the VL could be released on command through a tube (which was attached to the post) to blow dust off the window. Light which passed through the window was reflected by a mirror that nods up and down to provide the elevation scanning. Imaging data were acquired only during the relatively slow upward motion. Motion was controlled by a commutator-type dc torque motor. A tachometer provided servo damping, and a resolver provided position information. The resolver consisted of a dual unit: a coarse unit which provided low-resolution absolute position information over the complete rotation of the shaft for selecting the elevation field of view and a fine unit with a 36-times-higher angular sensitivity, which provided high-resolution relative position information for photogrammetric accuracy within the field of view. The light that was reflected by the nodding mirror was imaged by an achromatic triplet lens onto a photosensor array. The lens aperture diameter was 0.95 cm and the focal length was 5.37 cm. Light falling on the photosensor array was transduced into an electrical signal. Immediately below the lens was a dark reference shutter which consisted of a rotary solenoid that controlled a paddle-shaped black metal shutter. When energized, the solenoid shaft moved the shutter over the exit pupil of the lens to block external light from reaching the photosensor array. The design included a spring that forced the shutter to the open position in case of a failure of the solenoid or associated electronics. The dark reference shutter was closed for sampling the photosensor-preamplifier dark current which was stored for later subtraction from the signal current and for calibrating the photosensor array with a small tungsten filament lamp which was located below the shutter. The inner surface of the optical tunnel between lens and photosensor array contained a multiaperature baffle that was designed not only to reduce veiling glare but also to attenuate radio frequency interference from the VL antennas. The elevation assembly, which contained the camera elements described so far, tapered down to a narrow shaft below the photosensor array. All the cables that provided connections between the electrical elements in the elevation assembly and the control and signal processing electronics in the azimuth assembly spiraled down through the inside of this shaft. The azimuth servo assembly was mounted on the outside of the shaft. The servo consisted of a torque motor, tachometer, and resolver similar to the elevation servo components mounted on the mirror

shaft, but exposed to the ambient atmosphere. Other differences were that the motor has a higher torque capacity to handle the higher inertia of the elevation assembly and that the tachometer permitted nearly 360° rotation. The light sensitive part of the camera was the photosensor array: a miniature array of 12 silicon photodiodes. Four outer diodes were spaced at different distances from the lens for electrical focus selection for high-resolution (black and white) imaging. Six other diodes were covered with optical filters for multi-spectral (color or infrared) imaging. Another diode was unfiltered and used for directly viewing the Sun.

Meteorology instrument system.- The meteorology investigation measured the meteorological environment near the surface of Mars and obtained data on atmospheric dynamics which occurred in the Martian atmosphere. The time scales associated with these atmospheric dynamics ranged from a fraction of a second to many months.

The meteorology instrument operated during the postlanded portion of the nominal mission and during the extended mission. It measured the atmospheric parameters of pressure, temperature, and wind velocity (wind speed and wind direction) in the Martian boundary layer. Because of the composition and low surface pressures of the Martian atmosphere, the meteorology instrument had the capability to operate and make measurements over large variations in temperature and wind velocity. The instrument operating requirements were as follows:

Ambient temperature: The instrument measured Martian atmosphere ambient gas temperature over a range of 130 K to 350 K with accuracy of ±3 K.

Wind velocity: The wind sensors operated over a wind-speed range of 2 to 150 m/sec at ambient pressures between 2 and 20 millibars and ambient temperatures between 130 K and 350 K. The sensors had a wind-speed accuracy of ±4 m/sec or ±20 percent (whichever was greater) over most of the ambient conditions anticipated for the proposed landing sites. They had a wind-direction accuracy of ±20° at wind speeds of 5 to 25 m/sec and ±10° over the high accuracy ranges above a wind speed of 25 m/sec.

Pressure: The ambient-pressure sensor used in conjunction with the meteorology investigation was the same sensor as the one used during the parachute entry phase of the mission. This sensor measured the Martian surface pressure to an accuracy of ±0.5 mb over a pressure range of 1 mb to 30 mb.

The meteorology instrument consisted of three interconnected assemblies: meteorology sensor assembly, meteorology electronics assembly, and meteorology boom assembly. The MSA, shown in figure 102, supported the wind and temperature sensors and provided a housing for the low-level electronics. The wind-speed and wind-direction measurement utilized the technique of constant temperature hot-film anemometer consisting of a very thin conducting film (platinum) deposited on a substrate (glass rod). In operation this film was maintained at a constant temperature (approximately 100° C) above ambient temperature by controlling, with a feed-back amplifier (servo), the amount of power supplied to the platinum film. The amount of power supplied to the sensor was then a measure of the heat transfer from the sensor. The heat transfer from the cylinder (sensor) was primarily by convection if the sensor diameter was small and
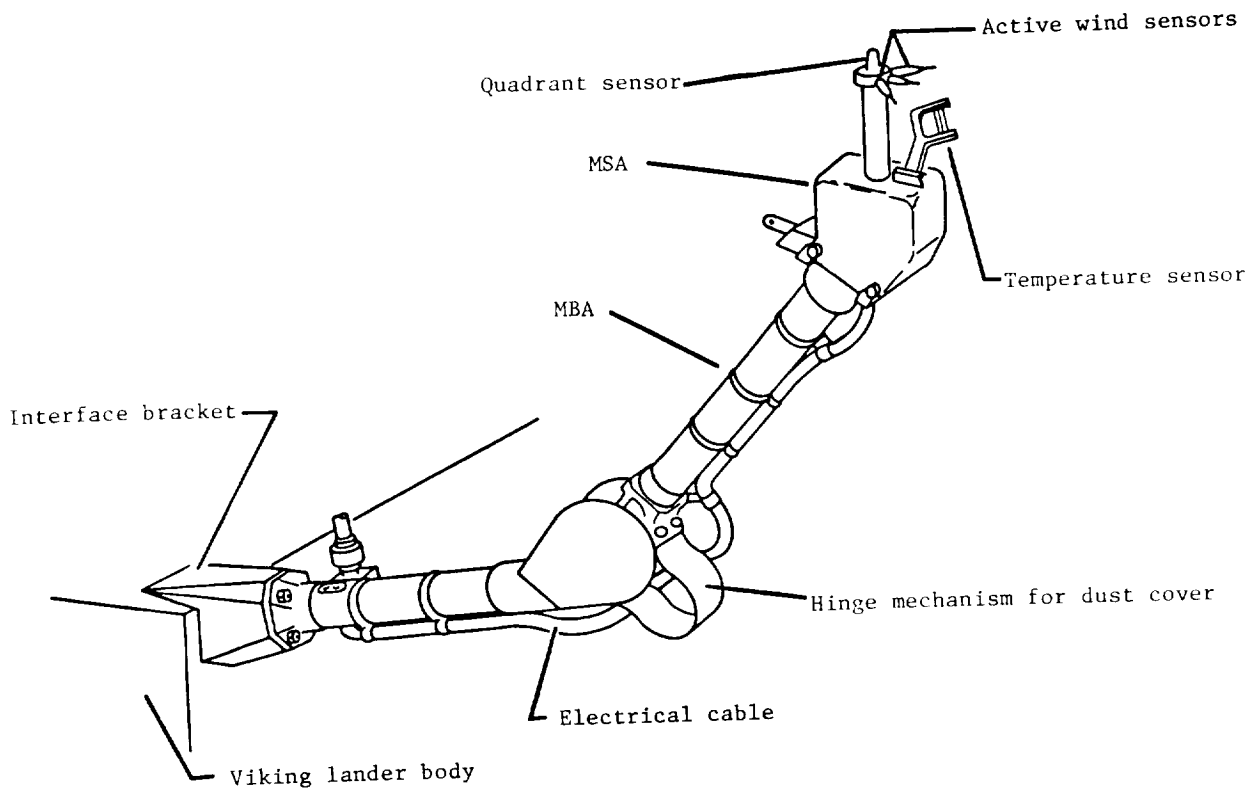
Figure 102.- Meteorology instrument boom assembly. Deployed configuration.

the wind speed was above some minimum value. If the power supplied to the sensor was measured, the convective heat transfer or wind velocity, normal to the sensor, could be determined. If two sensors were used, which were mounted at 90° with respect to each other, the power supplied to each sensor was then a function of the wind direction. The basic wind sensor could not distinguish wind from the positive or negative direction, which resulted in an ambiguity in wind direction. To eliminate this ambiguity in wind direction, a quadrant sensor was included in the system. This sensor consisted of a heated post and four thermocouple junctions mounted around the assembly. The post temperature was controlled at a nominal 100° C above ambient temperature similar to the wind sensors. The thermocouples measured a differential temperature due to the post thermal wake; therefore, by locating the position of the wake, a wind direction quadrant would be determined and wind sensor ambiguity would be removed. The temperature sensor was a three-thermocouple array; the thermocouples were chromel-constantan with all three junctions connected in parallel. The parallel connection was used to provide redundancy against breakage of a single thermo-couple wire. These junctions were connected in series with a reference junction located within the temperature module in the low-level electronics housing at the base of the wind sensor pedestal. The temperature module assembly provided a temperature controlled environment for the reference junction and the para-sitic junctions resulting from conversion of the thermocouple wire to copper wire for signal transmission to the MEA. The MEA provided the required elec-

172

tronics to support the sensors except for low-level electronics contained within the MSA. The MEA provided the power train for the two active wind sensors and the quadrant sensors and controlled their overheat temperatures at nominally 100° C. The sensor signals (wind, quadrant, and temperature sensors) were gathered, preconditioned, and converted into digital outputs. The MEA also formatted, stored, and delivered the data to the DAPU. The MBA (fig. 102) consisted of a deployable boom which supported the MSA in a stowed position during the launch, cruise, and entry phases of the mission. A short time after landing, a pyrotechnic activated pin puller was actuated to release the boom. The boom deployed under the action of a torsion spring contained at the hinge point, and latches provided a detent type locking of the boom in the deployed position.

Seismometer.- The seismology investigation provided information relevant to the structure, composition, and dynamics of the interior of Mars. In particular, the objectives of this investigation were to determine the amplitude, spectrum, polarization, and source of continuous background microseismic activity; to determine whether Mars is a tectonically active planet and to determine the level, nature, and location of tectonic activity; to determine the internal structure and composition of Mars, specifically, whether Mars has a crust and a core and whether the mantle of Mars is similar in composition to the mantle of the Earth; to determine the influx rate of meteorites; and to determine the mechanical properties of the material near the VL.

The seismometer operated during the postlanded mission to measure three perpendicular components of ground motion. The seismometer was capable of detecting ground displacement in all three axes of 50 mm, or less, at a frequency of 1.0 ± 0.2 Hz, and 1 mm, or less, at a frequency of 4.0 ± 1 Hz, with the unit operating at the level attitude (vertical axis of sensitivity parallel to the local gravity vector).

The seismometer consisted of two functional subassemblies contained in a single housing: the sensor subassembly and the electronics subassembly. (See fig. 103.) The sensor subassembly contained the following functional devices:

(1) Three mutually perpendicular seismic sensors, one vertical (X-axis) and two horizontal (Y- and Z-axes). These sensors were mass-coil assemblies suspended in such a way that the coil was positioned between the poles of two facing channel magnets. Motion of the coil normal to the field of the magnets generated an analog signal proportional to the amplitude and frequency of the respective components of ground motion. These outputs were hard-wired into the electronics assembly to be filtered, amplified, and then placed into a digital format.

(2) Calibration actuators for each sensor that operated in response to an external command and caused a mechanical displacement of the sensors.

(3) Three caging devices that released the moving elements of all three seismic sensors in response to external commands.

(4) A means of electrically testing the sensor and electronics while caged.
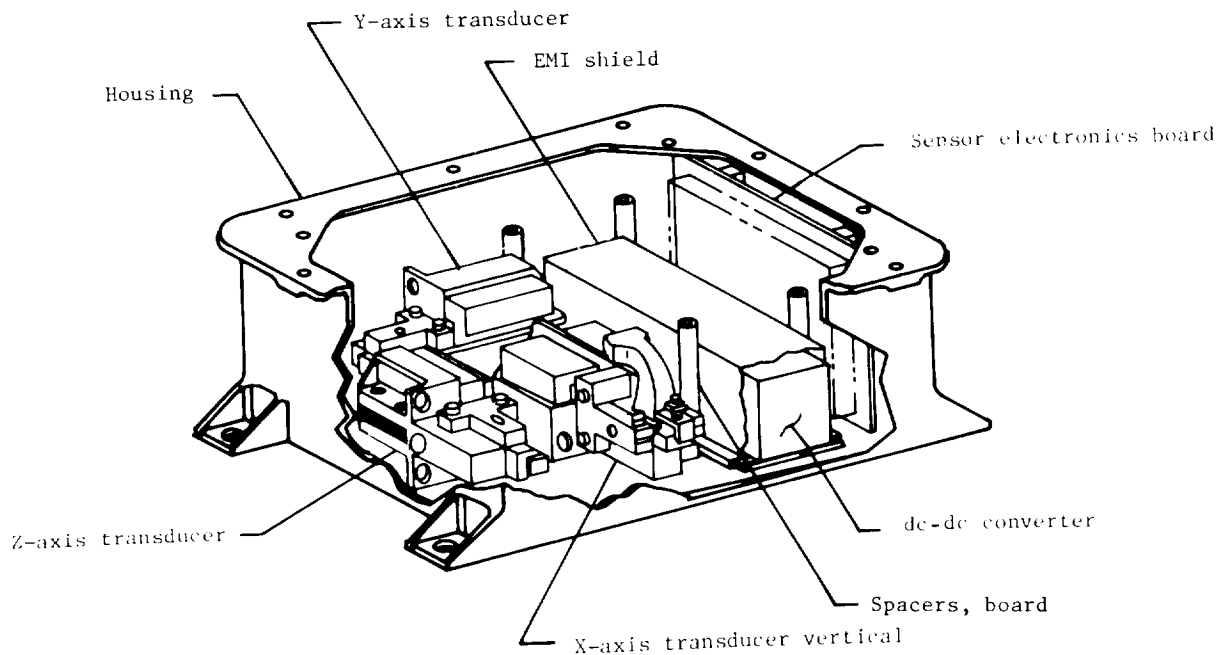
173

Figure 103.- Seismometer sensor subassembly.

The electronics assembly received analog inputs from the seismic sensors and serial digital command signals from the GCSC. Formatted data from the seismometer to the DAPU were serial digital signals that included experiment identification, synchronization, time information, and experiment data.

Surface sampler assembly.- The primary purpose of the SSA was to acquire, process, and distribute samples from the Mars surface to the GCMS, biology, and XRFS experiments. Secondary functions for the SSA included support of physical properties, magnetic properties, and meteorology investigations.

The SSA components (fig. 104) included the SSAA, GCMS PDA, biology PDA, and the SSCA. Related SSA/physical-magnetic properties support components (fig. 105) included boom-mounted mirrors, collector head backhoe magnets, magnet cleaning brush, ×4 magnifying mirror, and the crosshatched squares printed on top of the VL. The SSAA consisted of a controlled 3-axis 3-m (10-ft) furlable tube boom and collector head capable of acquiring surface samples at any location within an approximate 12.1 m^2 (130 ft^2) area in front of the VL and delivering 1000-μm sieved or raw samples to the required experiments. The GCMS PDA received 2000-μm particle size (and smaller) samples from the SSAA, sieved, and comminuted (ground) the samples to 300-μm particle size (and smaller), and delivered 1-cm^3 metered samples to the GCMS. The biology PDA received 2000-μm particle size (and smaller) samples from the SSAA, sieved the samples to 1500-μm particle size (and smaller), and delivered 7-cm^3 metered samples to the biology instrument. The SSCA consisted of the electronics necessary to provide control functions and data acquisition for the SSAA, biology PDA, and GCMS PDA. A
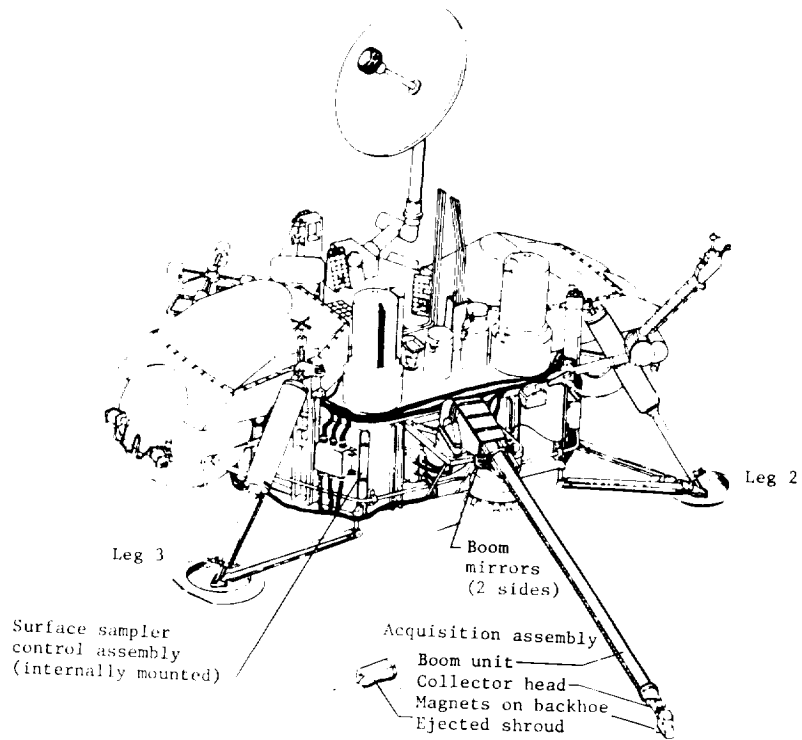
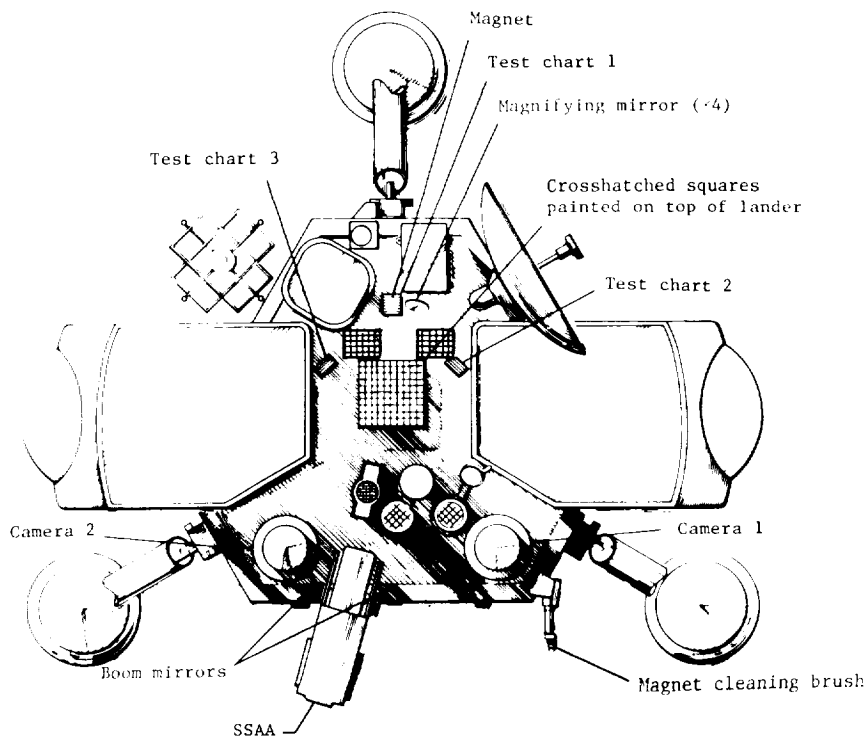Figure 104.- Surface sampler assembly components.

Figure 105.- SSA/physical-magnetic properties support components.

redundant side 2 operational capability provided for the control functions only (no data). Physical-magnetic properties support components consisted of boom-mounted mirrors for viewing footpads and terminal descent engine cratering effects, collector head backhoe magnet array for collecting magnetic material during normal sampling operations, magnet cleaning brush for removing magnetic material from the backhoe magnets, magnifying mirror (×4) for improved camera viewing of the collector head and backhoe magnets, crosshatched squares on VL top surface for collector head deposition of surface material, temperature sensor on the collector head lower jaw for surface temperature data, and boom and GCMS PDA comminutor motor current sensors for inferring surface properties.

The SSAA consisted of the boom unit (fig. 106), collector head (fig. 107), and shroud unit (fig. 106). The extendable/retractable boom element, combined with the integrated azimuth/elevation gimbal system, allowed the collector head to be commanded to any location within the articulation limits of the boom unit. The collector head, with its solenoid operated lid, backhoe, and 108° rotation capability, was designed to acquire samples from a variety of potential surface materials and to deliver raw samples or 2000-μm sieved samples to the various VL experiments. The backhoe permitted surface trenching operations, collection of magnetic surface materials, and the brushing of loose surface materials which could overlay a bedrock substrate.
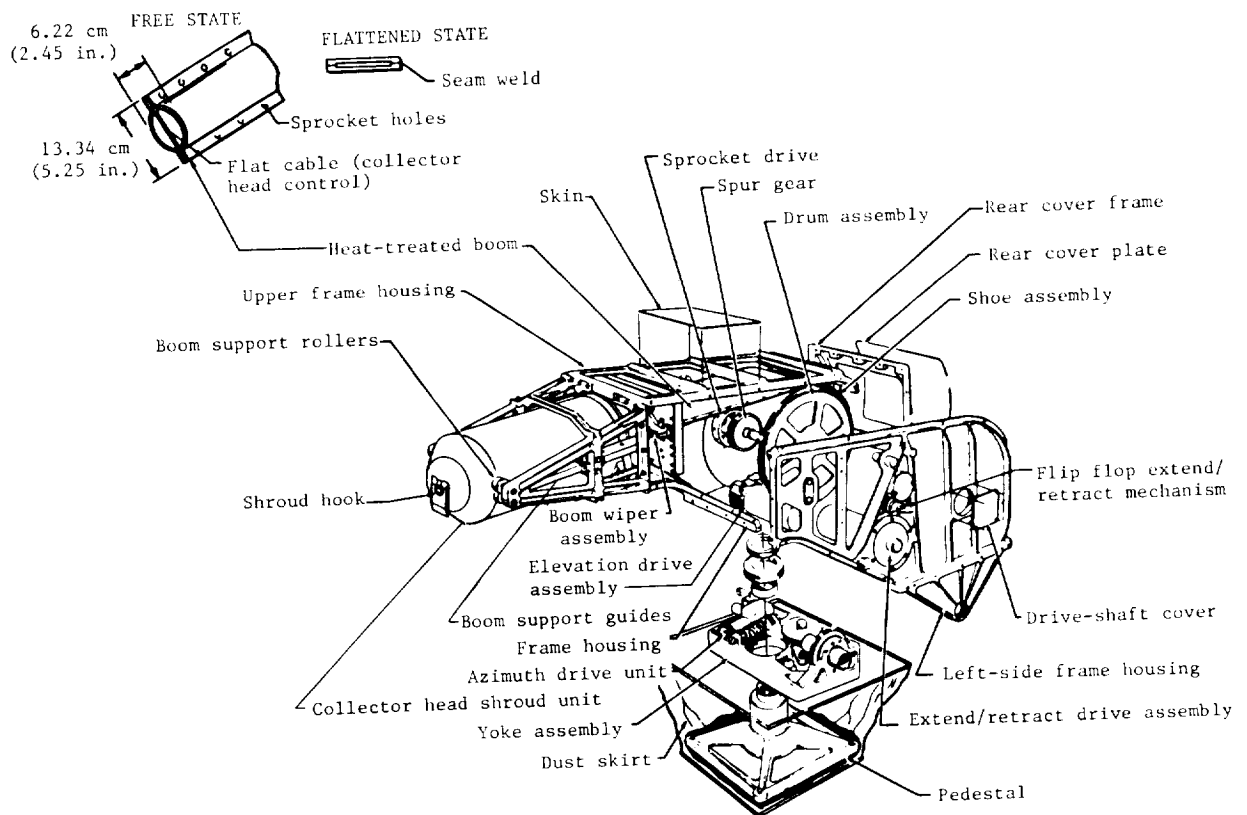

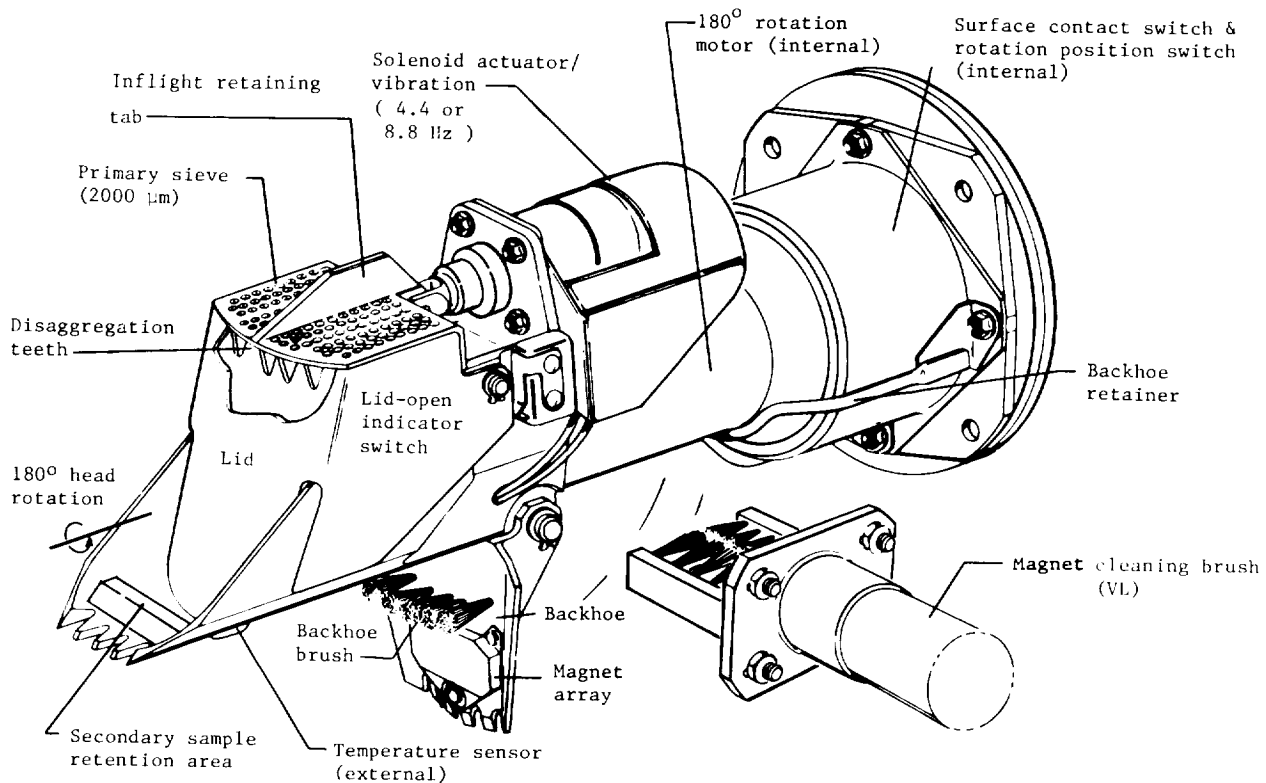Figure 106.- Boom unit with CHSU installed.

Figure 107.- Collector head and magnet cleaning brush.

The GCMS PDA (fig. 108) contained all the necessary elements for receiving a 2000-μm sieved sample from the collector head, sieving the sample through a 2000-μm sieve, comminuting a 600-μm sample, sieving this sample through a 300-μm sieve, and metering and delivering a 1-cm^3 sample to the GCMS instrument. Excess material was routed to a closed dump box. The PDA, dump box, and interfacing sample delivery tube were mounted directly to the GCMS instrument. The elements of the GCMS PDA were contained within pressurized lid-covered housing.

The biology PDA (fig. 109) contained all the necessary elements for receiving a 2000-μm sieved sample from the collector head, sieving the sample through a 1500-μm sieve, metering a 7-cm^3 sample and delivering it to the biology instrument. Excess material was routed to a closed dump box. The PDA, dump box, and interfacing sample delivery tube were mounted directly to the biology instrument. The elements of the biology PDA were contained within a lid-covered housing.

The SSCA contained all the necessary electronics to provide the control functions and data formatting for the three major electro/mechanical components of the SSA: the acquisition assembly, GCMS PDA, and biology PDA. Digital coded commands were received from the GCSC which were processed and transformed into stimuli for operating the various motors, solenoids, potentiometers, switches, temperature transducers, and sample level detectors located within the three

CROSS-SECTIONAL VIEW OF FUNNEL, AGITATOR, & SHUTTLE
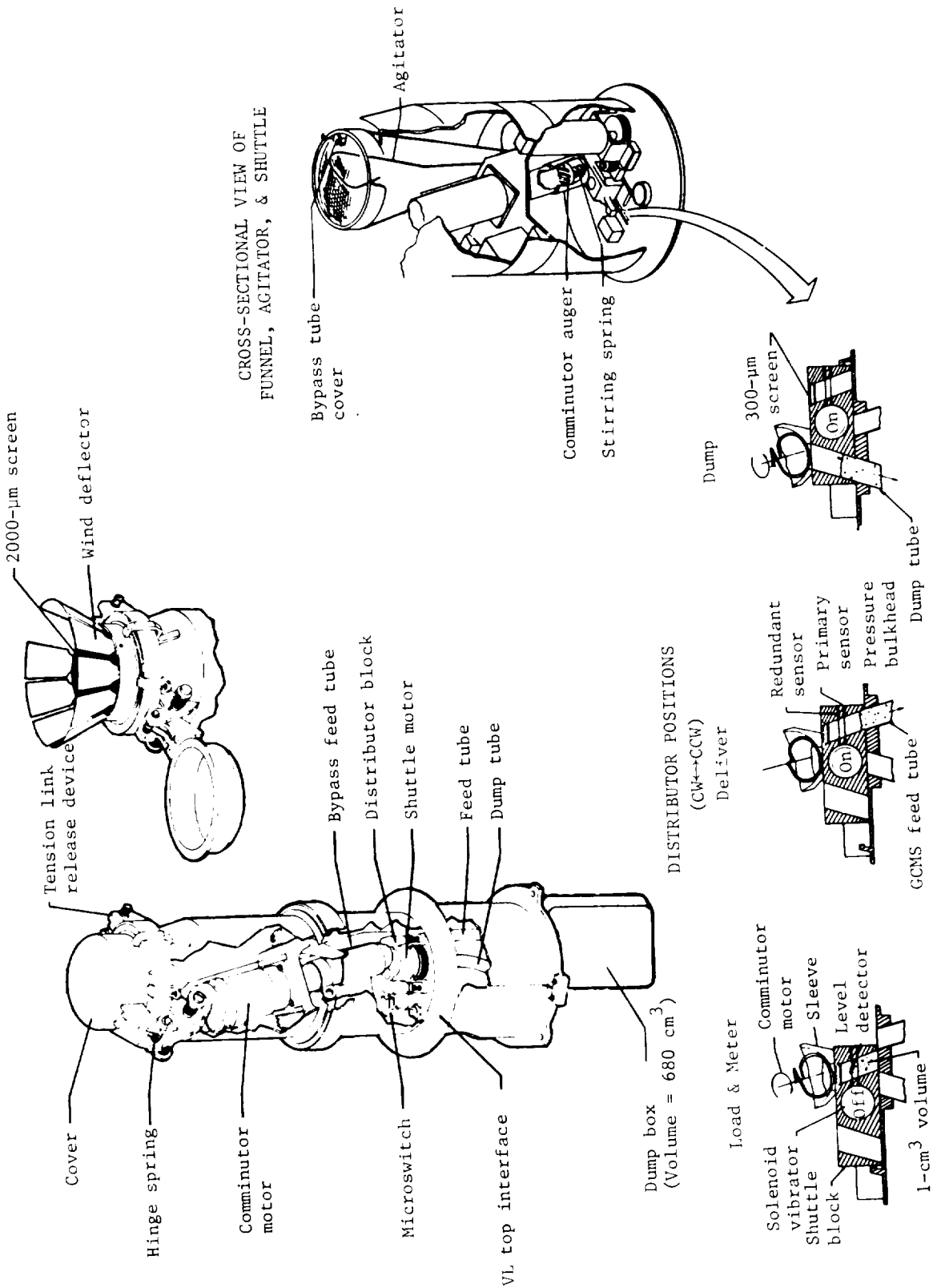
Figure 108.— GCMS processing and distribution assembly.

178

Figure 109.– Biology processing and distribution assembly.

CROSS-SECTIONAL VIEW OF
FUNNEL, AGITATOR, & SHUTTLE

1500-μm screen

Agitator

Wind deflector (deployed)
Bypass tube cover
Wind deflector (stowed)
Double-torsion spring
Charcoal filter
Bypass cover
Cover
Pin puller
Sand & dust ring
Agitator
Motor
Yoke
Distributor
Dump tube
Bypass tube
Funnel
Processor solenoid
Microswitch
Bulkhead
Tube junction
Delivery tube
Dump box
(Volume = 620 cm³)
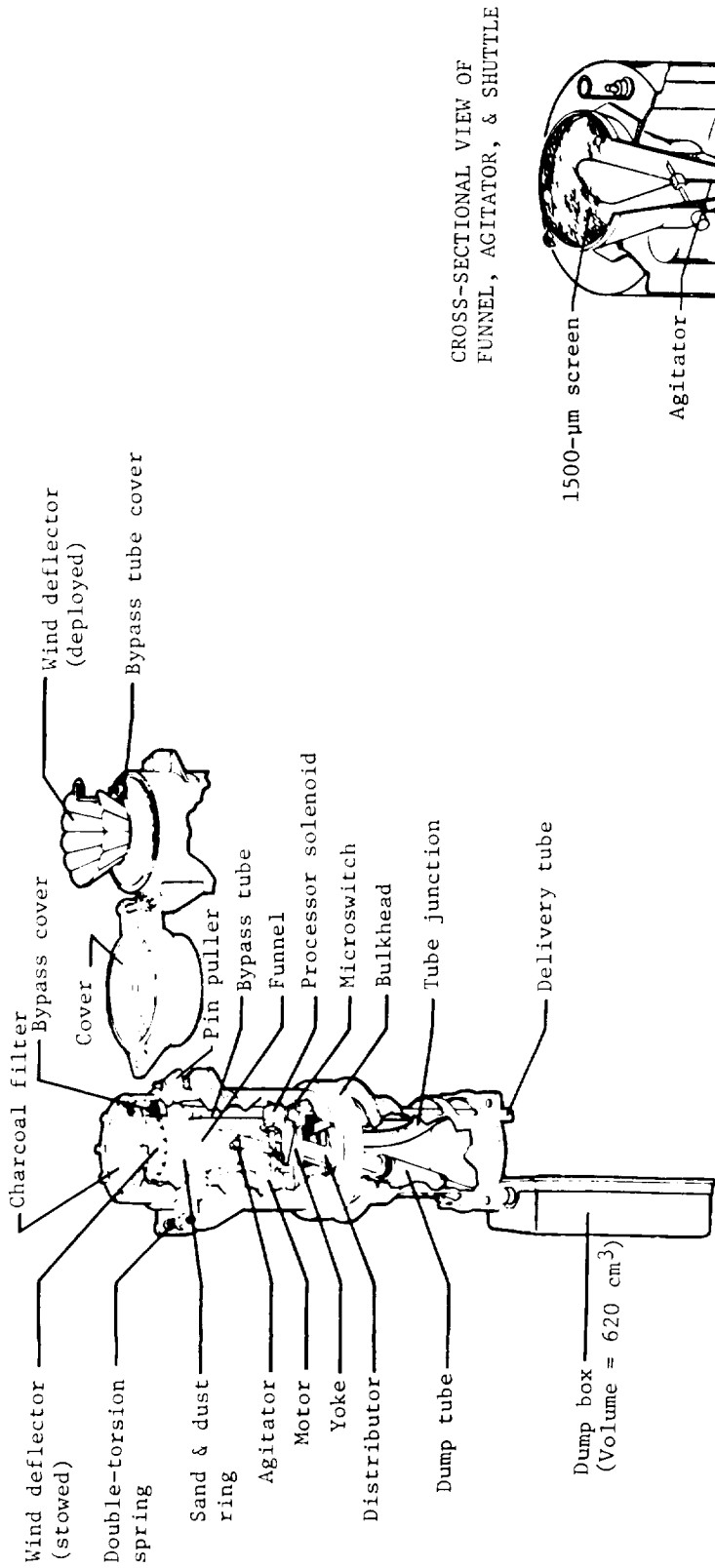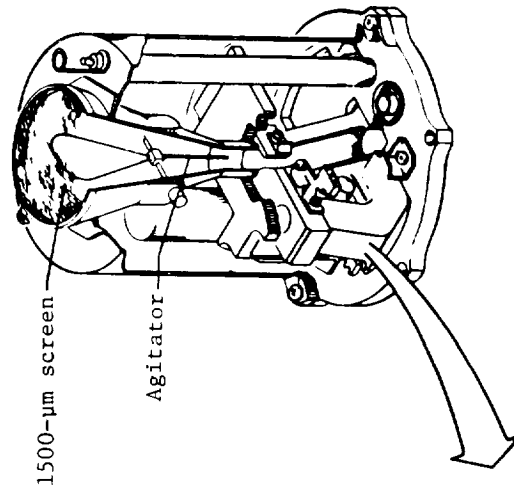
DISTRIBUTOR POSITIONS
(CCW→CW)

Load & Meter
Deliver
Dump

Agitator
Funnel
Shuttle
Level detector
Sample (6 to 8 cm³)
Bulkhead
Stop
Off
On

Biol distr sol (thumper solenoid)
Redundant sensor
Primary sensor

Stop

electro/mechanical components. Data were collected by the SSCA from the three components and digitally formatted for transmission to the DAPU. These data consisted of boom position in all three axes, temperature of the collector head and biology PDA distributor, six switches, sample level detectors, and motor/ solenoid operating currents.

X-ray fluorescence spectrometer.- The XRFS in the Viking lander performed inorganic chemical analyses of the surface material of Mars. The data from the XRFS were used by the Inorganic Chemical Team to determine the elements present on the Mars surface. From the determination, comparisons with compositions of geologic samples from the Earth, Moon, and meteorites were made.

The XRFS received samples from the Viking SSAA. The main method of delivery was made by setting the SSAA into the wind spoiler of the XRFS soil delivery system and vibrating the jaw of the SSCA. The sample material then gravity-flowed through a 1-cm screen into the XRFS funnel, through the XRFS delivery tube, and to the soil cavity within the electronics box. The XRFS bombarded the surface material with the radiosotope sources, Fe^{55} and Cd^{109}, and then measured the energy of the resultant X-rays emitted from the sample material. The Fe^{55} source excited the material with 5.9-keV X-rays and a set of proportional counters detected the X-rays emitted from the lighter elements of Mg through Ti. A second set of proportional counters detected the energy of the X-rays emitted from the sample bombarded by the 22.2-keV X-rays of the Cd^{109} source. The XRFS was capable of measuring the weight concentrations of elements from magnesium through the heavier elements. In particular it was capable of determining the concentration of 12 elements at detection limits as low as 50 ppm and with accuracies ranging from 70 ppm for zirconium to 3.0 percent for aluminum. The elements are Al, Ca, Fe, K, Mg, "O," S, Si, Ti, Rb, Sr, Ar; the element "O" is defined as the sum of the elements of atomic number less than 12. Soil was delivered by the SSAA to the XRFS measuring section, shown schematically as a top view in figure 110. The measuring cavity was made of 6061-T651 bar aluminum; the inside dimension was nominally 2.5 cm^2 (1 in^2); the height was 7.1 cm (2.8 in.); and the total volume inside the cavity was approximately 46 cm^3. The outer surface of the measuring cavity, facing the Fe^{55} source, was coated with between 2.54 to 5.08 m (0.0001 to 0.0002 in.) of nickel. Elevation cross sections in figures 111 and 112 show the source-window-plaque orientation and the detail parts for the Fe^{55} and Cd^{109} areas of the measuring section. A dump cavity having a volume of greater than 600 cm^3 total was located directly under the measuring cavity, thereby allowing the analysis of multiple soil samples. The electronics assembly received and amplified signals from the proportional counters and sent the signals to the discriminator circuit. The discriminator accepted signal pulses of the commanded level during the commanded counting period. The accumulated pulses during the counting period were shifted to the lander system as the primary data output from the XRFS.

Magnetic and physical properties.- The objectives of these investigations to find magnetic and physical properties were to determine the magnetic properties of the surface material and to determine the physical properties of the surface and the surface material.

Magnet arrays, magnifying mirrors, and standard mirrors were placed on the lander to obtain data for these investigations. See figures 104 and 105 for the
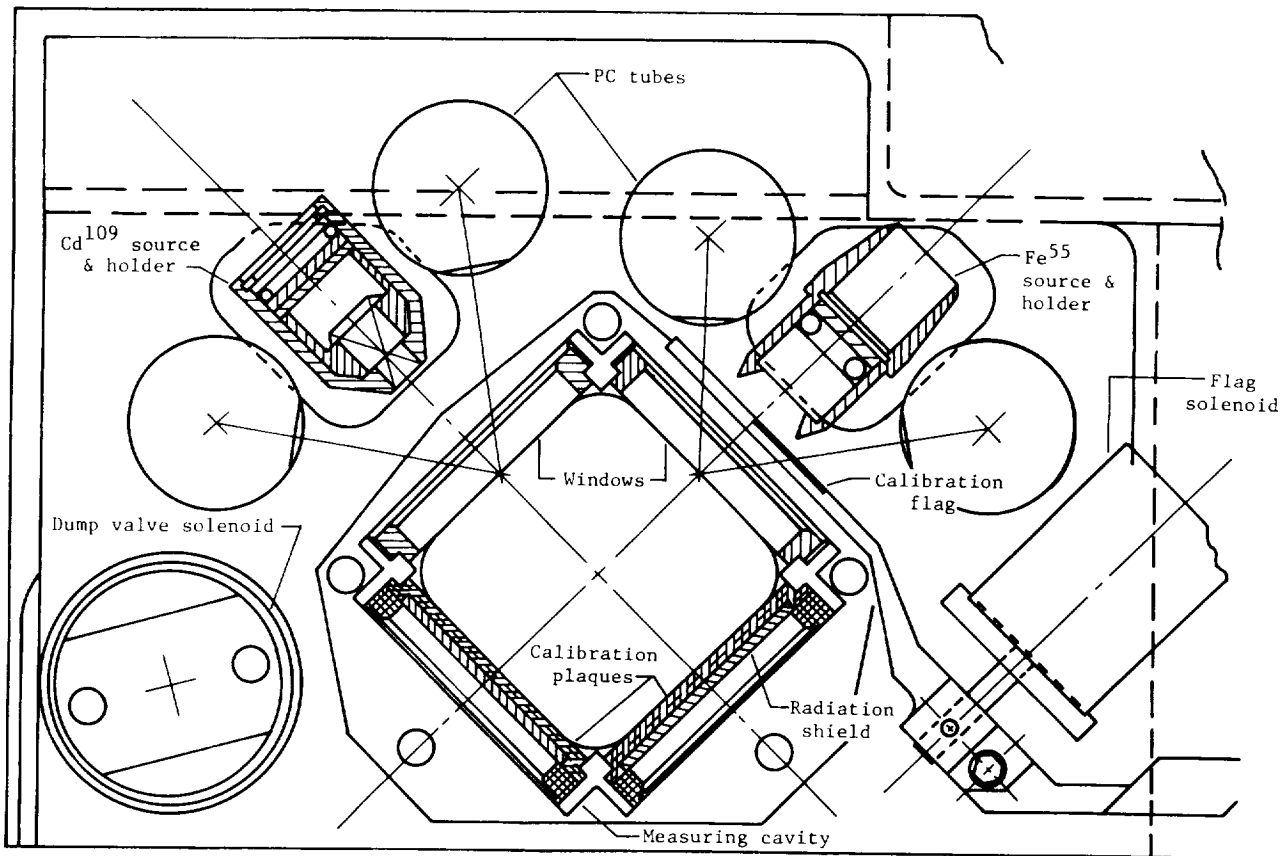
Figure 110.- Horizontal section of measuring cavity and source holders.
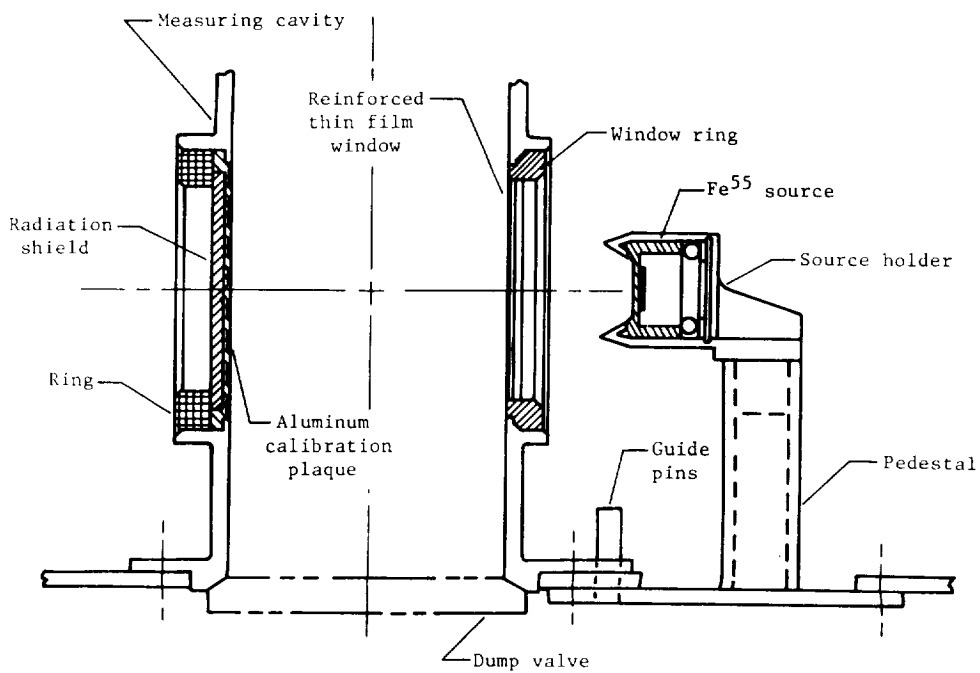
Figure 111.- Iron-55 source-window-plaque orientation.
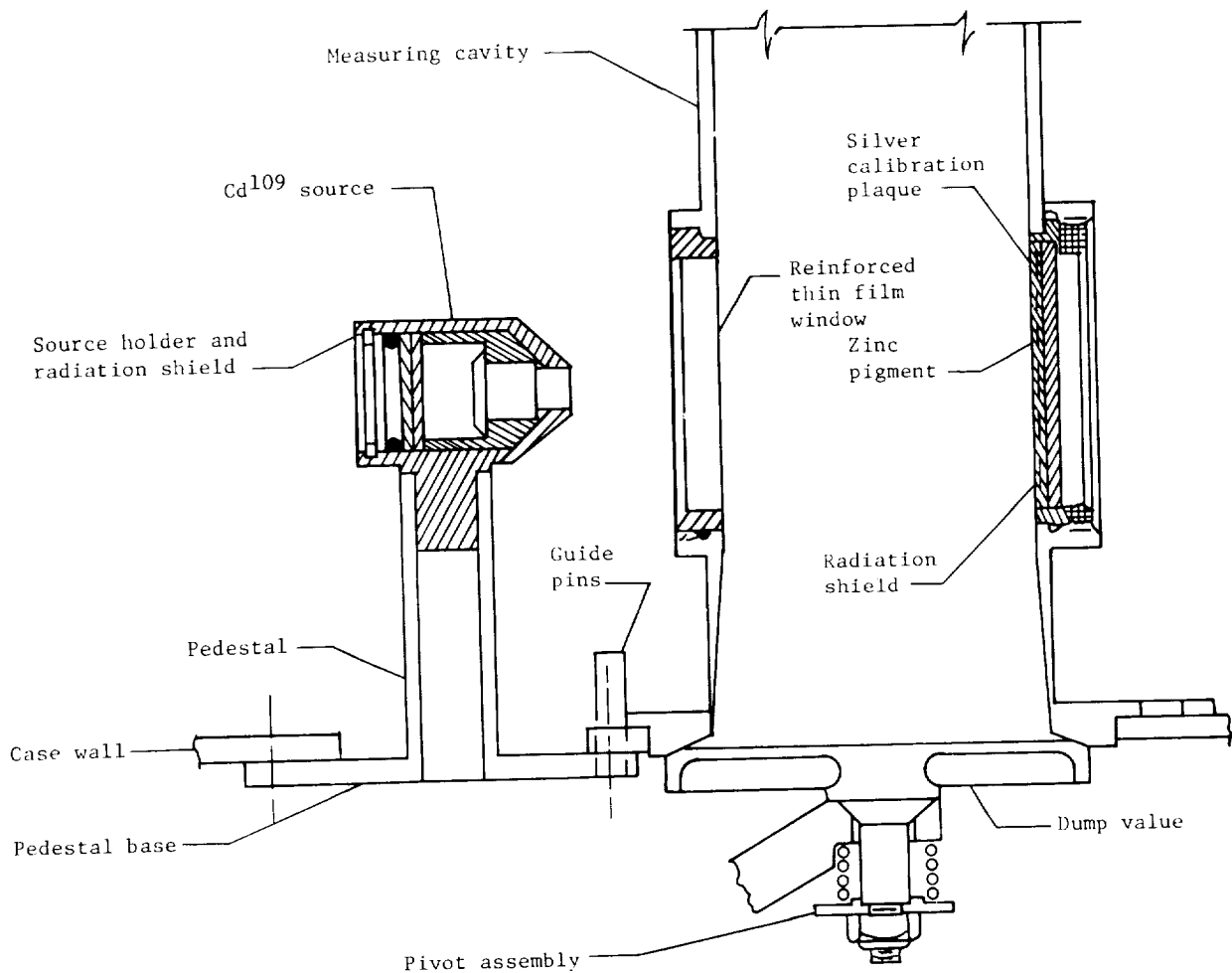
Figure 112.- Cadmium-109 source-window-plaque orientation.

location of these components. In addition, data from all other lander instruments were used to accomplish the objectives of these investigations.

Aerospace Ground Equipment

The VLS AGE included the equipment necessary to carry and test the VLC at the system level and to support the VLC during sterilization and the launch countdown phases of activity at KSC. The AGE was made up of the system test equipment; assembly, handling, and support equipment; launch complex equipment; and mechanical AGE.

System test equipment.- The STE was physically made up of two mobile test vans (vans A and B) and portable VLC vicinity equipment. A pictorial view of van A, van B, and the portable STE is shown in figure 113. Figure 114 shows the equipment layout of van A. Van A was a commercially purchased semitrailer designed to provide environmental conditioning and transport of the STE. Van B was a test operations trailer which was provided for test personnel and
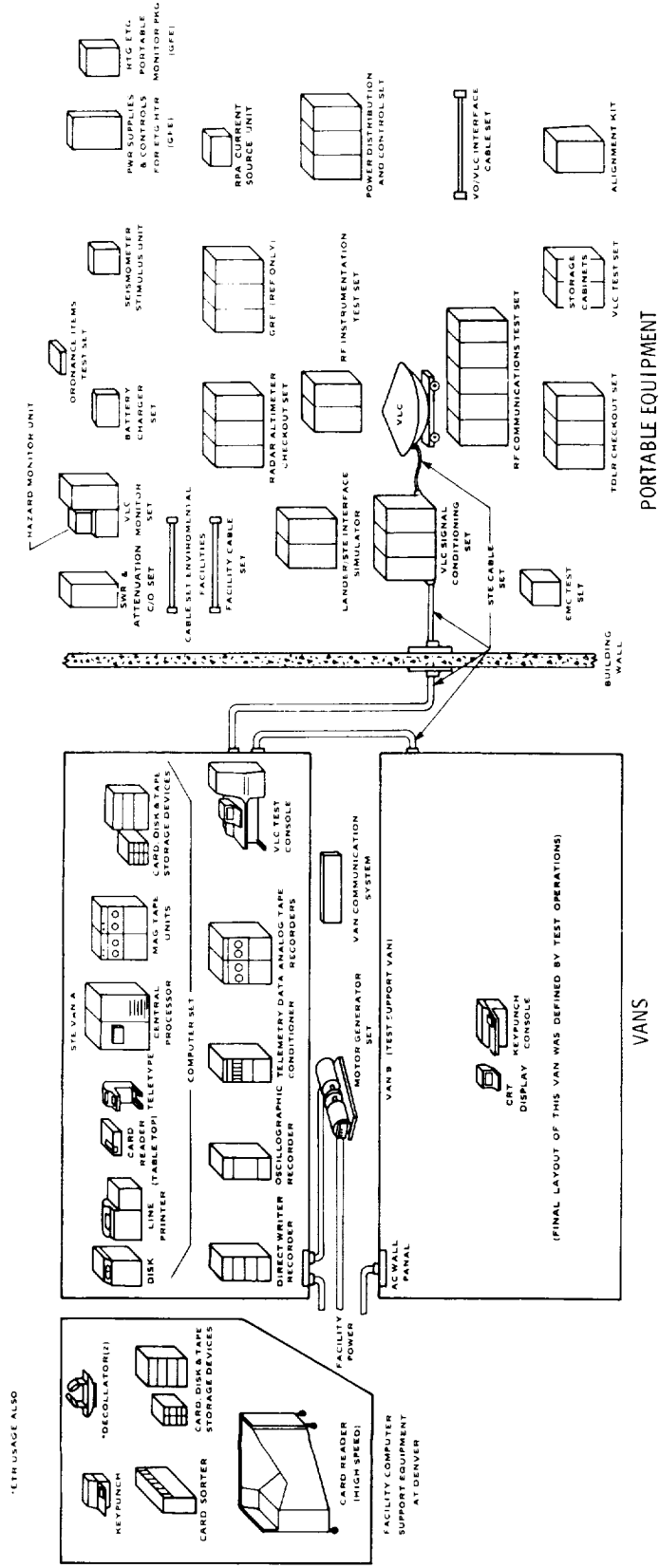
Figure 113.- System test equipment.

183
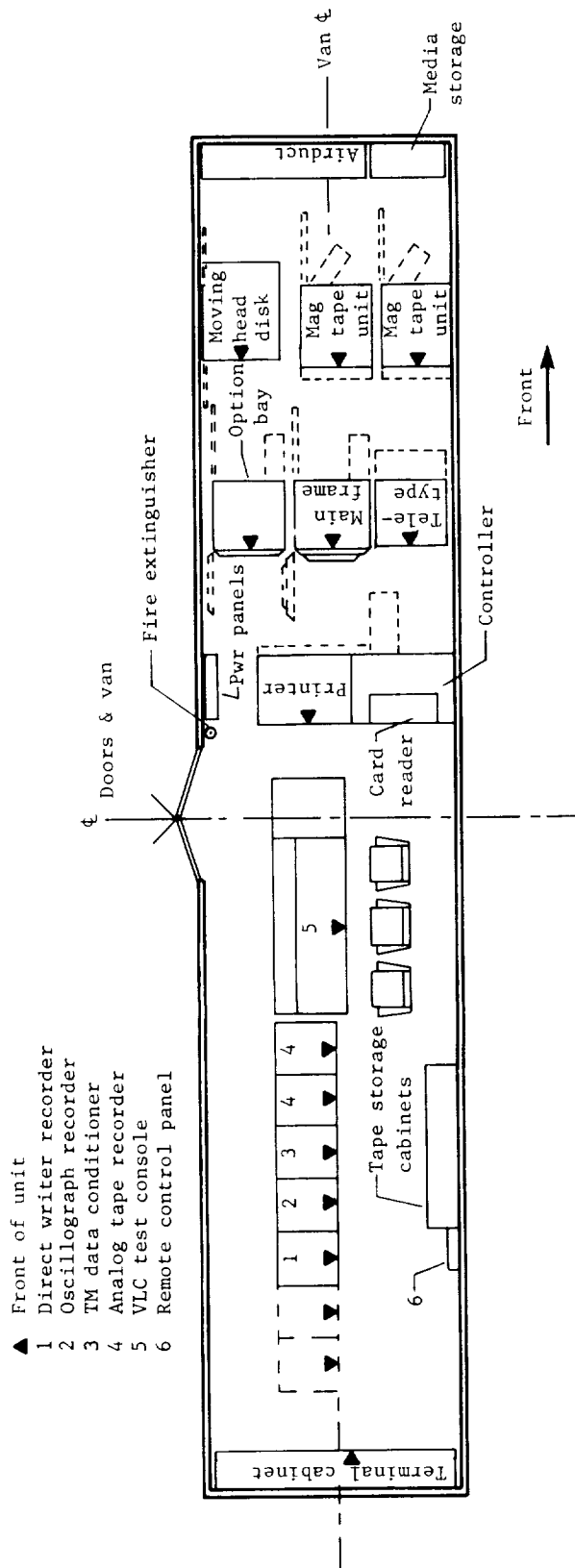
Figure 114.- Equipment layout of van A.

Front of unit
1 Direct writer recorder
2 Oscillograph recorder
3 TM data conditioner
4 Analog tape recorder
5 VLC test console
6 Remote control panel

Terminal cabinet

Tape storage cabinets

Doors & van

Fire extinguisher

Pwr panels

Printer

Card reader

Controller

Option bay

Moving head disk

Main frame

Tele- type

Mag tape unit

Mag tape unit

Airduct

Van

Media storage

Front

maintenance. Portable equipment was supplied only where conditions or frequency of usage precluded installation and operation in the equipment vans. A general functional block diagram of the STE is shown in figure 115. The STE was an assemblage of commercially purchased and contractor designed equipment integrated into a real time, computer controlled, data monitoring and checkout system.

A computer provided the basic control for test stimuli and data monitoring. Communication between the computer and the interface equipment was via the IOP data bus. The data bus provided a bidirectional 32-bit parallel data-transfer capability. The total transfer rate of the IOP data bus was approximately 150 000 32-bit words/sec. Control of data transfers between the computer interface unit and the computer memory bank was accomplished by the IOP and the data bus controller. This control consisted of timing, memory addressing, number of words to be transferred in or out of memory, and priority of units being serviced.

Under control of the on-line software subsystem, a formatted 32-bit discrete stimulus word was loaded into the discrete and time stimulus unit from the computer memory bank. The discrete stimulus word was then shifted serially to the three DOU's. The selected DOU decoded the discrete stimulus word and either set or reset a discrete. Each DOU was capable of issuing 250 mA current sink, driver output, and relay contact closure discretes.

The monitoring of discretes was accomplished by four remote discrete scanners and a DMU. Two discrete scanners were provided in van A and two were located in the VLC test area. Each discrete scanner was capable of monitoring the state (on/off) of 256 discrete signals. These data from each discrete scanner were serially shifted to the DMU once every 2.56 msec where each discrete channel was checked for a change of status (event change). If an event change had occurred, the discrete channel number and new status (on/off) were loaded into the computer memory bank via the IOP bus. Once in computer memory, the on-line software system time tagged the event change with range time and compared the new state against a predicted state (criteria table). In this manner, every discrete in the system was checked for proper status nearly 400 times a second.

All hardline analog data channels from the VLC or STE were routed to the analog patch unit where they could be patched to the oscillographic or direct writer recorders for strip chart recording. The analog hardlines were also routed to the analog multiplexer where each channel was sampled and presented to the ADC. The parallel digital output of the ADC was strobed into a holding register in the analog input unit. The analog input unit then loaded this data word into the computer memory via the IOP bus. This sequence of events was repeated until the multiplexer had scanned each analog channel and all the values were loaded into a table or buffer in computer memory. The on-line software subsystem tagged the buffer with range time and then checked each analog *value against* floating aperture limits to detect and record amplitude variations. This data compression technique removed redundant data values and allowed reconstruction of the analog channel (within the limitations of the sample rate) at a later time for historical purposes. The analog values were also checked against GO/NO-GO limits. NO-GO violations were displayed on the
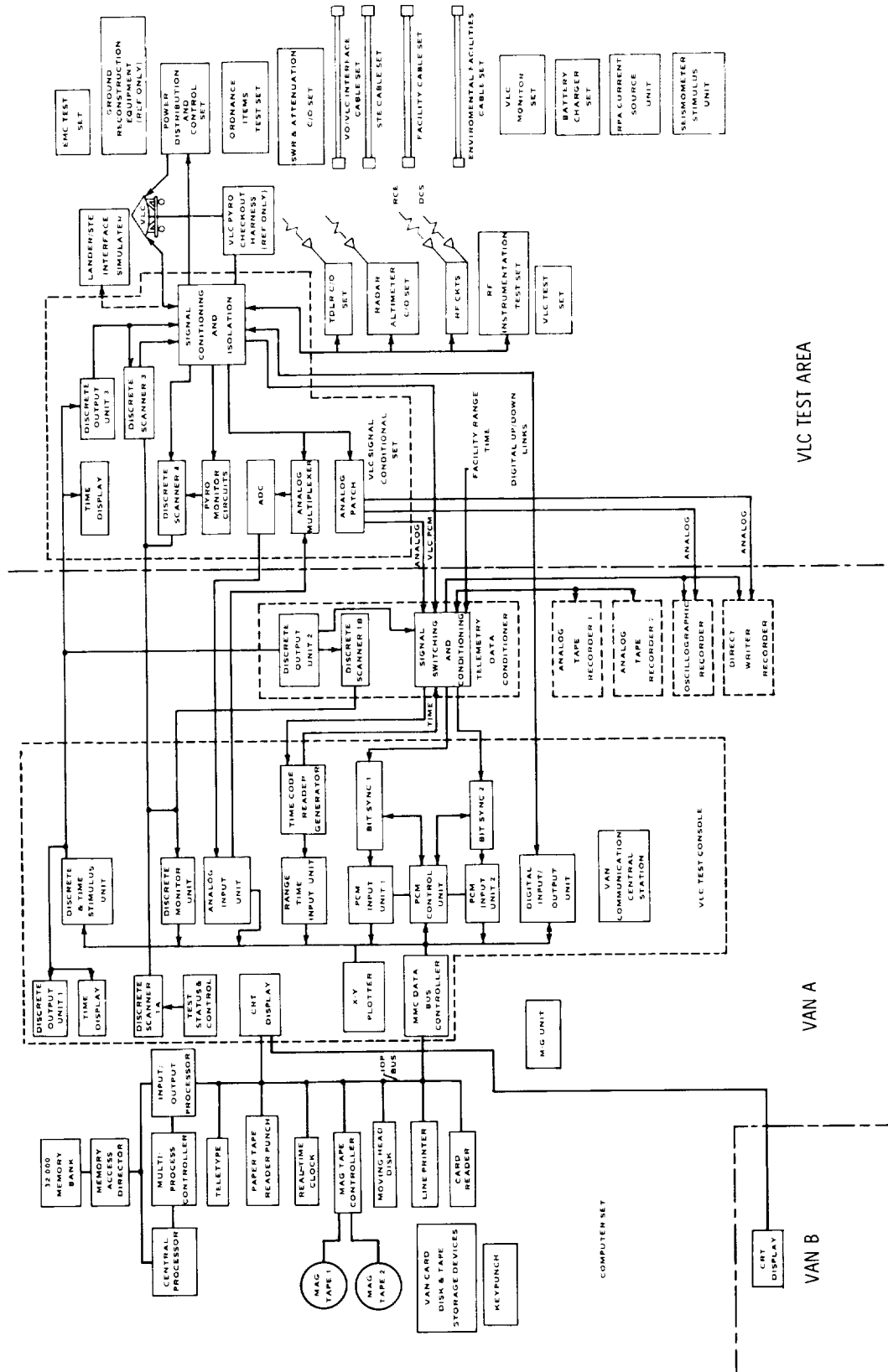
185

Figure 115.— Functional block diagram of STE.

186

line printer and CRT and could cause the test sequence to stop or go to an alternate test sequence.

Range time was used as a timing standard within the STE system. At test areas where a facility range time was available, the incoming signal was routed to the time code reader generator unit. At test locations where an incoming facility range-time signal was not available, the time code reader generator was operated with an internal high stability oscillator as the timing source. Test or simulated mission time provided an elapsed time reference during test operations. The test time format provided for days, hours, minutes, seconds, and an alpha prefix to indicate mission phase.

Dependent upon the STE test configuration, PCM data could be acquired as hardline data via the VLC signal conditioner or as radiated data captured by the rf communications test set with its attendant antenna couplers. These PCM data streams were routed to the TDC. The TDC performed functions such as patching, switching, and conditioning (demodulation, discrimination) for the various PCM data streams. Incoming PCM data were recorded on the analog tape recorders and were also routed to the bit synchronizers in the VLC test console for real-time processing.

The bit synchronizer established a bit clock synchronized to the incoming data. The output clock and data signals were then routed to the PCM input unit which contained logic to perform one or more of the following functions, depending upon the format of the incoming PCM data:

Block decoding

1 of 4 data discrimination

Bit deinterleaving

Alternate bit complementing

Direct coupling

After this preprocessing, the frame synchronizer logic performed a bit-by-bit examination of the data until the frame sync word was located. The data were then formatted into parallel 32-bit words and loaded into a buffer memory. When a complete frame of data had been loaded into buffer memory, it was tagged with range time and loaded into computer memory where the on-line software subsystem began decommutation and processing of the data.

The digital I/O unit provided the capability of acquiring serial digital data from the VLC. Incoming data were formatted into a 32-bit word containing data and source identification, which was then loaded into the computer memory via the IOP bus. Digital output words were formatted in the computer memory by the on-line software subsystem and loaded into appropriate channel registers of the digital I/O unit. The channel register then shifted the data out serially. The output clock rate and word length (number of shift pulses) for each output channel were variable and controlled by the on-line software.

Systems checkout of the VLC communications and radar subsystems was accomplished by four portable VLC vicinity test sets: TDLR checkout set, radar altimeter checkout set, rf communications test set, and rf instrumentation test set. These sets were capable of autonomous or manual operation for some of the rf testing performed on the VLC but relied on van STE for test and sequence control. Control of the VLC subsystem was accomplished by STE/GCSC digital uplinks and downlinks. Data values acquired by the test sets on hardlines were transmitted to the STE computer via serial data lines to the digital I/O unit. The on-line software performed automatic limit checking, data logging, and other data processing services on the data received.

The STE had two levels of self-test capability: Self-test capability while connected to the LIS and self-test capability while connected to the VLC. The LIS was a portable unit provided to permit verification of the STE prior to connection to the VLC. The LIS connected to the VLC signal conditioning set and provided signal turnaround or simulation that represented the signal range characteristics seen from the VLC. The LIS test sequence assured that every data channel and/or VLC interface point was functional. It also verified all STE modes and internal functional paths.

The STE self-test capability while connected to the VLC was sufficient to verify that general functional areas of the STE (such as power, PCM data acquisition, and analog monitoring) were operational. This initialization self-test sequence was normally performed after powering up the STE and prior to running VLC test sequences. It included functional checks of the following equipment:

Computer set and peripheral equipment

Timing subsystem

Discrete stimulus subsystem

Discrete monitor subsystem

Analog monitor subsystem

Digital input/output subsystem

Telemetry decommutation subsystem

Power subsystem

Radar and rf communication subsystems where applicable

STE self-tests that could be performed on-line while performing VLC test operations provided the following capabilities:

All discrete stimuli to the VLC and selected internal STE discrete stimuli were monitored by the discrete monitor subsystem. Channel 1 of each discrete scanner was a self-test channel which could be stimulated by a self-test discrete from each discrete output unit.

188

One high-level (0 to 5 V dc) and one low-level (0 to 40 mV dc) channel of the analog multiplexer was designated self-test channels and connected to an appropriate reference voltage.

STE devices that were connected to the IOP data bus provided status as required during data transfers over the bus.

The computer system provided the normal on-line system traps for operating errors such as parity errors, arithmetic errors, and undefined operations.

Assembly, handling, and support equipment.- The AHSE consisted of equipment with the capability to lift, transport, weigh, align, provide access to, and determine center-of-gravity location for balancing the VLC and subsystems. The equipment included assembly fixtures for use during VLC buildup and equipment installation; handling fixtures to lift, move, and rotate the VLC and components; transportation equipment for transfer of the VLC and assemblies between assembly, test, and operation facilities; protective containers for shipment of the VLC and assemblies; special test fixture adapters, tools, and carts to provide for VLC and component positioning and attachment to standard test equipment; access ladders and platforms for use during VLC assembly, test, and servicing; and logistic van to store, transport, and protect all spares for the program.

Launch complex equipment.- The LCE provided the necessary VLS monitoring, control, and display functions required during prelaunch and launch operations at the launch complex. The LCE consisted of the launch coordinators console and the lander hardline interface and signal conditioning set.

The LCC was a commercially available console structure configured to accommodate one seated operator. Front panel controls and displays were provided to perform the required functions, and voice communications for the operator was provided. The LCC was located in the payload control room at the VIB at KSC. The LCC provided indicator lights for monitoring status of specified AGE. The signals to drive these indicators were received from the LVS data transmission system. Two independent analog displays were provided, each of which was driven by a 0 to 5 V dc signal from the LVS ground PCM system. The LCC provided a means of selecting which parameter was transmitted by the LHISC via the LVS ground PCM system to drive each LCC display. Switches were also provided to control the functions identified for transmission to the LHISC via the LVS data transmission system. Seventy discrete inputs (21 to 31 V dc) were provided from the LVS transmission system.

The LHISC was packaged in standard equipment racks with front panel controls and displays provided as necessary to perform locally the required functions. The LHISC was located in the AGE building at Launch Complex 41 at KSC. Indicator lights were provided for monitoring the functions controlled by the LCC and those controlled locally. Two independent analog displays were provided and a means of selecting which of the parameters identified was displayed on each. The selected parameters were displayed in engineering units with the value of a measurement and the time of day printed whenever the measurement differed from the previous sample value by more than a predetermined value. Control was pro-

vided to allow the operator to cause a printout of all measurement values whenever desired. The LHISC provided circuitry to implement countdown logic for interconnection with the LVS automatic countdown control. This included monitoring of the vent valve, staging connector, and status of pyrotechnic functions. Discrete outputs were provided to the LVS CMG to indicate that the VLC/LCE was in a green ("go") condition; thus, the VLC vent and staging connectors were disconnected. These discretes were contact closures to the LVS AGE nominal 28 V dc power received from the CMG. Discrete inputs were also received from the LVS CMG. These discretes were used to turn on VLC pyrotechnic power and to arm, fire, and safety launch pyrotechnic events at the proper time in the launch countdown sequence. The hazard monitor unit which was part of the LHISC provided audible and/or visual alarms when specified limits for the functions considered essential to the VLC were violated. A battery source was provided which was capable of maintaining hazard monitor functions for up to 4 hr in the absence of primary ac input power. Switchover to battery power was automatic upon loss of ac input power and performance of the LHISC hazard monitor function was not degraded by the transfer. An interface with the GCMS PPU provided connection of PPU power to the GCMS ion pump, connection of ion pump current and voltage monitors to the PPU, and connection of the GCMS PPU alarm circuit to the LHISC. GCMS ion pump current and voltage measurements were monitored in parallel with the PPU with the measurements selectable for transmission to the LCC for analog display. The LHISC provided commands to control valves in the chilled water system to remotely start and stop each of the two water chillers and monitor the on and off status of each unit. The open and closed indication from each valve was monitored, and logic to sum certain valve indications for transmission to the LCC was provided. The flow, temperature, and pressure of the chilled water system was also monitored. In addition, commands for control valves in the chilled water flow control unit and commands to control application and removal of power to valves and heaters in the chilled water purge unit were provided. Control of a normally closed solenoid valve which vented excessive VLC bioshield pressure via the pressure makeup line was provided. Power to open the valve was maintained only while the operator continued to actuate a momentary control switch. Indication of the valve was also provided. Discrete commands provided to the VLC by the LHISC were used to initiate checkout of the VLC, to reset the VLC, to turn the VL tape recorder on before launch, and to control the launch pyrotechnics.

Mechanical AGE.- Mechanical AGE consisted of the following categories:

Propellant/pressurant servicing AGE which included all equipment for servicing the propulsion subsystems of the VLC as required during system and subsystem tests and preflight operations.

Environmental control AGE which included the equipment required to maintain necessary environmental conditions within the AGE vans as well as the portable equipment required to maintain VLC internal temperatures.

Sterilization AGE which included that equipment necessary for sterilizing both the VLC and its pressurant. Included in this category was equipment for VLC purge and pressurizaton before, during, and after sterilization.

Science servicing AGE which included the equipment required to maintain a positive pressure in the CHSU and the GCMS for maintaining cleanliness.

The alignment kit consisting of horizontal tooling bars, a vertical tool bar, corner cube, scopes, theodolites, their adapters, was used to read three-dimensional differences between any two points in the lander with respect to two orthogonal lander reference planes. Two horizontal tooling bars and one vertical bar were used to establish three coordinate axes orthogonal to the lander geometric axes. A reflective surface corner cube was used to obtain a perpendicular relationship between the two horizontal bars and to provide an orthogonal reference for the scopes. The lander tooling bars and scopes were leveled with respect to gravity by target arrays or an electronic level which compensated for vibration and, therefore, provided more accurate measurements. Angular alignment measurements consisted of IRU case, TDLR mount, terminal roll engines, camera mounts, high-gain antenna mount, aeroshell surface, deorbit engines, RPA mount, UAMS mount, and the VO/VL interface plane. Measurement accuracy was ±4 arc-sec. Location measurements consisted of terminal descent engines, terminal propulsion tanks, camera mounts, RCS deorbit tanks, aeroshell sockets, and VO/VL interface holes. Measurement accuracy was ±0.03 mm (0.001 in.).

The propellant/pressurant servicing AGE performed propellant and pressurant loading, off-loading and flushing, contamination control, and leak checks for the VLC propulsion system. This AGE transferred the specified amount of hydrazine or simulated propellant into the propellant subsystems and pressurized the pressurant subsystems with GN_2 to the specified pressure. This AGE also verified the accuracy of the amount of loaded propellant.

The propulsion subsystem was loaded for flight subsequent to sterilization of the VLC and before the VLC was removed from the sterilization chamber. Prior to commencing the sterilization cycle, all fluid line interfaces associated with propellant and pressurant loading were connected and remained connected during the sterilization process until completion of loading and lockup of the VLC propulsion systems. Pressurant introduced into the VLC propulsion systems after sterilization was sterile. The AGE off-loaded the propellant and pressurant, flushed the propellant subsystems with decontaminating fluid, and vacuum-dried the propellant subsystems prior to loading for flight. The AGE controlled the contamination level of fluids introduced by the AGE into the propulsion systems by initial cleaning of the wetted parts and by initial and final filtering of the fluids. In addition this AGE checked the propulsion subsystem for leaks. To accomplish propellant and pressurant servicing the following equipment was provided:

Propellant servicing unit: The PSU included the major components required to load and off-load the propellant or decontaminating fluid. The PSU loaded and off-loaded the liquids through the PLAU and the PLHS. The PSU was also connected to the PLVU to verify loading accuracy.

Propellant load verification unit: The portable PLVU verified and calibrated the loading accuracy of the PSU.

Propellant load adapter unit: The portable PLAU included shutoff valves, interconnecting piping, and other necessary components to direct the flow of propellant and/or sterile pressurant to the VLC during the loading operation. The PLAU interfaced with the PLHS to interconnect the PSU and the PCU with the VLC.

Propellant load hose set: The PLHS included all components necessary to interconnect simultaneously the equipment required for flight loading operation. The PLHS also included any additional components necessary to interconnect the equipment required for off-loading propellant, pressurant, or decontaminating fluids.

Pressurization control unit: The portable PCU pressurized to operating pressure the pressurant side of the VLC propellant tanks with sterile GN_2 during the propellant loading operation. The PCU also depressurized the propellant tanks and provided transfer pressurant for off-loading and flushing propellant tanks.

Pneumatic test unit: The PTU pressurized the propulsion system subassemblies and installed system, using helium and nitrogen, as required while they were being tested for leaks by means of the helium leak check unit and other equipment.

Helium leak check unit: The portable HLCU was used in conjunction with the PTU to detect helium leaks less than 10^{-9} cm^3/sec. The HLCU included all the accessories and adapters necessary for leak-testing the propulsion systems as well as the RTG cooling system located within the VLC.

The environmental control AGE provided van air conditioning and RTC cooling. The van air conditioning AGE controlled the environment within the van. The RTG cooling AGE limited the temperature of the RTG by circulating water at controlled temperature through the VLC RTG end-cap cooling subsystem. The RTG's required temperature control continuously from the time they were activated prior to lander encapsulation until just prior to launch. The AGE also cooled the VLC batteries during charging. For environmental control the following equipment was provided:

Van air conditioning unit: This unit was mounted externally on the van and discharged conditioned air through the wall for distribution to the cooled equipment through a floor plenum in the van.

Humidifier unit: The HU automatically maintained the relative humidity of the air in the van at a minimum of 30 percent.

Chilled water unit: The CWU chilled and circulated demineralized water through external supply and return lines to and from the VLC RTG cooling subsystem.

Chilled water piping system: The CWPS included the supply and return lines, valves, and other necessary components to transmit and control the flow of cooling/heating water to the VLC RTG cooling subsystem. The CWPS interconnected the CWU and the hot water system to the VLC through the sterilization chamber wall penetrations and the CWHS.

192

Chilled water hose set: The CWHS included all flexible hoses required for connecting the various subsystems of the RTG temperature control water system.

Chilled water purge unit: The CWPU purged with hot sterile GN_2 the VLC RTG cooling subsystem to remove all moisture just prior to launch. The CWPU was connected to the RTG cooling water piping in the umbilical tower.

Chilled water piping system - launch complex: The CWPS-LC included the supply and return lines, valves, and other necessary components to transmit and control the flow of cooling water and purge gas to the VLC RTG cooling subsystem at the launch complex. The CWPS-LC interconnected the CWU and the CWPU with the VLC.

Nitrogen supply unit: The NSU consisted of a manifold and interconnecting lines to connect K-bottles charged with nitrogen gas to the pressurization makeup unit and the CWPU on the umbilical tower.

Insulation (removable): The insulation was used to cover the RTG chilled water lines that ran up the outside of the bioshield cover to prevent the chilled water lines from sweating and allowing moisture to collect during the building phase. The insulation was removed from the lines just prior to the lander being installed in the shroud.

Storage container: The storage container was used to store the removable insulation when it was not installed on the RTG chilled water lines routed external of the lander.

Chilled water manifold: This manifold was required to allow connection of two CWU's to common supply and return umbilical hoses to the lander to allow operation of either CWU.

The sterilization AGE performed terminal sterilization of and maintained sterilization of the VLC. The AGE sterilized the encapsulated VLC and its pressurant by a dry-heat, inert-gaseous-atmosphere process. Subsequent to installation of the bioshield and thereafter until launch, the AGE pressurized the bioshield continuously to maintain VLC sterility. Before sterilization, the VLC was purged with GN_2 to reduce the oxygen content of the internal atmosphere to less than 2.5 percent by volume. During sterilization, the VLC was purged with GN_2 to reduce the moisture content of the internal atmosphere to less than 0.1 percent by weight and to purge the out-gassed organic materials. To accomplish terminal sterilization the following equipment was provided:

Sterilization chamber: The SC included a chamber in which the VLC and the specified propellant/pressurant loading equipment was sterilized. A separate control room housed controls and instrumentation required to control and monitor the sterilization process. Controls and instrumentation included a temperature controller and recorder, a pressure controller and recorder, and indication of moisture and oxygen content of both the chamber gas and the bioshield purge gas. The chamber was 6.4 by 6.4 by 4.3 m (21 by 21 by 14 ft) and included an independent air conditioning for maintaining suitable chamber conditions when sterilization was not being formed.

Pressurization makeup unit - ambient: The PMUA was connected to the VLC after the sterilization cycle and until launch. The unit maintained a pressure between 1.2 and 4.1 kPa (0.18 and 0.6 psig) on the VLC during this time period.

Pressurization makeup unit - sterilization: The PMUS was connected to the VLC bioshield before sterilization to purge the VLC, including the RPA, and remained connected throughout the sterilization cycle.

The science servicing AGE maintained cleanliness of the CHSU and the GCMS by means of controlled pressurization with high purity carbon dioxide. A positive pressure to 137.9 MPa (20 psig) maximum was maintained in the AGE and the surface sampler equipment continuously after cleaning until final bottom-up of the LVC prior to terminal sterilization. The AGE monitored and replenished the pressure in the AGE and surface sampler equipment intermittently. The AGE controlled the contamination level of the carbon dioxide introduced by the AGE into the surface sampler equipment by providing high purity gas, by initial cleaning of wetted parts, and by initial and final filtering of the fluid. The science servicing AGE included the following equipment:

Pressurization unit: The pressurization unit contained the carbon dioxide supply and storage tank, shut-off valves, self-sealing quick disconnect coupler, relief valve, flexible hoses, and other necessary components to pressurize the GCMS and the CHSU with high purity carbon dioxide.

Filtration assembly 1: This filtration assembly contained a final filter, pressure transducer, self-sealing quick-disconnect nipple, flexible hose, and other necessary components required to purify and transmit carbon dioxide from the pressurizaton unit to the GCMS.

Filtration assembly 2: This filtration assembly was identical to filtration assembly 1 except for different flex hose, tubing, and fitting arrangement required for connection to the CHSU.

Pressure readout unit: This unit contained a regulated power supply, digital voltmeter, switches, electrical lines, and other necessary components required to read out the pressure stimulus of the pressure transducer.

Langley Research Center
National Aeronautics and Space Administration
Hampton, VA 23665
August 30, 1979

194

APPENDIX

ABBREVIATIONS AND SYMBOLS

A	attitude
[A]	attitude direction cosine matrix
$[A]^T$	transpose of attitude matrix
$[\Delta A]$	error matrix
A_c	axial thrust command
$[A_d]$	desired (reference) attitude maneuver matrix
$[A_{d,i}]$	ith value of desired matrix
A/D	analog to digital
ADC	analog to digital converter
AFA	atmospheric filter assembly
AGC	automatic gain control
AGE	aerospace ground equipment
AHSE	assembly, handling, and support equipment
AO	auxiliary oscillator
AZ	azimuth
a	point in constant rate, engines off region
a_x	acceleration along X body axis
ac	alternating current
amp	amplifier
assy	assembly
atten	attenuator
BCE	bench checkout equipment
BLF	best lock frequency
BPA	bioshield power assembly

APPENDIX

BPF	band-pass filter
BRF	band reject filter
BS	bioshield
biol	biology
bps	bits per second
CCS	computer command subsystem
CCU	command control unit
CCW	counterclockwise
CHSU	collector head and shroud unit
CMG	command monitor group
CMU	controls mockup
C/O	check out
COSPAR	Committee on Space Research
CRT	cathode-ray tube
CSM	common services module
CW	clockwise
CWHS	chilled water hose set
CWPS	chilled water piping system
CWPS-LC	chilled water piping system - launch complex
CWPU	chilled water purge unit
CWU	chilled water unit
calib	calibration
cap	capacitor
c.g.	center of gravity
chgr	charger
ckt	circuit

APPENDIX

cmd   command

comb   combined

contr   contractor

DAPU   data acquisition and processing unit

Da   digital telemetry channel data interleaved with discrete and analog
          data on the telemetry data stream

Db   digital data formatted by a science instrument or GCSC and placed
          in telemetry stream when a data ready flag is generated

DCS   direct communications system

DMU   discrete monitor unit

DOU   discrete output unit

DR   down range

DSM   data storage memory

DSN   deep space network

DSS   data storage subsystem

dc   direct current

dc-dc   direct current to direct current

depress   depressurization

det   detector

diam   diameter

diff   difference

dipl   diplexer

distr   distributor

EL   elevation

EMC   electromagnetic compatibility

EMI   electromagnetic interference

EOM   end of mission

APPENDIX

ESS	electronic subsystem (biology)
ETG	electrically heated thermoelectric generator
ETR	Air Force Eastern Test Range
emerg	emergency
eng	engineering
equil	equilibration
exc	exciter
FAT	flight acceptance test
f_s	subcarrier frequency
G&C	guidance and control
GC	gas chromatograph
GCA	gas chromatograph assembly
GCMS	gas chromatograph mass spectrometer
GCSC	guidance, control, and sequencing computer
GDC	General Dynamics Corporation
GE	General Electric Company
GEX	gas exchange
GFE	government-furnished equipment
GRE	ground reconstruction equipment
g	acceleration of Earth's gravity
H	altitude
$\dot{H}$	rate of change in altitude
HGA	high-gain antenna
HGAC	high-gain antenna controller
HGADM	high-gain antenna deployment mechanism
HLCU	helium leak check unit

198

APPENDIX

HSA	hydrogen supply assembly
HTR	heater
HU	humidifier unit
H/W	hardware
IDS	instrument data system
IEA	instrument electronics assembly
IF	intermediate frequency
I/O	input/output
IOP	input/output processor
IR	infrared
IRD	interface requirements document
IRU	inertial reference unit
info	information
int	integrator
iso	isolation
JPL	Jet Propulsion Laboratory
K	altitude estimation constant
K_g	gravity constant
K_H	altitude constant
K_u, K_v, K_w	velocity radar data coefficients
KSC	John F. Kennedy Space Center
LaRC	Langley Research Center
LBS	lander body simulator
LCC	launch control console
LCE	launch complex equipment
LCS	lander camera systems

APPENDIX

LeRC	Lewis Research Center
LFOS	launch and flight operations system
LGA	low-gain antenna
LHISC	lander hardline interface and signal conditioning set
LIS	lander/STE interface simulator
LP	low pass
LPA	loading and pyrolyzing assembly
LPCA	lander pyrotechnic control assembly
LR	labeled release
LVS	launch vehicle system
M	manifold
MBA	meteorology boom assembly
MCA	microwave components assembly
MDS	modulation/demodulation subsystem (VO)
MEA	meteorology electronics assembly
M-G	motor generator
MMC	Martin Marietta Corporation (now Martin Marietta Aerospace)
MOI	Mars orbit insertion
MRO	memory readout
MS	mass spectrometer
MSA	mass spectrometer assembly (fig. 36); meteorology sensor assembly (fig. 102)
MSS	mechancial subsystem (biology)
mag	magnetic
m/e	mass ratio relative to mass of an electron
mem	memory
min	minimum

200

APPENDIX

mon	monitor
mult	multiplier
NBW	noise bandwidth
NC	normally closed
NO	normally open
NRZ	nonreturn to zero
NRZ-L	nonreturn to zero-level
NSU	nitrogen service unit
OC	overcurrent
O/S	overcurrent sensor
OS	overload sensor
OSC	oscillator
OVT	organic vapor trap
P_c	pitch command
PC	proportional counters
PCDA	power conditioning and distribution assembly
PCM	pulse code modulation
PDA	processing and distribution assembly
PKG	package
PLAU	propellant load adapter unit
PLHS	propellant load hose set
PLVU	propellant load verification unit
PMUA	pressurization makeup unit - ambient
PMUS	pressurization makeup unit - sterilization
PPS	pulses per second
PPU	portable power unit

PR	pyrolytic release
PS	power source
PSK	phase shift keyed
PSU	propellant servicing unit
PTU	pneumatic test unit
p,q,r	roll, pitch, and yaw angular velocity, respectively
ppm	parts per million
pream	preamble
presep	preseparation
press	pressure
prop	propulsion
pwr	power
pyro	pyrotechnic
QUAL	qualification tests
R	position vector
RA	radar altimeter
RAE	radar altimeter electronics
RAS	relay antenna subsystem
RCE	relay communication equipment
RCL	relay communicaton link
RCS	reaction control system
RFCTS	radio frequency communications test set
RFI	radio frequency interference
ROM	read only memory
RPA	retarding potential analyzer
RRS	relay radio subsystem

APPENDIX

RTD	resistance temperature detector
RTG	radioisotope thermoelectric generator
RTI	real-time interrupt
RTS	relay telemetry subsystem (VO)
RZ	return to zero
r	radius of Mars
rec	receiver
rf	radio frequency
SBRA	S-band radio assembly
SC	sterilization chamber
SCR	silicon controlled rectifier
SDA	sample distribution assembly
SFC	squib fire circuit
SPG	science payload group
S/S	subsystem
SSA	surface sampler assembly
SSAA	surface sampler acquisition assembly
SSCA	surface sampler control assembly
STE	system test equipment
SWR	standing-wave ratio
seq	sequence
sig	signal
sol	solenoid
TD	terminal descent
TDC	telemetry data conditioner
TDLR	terminal descent and landing radar

VO	Viking orbiter
VPC	Viking pressure cartridge

TDS	terminal descent system
TES	tape end signal
TESS	terminal engine shutdown switch
TM	telemetry
TMI	trans-Mars insertion
TR	tape recorder
TRS	transmit-receive selector
TWT	traveling wave tube
TWTA	traveling wave tube amplifier
t	time
Δt	change in time
typ	typical
UAMS	upper atmosphere mass spectrometer
UHF	ultrahigh frequency
u,v,w	velocity component along X, Y, and Z body axis, respectively

$\Delta\theta$	inertial reference unit attitude
ϵ	error
θ	angle between position vector and Z-axis
θ_c	pitch steering command
θ_L	limit cycle attitude limit
$\dot{\theta}_1, \dot{\theta}_2$	maneuver rate lower and upper boundary, respectively
σ	standard deviation
ϕ_e, θ_e, ψ_e	error in roll, pitch, and yaw angle, respectively
ψ_c	yaw steering command
ω	angular velocity

Subscripts:

b	body axis
I	inertial axis

REFERENCE

1. Cooley, C. G.; and Lewis, J. G.: Viking Lander System - Primary Mission Performance Report. NASA CR-145148, 1977.

207

1. Report No. NASA RP-1027	2. Government Accession No.	3. Recipient's Catalog No.
4. Title and Subtitle VIKING '75 SPACECRAFT DESIGN AND TEST SUMMARY VOLUME I - LANDER DESIGN		5. Report Date **November 1980**
		6. Performing Organization Code
7. Author(s) Neil A. Holmberg, Robert P. Faust, and H. Milton Holt		8. Performing Organization Report No. L-12087
9. Performing Organization Name and Address NASA Langley Research Center Hampton, VA 23665		10. Work Unit No. 815-00-00-00
		11. Contract or Grant No.
12. Sponsoring Agency Name and Address National Aeronautics and Space Administration Washington, DC 20546		13. Type of Report and Period Covered Reference Publication
		14. Sponsoring Agency Code

15. Supplementary Notes

16. Abstract

This publication, in three volumes, discusses the design of the Viking lander and orbiter as well as the engineering test program that was developed to achieve confidence that the design was adequate to survive the expected mission environments and to accomplish the mission objective. Volume I includes a summary of the Viking Mission and the design of the Viking lander. Volume II consists of the design of the Viking orbiter and Volume III comprises the engineering test program for the lander and the orbiter.

17. Key Words (Suggested by Author(s)) Viking Project Viking lander design	18. Distribution Statement Unclassified - Unlimited Subject Category 18

19. Security Classif. (of this report) Unclassified	20. Security Classif. (of this page) Unclassified	21. No. of Pages 211	22. Price A10

NASA-Langley, 1980